The Role of BRCA1 in Telomere Maintenance

A thesis submitted for the degree of Doctor of Philosophy

By

Kobra Kargaran

College of Health and Life Sciences
Department of Life Sciences,
Division of Biological Sciences
Brunel University London

October 2015

Declaration

I hereby declare that the research presented in this thesis is my own work, except where otherwise specified, and has not been submitted for any other degree.

Kobra Kargaran

Abstract

Telomeres are fundamental structures found at the end of all eukaryotic chromosomes that function to protect the end of chromosomes from end-to-end fusion, erosion and subsequent telomere dysfunction. Telomerase and alternative lengthening of telomere (ALT) mechanisms maintain the telomeres by compensating natural telomeric loss. ALT is found to be present in 15% of human tumours lines and it may be expressed at low levels in the normal mouse tissues. However, the exact mechanism behind ALT depression and/or activation in the mammalian cells is not fully understood. Previous studies have highlighted the role of BRCA1 in telomere dysfunction. Also, it has recently been shown that BRCA1 co-localises at telomeres in the ALT $^{+}$ human cells through BLM and Rad50. However, it is still unclear whether BRCA1 plays a direct role on telomere length maintenance and integrity.

The aim of this project was to examine the role of BRCA1 in telomere maintenance associate with ALT in *BRCA1* defective mammalian cells. Therefore to achieve this, we have set up series of experiments to look at, (a) hallmarks of ALT activity at the cytological level, (b) measuring of ALT activity using biochemical and immunocytochemistry techniques and (c) understanding the role of BRCA1 in DNA damage response mechanism and telomere dysfunction.

Firstly, we found elevated levels of recombination at telomeres in the two human *BRCA1* carrier cell lines and mouse embryonic stem cell with deficiency in *Brca1*$^{-/-}$. Secondly, our data showed that human and mouse *BRCA1* defective cells are significantly more sensitive to ionizing radiation in line with the DNA repair function of BRCA1. Moreover, we found persistent DNA damage at telomeres in the BRCA1 defective environment when after exposure of cells to ionizing radiation. Thirdly, we found evidence of ALT activity in some mouse cell lines, and elevated ALT in mouse cells defective in Brca1. Finally, we examined

some other ALT markers using immunofluorescence. Our data indicate differences between human and mouse cells in regulating ALT.

Taken together data presented in this thesis revealed that (i) BRCA1 plays a major role in telomere maintenance and defective BRCA1 mammalian cells show evidence of telomere dysfunction and telomere length shortening in line with previous publish data, (ii) BRCA1 defective mouse cells have elevated levels of ALT, (iii) the mouse lymphoblastoid LY-S cells have complete absence of ALT.

Publications arising from this thesis

Kargaran P.K., Yasaei H., Anjomani-Virmouni S., Mangiapane G and Slijepcevic P. (2016) Analysis of Alternative Lengthening of Telomere Markers in BRCA1 Defective Cells, Genes Chromosomes Cancer. 2016 Jun 13. doi: 10.1002/gcc.22386.

Kargaran K., Yasaei H., and Slijepcevic P. (2016) Mouse Lymphoma radiosensitive cells lack ALT-mediated telomere maintenance, Mutation Research (In preparation).

Acknowledgement

I would firstly like to thank my supervisor Dr Predrag Slijepcevic for his expertise and continuous advice, and second supervisor Dr Amanda Harvey for her guidance and opinion.

I would like to thanks Dr Amir Hassan Khani the managing director of Bent Al Hoda Hospital in Mashhad, Iran for providing part scholarship towards the completion of this thesis.

I would also like to acknowledge Dr Sahar Al-Mahdavi, Dr Hemad Yasaei, and Dr Terry Roberts, for showing me the ropes in the lab and sharing their knowledge with me.

I have to thank my friends who have all helped in their own way: Chetana, Savi, Sheila and Giovanna Mangiapane various lab discussions and help in managing and running the day-to-day activities in the lab. Also big thanks to my lovely friend Sara Anjomani Virmouni for all her advice over the past years.

Lastly, I would like to say a BIG thank you to my family, especially my mother and father for their endless support, love and always giving the right advice during difficult time that made the huge difference. I also want to say a big thank you and love to my sister and brother for believing in me and giving support that helped me to get through the four years.

Table of Contents

Declaration I

Abstract II

Publications arising from this thesis IV

Acknowledgement V

Table of Contents VI

List of Figures XIV

List of Tables XXIII

List of Abbreviations XXIV

1 General Introduction 1

1.1 Introduction 1

1.2 Structure and Function of Mammalian Telomeres 3

1.2.1 Structural biology of Telomeres 3

1.2.2 End replication problem 5

1.2.3 The G-quadroplex structure of telomeres 6

1.3 Proteins associated with telomeric DNA 8

1.3.1 Telomeric nucleosome 8

1.3.2 Shelterin 8

1.3.2.1 TRF1 9

1.3.2.2 TRF2 10

1.3.2.3 TIN2 10

1.3.2.4 Rap1 11

1.3.2.5 TPP1 11

1.3.2.6 POT1 11

1.4 The role of shelterin in chromosomal end protection 13

1.5 *BRCA1* gene and protein structure 15

1.6 The role of telomere and shelterin in DNA damage response 17

1.6.1 Functional role of BRCA1 within DNA-damage response 19

1.6.2 How does shelterin repress telomere-mediated DNA damage response? 20

1.7 DNA repair and response at dysfunctional telomeres – How does BRCA1 play a part? 23

1.8 The role of BRCA1 in non-homologous end joining (NHEJ) 24

1.9 BRCA1 and HR 27

1.9.1 HR at telomeres 29

1.9.2 NHEJ and HR in cell cycle 30

1.10 The role of BRCA1 in telomere maintenance 31

1.11 Telomere length regulation by telomerase 33

1.11.1 The human telomerase structure 34

1.11.1.1 Human TR (hTR) 34

1.11.1.2 Human TERT (hTERT) 34

1.11.2 Telomerase assembly and regulation at telomeres 35

1.11.3 BRCA1 inhibition of telomerase activity 36

1.12 Telomere length regulation through Alternative Lengthening of Telomere (ALT) and the role of BRCA1 37

1.12.1 Telomeric phenotype of ALT positive cells 37

1.12.2 Telomeric recombination in ALT cells 41

1.12.3 Proteins involved in HR-mediated telomere maintenance in ALT cells 42

1.13 Aim of the thesis and outline of chapters 43

2 Materials and Methods 45

2.1 Cell lines and tissue culture conditions 45

2.1.1 Human epithelial cancer cell lines 45

2.1.2 Human B-lymphocytes 45

2.1.3 Mouse lymphoma cell lines 46

2.1.4 Mouse embryonic stem cells 46

2.1.5 Human ALT^{+} cell lines 46

2.2 Tissue culture procedure 47

2.2.1 Cell counting 47

2.2.3 Cell cryopreservation 49

2.2.4 Thawing of cryopreserved cells 49

2.2.5 Irradiation of cells 49

2.3 Cytogenetic Analysis 50

2.3.1 Metaphase preparation using lymphoblastoid cell lines 50

2.3.2 Metaphase preparation using mouse embryonic stem cell lines 50

2.3.3 Giemsa staining 50

2.3.4 Chromosomal aberration analysis 50

2.3.5 Micronuclei assay 51

2.4 Interphase Quantitative Fluorescence *in situ* Hybridization (I-QFISH) 52

2.4.1 Pre-hybridisation washes 52

2.4.2 Hybridisation 52

2.4.3 Post-hybridisation washes 52

2.4.4 Image capture and telomere length analysis 53

2.5 Chromosome Orientation Fluorescence *in situ* Hybridisation (CO-FISH) 55

2.5.1 Washing, digestion, and fixation 55

2.5.2 Image Analysis 56

2.6 Immunocytochemistry 56

2.6.1 Single immunofluorescence detection of γ-H2AX foci 56

2.6.2 Telomere dysfunction-induced foci (TIF) assay 57

2.6.3 Single immunofluorescence detection of PML foci 57

2.6.4 Immunofluorescence and FISH (Immuno-FISH) 58

2.6.5 Single immunofluorescence detection of ATRX foci 58

2.6.6 Single immunofluorescence detection of BRCA1 foci 59

2.6.7 Single immunofluorescence detection of BLM foci 59

2.6.8 Double immunofluorescence detection of BRCA1 with BLM 60

2.7 Western Blot 60

2.7.1 Protein gel electrophoresis 60

2.7.2 Blotting and transfer 61

2.7.3 Blocking and antibody incubation 61

2.7.4 Protein detection with chemiluminescence 62

2.8 Quantitative telomere-repeat amplification (TRAP) assay 64

2.8.1 Protein isolation 64

2.8.2 Determination of protein concentration 64

2.8.3 TRAP PCR reaction set-up 66

2.8.4 PAGE-gel electrophoresis and data analysis 67

2.8.5 Quantitation and data analysis using Image-Lab software 69

2.9 C-Circle assay for detection of *A*lternative *L*engthening of *T*elomeres (ALT) activity 70

2.9.1 Genomic DNA extraction 70

2.9.2 DNA quantification 72

2.9.3 C-circle amplification 73

2.9.4 Slot-blotting 73

2.9.5 Hybridization with P^{32}-labelled telomeric probe 74

2.9.5.1 Preparation of P^{32} probe 74

2.9.5.2 Purification of P^{32} probe 74

2.9.5.3 Hybridization 74

2.9.5.4 Image analysis of CC assay (Quantification) 75

2.10 Graphical display and Statistical Analysis 76

3 Analysis of Telomere Function in *BRCA1* Defective Human Cell Lines 77

3.1 Introduction 77

3.2 Results 80

3.2.1 Cell lines and rationale 80

3.2.2 Telomere sister chromatid exchange in *BRCA1* lymphoblastoid cell lines 81

3.2.3 Telomere length analysis in *BRCA1* lymphoblastoid cell lines 83

3.2.4 Cytogenetic analysis of chromosomal aberrations in human lymphoblastoid BRCA1 defective cell lines 86

3.2.5 Chromosomal abnormalities in the BRCA1 defective human cells – the G1 assay 87

3.2.6 Chromosomal abnormalities in the BRCA1 defective human cells – the G2 assay 89

3.2.7 Establishment of micronucleus assay for assessing chromosome damage in BRCA1 defective cell lines 90

3.2.8 Immunofluorescence analysis of γ-H2AX in human lymphoblastoid cell lines 93

3.2.8.1 Analysis of γ-H2AX kinetics in human lymphoblastoid cell lines 93

3.2.8.2 Analysis of γ-H2AX after exposure to different doses of gamma rays 95

3.2.9 Telomere dysfunction-induced foci (TIF) analysis in human lymphoblastoid cell lines 97

3.2.9.1 Analysis of TIF kinetics in human lymphoblastoid cell lines 97

3.2.9.2 Analysis of TIF response after acute dose response in human lymphoblastoid cell lines. 98

3.3 Discussion 99

4 DNA damage response in mouse embryonic stem cells 103

4.1 Introduction 103

4.2 Results 106

4.2.1 Establishment of an immunofluorescence assay protocol in mESCs cells ... 106

4.2.2 Telomere dysfunction-induced foci (TIF) analysis in normal and homozygous Brca1 mESCs 110

4.2.3 Radiation induced chromosomal abnormalities in Brca1 mutant mouse embryonic stem cells 112

4.2.4 Analysis of CAs induced by IR in mESCs 112

4.2.4.1 Setting up a modified micronuclei assay protocol for assessing chromosome damage in mouse BRCA1 homozygous embryonic stem cells 115

4.3 Discussion 118

5 Analysis of ALT markers in mESCs 121

5.1 Introduction 121

5.2 Results 124

5.2.1 CO-FISH analysis of BRCA1-defective mouse embryonic stem cells 124

5.2.2 Analysis of end-to-end telomeric fusion in mouse embryonic stem cells 125

5.2.3 Telomere length analysis using IQ-FISH in mouse embryonic stem cells 127

5.2.4 Co-localization of PML bodies and telomeres in mouse embryonic stem cells 129

5.2.5 ATRX as a marker of ALT activity 133

5.3 Discussion 137

6 Assessment of additional ALT markers in mouse and human cells 140

6.1 Introduction 140

6.2 Results 142

6.2.1 Cell lines 142

6.2.2 Detection of ALT activity by C-circles assay 142

6.2.3 Detection of Telomerase activity in mESCs 145

6.2.4 Investigation of BRCA1 protein in ALT and non ALT cell lines 148

6.2.5 Immunofluorescence analysis of BRCA1, BLM and ATRX 149

BRCA1 and BLM 159

6.3 Discussion 166

7 General Discussion and Future Research Direction 171

7.1 Introduction 171

7.2 Telomere dysfunction in *BRCA1* mutation carriers 172

7.3 Evidence for ALT activity in BRCA1 defective mESCs 173

7.4 Future Research Direction 175

8 References..... 177

List of Figures

Figure 1-1. Proposed structure of the mammalian telomeres. 4

Figure 1-2. The end replication problem at telomeres. 6

Figure 1-3. The G-quadroplex structure of telomeric DNA (Phan et al., 2007)..... 7

Figure 1-4. The schematic diagram of mammalian telomeric complex containing shelterin units (Verdun and Karlseder, 2007)..... 13

Figure 1-5. The protein structure of the BRCA1 tumour suppressor (Adapted from (Clark et al., 2012)..... 16

Figure 1-6. DNA is constantly under attack through exogenous agents (Shiloh, 2003)..... 20

Figure 1-7. DNA double-strand break repair in mammalian cells (Lans et al., 2012). DNA DSBs are predominantly repaired by either non-homologous end-joining (NHEJ) or homologous recombination (HR)..... 24

Figure 1-8. The mechanism of NHEJ (Samarasinghe, 2013). BRCA1 plays an important role in NHEJ mechanisms. A double stranded and break is detected by and repair proteins which bring together two ends and join them. 25

Figure 1-9. The HR repair pathway in the mammalian cells (Bugreev et al., 2011). Stalled replication forks can be rescued by HR via a mechanism that relies on DNA strand exchange activity of RAD51. 28

Figure 1-10– Irradiation induces G1 and G2 cell cycle checkpoint activation and DNA repair. Most cancer cells are defective in G1checkpoint, commonly due to the mutation/alterations of the key regulators of the G1 checkpoint (in blue), but contain a functional G2 checkpoint (Hein et al., 2014). 31

Figure 1-11. Evidence of telomeric copying via HR in the ALT cells. 39

Figure 2-1. Representative images of cultured mouse ESCs. 46

Figure 2-2. Representative images of ALT^+ human cell lines. 47

Figure 2-3. Schematic diagram showing formation of micronuclei (MN). 51

Figure 2-4. Schematic representation of the IQ-FISH workflow. 53

Figure 2-5- Image shows a typical segmented image with cell nuclei stained in green..... 54

Figure 2-6- Image shows a snapshot of the mathematical manipulations behind the process of telomere fluorescence intensity measurement. 54

Figure 2-7. Schematic representation of CO-FISH. 56

Figure 2-8. BSA standard curve for protein estimation. 65

Figure 2-9. Workflow used for TRAP measurement. 69

Figure 2-10. CC quantification using Image J. 75

Figure 3-1. Examples of T-SCEs in lymphoblastoid cell lines after CO-FISH. 82

Figure 3-2. T-SCE analysis of human lymphoblastoid cells by CO-FISH. 83

Figure 3-3. Representative examples of telomere FISH in the interphase nuclei of human lymphoblastoid cell lines. 84

Figure 3-4. Representative examples of telomere FISH in mouse LY-R (A and B) LY-S cells (C and D). Blue: nuclei stained with DAPI (A and C). Green: telomere staining by the FITC labelled probe (B and D). 85

Figure 3-5. Mean values of telomere fluorescence measured using IQ-FISH. 86

Figure 3-6. Representative example of radiation-induced CA in G1 from the BRCA1 defective human cells..... 88

Figure 3-7. Frequencies of chromosomal abnormalities in three human cell lines after exposure to various doses of gamma radiation. 88

Figure 3-8. Frequencies of radiation induced chromatid breaks and gaps (G2 assay) in the BRCA1 defective cell lines (GM13705 and GM14090) and the control cell line (GM00893). 90

Figure 3-9. An example of chromosomal abnormalities in the G2 phase of the cell cycle in a human lymphoblastoid cell line. 90

Figure 3-10. Analysis of binucleated cells in *BRCA1* human lymphoblastoid cell lines. 92

Figure 3-11. Mean frequency of micronuclei in un-irradiated and irradiated cell lines. 93

Figure 3-12. Frequencies of γ-H2AX foci induced with 1.0Gy of gamma-rays. 94

Figure 3-13. Representative example of γ-H2AX foci detected by immunofluorescence in human lymphoblastoid cell line GM14090 (BRCA1$^{+/-}$) induced with 1.0Gy gamma radiation. 95

Figure 3-14. Frequencies of γ-H2AX and TIF foci after exposure to 0.5Gy, 1.0Gy, and 2.0Gy of gamma rays in BRCA1 defective cell lines (GM14090 and GM13705) and the control cell line (GM00893). A) Average frequencies of spontaneous γ-H2AX foci. B) The difference in the levels of γ-H2AX was significant between the two BRCA1 defective (GM14090 and GM13705) cell lines and the BRCA1 WT control (GM00893) (***P<0.001). Asterisks indicate significant differences between the BRCA1 and control cell lines (*P<0.5; **P< 0.001; ***P< 0.0001). T-test used in all statistical comparison. 96

Figure 3-15. Immunofluorescence microscopy showing γ-H2AX foci formation in nuclei of human lymphoblastoid cell line GM14090. 96

Figure 3-16. An example of TIF foci in BRCA1 carrier (GM14090). 97

Figure 3-17. Average frequencies of TIF foci in each cell line irradiated with 1.0Gy. 98

Figure 3-18 Average TIFs in BRCA1 defective cell lines (GM14090 and GM13705) and control cell lines (GM00893) exposed to various doses of IR. 99

Figure 4-1. Analysis of γ-H2AX foci in mESCs. 109

Figure 4-2. Detection of γ-H2AX by immuno-FISH in mouse embryonic stem cell line (408 Brca1$^{-/-}$) after different time post 1.0 Gy gamma irradiation. 110

Figure 4-3. Average frequencies of TIF foci in each cell line after 0.5hrs, 5hrs, 24hrs and 48hrs post-irradiation. A) levels of TIFs per cell nuclei measured in the un-irradiated E14 and 408 cell lines. B) a total of 50nuclei scored for each time point and cell line (E14 and 408) in two independent experiments. C) T-test analysis comparing the untreated samples with irradiated samples. There were no significant differences between the average frequency of TIF foci in the E14 cell line 24hrs and 48hrs post-irradiation when compared to the untreated E14 cells, whereas 408 Brca1 defective mESC showed significantly elevated levels of TIF at all time points compared to the un-irradiated 408 sample but to a lesser extent at 48hrs.

Error bars indicate SEM and asterisks indicate significant differences between the 408 and the control cell line (E14) (***P<0.001). 111

Figure 4-4. Detection of TIF in mESC*: Brca1*+/+ and *Brca1-/-* (E14 and 408 respectively). Interphase cells were permeabilised and stained with antiphospho-histon γ- H2AX (green) and telomeric Cy3-labeled PNA probes (red). Nuclei were counterstained with DAPI. 112

Figure 4-5. Examples of chromosomal abnormalities in mouse embryonic stem cells. A) Untreated cells, with classical Giemsa staining method, B) chromosomal abnormalities in 408 cell line (dicentric and fragment) after exposure with IR. 113

Figure 4-6. Frequency of chromosomal abnormalities in mouse embryonic stem cell lines: E14 (*Brca1+/+)* and 408 (*Brca1-/-)* induced by IR in the G1 phase. *=P<0.05, **=P<0.01, ***=P<0.001. The error bars represent SEM. 114

Figure 4-7. Relative frequencies of chromatid breaks in mouse embryonic stem cell lines (E14 and 408): all cells collected at 1.5hrs, 3hrs and 4hrs after exposuere to 0.5Gy IR. The error bars represent SEM. 114

Figure 4-8. Examples of initial images generated by the MN assay in mESCs A) after 24hrs with 3µg/ml of Cyt-B, B) after 24hrs with 6µg/ml Cyt-B, C) after 48hrs with 3µg/ml of Cyt-B. 115

Figure 4-9. Mean MN after irradiation in mouse embryonic stem cell lines: E14 (Brca1+/+) and 408 (Brca1-/-). The basal levels of MN induced by IR 48hrs after exposure to different Gy in cultures of normal *Brca1* cell line (E14) and *Brca1* homozygous cell line (408) treated with cytochalasin B. Mean ± SEM from 500 scored binucleated cells. T-test used for statistical analysis. * (P<0.05); ** (P<0.001). 117

Figure 4-10. Scoring binucleated cells in mESC. A) an examlpe of a MN; B and C) binucleated cells with three MN; D, E and F) viable mono, di and quadrinuclear cells..... 118

Figure 5-1. Mean value of T-SCEs in mESCs. Error bars indicate SEM. A total of 100 metaphases were scored for the presence of T-SCE in two independent experiments. 125

Figure 5-2. Examples of T-SCEs in the mESCs. A) A metaphase spread from the E14 cell line. B) A metaphase spread from the 408 cell line. The yellow arrows indicate examples of T-SCEs and enlarged on the right. 125

Figure 5-3. Frequencies of telomeric end-to-end fusions in E14 and 408 cell lines. The error bar indicates SEM. A total of 100 metaphases were scored for the presence of ECFs in two independent experiments. 126

Figure 5-4. Detection of telomeric fusion in mouse embryonic stem cells: A) control cell line (E14), and B) Brca1$^{-/-}$ (408). 127

Figure 5-5. Telomere fluorescence analysis by IQ-FISH. CCFL. corrected calibrated fluorescence after calibration using LY-R and LY-S cells. Error bars indicate SEM. 128

Figure 5-6. Telomere fluorescence analysis using IQ-FISH. A and B) Radioresistance LY-R and Radiosensitive LY-S in interphase; C and D) show mESCs: 408 and E14, respectively. 128

Figure 5-7. Total number of APBs in human and mouse cells. Frequency of APBs counted in: BRCA1-positive human cells (U2OS and HeLa) and BRCA1-defective human cells (HCC1937); and mouse Brca1-positive ESC (E14) and Brca1-defective ESC (408) cells; mouse Brca1-positive lymphoblastoid (LY-R and LY-S) cells. Data from 50 nuclei counted in two independent experiments. T-test used for statistical analysis..... 130

Figure 5-8. Co-localisation of APBs with telomeres in human and mouse cell lines. Green lines indicate the means. T-tests were used for statistical analysis. 131

Figure 5-9. Immuno-FISH analysis in ALT^{+} (U2OS) and ALT^{-} (HeLa and HCC1937). U2OS was used as the positive control while HeLa served as the negative control. Interphase cells were permeabilised and stained with anti-PML (green) and telomeric Cy3-labeled PNA probes (red). Nuclei were counterstained with DAPI. 132

Figure 5-10. Detection of APBs by immuno-FISH in mESCs, LY-R and LY-S cells. Interphase cells were permeabilised and stained with anti-PML (green) and telomeric Cy3-labeled PNA probes (red). Nuclei were counterstained with DAPI. 133

Figure 5-11. Total number of ATRX signals in human and mouse cells. Data is from 50 nuclei from two independent experiments. T-test is used for statistical comparison. 134

Figure 5-12. Co-localisation of ATRX with telomeres. The green bar indicates mean. T-test is used for statistical analysis..... 135

Figure 5-13. ATRX (green) is absent in U2OS cells and present in HeLa and HC1937 cells. Telomeres shown in red..... 136

Figure 5-14. ATRX signals (green) present in all mouse cells. Telomeres shown in red.... 137

Figure 6-1. The CC assay in human and mouse cells. A) Slot-blot examples of the CC assay using 30ng of gDNA. B) The human ALT-positive U2OS cells used to create a standard curve with concentrations of DNA ranging from 3.75ng-60ng. C) Standard curve of the CC assay of the ALT-positive U2OS. The R^2 was equal to 0.9207. The CC assay unit is calculated based on arbitrary unit (a.u.). 143

Figure 6-2 CC assay on 30ng genomic DNA. A) from U2OS (ALT^+), HeLa, GM00893, GM13705 ($BRCA1^{+/-}$), HCC1937 ($BRCA1^{-/-}$), SKLU-1, G292. B) E14 ($Brca1^{+/+}$), 408 ($Brca1^{-/-}$), LY-R, and LY-S. The quantitation was done using the Image J software. Error bars indicates SD. T-test used for statistical analysis. *P= 0.0341, **P=0.0169. 145

Figure 6-3. Telomere Repeat Amplification Protocol (TRAP). 200ng of CHAPS lysed proteins used in all samples. The heat-treated samples were heated at 85°C for 10 minutes to inactivate the telomerase enzyme. The Standanrd Internal Control (SI-C) at 36bp is indicative of complete PCR amplification. In high telomerase samples the SI-C is weaker than in low telomerase samples since the SI-C competes proportionaly with the telomerase enzyme. The 25bp DNA ladder is shown in the first lane. The last lanes are TSR8 (2 units of telomerase quantitation positive control. TSR8 is an oligonucleotide with a sequence identical to the TS primer extended with 8 telomeric repeats $AG(GGTTAG)_7$. This control serves as a standard for estimating the amount of TS primers with telomeric repeats extended by telomerase in a given extract provided by the kit manufacturer) and CHAPS buffer used as internal positive and negative controls respectively..... 147

Figure 6-4 Telomerase activity in the human and mouse cell lines. U2OS (ALT^{+}), HeLa (ALT^{-}), LY-R, LY-S, E14 ($Brca1^{+/+}$), and 408 ($Brca1^{-/-}$) calculated using the TRAP gels from the 200ng protein . The artibtary unit of telomerase units calcualted using the formula described in chapter 2. T-test is used for statistical analysis. The 200ng data is based on three independent experiments from two independent CHAPS lysed proteins. 148

Figure 6-5 Immunoblotting of BRCA1 in the human and mouse cell lines. A) Western blot showing the BRCA1 expression. B) Protein bands were quantified by densitometry, expressed relative to actin, and normalized to the control (HeLa). C) Protein bands were quantified by densitometry, expressed relative to actin, and normalized to the control (E14). 149

Figure 6-6- BRCA1 co-localise at telomere in human cell lines. Examples of immunofluorescence colocalisation of BRCA1 with telomeres in the human HCC1937 BRCA defective and HeLa and U2OS BRCA1 positive cells. . Interphase cells were permeabilised and stained with anti-BRCA1 (green) and telomeric Cy3-labeled PNA probes (red). Nuclei were counterstained with DAPI. 151

Figure 6-7- BRCA1 co-localise at telomere in mouse cell lines. Examples of BRCA1 colocalisation with telomeres. 408 cell line served as the negative controls, and E14 was used as the positive control. Interphase cells were permeabilised and stained with anti-BRCA1 (green) and telomeric Cy3-labeled PNA probes (red). Nuclei were counterstained with DAPI. 152

Figure 6-8- Total number of BRCA1 foci per cell in the human and mouse cells. Immunofluoresence of the total number of BRCA1 foci in the human ALT-positive (U2OS) and ALT-negative (HeLa and HCC1937) cells and the mouse ES cells (E14 and 408) and lymphoblastoid (LY-R and LY-S) counted in 50 cell nuclei in two independent experiments. T-test is used for statistical analysis. 153

Figure 6-9- Co-localisation of BRCA1 with telomeres in the human and mouse cells and human cell lines. Number of BRCA1 foci colocalised with telomeres in the human ALT-positive (U2OS) and ALT-negative (HeLa and HCC1937) cells and the mouse ES cells (E14

and 408) and lymphoblastoid (LY-R and LY-S) cells. In total 50 cell nuclei counted in two independent experiments. The green bar indicates mean. T-test is used for statistical analysis. 154
Figure 6-10- BLM (green) co-localisation with telomeres (red) in the human cell lines. . Interphase cells were permeabilised and stained with anti-BLM (green) and telomeric Cy3-labeled PNA probes (red). Nuclei were counterstained with DAPI. 156
Figure 6-11- BLM (green) co-localisation with telomeres (red) in the mouse cell lines..... 156
Figure 6-12- Number of BLM foci per cell in the human and mouse cells. A total of 50 cell nuclei in two independent experiments were analysed. Statistical analysis carried out by T-test. 157
Figure 6-13- Co-localisation of BLM with telomeres in the human and mouse cells. A total 50 cell nuclei/sample counted in two independent experiments. The green bars indicate the means. T-test is used for statistical analysis. 158
Figure 6-14- Examples of immunofluorescence showing co-localisation of BRCA1 with BLM in human cell lines. Interphase cells were permeabilised and stained with anti-BRCA1 (green) and anti-BLM (red) antibodies. Nuclei were counterstained with DAPI. 160
Figure 6-15- Examples of immunofluorescence showing co-localisation of BRCA1 with BLM in mouse cell lines. Interphase cells were permeabilised and stained with anti-BRCA1 (green) and anti-BLM (red) antibodies. Nuclei were counterstained with DAPI. 161
Figure 6-16- A) Co-localisation of BRCA1 with BLM in the human and mouse cells. B) Quantitation of percentage of cells with BRCA1-BLM co-localisation. A total 50 cell nuclei/sample counted in two independent experiments. The green bar indicate the means. T-test is used for statistical analysis. 162
Figure 6-17- Examples of immunofluorescence showing co-localisation of BRCA1 with ATRX in the human cell lines. Interphase cells were permeabilised and stained with anti-BRCA1 (green) and anti-ATRX (red) antibodies. Nuclei were counterstained with DAPI..... 163

Figure 6-18- Examples of immunofluorescence showing co-localisation of BRCA1 with ATRX in the mouse cell lines. Interphase cells were permeabilised and stained with anti-BRCA1 (green) and anti-ATRX (red) antibodies. Nuclei were counterstained with DAPI..... 164
Figure 6-19- Co-localisation of BRCA1 with ATRX in the human and mouse cells. A) Number of BRCA1 and ATRX colocalisation in the human ALT-positive (U2OS) and ALT-negative (HeLa and HCC1937) cells and the mouse ES cells (E14 and 408) and lymphoblastoid (LY-R and LY-S) cells. B) Quantitation of percent of cells with ATRX-BRCA1 colocalisations in the human and mouse cells. In total 50 cell nuclei counted in two independent experiments. The green bar indicates mean. T-test is used for statistical analysis. 165
Figure 6-20- Co-localised foci of APBs, ATRX, BRCA1 and BLM with telomeres in human and mouse cells. 166

List of Tables

Table 1-1. Summary of proteins involved directly with the telomere (the shelterin unit) (de Lange 2006)..... 14

Table 1-2. Interaction of DNA repair and damage response proteins with telomeres ((Slijepcevic, 2006) de Lange 2006)..... 22

Table 2-1. A detail summary of all cell lines used in this thesis. 48

Table 2-2. Summary of antibodies used in this thesis..... 63

Table 2-3. Preparation of diluted BSA standards for BCA analysis..... 65

Table 2-4. DNA concentration of all samples 72

Table 4-1- Establishment of the H2AX assay protocol..... 107

Table 4.2- Establishment of a micronucleus assay..... 116

List of Abbreviations

ALT Alternative lengthening of telomeres

APB ALT Promyelocytic leukemia Bodies

APS Ammonium persulphate

ATM Ataxia telangastia mutated protein

ATR ATM-and Rad3-related proteins

ATRX alpha thalassemia/mental retardation syndrome X-linked

BCA Bicinchoninic acid

BER Base excision repair

BLM Bloom syndrome

BP Base pair

BRCA1 Breast Cancer susceptibility gene 1

BRCA2 Breast Cancer 2 susceptibility protein

BRCT BRCA1 C-terminal

BSA Bovine Serum Albumin

CCFL Corrected Calibrated Fluorescence

cDNA Complementary DNA

CC C-circle assay

CF Correction Factor

COD-FISH Chromosome Orientation and Direction FISH

CO-FISH Chromosome Orientation Fluorescence in situ Hybridization

DDR DNA damage response

DKC Dyskeratosis Congenita

DMEM Dulbecco modified eagle medium

DMSO Dimethylsulfoxide

DNA-PKcs DNA-protein kinase catalytic-subunit

dNTP Deoxynucleotide triphosphate

DSB Double strand breaks

DTT Dithiothreitol

DW Distilled water

ECL Enhanced chemiluminescence

EDTA Ethylene diamine-tetra acetic acid

ES Embryonic stem cells

FA Fanconi Anemia

FBS Fetal bovine serum

FCS Fetal calf serum

FISH Fluorescence in-situ hybridization

FITC Fluorescein isothiocynate

gDNA Genomic DNA

Gy Gray

HR Homologous recombination

HRP Horseradish peroxidise

IPA Isopropyl alcohol

IQ-FISH Interphase Q-Fish

IR Ionising Radiation

Kb Kilobase

KCL Potassium Chloride

kDa Kilo Dalton

LY-R Radioresistant mouse lymphoma cells

LY-S Radio-sensitive mouse lymphoma cells

MgCl2 Magnesium chloride

ml Mililiter

mESC Mouse embryonic stem cell

MMEJ Microhomology-mediated end joining

MRN MRE11/RAD50/NSB1

NER Nucleotide Excision Repair

NHEJ Non-homologous end joining

PAR Poly ADP-ribose

PBS Phosphate buffer saline

PCR Polymerase chain reaction

PNA Peptide nucleic acid

POT1 Protection of telomeres 1

PVDF Polyvinylidene fluoride

Q-FISH Quantitative in-situ hybridization

RNA Ribonucleic acid

RNAi Ribonucleic acid interference

RPA Replication protein A

RPM Rotations per minute

RPMI Roswell Park Memorial Institute

RS-SCID Radio sensitive severe combined immunodeficiency RT Room Temperature

RT-PCR Reverse transcriptase-polymerase chain reaction SCID Severe-combined immunodeficiency syndrome

SDS Sodium dodecyl sulphate

siRNA Short interfering ribonucleic acid

ss Single stranded

SSB Single strand breaks

SSC Sodium chloride sodium citric acid

ssDNA Single stranded DNA

T Thymine

TBE Tris-borate-EDTA

TBST Tris-buffered saline tween-20 TEMED Tetramethylethylenediamine

TERT Telomerase Reverse Transcriptase TFUs Telomere fluorescence units

TIF Telomere dysfunction induced foci TIN2 TRF1-interacting factor

T-loop Telomeric-loop

TRAP Telomere repeat amplification protocol

TRF1 Telomeric repeat binding factor 1

TRF2 Telomeric repeat binding factor 2

T-SCEs telomere Sister Chromatid Exchanges

UV Ultra violet

H2AX Histone H2AX phosphorylated on serine-139

µl Microlitre

CHAPTER 1

1 General Introduction

1.1 Introduction

Telomeres are unique DNA-protein structures at the end of all eukaryotic chromosomes that play a critical role in chromosomal end protection and recombination. The loss of telomeres causes end-to-end chromosome fusions, cell cycle arrest and/or apoptosis/senescence (Blasco et al., 1997, Gilley et al., 1995, Hackett and Greider, 2003, Campisi et al., 2001, Maser and DePinho, 2002). In humans telomere dysfunction leads to some genetic and common diseases including cancer (Harley et al., 1990, Blackburn et al., 2006, Donate and Blasco, 2011). The molecular analysis of telomeres began in the 1970s by the detection of the DNA sequence of telomeres in a single cell protozoan *Tetrohymena thermophila* (Blackburn and Gall, 1978). Blackburn eventually discovered that the DNA sequence at chromosome ends of the *T. thermophile* contained 50 tandem repeats of the (Makarov et al., 1993) hexanucleotide unit CCCCAA/GGGGTT and that these tandem repeats ranged from 20 to about 70 suggesting a heterogeneity of the telomeric repeat

sequences (Blackburn et al., 2006). In the subsequent decades (from 1970s to 1990s), it emerged that DNA ends of other eukaryotic cells such as *Physarum* and *Dictyostelium* contained similar tandem repeats including a 3' overhang of the GGGGTTTT repeat strand (Oka et al., 1980, Klobutcher et al., 1981). It was later identified that vertebrate telomeric DNA also contained a highly conserved tandem repeat of $(TTAGGG)_n$ on all chromosome ends (Moyzis et al., 1988, Meyne et al., 1989). Blackburn and Greider also discovered that the telomeric DNA is elongated and maintained by an enzyme termed telomerase (Greider and Blackburn, 1985). They both received the 2009 Nobel Prize in Medicine and Physiology for their discovery. The main function of the telomerase enzyme is to maintain telomere length homeostasis in eukaryotic cells but it is shown that telomerase has non-canonical function specially in NF-κB and Wnt/β-catenin pathways with critical role in cancer development and progression (for review see (Li and Tergaonkar, 2014).

The problem with telomere replication was noted as far back as 1960's and prompted the Russian scientist Alexsei Olovnikov to propose the end-replication problem hypothesis at telomeres that explains telomere shortening (Olovnikov, 1971, Olovnikov, 1973). Independently of Olovnikov, Hayflick discovered in the 1960's that human cells grown *in vitro* have limited proliferative capacity which was later linked to telomere shortening leading to the concept of a biological clock (Hayflick and Moorhead, 1961, Hayflick, 1965, Harley et al., 1990). The discovery of telomere shortening and the function of telomerase enzyme in human cells made a link between telomere maintenance and human health from the carcinogenesis and aging perspective. It became clear that human cancer cells grown *in vitro* have infinite capacity to proliferate without losing telomere length as a result of activation of the telomerase enzyme (Harley et al., 1990, Kim et al., 1994). Telomere erosion that occurs *in vitro* was later linked to cellular senescence termed replicative senescence (Wright and Shay, 1992, Shay and Wright, 2005). Cellular senescence is usually interpreted as a natural anti-proliferative mechanism operational both *in vitro* and *in vivo* (Herrera et al., 1999, Meeker and De Marzo, 2004) in mammalian cells with a functional role as a barrier to

carcinogenesis (Wright and Shay, 1992). Other functional aspect of telomere biology is the link to cellular aging (Harley, 2002). Interestingly, it was found that the expression of telomerase is suppressed in human diploid somatic cells whereas telomerase activity is exhibited in gametes, stem cells and tumour cells. Over 85% of human tumours have active telomerase making it a target for future anti-cancer therapy (Harley and Villeponteau, 1995, Ducrest et al., 2002). However, the complicating factor is the Alternative Lengthening of Telomeres (ALT) pathway active in the remaining 10-15% of cancers functioning independent of telomerase-enzyme. The ALT pathway utilises the homologous recombination process of DNA replication. The exact mechanism of activation and the roles of various proteins involved in the ALT activation and process remain to be fully elucidated.

Here we will review the biology of mammalian telomeres, look at the key proteins involved, highlight the mechanism behind telomere length homeostasis, assess the current knowledge on the role of DNA damage response proteins and telomere maintenance and finally review the role of BRCA1 (a tumour suppressor) in the maintenance of telomere structural integrity in mammalian cells.

1.2 Structure and Function of Mammalian Telomeres

1.2.1 Structural biology of Telomeres

Telomeres are highly conserved repetitive non-coding DNA sequences associated with a set of specialized proteins located at the end of linear eukaryotic chromosomes. Telomeric DNA is predominantly double stranded with a protruding 3’ overhang that invades the double stranded portion of the telomere to form a bigger t-loop and smaller d-loop (Figure 1A). The first evidence for the lariat structure of the telomeric loop (t-loop) was provided by (Griffith et al.) (1999) (Figure 1B). It was proposed that these t-loop structures are formed by the 3’ overhang strand invasion into the duplex part of the telomere. The main function of the t-loop formation was thought to be sequestration of the chromosomal end. Recently, a super-resolution fluorescence imaging using stochastic optical reconstruction microscopy (STORM), verified the formation of t-loop within chromosomes (Doksani et al., 2013) (Figure

1C). The t-loop configuration of telomere is maintained by a group of telomeric proteins (discussed in section 1.2.4 below).

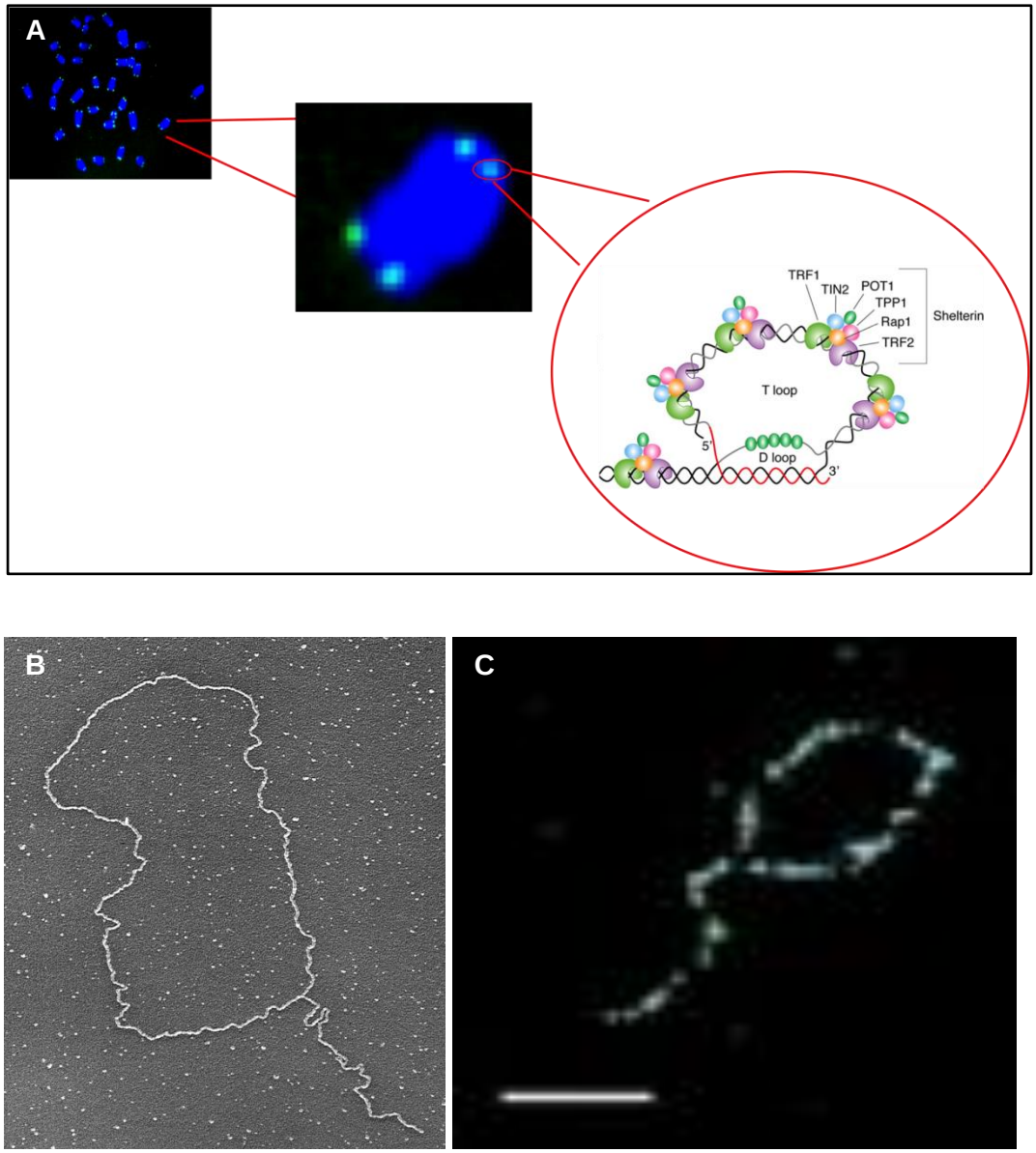

Figure 1-1. Proposed structure of the mammalian telomeres.

A) Telomeric DNA sequences are located at ends of chromosomes. Telomeres can be visualised using fluorescently tagged probe specific to the telomeric tandem repeats $(TTAGGG)_n$ (Green) whereas genomic DNA can be counterstained with fluorescently tagged DAPI (Blue). **B)** Electron microscopy has revealed the lariat structure of the telomeres forming a large t-loop (Griffith et al., 1999). **C)** These structures was recently shown using fluorescence tagged FISH and STORM imaging (Doksani et al., 2013).

The length of telomeric DNA varies in size in different species. For example, telomeres are typically found to have a length of about 10-15 kb in human primary cells and 20-50 kb in mouse and rats cells (Broccoli et al., 1996). In canine chromosomes the range is 12-23 kb

(Nasir et al., 2001). In all vertebrates telomere sequence consist of a 3` tandem repeat of $(TTAGGG)_n$. The double stranded 5' end and single stranded 3' end of the telomere sequence is attached with a highly conserved protein set known as shelterin (de Lange, 2005a). The shelterin complex protects the integrity of the telomeres and prevents illegitimate recombination, repair and sequence end-fusion thus helping create a stable linear chromosomal end. The shelterin complex consists of 6 proteins: telomere repeat factor 1 and 2 (TRF1/2), POT1, TIN2, Rap1 and TPP1 (see section 1.2.3 for detail). Telomeres face another problem due to their unique structure and position at the ends of linear chromosome known as end-replication problem first described by (Olovnikov, 1971).

1.2.2 End replication problem

Replication of DNA is the process of doubling DNA molecule that occurs in the S-phase of cell cycle. It has been recognized that the ends of linear chromosomes are replicated differently from the rest of the genome. In 1971 Olovnikov established a theory of telomere replication known as the 'End Replication Problem'. The theory revealed that in somatic cells in each round of DNA replication a portion of telomeric DNA is lost because of end under-replication which contributes to the gradual change in cellular phenotype, from normal and young to an old phenotype. The experimental work by Hayflick demonstrated the existence of cellular senescence (Hayflick and Moorhead, 1961, Hayflick, 1965) thus providing a logical background for the Olovnikov hypothesis. Furthermore, it was confirmed experimentally that germline and tumour cells are able to protect their telomeric DNA from shortening by expression of Telomerase, which is suppressed in normal somatic cells (Greider and Blackburn, 1985, Greider and Blackburn, 1989).

Based on this idea the traditional DNA replication machinery, which replicates the middle regions of chromosomes, is naturally unable to replicate their termini. Conventional DNA polymerases extend RNA primers, which are subsequently removed, thus creating gaps at lagging DNA strands (Figure 1.2).

However, DNA sequence loss at telomeres is not consistent with the RNA primer size which is in the region of 10 base pairs (Okazaki et al., 1967). Measurements indicate that the size of DNA sequence loss at chromosome ends is in the region of 150-200 bp suggesting the involvement of mechanisms such as exonucleolytic degradation (Makarov et al., 1997).

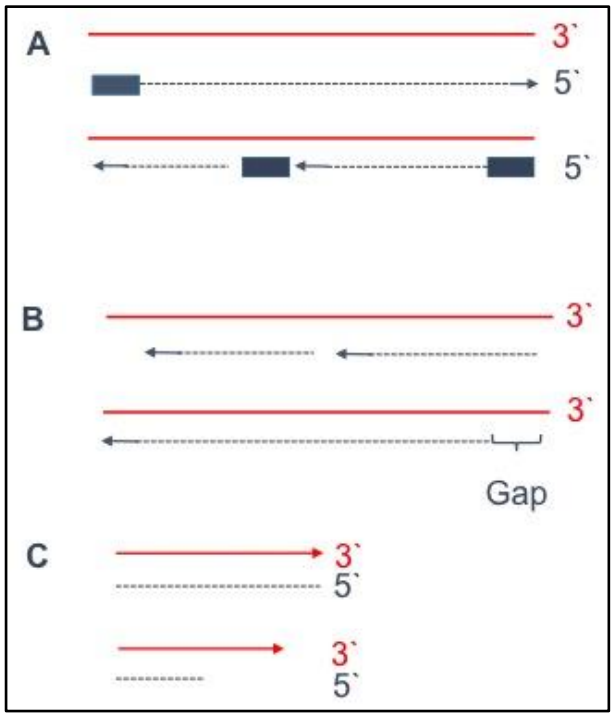

Figure 1-2. The end replication problem at telomeres.

The end replication problem is associated with the lagging strand during DNA replication process. **A)** The leading strand is replicated in continues fashion. **B)** The lagging strand on the other hand is encountered with gaps as a result of the primers (grey boxes) known as Okazaki fragment. At ends of chromosome this leaves a gap where the cell is not able to fully replicate. **C)** This model was first proposed by Makarov et al. 1997 following Olovnikov 'end replication problem; theory. In here Makarov proposes that there is a greater degradation at the 5' end of both DNA strands (lagging and leading), leaving a long 3' overhang at both ends (Makarov et al., 1997).

1.2.3 The G-quadroplex structure of telomeres

Interestingly, the unique sequence repeats of the telomeric structure containing three or four guanines on the single stranded overhangs gives the structure the ability to form G-quadruplexes (Rhodes et al., 2006). These structures in theory can provide additional end protection and have the ability to be self-recognised due to its unique sequence. These

unique G-quadruplexes are shown to form *in vivo* and have a biological function (Henderson, 1995). These G-quartets arise from the association of four guanines into a cyclic hydrogen bonding arrangements (Fig. 1.3 c). In human cells, the G-quadruplex structure will form without any kinetic barriers as a result of long G-overhangs (50 – 200 nucleotides) since it is strand concentration independent. It was found that one of the functions of the telomeric proteins, TPP1 and POT1 is to prevent the formation of G-quadruplexes (Xin et al., 2008). The structure of the G-quadruplex human DNA was first described by Parkinson et al. (2002). It was shown that the polymorphic structure of the G-quadroplex is affected by the concentration of the K^+ and Na^+ (Rhodes, 2006). However, the most likely structure is thought to be the one affected by the K^+ concentration as it exceeds the Na^+ concentration *in vivo* (Rhodes, 2006). G-quadruplexes in human cells are shown to inhibit the action of telomerase thereby preventing telomere elongation, by sequestering the 3' overhang and preventing telomerase access. This interesting observation provided a possible anti-tumour strategy whereby a specific G-quadruplex ligand can be used in human telomerase positive tumours to prevent telomere elongation and hence initiate cellular senescence (Riou et al., 2002) (Cao et al., 2003).

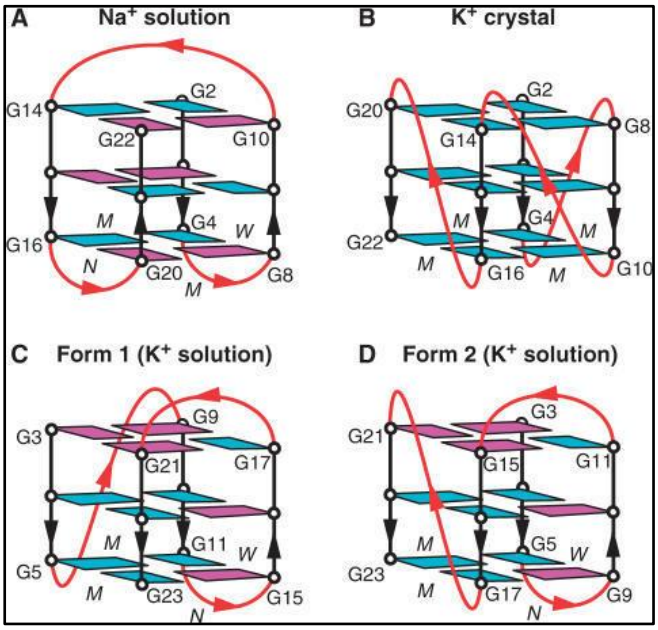

Figure 1-3. The G-quadroplex structure of telomeric DNA (Phan et al., 2007).
Structure of two intramolecular G-quadruplexes formed by natural human telomere sequences in K^+ solution.

1.3 Proteins associated with telomeric DNA

Mammalian telomeres are associated with three types of factors that collectively protect the structural integrity of the telomere. These factors are: nucleosomes, the shelterin complex and factors/proteins associated with the shelterin complex, known as telomere associated proteins.

1.3.1 Telomeric nucleosome

It has been shown that telomeres in rat cells are packaged in nucleosomal chromatin containing histone H1 (Makarov et al., 1993). The t-loop electron microscopy analysis also shows the nucleosomes throughout the tail and the circle very similar to the nucleosomal array of the genome. The telomeric chromatin also contains histone H3 that is di- and tri-methylated on lysine 9 and these methylation patterns of telomeric and sub-telomeric regions within the heterochromatin are shown to be regulated epigenetically and function to maintain normal telomere length (Blasco, 2007). An important action of demethylation of the genome has its effect on telomere stability in cancer. Most cancers have deregulated methylation pattern (Baylin, 2005) and these are thought to have an impact on telomere length stability and therefore contribute to disease phenotype (Blasco, 2007). Subsequently, telomere shortening leads to epigenetic defects at mammalian telomeres and sub-telomeres as shown by a decrease in DNA and histone methylation and increase in histone acetylation (Blasco, 2007).

1.3.2 Shelterin

Over that last 15 years research on telomere structure indicated strongly the existence of the shelterin complex contributing to the structural integrity of telomeres. The members of the complex, TRF1 and TRF2, directly bind the double-stranded telomeric DNA whereas protection of telomeres 1 (POT1) binds to the singe-stranded form of TTAGGG repeats (Palm and de Lange, 2008). These three proteins held together via protein interactions provide a strong protective role for the telomere structure (Celli et al., 2006). The shelterin complex is ubiquitously expressed throughout the cell cycle and does not accumulate

elsewhere in the nucleus suggesting that the function of shelterin is limited to telomeres (Celli et al., 2006). There are hundreds of copies of shelterin proteins within telomeres and their concentration increases with increased telomere length (Smogorzewska et al., 2000, Li and de Lange, 2003).

The shelterin complex plays a number of important functions: (i) the t-loop formation, (ii) the structure of the telomeric terminus, (iii) the control of the synthesis of telomeric DNA by telomerase, (iv) protection of chromosome ends from DNA damage surveillance and repair pathways (Celli et al., 2006). The latter protective function of shelterin will be analysed in subsequent sections, but first a detailed look at each of the subunits of the shelterin complex will be provided below.

1.3.2.1 TRF1

Zhong and colleagues identified the first shelterin component, TRF1, from HeLa cell extracts as a DNA-binding activity that associates specifically with duplex TTAGGG sequence (Zhong et al., 1992). TRF1 is also found to be expressed *in vivo* and binds TTAGGG repeats independently of their location within the chromosome (Smogorzewska et al., 2000). The core domain of the TRF1, TRF homology domain (TRFH) is evolutionary conserved. In human cells there are two variants of TRF1 due to splice variants, whereas in mouse cells there is only one functional form of the TRF1 (Broccoli et al., 1996). It was revealed, through immunofluorescence and chromatin immunoprecipitation (ChIP), that TRF1 is localised within telomeres at all stages of the cell cycle during both mitosis and meiosis (Crabbe et al., 2004). Two-hybrid protein-protein screening revealed other proteins that directly interact with TFR1 in human cells. These proteins are TRF1- and TRF2- interacting nuclear protein 2 (TIN2), tankyrase, ku70/80 heterodimer, the bloom's syndrome (BLM) helicase and Ataxia telangiectasia mutated (ATM) kinase that can phosphorylate TRF1 at ser-219 (Celli et al., 2006).

TRF1 is also shown to act as a negative regulator of telomere length through inhibition of telomerase. Knocking-down of TRF1 protein activity leads to telomere elongation (Iwano et

al., 2004). Interestingly, TRF1 is shown to be essential in the mouse during development as *Terf1*$^{-/-}$ mouse embryos die early during maturation at E5-E6 with apoptosis activated within the inner blastocysts (Karlseder et al., 2003), most likely because of the p53-dependent telomere deprotection.

1.3.2.2 TRF2

Another protein that directly binds the telomeric double stranded sequence is TRF2. Both TRF1 and TRF2 have a conserved Myb domain that mediates sequence-specific binding to telomeric DNA (Bilaud et al., 1997) (Hanaoka et al., 2005). Structurally, TRF1 and TRF2 are similar (a central TRFH domain and C-terminal DNA binding domain) but functionally they have distinct roles in protection of telomeric ends and t-loop formation. TRF2 interacts with TIN2 and Rap1, as well as POT1, and other DNA repair proteins such as Ku70, ATM, Apollo, MRN complex, WRN, PARP1 and PARP2 (Arat and Griffith, 2012, Celli et al., 2006). TRF2 is essential for the formation of the large t-loop and *TRF2*$^{-/-}$ mice die early in the developmental embryogenesis. Conditional knock-down of *TRF2* in mouse embryonic fibroblasts (MEFs) results in p53-mediated senescence, chromosomal end fusions and DNA-damage response activation, suggesting the critical functional role of TRF2 in chromosomal end protection (Celli et al., 2006).

1.3.2.3 TIN2

TIN2 is a small protein factor (40kDa) that binds to TRF2 and to TPP1, as well as to TRF1 (Kim et al., 1999). It binds to the TRF1 through the TRFH domain, whereas it binds to TRF2 and TPP1 through central domain of the protein and the amino terminal half respectively. Immunofluorescence and ChIP analysis has shown accumulation of TIN2 with TRF1, TRF2 and TPP1 in vivo at telomeres (Kim et al., 1999). TIN2 has a central role in the shelterin complex as it connects TRF1, TRF2 with POT1 (through TPP1) and can bind to both TRF1 and TRF2 in vivo simultaneously resulting in stabilisation of TRF2 binding to telomeres (Kim et al., 2004).

1.3.2.4 Rap1

Rap1 protein was identified through homology search and was found unexpectedly to interact with TRF2 in yeast (Li et al., 2000, Zhu et al., 2000). Rap1 is a 49kD, with a single Myb domain and has a nuclear localisation sequence and evolutionary is very diverse compared to the budding yeast Rap1. The Myb domain of human Rap1 does not have enough positive charge to bind to DNA and therefore it is more likely to mediate protein-protein interactions. Interestingly, when TRF2 is absent from cells Rap1 does not bind to telomeres suggesting a close interaction between TRF2 and Rap1. Functionally, Rap1 has a role in telomere length regulation and is shown to affect telomere length heterogeneity (Li et al., 2000) and (Li and de Lange, 2003). Similar to TRF1 and TRF2, mice cells lacking Rap1 are not viable suggesting an important role of Rap1 to the shelterin activity and protection of telomeres (Celli et al., 2006).

1.3.2.5 TPP1

Another recently identified shelterin protein is TPP1 that was identified through mass spectrometry of TRF1/TIN2- associated proteins and a two-hybrid screen with TIN2 (Celli et al., 2006). TPP1 binds to POT1 through the carboxyl-terminal half. TPP1 has the role of recruiting POT1 to the telomeres and short hairpin knock-down of TPP1 is associated with inappropriate telomere elongation that is consistent with reduced POT1 activity at telomeres.

1.3.2.6 POT1

Another shelterin protein, POT1, was identified through homology search with the DNA-binding domain of TEBPα (a ciliate telomere binding factor). POT1 binds to the single-stranded telomeric sequence through the oligonucleotide/oligosaccharide-binding (OB) folds and is highly specific for the 5'-(T)TAGGGTTAG-3'(Lei et al., 2004, Loayza and De Lange, 2003). POT1 is shown to have a favourite target site such as TAG-3' ends of telomeres but has the capacity to bind to any site along a single stranded TTAGGG repeat arrays (Lei et al., 2004),(Loayza and De Lange, 2003). The binding of TPP1 to POT1 helps it to localise and binds to telomeres whereas the DNA-binding site of POT1 does not have any effect in this sense (Loayza and De Lange, 2003). The main function of POT1 is in telomere

homeostasis and end-protection. Interestingly the interaction between POT1 and TPP1 and/or TIN2 creates together with TRF1/2 and RAP1 a bridge that makes the t-loop inaccessible to telomerase and it forms a protective loop at the telomeric end. Two reports provided contradictory findings – in one report a knock-down of POT1 expression resulted in telomere elongation therefore suggesting telomerase inhibitory function of POT1 (Ye et al., 2004) whereas overexpression of POT1 also resulted in telomere elongation (Colgin et al., 2003). The question is: how is it possible that both overexpression and reduction of POT1 activity results in telomere elongation? Two reports provide contradictory findings: in one report POT1 knock-down resulted in telomere elongation therefore suggesting telomerase inhibitory function of POT1. In addition to the role of POT1 in inhibition access of telomerase to the telomere other observation explain that overexpression of human POT1 also cause telomere elongation (Colgin et al., 2003). Basically to explain why increasing and reducing of POT1 result in telomere elongation may bring up the key role of TPP1 to interact with both TIN2 and POT1 (O'Connor et al., 2006). POT1 links to TRF1, TRF2, and RAP1 through TIN2-TPP1, so a bridge, can be formed between the single and double stranded of the telomere. This bridge can force the telomere into a closed conformation in which the 3`end is inaccessible to telomerase (Palm and de Lange, 2008). However when this bridge (known as shelterin) is less stable the telomere is more likely to be open and linear conformation accessible to telomerase. Overexpression of POT1 can disrupt the closed conformation when different POT1 molecules bind to TPP1/TIN2 and the G-strand overhang, thereby breaking the protein bridge. Such a mechanism implies that a closed conformation of the telomere rather than simple POT1 binding to single-stranded telomeric DNA is required to inhibit telomerase in *vivo* (Baumann and Price, 2010). Figure 1.4 shows interacting partners of shelterin proteins.

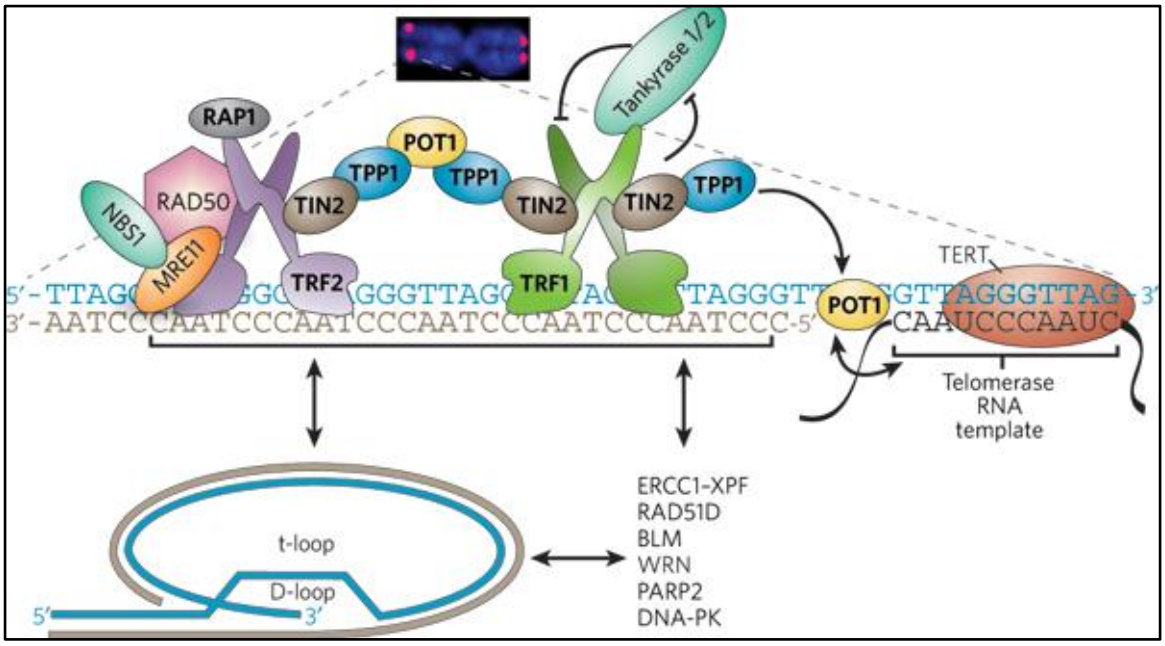

Figure 1-4. The schematic diagram of mammalian telomeric complex containing shelterin units (Verdun and Karlseder, 2007).

1.4 The role of shelterin in chromosomal end protection

The six proteins discussed above form a unique complex that is only found accumulated at telomeres and not anywhere else in the cell. This is due to a high affinity of the shelterin proteins such as TRF1/2 to the TTAGGG telomeric sequence through a Myb-specific DNA binding domain. Similarly, POT1 has a strong affinity to the 3' end of telomeres with 5'-(T)TAGGG TTA-3' and at internal positions. The three proteins are then connected through a protein-protein interaction giving a strong five DNA-binding domain (two TRF1/2 and one POT1) giving shelterin complex a specific ability to recognise only telomeric sites and no other regions within the genome (de Lange, 2005). The unique structure of the shelterin complex gives it a specific functional role at protecting telomeres. These functional roles of shelterin are: (i) determination of the structure of telomere ends, (ii) generation of t-loops, and (iii) control of synthesis of telomeric DNA by telomerase (Table 1-1) (de Lange, 2005a).

The formation of t-loop lariat structure in mammalian telomeres is thought to be a critical aspect of shelterin complex. It is thought that shelterin complex helps the formation of t-loop. Conditional knock-down of shelterin components have shown that TRF2 is required for the

formation and maintenance of t-loops whereas TRF1, Rap1 or POT1 do not significantly affect t-loop formation (Doksani et al., 2013).

Table 1-1. Summary of proteins involved directly with the telomere (the shelterin unit) (de Lange 2006).

Shelterin proteins	Function	References
TRF1	Telomere length regulation	Zhong et al., 1992
TRF2	Protect chromosome end	Bilaud et al., 1997
POT1	Modulate telomere length	McKay and Cooke 1992
TPP1	Regulating and protecting of telomere length	Houghtaling et al., 2004
TIN2	Providing the bridge between single strand and double stranded telomeric	Kim et al., 1999
hRAP1	With TRF2 inhibiting homologous recombination	Li et al., 2000; Zhu et al., 2000
Tankyrase1	Positive regulator of telomere length	Smith et al., 1998
Tankyrase2	Positive regulator of telomere length	Smith et al., 1998
EST1A	Positive regulator of telomerase	Reichenbach et al., 2003

Inhibition of TRF1 or POT1 diminishes the overall repeats of TTAGGG, suggesting a direct effect of TRF1 or POT1 on the 3’ end of telomeres (Hockemeyer et al., 2005). Interestingly, when TRF1 is inhibited ERCC1/XPF (an endonuclease) cleaves the 3’ end of telomeric DNA and the telomere can lose all of the ssDNA. Similarly, POT1 binding to the 3’ end can protect the ssDNA from CRCC1/XPF degradation (de Lange, 2005a).

The effect of shelterin complex on telomere length is through the *cis*-acting inhibition, influenced by the total amount of shelterin proteins. The longer the telomere lengths the more shelterin is abound to the telomere and this inhibits the access of telomerase whereas shorter telomeres with fewer shelterin units have a relaxed structure therefore allowing

access of telomerase to the telomeric site. This control of the telomerase by shelterin is mediated by POT1 on the ssDNA. In cells where POT1 activity is diminished through knock-downs irregular telomere length maintenance is apparent as evidenced by formation of very long telomere tract by telomerase despite heavier loads of shelterin proteins (Hockemeyer et al., 2006).

The shelterin complex also interacts with some proteins involved in DNA damage response as shown in Table 1-2. The focus of this dissertation is the role that BRCA1, a DNA damage response protein, plays in the functional interplay between telomere maintenance and DNA damage response.

1.5 *BRCA1* gene and protein structure

The breast and ovarian cancer susceptibility gene 1 (*BRCA1*) was first identified and cloned in 1994 by Miki and colleagues. One year later the second breast and ovarian cancer susceptibility gene 2 (*BRCA2*) was identified and cloned (Wooster et al., 1995). *BRCA1* gene was shown to contain 24 exons with 22 of it having coding sequences and 2 non-coding sequences (Miki et al., 1994). Exon 11 was the biggest exon encoding 60% of the BRCA1 protein. The *BRCA1* gene produces 1863 amino acid long protein with a molecular weight of 220 kDa. The protein structure of BRCA1 contains various features that are found in other DNA repair and cell cycle checkpoints proteins. For example, the N-terminal RING domain and a C-terminal BRCA1 domain (BRCT) has a DNA binding capacity similar to the C-terminal acidic domain (Monteiro et al., 1996, Bork et al., 1997) (See Figure 1.5). Each structural domain of the BRCA1 is important for its various functions within the cell. For example, the RING domain activates the E3 ubiquitin ligase activity through its interaction with E2 enzyme (Jiang and Greenberg, 2015). The HR and checkpoint function of the BRCA1 is performed by the central domain, which is coded entirely by the exon 11, and this poorly conserved central domain is shown to also have tumour suppressive activity (Xu et al., 1999b). Nearer the C-terminal there resides a coiled-coiled region that interacts with PALB2 that forms a bridge between BRCA1 and BRCA2 creating a tumour suppressive

supercomplex (Jiang and Greenberg, 2015). Interestingly, mutations in *PALB2* is linked to high penetrance breast cancer (similar to *BRCA1* and *BRCA2* mutation) suggesting an important biochemical activity of the PALB2 and the coiled-coiled region in the C-terminal domain of the BRCA1 (Antoniou et al., 2014). Finally, near the C-terminal resides BRCA1 C-terminal repeats (BRCT), which bind to phosphopeptides. Many proteins interact with the BRCT domain that provide various functions of the BRCA1 protein. For example, interaction of BRCA1 with BARD1 stabilises the two proteins and enhances the DNA damage sensing capability of the BRCA1. Crystal structure has shown direct interaction of the BRCA1/BARD1 with the nucleosome (McGinty et al., 2014). BRCA1/BARD1 also interacts with poly (ADP) ribose (Li and Yu, 2013) as well as with HP1 protein that helps to anchor the BRCA1/BARD1 complex to the DNA damage sites (Wu et al., 2015).

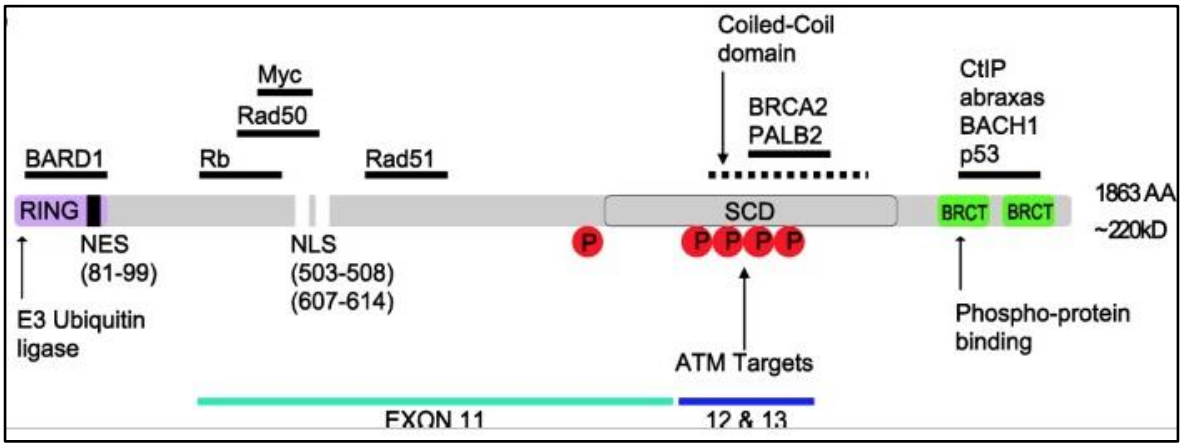

Figure 1-5. The protein structure of the BRCA1 tumour suppressor (Adapted from (Clark et al., 2012).

When DNA damage occurs, BRCA1 is phosphorylated at various sites by DNA damage sensing proteins such as ATM, CHK1 and ATR, which then makes BRCA1 to form complexes that is then recruited to the DNA damage sites. BRCT domain can form mutually exclusive interaction with phosphorylated CtIP, BACH11and abraxas. BRCA1 can also recruit BRCA2 to sites of DNA damage via PALB2. The interaction between BARC1 with the N-terminal RING domain produces the tumour suppressive function of the BRCA1 since mutations within this domain is shown to lead to cancer.

BRCA1 is also found to regulate the activity of many transcription factors although BRCA1 itself does not have sequence-specific DNA-binding transcription factor. Examples of BRCA1 interaction with various transcription factors include p53, estrogen receptor, progesterone receptor, androgen receptor, STAT1, c-Myc, NF-κB, octamer-binding transcription factor 1

(OCT1), and others (Rosen et al., 2006, Rosen, 2013). The BRCA1 co-transcriptional activity can be stimulatory (p53, androgen receptor) or inhibitory (estrogen, progesterone or c-MYC) (Rosen et al., 2006) that offers it a role as transcription co-regulator. BRCA1 is now known to have various other functions within the cell such as in DNA damage response, DNA repair and cell cycle regulation and these are reviewed in detail in the subsequent sections of this chapter.

1.6 The role of telomere and shelterin in DNA damage response

One of the main functions of the shelterin complex is to hide the telomeric ends from recognition by the DNA damage response proteins. Since mammalian chromosomes are linear they face a problem of end protection. Unprotected telomeric ends resemble that of DNA double strand breaks, lesions that initiate the DNA damage response. It is therefore proposed that shelterin complex hides the telomeric ends from been recognised as sites of double strand breaks through the interaction of the shelterin proteins. This was shown initially through a series of delicate experiments whereby the function of TRF2 was conditionally knocked-down in mouse cells or through expression of dominant-negative allele of TRF2 ($TRF2^{\Delta B \Delta M}$). Through this dominant-negative allele of TRF2 that lacks functional carboxylic terminal forms an inactive heterodimer causing a total loss of TRF2, Rap1 and portion of POT1 from telomeres (van Steensel et al., 1998). De-protection of telomeric ends from TRF2, Rap1 and part of POT1 but not TRF1 or TIN2 (they remain attached to the telomere) are shown to activate DNA damage response factors such as 53BP1, Nbs1, ATM, Rad17, Rif1 and MDC1 in mouse cells (d'Adda di Fagagna et al., 2003, Takai et al., 2003). The formation of telomere dysfunction-induced foci or TIFs within telomeres is indicative of a DNA-damage domain as a result of telomere structural de-protection. When TRF2 was deleted in the mouse cells majority of the TIFs were associated with most telomeres (but not all telomeres had TIFs) (Celli and de Lange, 2005). In the presence of functional ERCC1/XPF or non-homologous-end joining (NHEJ) machinery it has been shown that approximately 50% of the single stranded TTAGGG is lost through end-to-end fusion (van Steensel et al., 1998). Interestingly the two mechanisms, TIF-associated DNA-damage

response and DNA double strand breaks, are not linked meaning that in cells where the action of NHEJ is diminished formation of TIFs still persist at telomeres (Celli and de Lange, 2005). On the other hand, ATM kinase is shown to be the major component of the activation of DNA-damage response, as TIF are not formed in AT cells (where ATM in mutated) (Takai et al., 2003). In the absence of ATM, another DNA damage response related protein ATR (ataxia telangiectasia/Rad3 –related) protein is observed at dysfunctional telomeres in AT cells (Herbig et al., 2004). However, when both proteins are inhibited (ATM and ATR) using caffeine this results in disappearance of TIFs (Takai et al., 2003) suggesting that signalling of DNA damage performed by the two proteins is made through phosphatidyl inositol 3' kinase-related kinases (PIKK). Other factors that seems to be involved during telomere deprotection, e.g. DNA damage sensor such as the Mre11 complex (Mre11/Rad50/Nbs1), most likely contribute to the upstream sensing step in the DNA damage response and inhibition of ATM does not affect its accumulation at dysfunctional telomeres. The Mre11 complex is part of the homologous recombination DNA damage repair and it will be covered in more detail in the subsequent chapters.

When telomeres are deprotected through dysfunction of the shelterin units, the activation of ATM leads to downstream events that result in cell cycle arrest and delay in cycle progression, apoptosis or senescence (de Lange, 2006). Depending on the cell type apoptosis or senescence is activated and mediated by p53. For example, it has been shown that some epithelial cells or lymphocytes activate apoptosis in response to telomere dysfunction whereas fibroblasts go through senescence (de Lange, 2006). Stabilization of p53 results in increased levels of p21 that inhibits Cdk2 and arrests the cell entry into the S-phase. Telomere damage also results in p16 mediated cell cycle arrest through inhibition of Cdk4/6. This is shown to occur when p21 is displaced (possibly through p53 impairment) where p16 takes over the mechanism of entry into S-phase. In this scenario, elevated p16 act as the back-up mechanism of cell cycle regulation, although it has been shown that in mouse cells p16 does not induce G1/S arrest following telomere dysfunction

(Smogorzewska et al., 2002). TIN2 and POT1 also activate TIFs when abrogated through either overexpression of TIN2 mutants that result in loss of TRF2 from telomeres (Kim et al., 2004) or shRNA-mediated knock-down of POT1 with similar effect (Hockemeyer et al., 2005). The one difference observed between TIN2-mediated TIFs formation and POT1 is that, in POT1 knocked-down cells undergo a G1 arrest and TIFs largely disappear by the time cells enter the S-phase (de Lange, 2006).

1.6.1 Functional role of BRCA1 within DNA-damage response

When DNA damage occurs (Figure 1.6) ATM is recruited to the sites of DNA damage and it phosphorylates very quickly the variant of histone H2AX on serine-139 producing a phosphorylated H2AX, known as γH2AX (Burma et al., 2001) (Wang et al., 2005). Subsequently, the γH2AX is sensed by the mediator of DNA damage checkpoint 1 (MDC1) and this rapid recruitment of the MDC1 serves as a scaffold to other DNA damage repair proteins (Stewart et al., 2003, Lou et al., 2006, Lee et al., 2005). MDC1 then recruits the MRN complex through the binding of the phosphorylated casein kinase 2 (CK2) of the NBS1 (Spycher et al., 2008). The localisation of BRCA1 to the sites of DNA damage, especially within the ionising radiation-induced DNA damage foci, occurs very quickly (Rosen, 2013). The focus of this dissertation is the functional role of BRCA1 within the DNA damage response (DDR) and its link with telomere maintenance. The earliest evidence implicating *Brca1* deficiency in DDR emerged through the study of fibroblast cells and tumours that showed extensive genomic instability, including aneuploidy, centrosomal amplification and chromosomal aberrations (Tirkkonen et al., 1997) (Xu et al., 1999b) (Weaver et al., 2002). It was also revealed that BRCA1 is co-localised with Rad51 during S-phase. When DNA damage occurs BRCA1 is phosphorylated and translocated to proliferation cell nuclear antigen (PCNA)-positive DNA structures containing Rad51 and BARD1 (Scully et al., 1997). Similarly, it has been shown that BRCA1-defective cells are sensitive to ionising radiation (Shen et al., 1998, Scully et al., 1999, Ruffner et al., 2001), providing evidences for the role of BRCA1 as a (i) caretaker gene involved in DNA repair with monitoring and maintenance

role within genome stability, and (ii) as a DNA damage response protein involved in response to the DSBs (Rosen, 2013).

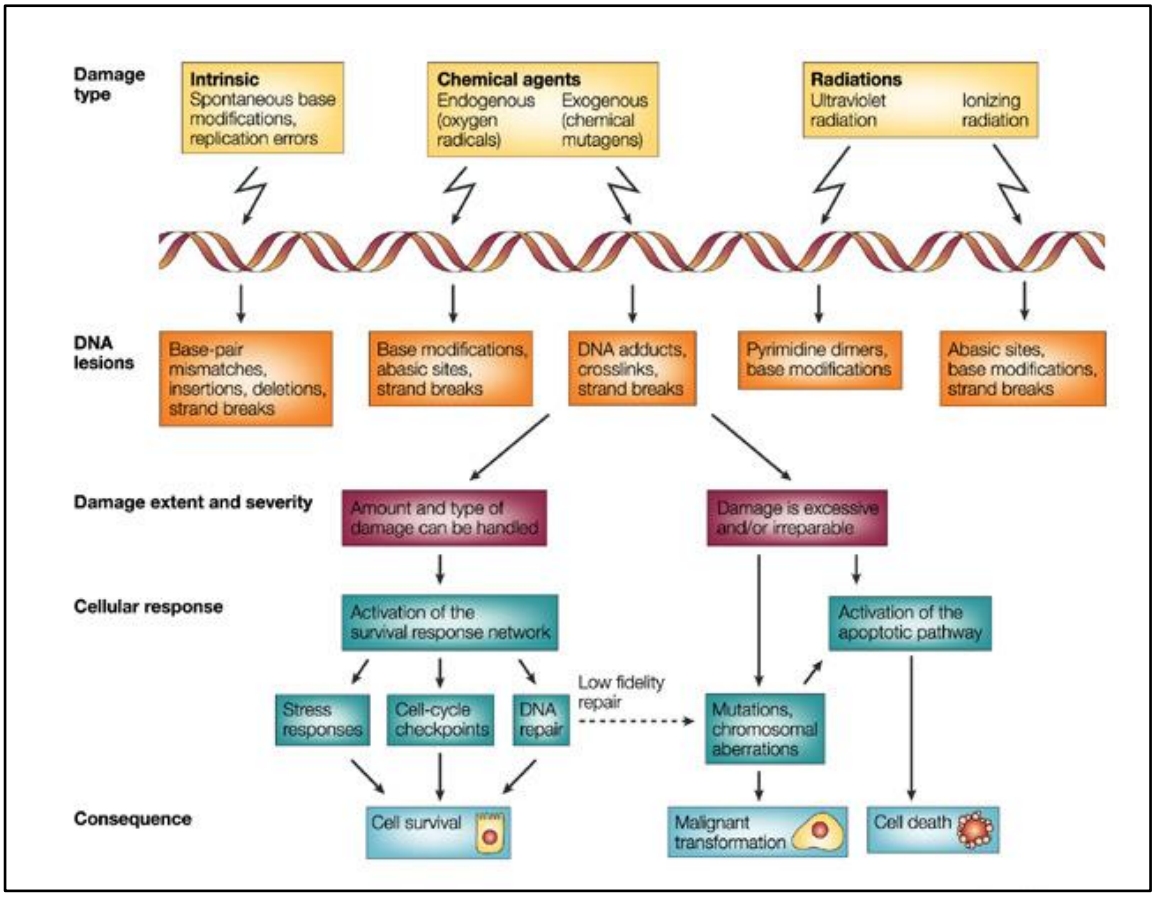

Figure 1-6. DNA is constantly under attack through exogenous agents (Shiloh, 2003).

1.6.2 How does shelterin repress telomere-mediated DNA damage response?

Interestingly, a question that comes to mind is that why telomeres containing functional shelterin complex are not sensed by ATM kinase pathway. We did argue that this could be because shelterin complex creates the t-loop structure that hides telomeric ends hence preventing DNA ends to be recognised as DNA DSBs. Another suggested possibility is that the shelterin factors at telomeres create a nucleosomal organisation similar to that of intact chromosome internal DNA (de Lange, 2006). The latter hypothesis was tested when chromatin organisation of telomeric ends was disrupted leading to ATM activation (Huyen et al., 2004). Interestingly, it has been shown recently that TRF2 binds to ATM kinase (*in vitro* and *in vivo*) and suppresses the activity of ATM (Karlseder et al., 2004). TRF2 was overexpressed leading to diminished activity of ATM authophosphorylation suggesting that

telomere-bound TRF2 could suppress ATM activation on chromosomal terminus (de Lange, 2006). Similarly, it was shown that the t-loop structure can block the end-loading of Ku protein by the NHEJ activation (Celli et al., 2006). POT1 also can inhibit ATR activation suggesting that both TRF2 and POT1 are needed for the efficient suppression of DNA-damage response activation at telomeres and that TRF2 and POT1 function independently (Denchi and de Lange, 2007).

Table 1-2. Interaction of DNA repair and damage response proteins with telomeres ((Slijepcevic, 2006) de Lange 2006)

Protein	Main function	Function at telomeres	Shelterin interactions
Mre11/Rad50/Nbs1	Recombinational repair, DNA damage sensor	T-loop formation/resolution? Required for t-loop HR	Associated with shelterin
ERCC1/XPF	NER, crosslink repair3`flap endonuclease	Deficiency leads to formation of TDMs; implicated in overhang processing after TRF2 loss	Associated with shelterin
WRN helicase	Branch migration G4 DNA resolution	Deficiency results in loss of lagging-strand telomeres	TRF2
BLM helicases	Branch migration crossover repression	T-loop formation/resolution?	TRF2
DNA-PK	NHEJ	Deficiency leads to mild fusion phenotype	Associated with shelterin
PARP-2	BER	Not known	TRF2
Tankyrases	Role in mitosis (tankyrase 1)	Positive regulator of telomere length through inhibition of TRF1	TRF1
Rad51D	Unknown (HR)	Deficiency leads to mild fusion phenotype	unknown
ATM	Damage signaling	DNA damage activation at telomeres	TRF2
Ku	NHEJ	Deficiency leads to telomere shortening	TRF1,TRF2
RAD54	HR	Activity plays an essential role in telomere length maintenance	TRF2
FANCA	Damage sensing	Deficiency leads to breakage at telomeres and end-to-end fusion.	Not known
BRCA1	HR shorter	Deficiency leads to accelerated telomere shortening and mild telomere dysfunction	TRF1, TRF2
Rad9	Damage sensing	Inactivation increases in chromosome end-to-end associations	TRF2
PARP-1	BER	Function as capping of normal telomeres and its deficiency leads to chromosome end-to-end fusions	TRF2

Other event that leads to DNA-damage response activation is the programmed shortening of telomeres during each round of cell cycle. Even when a single telomere becomes dysfunctional, as a result of shortening, this leads to activation of DNA-damage response and p53-mediated cell cycle arrest (Hemann et al., 2001). Short telomeres contain fewer shelterin complex units (Loayza and De Lange, 2003) causing the diminished loading of TRF2 and POT1 on short telomeres and activation of ATM and ATR kinases leading to cell cycle arrest and inappropriate DNA repair at telomeres (formation of end-to-end fusion) (Denchi and de Lange, 2007). Table 1-2 lists all the known proteins that are associated with shelterin at telomeres with a brief description of their function. Some of these proteins are found to be critical component of DNA DSB repair machinery that is discussed below.

1.7 DNA repair and response at dysfunctional telomeres – How does BRCA1 play a part?

When telomeres become dysfunctional, either as a result of defective shelterin complex or telomere length attrition, this leads to activation of DNA DSB repair pathways. Two main DSB repair pathways in mammalian cells are NHEJ and HR (Figure 1.7). NHEJ is responsible for the formation of end fusions leading to dicentric chromosomes, and genomic instability, whereas HR causes deletion of large segments of telomeric DNA and mediate exchange of sequences between sister telomeres (leading to sister chromatic exchange – this is reviewed in detail in subsequent sections).

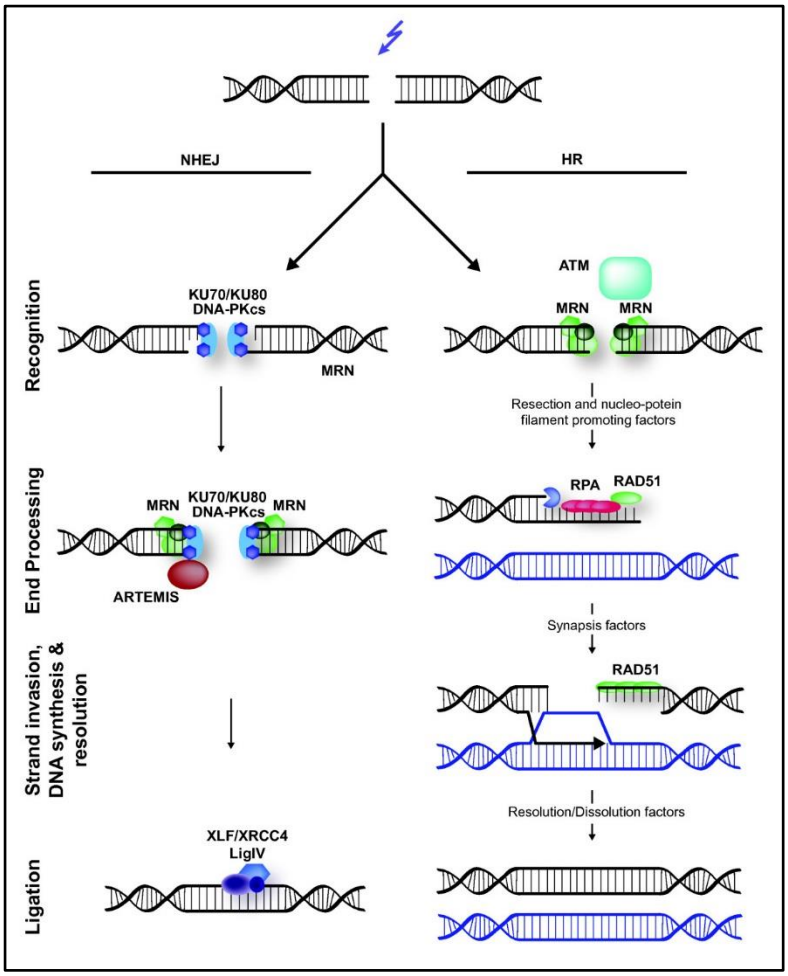

Figure 1-7. DNA double-strand break repair in mammalian cells (Lans et al., 2012). DNA DSBs are predominantly repaired by either non-homologous end-joining (NHEJ) or homologous recombination (HR).

1.8 The role of BRCA1 in non-homologous end joining (NHEJ)

The human genome receives constant insult from endogenous and exogenous agents that cause damage in DNA including DSBs. Induction of DSBs can be mediated endogenously by reactive oxygen species (ROS) generated by cellular metabolism and replication errors and by exogenous agents such as ionising radiation (IR) and chemotherapeutic agents. Programmed DSBs occur during the T- and B-cell development as part of V (D) J recombination. Figure 1.6 in the above section shows a summary of endogenous and exogenous agents that cause DNA damage. Unrepaired DSBs can activate cellular senescence or apoptosis (mediated by p53), or lead to chromosomal translocations and deletions with end result of loss of heterozygosity. Unrepaired carry abnormalities accumulate and can contribute to carcinogenesis. The main mechanism of DSB repair in

human cell is the NHEJ that takes place throughput the cell cycle. HR also has a role in repair of DSBs in the late S-G2 phase with the third mechanism of DBS repair known as microhomology-mediated end-joining (MMEJ) details of which are not well characterised. The restriction of HR to the late S-G2 phase is because it requires a template that only becomes available during the S-G2 phase as a sister chromatid, whereas NHEJ does not require homologous template and can, in theory, take place throughout the cell cycle.

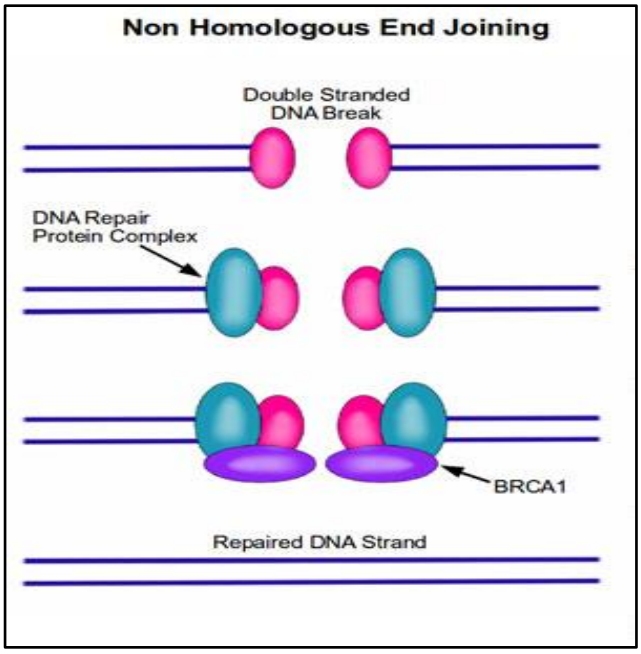

Figure 1-8. The mechanism of NHEJ (Samarasinghe, 2013). BRCA1 plays an important role in NHEJ mechanisms. A double stranded and break is detected by and repair proteins which bring together two ends and join them.

The NHEJ process DNA DSB through a number of proteins and kinases and the process is divided into the following sequential steps: (i) DNA end recognition and assembly of DNA repair proteins, (ii) bridging of DNA ends and promotion of DNA end stability, (iii) DNA end processing by NHEJ factors, (iv) ligation of DNA ends and dissolution of the assembly (Figure 1.8).

The first step in the NHEJ process is the recognition of DNA ends by the Ku heterodimer. Ku heterodimer is made up of Ku70 and Ku80 subunits that as a heterodimer have a high affinity to the DNA ends. This is shown to occur within seconds of a laser-generated DSB (Mari et al., 2006) and shows its abundant occurrence throughout the cell (500,000 units of

Ku molecules per cell) (Downs and Jackson, 2004) (Davis and Chen, 2013). The sequence independent biding of Ku heterodimer is because of its ability to bind to the sugar backbone of the DNA instead of the bases. It forms a ring-shape structure that slides onto the DNA end (Walker et al., 2001). The quick formation of Ku heterodimer binding with broken DNA ends forms a scaffold-like structure that allows other NHEJ factors to bind. The direct and indirect recruiting of other NHEJ factors by Ku heterodimer such as DNA-PKcs, x-ray cross complementing protein 4 (XRCC4), DNA-ligase IV, XRCC4-like factor (XLF) and Aprataxin-and-PNK-like factor (APLF).

Ku heterodimer directly recruits DNA-PKcs to the DSBs and this recruitment is only possible due to extreme C-terminal 12 residues of Ku80 mediating the recruitment (Gell and Jackson, 1999). Binding of Ku70/80 with DNA-PKcs requires the presence of DNA. Recruitment of DNA-PKcs to the ends of the DNA pushes the Ku heterodimer inwards thus activating the kinase activity of the DNA-PKcs. Although it is predicted that both N- and C-terminal units of the Ku70/80 make contacts with DNA-PKcs it is the N-terminal that is shown to be absolutely necessary for the formation of the DNA-PKcs-Ku-DNA complex and subsequent stabilisation of the DNA DSB ends (Davis and Chen, 2013).

The role of BRCA1 within the NHEJ is controversial, as conflicting evidence has been reported for a requirement of BRCA1 in NHEJ (Baldeyron et al., 2002) (Zhong et al., 2002b, Zhong et al., 2002a, Bau et al., 2004), while others find no defect in NHEJ in BRCA1-deficient cells (Moynahan et al., 1999) (Wang et al., 2001) (Merel et al., 2002). This may possibly be due to the fact that there are several NHEJ processes described; an error-prone and an error-free NHEJ mechanism (Durant and Nickoloff, 2005, Gudmundsdottir and Ashworth, 2006). BRCA1 is thought to be involved in promotion of the error-free pathway of the NHEJ process (Rosen, 2013). BRCA1 is thought to inhibit the nuclease action of the MRE11 (part of the MRN complex) when bound to the DNA therefore limiting the DNA end resection activity (Durant and Nickoloff, 2005). It is therefore, still unclear as to how exactly BRCA1 is involved in the NHEJ, since levels of BRCA1 during G1 phase of the cell cycle are

low and slowly increase during the S- and G2-phases of the cell cycle. Accumulation of BRCA1 during the S- and G-2 phases counteracts the ability of the 53BP1-RIF1 to stimulate NHEJ and therefore this pathway is inhibited in favour of HR, whereas in the G1-phase with low levels of BRCA1, 53BP1-RIF1 is able to accumulate at sites of DNA DSB to promote NHEJ (Escribano-Diaz et al., 2013, Feng et al., 2013) The tussling between NHEJ and HR is partly controlled by levels of BRCA1 and does explain the cell-cycle dependent activation of NHEJ during DNA DSB repair.

1.9 BRCA1 and HR

Another mechanism of DNA DSB repair in mammalian cells is HR, characterised by high-fidelity and template-dependant repair of complex DNA damages. HR also provides repair to DNA intra-strand cross-links and DNA gaps. In addition of providing genomic stability and integrity, HR plays a critical role in DNA replication and telomere maintenance. HR is the preferred DNA repair pathway during S and G2 phases of the cell cycle when identical sister chromatids are present and HR can access telomeres when the shelterin function is suppressed leading to irregular telomere length replication and activation of alternative lengthening of telomeres (ALT) in the absence of telomerase. The similarity between telomere maintenance and HR is quite striking. For example, the t-loop formation at telomeres as a result of 3’ overhang invasion of the duplex telomeric DNA is similar to the 3’ single-stranded overhang at the break site that is followed by invasion of duplex DNA (Verdun and Karlseder, 2007). Other similarities exist between DNA repair proteins, DNA damage responses and telomeres suggesting that the mechanism of telomere homeostasis and DNA repair/damage proteins are very similar (Verdun and Karlseder, 2007).

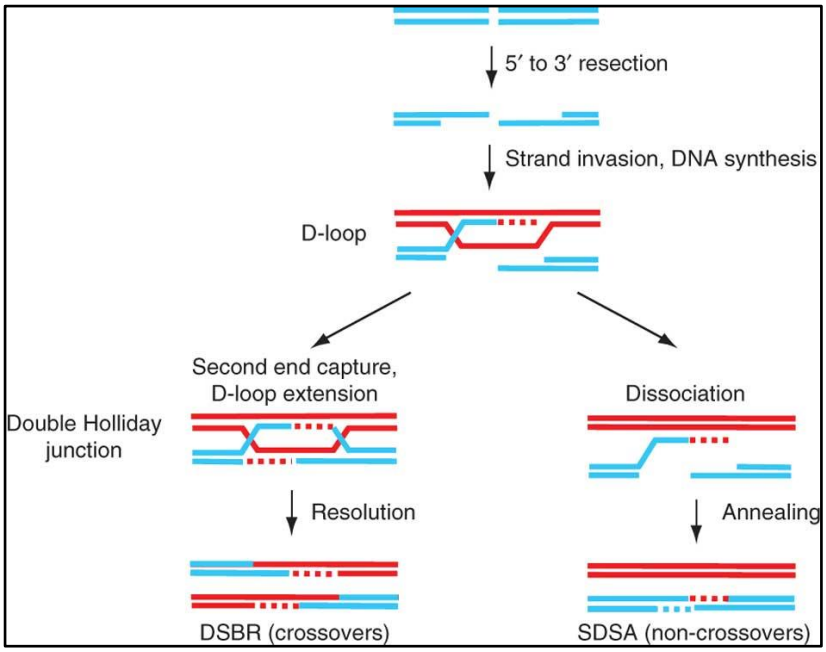

Figure 1-9. The HR repair pathway in the mammalian cells (Bugreev et al., 2011). Stalled replication forks can be rescued by HR via a mechanism that relies on DNA strand exchange activity of RAD51.

HR is activated following a replication fork stalling, at crossovers at meiosis and it is linked to telomere maintenance. In any case when HR is activated through DNA damage sensory proteins (ATM and ATR) the search for homology begins. This process is dependent on Rad51, a recombinase enzyme (Li and Heyer, 2008). Rad51 binds specifically to the ssDNA and promotes strand invasion of the template strand which creates the holiday junction (Figure 1.9). BRCA2 is needed for this process as it functions to deliver Rad51 to the DNA using shared motifs between the evolutionary conserved BRC motifs of BRCA2 and the RecA-homology domain of Rad51 (Pellegrini et al., 2002). Similarly, BRCA1 plays a central role in the HR process possibly in a regulatory capacity but the exact biochemical role of BRCA1 in HR is still unknown (O'Driscoll and Jeggo, 2006, Zhang, 2013). Moynahan provided the earliest evidence for the role of BRCA1 in the HR by clearly demonstrating that a Brca1- deficient reporter mouse embryonic stem (ES) cell line failed to accurately repair a chromosomal DSB created by the I-Sce 1 endonuclease (Moynahan et al., 1999). They also showed that BRCA2 was required for HR as well and provided evidence that Brca1-deficient cells could recover HR activity when a WT BRCA1 is transfected (Moynahan et al., 2001).

Figure 1.9 provides an overview of the main processes involved in the HR repair pathway in mammalian cells. In brief, following formation of DNA DSBs and resection of the ends to form the 3' overhang, the ssDNA is coated with replication protein A (RPA), that aids the binding of Rad52 (a protein homologous to Rad51), which in turn interacts with Rad51 to recruit it to the ssDNA with BRCA2 shown to have binding specificity to this structure. This forms the active nucleoprotein filament and enables the strands invasion of the ssDNA with the homologous dsDNA and formation of Holliday junction (West, 2003). After formation of the Holliday junction, the two strands function as a primer for DNA re-synthesis following assembly of the DNA polymerases. Following this the site of Holliday junction must be resolved after recombination and in eukaryotes this is done by the Rad51 paralog, XRCC3 and Rad51C that is associated with the resolvase activity (Wyman and Kanaar, 2006). It is thought that BRCA1 forms a complex with the CtBP-interacting protein (CtIP) facilitating the end resection by allowing the recruitment of replication protein A (RPA), a ssDNA-binding protein to the site of the DNA damage (Sartori et al., 2007, Buis et al., 2012, Escribano-Diaz et al., 2013). It must be noted that the role of BRCA1 is much broader than BRCA2 in the HR repair pathway since BRCA1 is also involved in cell-cycle checkpoint activation (Rosen, 2013).

The types of proteins involved in the HR depend on the origin of DSBs: whether they result from replication fork stalling or IR or cross linked-induced damage.

1.9.1 HR at telomeres

As mentioned previously, the t-loop at the telomere closely resembles a structure formed during HR with a 3' overhang generated that is used to make the invasion within the dsDNA portion of the telomeric region. In the absence of TRF2 domain, it is shown that the formation of the t-loop is altered to form a single or double HR that is subsequently resolved by the HR resolvase (such as XRCC3 or Rad51C) (Wang et al., 2004) de Lange, 2006). This results in the formation of telomeric circle (t-circle) and causes telomere shortening that could lead to DNA-damage signal or a reformation of another t-loop (See Figure 1.10 in

section 1.12.1). These (formation of t-circles and heterogonous telomeric lengths) are all hallmarks of ALT activity in telomere length maintenance and suggest that this type of HR is derepressed in ALT positive cells. This is further discussed in sections below. However, studies have shown that, HR-mediated telomere replication is dependent on the MRE11/RAD50/NBS1 (Mre11 complex), as mutations in the Nbs1 fail to show loss of telomeric DNA after TRF2 mutant overexpression (Helt et al., 2005b) de Lange, 2006). Another problem associated with the activation of HR at dysfunctional telomeres is the formation of post-replication exchanges that can be visualised using chromosome-orientation FISH (CO-FISH), also referred to as telomere-sister chromatic exchanges (T-SCE). The formation of double telomeric signals observed with CO-FISH experiment is likely to occur subsequent to DNA replication (Londono-Vallejo et al., 2004, Bailey et al., 2004b).

1.9.2 NHEJ and HR in cell cycle

The most dangerous type of DNA damage, in which both strands in the DNA double helix are severed is termed DSB. It is clear that DSBs, which are unrepaired or are repaired incorrectly, result in loss of genetic material and subsequently cause genomic rearrangements or cell death (Mao et al., 2008). Therefore, cell cycle checkpoints become activated as a first response to DNA damage (Sancar et al., 2004). Depending on the cell cycle phases at which the damage is occurred, cells can be blocked at either G1/S or G2/M (Sancar et al., 2004). However, if the damage is permanent or cell cycle checkpoint is dysfunctional, apoptosis may be triggered to remove the injured cells (Sancar et al., 2004). It is now well known that the G1 checkpoint is defective in most cancer cells, due to mutations/alterations of key regulators of the G1 checkpoint (p53, Cyclin D, etc.) (Kastan et al., 1991), whereas the G2 checkpoint is rarely impaired in cancer cells, as this checkpoint operates primarily via a p53-independent mechanism (Figure 1.10)(O'Connell and Cimprich, 2005). In fact, in cancer cells absence of G1 checkpoint abrogation of the G2 checkpoint often sensitises the cells to radiation (Chen et al., 2012). Mao et al., 2008 measured the efficiency of NHEJ and HR at all stages of cell cycle in hTERT-immortalized diploid human fibroblasts. The results indicated that NHEJ is active throughout the cell cycle, and its activity

increases from G1 to G2/M. HR is nearly absent in G1 and most active in the S phase, and decline in G2/M. Therefore this is in contrast with the notion that NHEJ is most active in G1, while HR is active in S, G2 and M. Overall, the efficiency of NHEJ was higher in all cell cycle stages than the HR. As a result, human somatic cells utilise error-prone NHEJ as the major pathway at all cell cycle stages, whereas HR is used primary in the S phase (Mao et al., 2008).

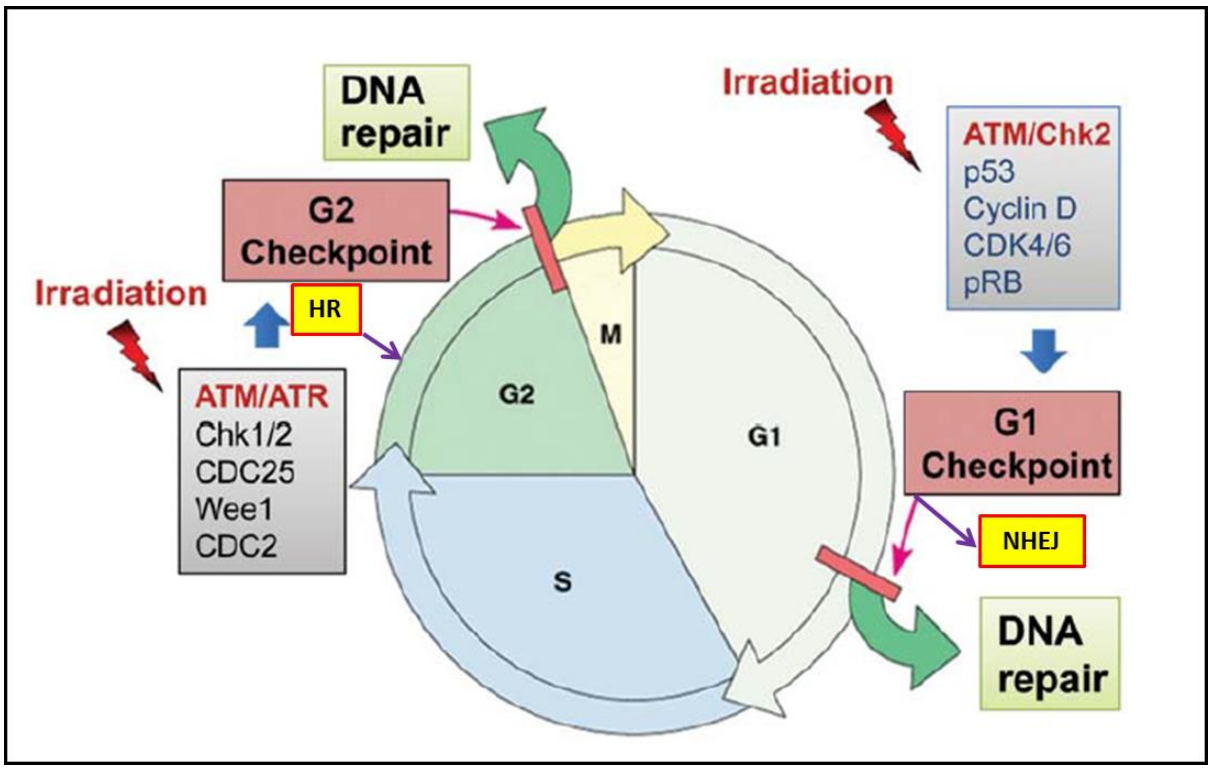

Figure 1-10– Irradiation induces G1 and G2 cell cycle checkpoint activation and DNA repair. Most cancer cells are defective in G1checkpoint, commonly due to the mutation/alterations of the key regulators of the G1 checkpoint (in blue), but contain a functional G2 checkpoint (Hein et al., 2014).

1.10 The role of BRCA1 in telomere maintenance

BRCA1 plays an important role in DDR by being involved in HR and NHEJ (see sections 1.8 and 1.9). BRCA1 is recruited to the sites of DNA damage by the MRN complex and it is

critical in recruitment and assembly of further recombination proteins to the site of DNA damage.

BRCA1 was identified as a tumour suppressor in the breast cancer and ovarian cancer in the early 1990s through positional cloning and was linked to chromosome 17q21 (Hall et al., 1990) (Miki et al., 1994). In the subsequent years evidence linked inactivating mutation in the *BRCA1* gene to increased risk of familial breast and ovarian cancer (for reviews see(Narod and Foulkes, 2004). Because of its important role in various aspects of DSB repair, S-phase, G2/M and spindle checkpoints, as well as in centrosomal regulation (Zhang and Powell, 2005), (Roy et al., 2011) any perturbation in its function can have severe consequences for the cell. For example, biallelic inactivation of the BRCA1 leads to genomic instability and cancer development. Indeed, mutations in the high penetrance genes, *BRCA1* and *BRCA2* are linked to an increased risk of familial breast cancer (King et al., 2003). Considering *BRCA1's* various essential roles in the cell, it is still unclear as to why *BRCA1* mutation preferentially leads to a subset of ovarian and breast cancer and not other types of cancers, even when important cancer-causing genes such as p53 and ATM are intact (Musolino et al., 2007) (Tlsty, 2011). Mutations in other DNA damage genes such as *p53* and *ATM* is found in many cancers (Musolino et al., 2007) (Tlsty, 2011). For instance, *p53* mutation is found in almost 50% of all cancers (Vogelstein et al., 2000). Similarly, it is not known why *BRCA1* mutation in one allele (leading to haploinsufficiency) early in the life causes rapid onset of the breast cancer (Whittemore et al., 1997), (Komenaka et al., 2004), whereas total inactivation of both alleles only occurs as a late event in the tumour development (Clarke and Sanderson, 2006, Martins et al., 2012). The exact role of the BRCA1 in genome integrity and DDR is not fully elucidated and probably involves other proteins that act as partners of BRCA1 in various pathways. In a recent study it was shown that cells from primary mammary epithelial cells (HMECs) with mutations in $BRCA1^{mut/+}$, show premature senescence as a result of genomic instability (Sedic et al., 2015). This unique type of cellular senescence caused by haploinsufficiency of a tumour suppressor such as *BRCA1* is termed

haploinsufficiency-induced senescence (HIS). The spontaneous bypass of this senescence which is triggered by pRb pathway activation rather than p53 induction is thought to be involved in the early onset of breast cancer development in individuals with *BRCA1* mutation (Sedic et al., 2015). Although these immortalised non-tumourigenic *BRCA1*$^{mut/+}$ HMECs showed rapid genomic instability, increased DNA damage, increased telomere length rate the exact mechanism by which the telomere maintenance is affected is not known (Sedic et al., 2015). Indeed it is not known whether BRCA1 haploinsuficiency leads to activation of telomerase or ALT mechanism as these experiments have not been performed. Recent findings suggest that BRCA1 does accumulate at telomeres in the ALT-positive cancer cells but not in telomerase-positive cancer cells most likely with the help of BLM and PML bodies (Acharya et al., 2014). One of the aims of this dissertation is to elucidate some of uncertainties surrounding the BRCA1 role in telomere homeostasis.

1.11 Telomere length regulation by telomerase

The linear genome in all mammalian cells requires a special mechanism to (i) fully replicate the DNA ends due to the DNA end replication problem as described earlier (1.2.2 above) and (ii) the nucleolytic processing of telomere ends after semiconservative DNA replication (Cristofari and Lingner, 2006). The end-replication problem is most commonly overcome through the ribonucleoprotein reverse transcriptase telomerase enzyme discovered by Greider and Blackburn in Tetrahymena thermophila (Greider and Blackburn, 1985). Subsequently, Greider and Blackburn received the 2009 Nobel Prize in Physiology or Medicine for their discovery of this unique RNP enzyme that has important physiological implication to human health as seen cancer and aging. Telomerase was subsequently demonstrated to have an RNA moiety, which co-purifies with enzymatic activity (Greider and Blackburn, 1989). Subsequent experiments revealed a highly conserved reverse transcriptase sequence motifs within the enzyme (Lingner et al., 1997).

1.11.1 The human telomerase structure

1.11.1.1 Human TR (hTR)

The telomerase enzyme has two major structural features: an RNA moiety of telomerase (TERC) and the telomerase reverse transcriptase (TERT). The TERC component of telomerase act as a template for telomere elongation and it is shown to be conserved in the secondary structures in all species, but the primary structure (length and sequence) diverge between species (153-192 nucleotides in ciliates and 1.3kb in *Saccharomyces cerevisiae* (Romero and Blackburn, 1991, Lingner et al., 1994). For example, the template of all telomerases is single stranded allowing conventional Watson-Crick base-pairing with the 3' single stranded overhangs of telomere with the active site of the TERT closely linked (Cristofari and Lingner, 2006). The whole RNA template is approximately 1.5–2 times the telomeric repeat length providing access to both annealing of the telomeric 3' end and the template providing the addition of one telomeric repeat per elongation cycle (Cristofari and Lingner, 2006). The TERC component of telomerase also has a pseudoknot domain at the 5' end that is conserved in all species. The hTERC is ubiquitously expressed in both the normal and tumour cells (Feng et al., 1995) but it is shown to be up-regulated in tumour cells by almost five-fold when measured by *in situ* hybridisation (Heine et al., 1998) possibly due to longer half-life of the transcribed RNA.

1.11.1.2 Human TERT (hTERT)

The second structural unit of telomerase is the TERT that has the reverse transcriptase activity. TERT was initially identified through biochemical purification of telomerase in *E. aediculatus* (Lingner and Cech, 1996) and *S.* cerevisiae (Lendvay et al., 1996) that eventually led to the full identification of the structure (Lendvay et al., 1996). Subsequently, hTERT was identified through homology search and the cDNA prepared and cloned (Meyerson et al., 1997). In humans, the *hTERT* was mapped to Chr 5p15.33 near the tip of the chromosome 5 and the *hTERT* gene spanned 40kb in size containing 16 exons. The hTERT protein is 127kDa in size and has a conserved telomerase-specific motif (T), seven reverse transcriptase (RT) motifs in their carboxyl-terminal half (1, 2, A, B′, C, D and E)

forming a finger-palm-thumb structure (Nakamura and Cech, 1998). Phylogenetic studies have suggested that the TERT is most related to RTs encoded by the non-long terminal repeat retrotransposons and viruses therefore providing evidence that telomerase is among the most ancient eukaryotic RTs (Eickbush, 1997). The RTs are very important in the function of the reverse transcriptase as mutations in the RT motifs prevent telomerase activity (Harrington et al., 1997, Nakayama et al., 1998). Through the RT motifs the hTERT protein recognises the RNA template and transcribes the telomeric sequence leading to telomere length elongation.

Other molecular chaperons such as p23 and heat-sock proteins (Hsp90) associate with hTERT to promote hTERC and hTERT assembly *in vitro* in rabbit retinulocyte lysates (Weinrich et al., 1997). It is also shown that both chaperons are associated with the mature telomerase in cell extracts as inhibition of Hsp90 leads to blocking of telomerase formation (Holt et al., 1999). Interestingly, Weinrich and colleagues have shown that hTERT is the rate limiting factor for the telomerase absent in normal somatic cells but actively expressed in tumour-derived tissues and cells (Weinrich et al., 1997).

1.11.2 Telomerase assembly and regulation at telomeres

The large telomerase complex (~1000kDa) in human cells have the ability to form dimers or higher order multimers and the hTERT is implicated in multimerization (Cristofari and Lingner, 2006). This dimerization is mediated by the RNA-RNA interaction involving pseudoknot formation in trans (Ly et al., 2003). Biochemical analysis has shown that the telomerase enzyme is associated with many chaperons and proteins including telomerase associated protein 1 (TEP1), Hsp23, Hsp90, hStau and dyskerin but the exact function of these and other associated chaperons and proteins are not fully understood. For example, it is known that Hsp23 and Hsp90 are required for the assembly of the telomerase in the nucleus and mutations in dyskerin lead to the congenital disorder *dykeratosis congentia* (DC) (Pendino et al., 2006).

The telomerase activity is limited to the nucleus and its function on telomeres is regulated by several shelterin proteins. TPP1 and TIN2 recruit telomerase and retain it at telomeres as their depletion is shown to lead to diminished activity of telomerase at telomeres (Abreu et al., 2010). On the other hand POT1 is shown to inhibit telomerase binding to the 3' single stranded telomeric DNA through its OB1 motif as studies have shown that lack of POT1 OB1 domain induces rapid telomere elongation (Loayza and De Lange, 2003). Therefore, POT1 is a negative regulator of telomerase as it acts as a terminal transducer that converts telomere length information into a regulatory signal at the telomere terminus (de Lange, 2006).

1.11.3 BRCA1 inhibition of telomerase activity

It must be noted that a single study suggested inhibition activity of BRCA1 overexpression on telomerase in cells grown *in vitro* with the consequence of telomere shortening (Xiong et al., 2003). This inhibition occurs through reduction of the hTERT activity and had no effect on other components of the telomerase holoenzyme (e.g. TP1, HSP90, hTR, and dyskerin), the hTERT transcriptional activator c-MYC or the shelterin components TRF1 and TRF2 (Xiong et al., 2003). The WT BRCA1 overexpression caused c-myc-induced hTERT repression, which was consistent with previous findings (Wang et al., 1998) (Li et al., 2002). Inhibition of the telomerase activity resulted in shortening of telomeres in the subclones of the overexpressed WT BRCA1 cells, but this telomere shortening did not result in senescence or apoptosis as the cells were able to maintain short telomere lengths. The mechanism behind the maintenance of the short telomeres is not known by the author but predicted to be due to low-levels of telomerase activity (Xiong et al., 2003). However, the authors failed to assess alternative telomere length maintenance activity in these cells (discussed in more detail below).

Overall, limited evidence thus far has been provided that have shown non-physiological overexpression of WT BRCA1 in cells with mutant BRCA1 activity leading to telomerase inhibition and rapid telomere shortening. However, the study but failed to identify the

potential mechanism for the short telomere length maintenance or indeed assess the ALT mechanism.

1.12 Telomere length regulation through Alternative Lengthening of Telomere (ALT) and the role of BRCA1

Immortalised mammalian cells which proliferate for many population doublings (PD) without telomerase activity (measured through the conventional telomerase repeat amplification protocol or TRAP assay) maintained telomeres through ALT (Bryan et al., 1995, Reddel et al., 1997, Hande et al., 1999). Evidence for ALT activity have so far only been found in human immortalise cancer cell lines and telomerase-null mouse cell lines (Bryan et al., 1995, Henson et al., 2002). Although, ALT activity has been found in breast carcinoma and other human cancers including glioblastoma multiforme, osteosarcoma and some types of soft tissue cancer, it is more prevalent in tumours of mesenchymal origins (Cesare and Reddel, 2010). The exact reasons for ALT preference in tumours of mesenchymal origin is not known. The human mesenchymal stem cells are shown to have a preference for ALT activity (Lafferty-Whyte et al., 2009). ALT cells have distinct phenotype that makes it unique to its mode of telomere length maintenance. Therefore, understanding the mechanism of ALT activation in the cancer setting offers particular clinical significance through development of ALT-targeted treatment.

1.12.1 Telomeric phenotype of ALT positive cells

Telomeres in ALT-positive cancer cells have the exact features of telomerase-positive cells: telomeres are able to form the t-loop structure with shelterin protection and have TTAGGG telomeric repeats and the overhang of the G-rich strand (Cesare and Reddel, 2010). However, ALT-positive cancer cells are shown to have heterogeneous telomere length ranging from <3kb to >50 kb with an average of ~ 20 kb (Bryan et al., 1995, Bryan et al., 1997a, Grobelny et al., 2000, Murnane et al., 1994, Opitz et al., 2001). To put this in perspective, telomerase-positive human cancer cells have on average telomere length of <10 kb (de Lange et al., 1990). In some breast cancer cells telomeres are only 2-3 kb in length (Motevalli et al., 2014). In human germline cells the telomere length are averaged at ~

15 kb (de Lange et al., 1990). In normal human somatic cells, in the absence of telomerase and ALT activity, telomeres get progressively shorter with every cell division at a rate of 40 – 200 bp until the telomere length gets to 5 – 8 kb at which point the cell triggers the p53-dependant cellular senescence mechanism and ceases proliferation (Harley et al., 1990, Wright et al., 1997, Shay and Wright, 2005) Neumann and Reddel 2006).

The heterogeneity in telomere size in ALT-positive cells is observed using *in situ* hybridization (FISH). Some chromosomes have no telomeric signal whereas others have strong telomeric signal reflecting the heterogeneity in the telomere lengths observed (Blasco et al., 1997, Perrem et al., 2001). Interestingly, fluctuations in telomere length measured using Flow-FISH method, were observed in an ALT-negative mouse lymphoma cell line (L5178Y also known as LY-R) with emergence of a subpopulation of cells after 20PDs (Cabuy et al., 2004). This unusual event in the telomerase-positive LY-R cells reveals significant gains and losses of telomeric DNA for which the mechanism of changes has not been elucidated (this observation is discussed in more detail in Chapter 6).

The second most striking feature of telomeres in ALT positive cells is the presence of *extrachromosomal telomeric DNA* which takes many forms including double-stranded telomeric circles (t-circles) (Cesare and Griffith, 2004, Wang et al., 2004), the single stranded circles referred to as C- or G-circles depending on whether the strand is C- or G-rich (Nabetani and Ishikawa, 2009, Henson et al., 2009) (the mechanism of C-circle formation is discussed in detail in Chapters 2 and 6), linear double-stranded DNA (Tokutake et al., 1998, Ogino et al., 1998) and very high molecular weight ‘t-complex’ DNA containing abnormal and branched structures (Nabetani and Ishikawa, 2009).

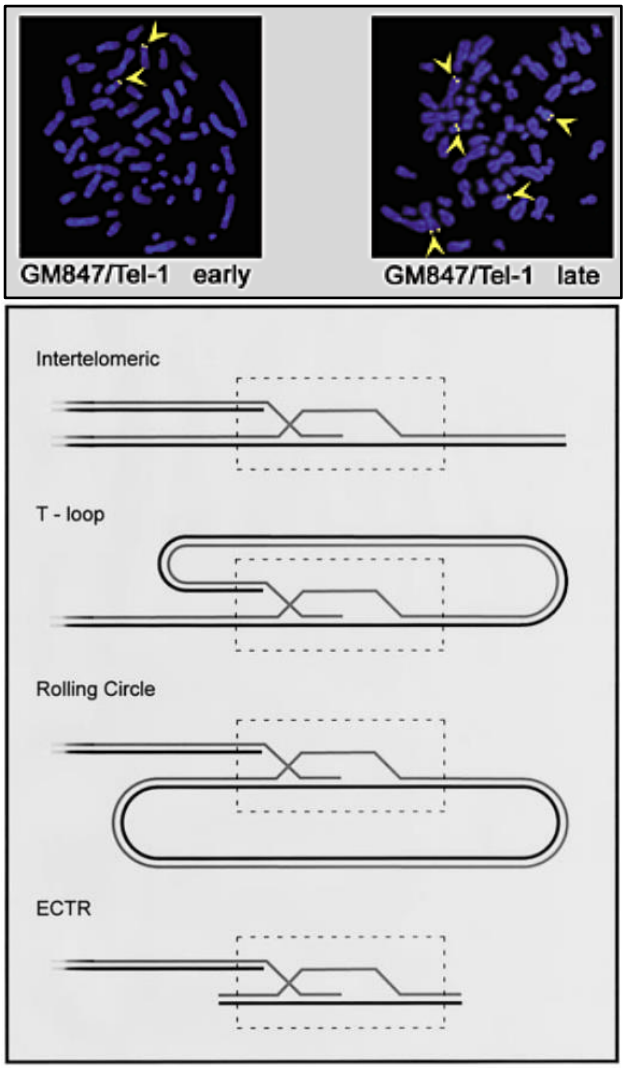

Figure 1-11. Evidence of telomeric copying via HR in the ALT cells.

A) The detection of telomere copying using FISH of an intratelomeric plasmid DNA tag (yellow) in a clonal ALT cell lines in early and **B)** late passage cells (Dunham et al., 2000). **C)** The four proposed model of ALT recombination in human cells (Henson et al., 2002).

The third hallmark common in all human ALT positive cell lines is the occurrence of specific nuclear structures, referred to as ALT-associated promyelocytic leukaemia nuclear bodies (PML nuclear bodies) or APBs (Yeager et al., 1999). These are PML nuclear bodies (PNBs) that are PML aggregates bound to the nuclear matrix (Henson et al., 2002). PNBs have a vast array of functions including tumor suppression, cell cycle regulation, senescence, apoptosis and immune response just to name a few (for detailed review of PNBs see (Lallemand-Breitenbach and de The, 2010). PNBs perform their function by sequestering and releasing proteins and localising proteins to their site of action – be it on the chromatin, on the DNA or through interactions with other proteins (Henson et al., 2002). However, APBs

differ from other PNBs in that they contain telomeric DNA, as well as having TRF1 and TRF2 proteins association (Yeager et al., 1999). It has recently been shown that APBs contain many other proteins involved in DNA recombination and replication such as RAD51, RAD52, RPA, MRE11, RAD50, NBS1, BLM, WRN, ATM and ATR (Henson et al., 2002, Cesare and Reddel, 2010, Nabetani and Ishikawa, 2009). APBs formation in ALT-positive cells is cell cycle dependant and occurs in specific phases of the cell cycle. Therefore APB frequency typically varies between 5 – 10% in ALT-positive cells (Yeager et al., 1999). APBs have been observed in all ALT-positive human tumour cell lines (Neumann and Reddel, 2006) including human tumour specimen obtained from needle aspirates, frozen sections and paraffin-embedded blocks (Henson et al., 2002), Neumann and Reddel, 2006). However evidence is emerging that not all ALT-positive human cells have APBs associated with telomeric DNA (Cerone et al., 2005). This inconsistent observation was made only in one ALT-positive human cell line. This unexpected observation suggests that there may be more than one class of APBs; those that accumulate and are involved in cell cycle and cellular senescence and those that is involved in the ALT activity and telomere length maintenance (Cesare and Reddel, 2010).

A forth hallmark of ALT cells is the frequent occurrence of post-replicative exchanges between telomeric repeats that results in telomere-sister chromatid exchange (T-SCE) (Bechter et al., 2004a, Londono-Vallejo et al., 2004). These T-SCEs can only be visualised using a strand-specific *in situ* hybridization technique known as chromosome orientation (CO)-FISH (Bailey et al., 2004b) (Bailey et al., 2001) (See Chapter 2 for more detail). With this technique it is possible to analyse the frequency of SCEs involving telomeres. However, the exact mechanism behind the formation of T-SCEs is not fully known. It is predicted that these may occur as a result of recombination mediated repair of replication forks (Wilson and Thompson, 2007). Though the exact molecular mechanism of T-SCEs is not understood, these features are commonly observed at high frequencies in all ALT-positive human cell lines and very rarely in telomerase-positive human cells (Neumann and Reddel,

2006; Table 1 p. 170, (Londono-Vallejo et al., 2004). The result of unequal T-SCEs in ALT cells is proposed to cause one daughter cell to have elongated telomeres, and therefore higher proliferation capacity relative to the daughter cell with shorter telomeres, and hence lower capacity for cell division (Bailey et al., 2004b). It must be noted that this is only a hypothesis and no evidence of differential segregation of telomeres has been observed in human cells (Cesare and Reddel, 2010). It is thought that the high frequency of telomeric exchanges in ALT positive cells could be due to the recruitment of proteins involved in HR to the sites of telomeres resulting in the accumulation of proteins that results in generating telomeric SCEs (Londono-Vallejo et al., 2004).

1.12.2 Telomeric recombination in ALT cells

The occurrences of long but heterogeneous telomeres in ALT positive cells suggested that their telomeres may be maintained by HR (Murnane et al., 1994) Neumann and Reddel, 2006). A total of four HR derived mechanisms were proposed (Figure 1.10) suggesting inter-telomeric recombination as a primary mechanism (Reddel et al., 1997). Dunham and colleagues (Dunham et al., 2000) provided evidence for inter-telomeric recombination by showing telomere to telomere copying using fluorescently-tagged plasmids targeted into telomeres. These experiments showed for the first time that telomeres from one chromosome can be used as templates for extending another telomere from a separate chromosome (Figure1.10), and that these events were unique to ALT positive cells (Dunham et al., 2000). This model of HR-mediated telomere length maintenance is seen as a favourable model of telomere length homeostasis in the ALT positive cells (over the unequal exchanges and asymmetric segregation model) since recombination can occur both from inter-telomeric (Dunham et al., 2000) and intra-telomeric sequences (Muntoni et al., 2009). Therefore, telomeres can copy themselves through t-loop formation or template-directed DNA-copying of one sister chromatid by another (Cesare and Reddel, 2010).

1.12.3 Proteins involved in HR-mediated telomere maintenance in ALT cells

Several proteins have been shown to be important in recombination at telomeres. These are classified into (i) proteins that keep telomere elongated and (ii) proteins that prevent telomere loss (Cesare and Reddel, 2010).

Central to the recombination process is the MRN complex, which includes a trio of MRE11, RAD50 and NSB. MRN is shown to be necessary to the recombination in ALT cells (Jiang and Greenberg, 2015, Zhong et al., 2007) as MRN recruits ATM and is responsible for resection of 5' to 3' of the DNA at the DSB sites creating a 3' overhangs necessary for strand invasion during the HR process (Lee and Paull, 2007) (See section 1.9 above). The localisation of MRN occurs on telomeres during the S and G2 phases of the cell cycle and is bound directly to the TRF2 (Zhu et al., 2000). Since the DNA elongation at telomeres occurs at the 3'overhang section it requires DNA polymerases which are though to be recruited to the telomeric sites by the ATM after its activation via the MRN complex (Cesare and Reddel, 2010). This is shown in various experiments whereby the MRN activity was diminished by various means (using SP100 protein to sequester NBS1, or shRNA targeting RAD50) causing long-term disruption of the MRN complex and massive telomere shortening in the ALT positive cells (Jiang and Greenberg, 2015, Zhong et al., 2007).

Other proteins that are shown to be involved in the ALT mechanism are WRN and BLM, both present in APBs (Yankiwski et al., 2000) (Johnson et al., 2001). The BLM RecQ helicase functions at telomeres to regulate the D-loop formation following strand invasion and may also be involved in resolving recombination events in mortal and telomerase-positive cells (Neumann and Reddel, 2002). The 3' and 5' exonuclease activity of the WRN is shown to function both in recombination repair at telomere and in the dissociation of a 3' telomeric tail from inappropriate recombination event by resolving telomeric D-loops (Opresko et al., 2002) (Opresko et al., 2004). Similarly, it is shown that Replication protein A (RPA), RAD51, RAD52 and BRCA1 are associated with ALT through APBs (Yeager et al., 1999) (Naka et al., 2002, Acharya et al., 2014). Recently, it is shown that BLM and BRCA1 are co-localised

with Rad50 at telomeres during S- and G2-phases of the cell cycle in the ALT positive cells but not in telomerase-positive cells (Acharya et al., 2014), further highlighting the involvement of BRCA1 via BLM and RAD50 in telomere maintenance in the ALT cells.

1.13 Aim of the thesis and outline of chapters

Maintaining telomere structure and length in the mammalian cells is extremely important as functional telomeres can prevent unwanted genomic instability, an important hallmark of cancer. Telomere dysfunction is caused by (i) disrupted shelterin proteins, (ii) telomere length shortening and (iii) defective DNA damage repair and sensing proteins. BRCA1 is an important DNA damage repair protein that is recruited to sites of DNA DSB damage including telomeres and it repairs the damaged DNA mainly through HR and to lesser extent through NHEJ. Cells lacking functional BRCA1 suffer from premature senescence but the exact role of telomere maintenance in the process is not known.

Aims of this thesis are:

(a) To assess the effect of *BRCA1* heterozygous mutation on DNA damage repair and sensing capacity at telomeres in human and mouse cells;

(b) To assess whether BRCA1 defects plays a role in ALT in human cells and mouse stem cells.

(c) To elucidate uncertainties surrounding BRCA1 role in telomere homeostasis described earlier (see pages 40-41).

To achieve the above aims we used human lymphoblastoid cell lines derived from patients with heterozygous *BRCA1* mutations and mouse embryonic stem cells (mESCs) lacking both copies of *BRCA1*. Using a range of techniques we measured DNA damage response and telomere maintenance in these cells.

Chapter 3 describes DNA damage response and telomere maintenance following low doses of IR in human lymphoblastiod cells lines.

Chapter 4 describes DNA damage response in mESCs.

Chapter 5 focuses on telomere maintenance and searching for evidence of ALT in mECS.

Finally, in Chapter 6 we used the same mESCs described in chapters 4 and 5 and human ALT-positive cell lines U2OS, SKLU-1 and G292, as well as ALT-negative human cells HeLa and HCC1937, to further characterise the relationship between *BRCA1* wild-type and heterozygous mutant with *BLM* at telomeres, with the aim of identifying the mechanism behind ALT activity in the above cells.

CHAPTER 2

2 Materials and Methods

2.1 Cell lines and tissue culture conditions

2.1.1 Human epithelial cancer cell lines

The HeLa cell line (Table 2-1) was originally established from a patient with cervical cancer. HeLa cells were grown in Dulbecco's modified Eagle medium (DMEM) (Gibco/Sigma), supplemented with 10% fetal calf serum (Gibco/Sigma) at 37°C in the atmosphere of 10% CO_2. The breast cancer cell line HCC1937, which has a truncated, non-functional BRCA1 was cultured in RPMI 1640 (Gibco/Invitrogen) supplemented with 15% fetal calf serum at 37°C in a humid atmosphere containing 5% CO_2. In order to avoid contamination, Penicillin and Streptomycin were added (1µl per 100ml medium) to both media.

2.1.2 Human B-lymphocytes

Normal human B-lymphoblast cell lines GM00893 and GM13705,and GM14090 cell lines derived from carriers of $BRCA1^{+/-}$ mutations were cultured in RPMI 1640 medium (Gibco/Invitrogen) and 10% fetal calf serum and antibiotics at 37°C in the atmosphere of 5% CO_2. All these cell lines have been obtained from the Coriell Cell Repository.

2.1.3 Mouse lymphoma cell lines

Mouse lymphoma LY-R (radio-resistant) and LY-S (radio-sensitive) cells were cultured in RPMI 1640 medium (Gibco/Invitrogen) supplemented with 10% fetal calf serum and antibiotics at 37°C in the atmosphere of 5% CO_2 and were used as a reference for cytological testing telomeric measurements using interphase Q-FISH (IQ-FISH) technique.

2.1.4 Mouse embryonic stem cells

Mouse embryonic stem cell lines E14 and 408 were obtained from Dr Beverly Koller, Duke University, USA. They represent undifferentiated embryonic stem cells and were cultured at 37°C in the atmosphere of 5% CO_2 on gelatine coated dishes in KnockOut DMEM medium supplemented with 20% KnockOut serum replacement, 2 m*M* L-glutamine, 0.001% b-mercaptoethanol (Sigma-Aldrich, St. Louis, MO), 1000 U/ml ESGRO (Chemicon, Temecula, CA), 10 U/ml penicillin, 10 U/ml streptomycin (all purchased, except where stated, from Gibco/Invitrogen). Medium was changed every 2 days, and cells were subcultured initially at the ratio 1:2. The ratio progressively increased up to 1:8.

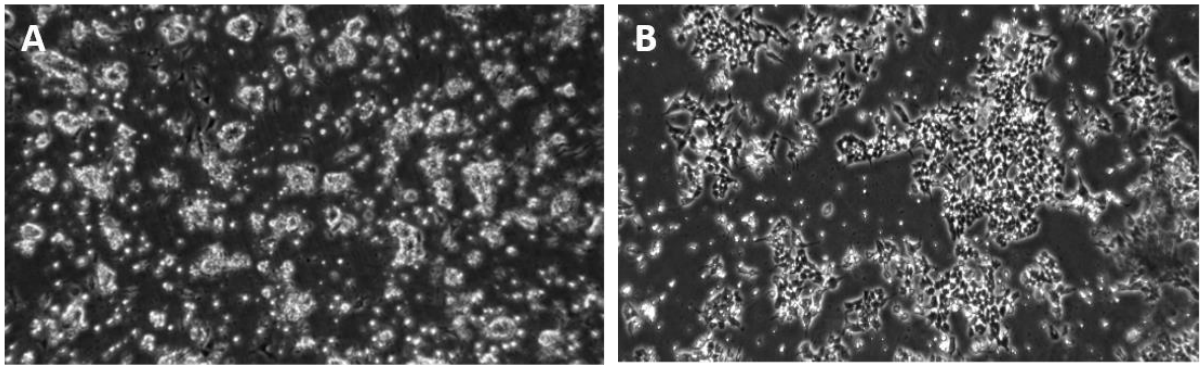

Figure 2-1. Representative images of cultured mouse ESCs.
A) Brca1 wild type E14. **B)** Brca1$^{(-/-)}$ homozygous 408. Images taken at x40 magnification using inverted microscope.

2.1.5 Human ALT^{+} cell lines

The human osteosarcoma cell line U2OS and G292 originally derived from a 15 and 9 years old female, exhibit epithelial adherent morphology were grown in McCoy`s 5a culture medium (Sigma), supplemented with 10% FBS (Gibco/Sigma) and 2mM glutamine (Gibco) at 37°C. the lung adenocarcinoma SK-LU-1 cell line derived from 60 years old female (ECACC, Cat. No.93120835) was grown in EMEM (Sigma), supplemented with 10% FBS

(Gibco/Sigma) and 2mM glutamine (Gibco). In order to avoid contamination, penicillin and Streptomycin were added (1µl per 100ml medium) to all media.

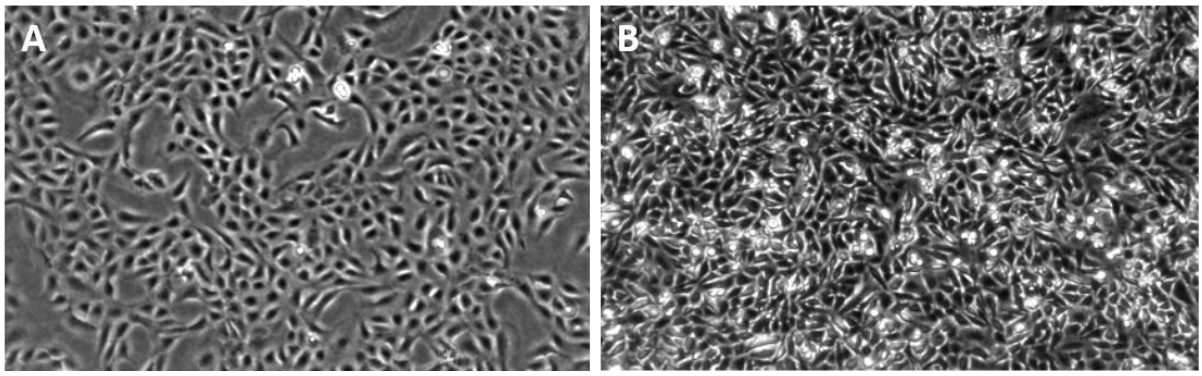

Figure 2-2. Representative images of ALT$^+$ human cell lines.
A) Human U2OS osteosarcoma cell line. **B)** Human ALT- HeLa cells. Images taken at 40x magnifications.

2.2 Tissue culture procedure

All cell lines were kept frozen in liquid nitrogen. When required vials of frozen cells were thawed and set up in either 25cm^2 or 75cm^2 filter head flasks (Nunc) to prevent any contamination. Cells were incubated in a humidified incubator (Heracell 150) at 37°C. All primary fibroblast cell lines were subcultured 1:3 following gentle trypsinization with trypsin-EDTA (Gibco/Invitrogen) for about 5 minutes at least every three days at 80 percent confluence. After trypsinization cells were spun down using a Megafuge 1.0, Heraeus centrifuge for 5 minutes at 1200rpm.

2.2.1 Cell counting

Cell counting was carried out using automatic method a Countess Automated Cell Counter from Invitrogen was used. A mixture of 10µl of Trypan blue and 10µl of cell suspension was prepared. Then a total of 10µl of mixture was taken and added to each slides. The slide is then inserted into the allocated slot in the machine. Finally, the result of the total number of cells per ml displayed on the screen.

Table 2-1. A detail summary of all cell lines used in this thesis.

Cell lines	Species	Origin and gene affected	Cell type	Sex	References
GM00893	Human	Healthy individual (32 years old)	B-lymphocyte	Female	Coriell Institute for medical research
GM13705	Human	BRCA1 carrier (*BRCA1*$^{+/-}$) (38 year old)	B-lymphocyte	Female	Castilla LH et al 1994
GM14090	Human	BRCA1 carrier (*BRCA1*$^{+/-}$) (43 years old)	B-lymphocyte	Female	Struewing JP et al 1995
U2OS	Human	Human osteosarcoma (15 years old)	Mesenchymal adherent cells	Female	Ponten J and Saksela E 1967
HeLa	Human	Human cervical carcinoma (31 years old)	Epithelial adherent cells	Female	Gey Go et al. 1952
HCC1937	Human	Human breast adenocarcinoma (23 years old)	Lymphoblast, epithelial	Female	Tomlinson GE et al. 1998
L5178Y (referred to as LY-R)	Mouse	Mouse lymphoma, Normal	Lymphoma	Unknown	Alexander P et al 1961
L5178Y-S (referred to as LY-S)	Mouse	Mouse lymphoma, Radiosensitive	Lymphoma	Unknown	Alexander P et al 1961
E14TG2a (referred to as E14)	Mouse	Mouse embryonic stem cells with functional *Brca1*	Stem cell	Unknown	Hooper et al. 1987; Snouwaert J et al 1999
408	Mouse	Mouse embryonic stem cells with defective Brca1 (*Brca1*$^{-/-}$)	Stem cell	Unknown	Snouwaert J et al 1999
SKLU-1	Human	Human lung adenocarcinoma (60 years old)	Epithelial adherent cells	Female	Fogh J et al 1977
G292	Human	Human osteosarcoma (9 years old)	Fibroblast adherent cells	Female	Peebles P et al 1978

2.2.3 Cell cryopreservation

Cells were preserved in liquid nitrogen, so before that cell suspension mixed with 1ml of freezing medium consisting of 90% foetal calf serum (Gibco/Invitrogen) and 10% DMSO (dimethylsulfoxide, Sigma). The cell suspension was aliquot into cryogenic vials for storage in liquid nitrogen. Prior to storage in liquid nitrogen the vials were kept in a Nalge nunc cooler for 24 hours at -20°C, which contained Isopropyl Alcohol (IPA).

2.2.4 Thawing of cryopreserved cells

The cryopreserved cells after taken out from liquid nitrogen, warmed for 2-3 minutes at 37°C and then transferred to flasks containing pre-warmed medium. After 24 hours the medium was changed to wash away any DMSO residual.

2.2.5 Irradiation of cells

Cells were exposed to ionising radiation using a Cobalt-60 source. Adherent cells were grown up to 80-90% confluence either in non-filtered tissue culture flasks (Nunc, Fisher) for metaphase preparation, or on polyprep slides (Sigma) depending on the relative assay. Cells were exposed to different doses of ionizing radiation including: low dose 0.5 Gray (Gy) or high dose (1.0Gy, 2.0Gy, and 4.0Gy) which was calculated using datasheets provided by the physicists in charge of the facility.

The formula was used to calculate:

$$Time\ (mins) = \frac{Dose\ Needed\ (Gy)}{Dose\ Rate\ (Gy\ min^{-1})}$$

The calculation of radiation dosages was measured in Gy per minutes. In our research, cells were only subjected to relatively low doses of radiation (0.5Gy and 1.0Gy), however 2.0Gy was used as a maximum dose.

2.3 Cytogenetic Analysis

2.3.1 Metaphase preparation using lymphoblastoid cell lines

All cell lines were treated in the presence of Demecolcine (10µg/ml) for about 1- 12 hours depending on the cell line and assays. Demecolcine was used to block the formation of microtubules, therefore can arrest the cells in metaphase. Cells were washed with PBS, trypsinised for 5 minutes and after spun down at 1000rpm for 5 minutes, treated with 3ml of hypotonic buffer (75 Mm KCl) for 15 minutes in a 37°C water bath and this will cause cells to increase their fluid intake. The 1ml of fresh fixative (Methanol: Acetic acid 3:1) was gently added and the cells were centrifuge at 1000rpm for 5 minutes. The fixation process was repeated at least 3 times. Finally, cells were then re-suspended in fresh fixative and 20µl of this suspension was dropped on to pre-cleaned slides. The fresh fixative confirmed that mitotic cells were spread over the surface of slide effectively. The slides were checked under a phase contrast microscope.

2.3.2 Metaphase preparation using mouse embryonic stem cell lines

2.3.3 Giemsa staining

Next, metaphase cells were stained with 7 percent (v/v) Giemsa (Sigma-Aldrich) for about 5 minutes in 5 ml of ddH_2O. To ensure better staining, Giemsa was filtered using standard filter paper (3MM Watman paper). After staining slides were washed gently with ddH_2O and left to air dry. Slides then were mounted with DPX (BDH laboratories), covered with cover slip, and left for maximum 2 hours to dry. Analysis was carrying out using light microscopy (Zeiss Axioplan 2) equipped with CCD camera and Metasystem software (Altlussheim, Germany).

2.3.4 Chromosomal aberration analysis

To detect any damage at chromosomal level, metaphase chromosome was stained using either DAPI (fluorescence microscopy), or Giemsa (light microscopy) and were analysed at G1 and G2 phases of the cell cycle. For both human lymphoblastoid cell lines and mouse embryonic stem cell lines following protocol were performed.

For G1 assay, cells were irradiated as confluent, sub-cultured and incubate about 18 hours. Then 10µg/ml colcemid was added for 2 hour. The cells were harvested as described above. The duration of one single cell cycle in the case of mouse embryonic stem cells is approximately 20 hours and incubation for 18 hours plus 2 hours colcemid treatment allow capturing of metaphase G1 cells exclusively.

Semi-confluent cells were exposed to ionizing radiation in G2 assay. Cells were then incubated for 20 minutes before adding colcemid and kept them in presence of colcemid for 1 hour. The cells were harvested at 1.5, 3.0 and 4.0 hours after radiation.

2.3.5 Micronuclei assay

Growing cells were treated with 6µg/ml of Cytochalasin B (Sigma) for 48hours. The cells were then centrifuge at 800rpm for 8 minutes. After discarding the supernatant, the pellet was gently re-suspended in 3ml of hypotonic KCl (75mM) solution and left at 4°C for 3 minutes. A few drops of fixative (Methanol: Acetic Acid; 3:1) were added to the cells, and they were centrifuged at 800 rpm for 5mins. After that the supernatant was aspirated and the cells were re-suspended in 3ml of fixative and left for 10 minutes at room temperature. After centrifuging the supernatant was aspirated and a total of 500µl of fixative was added, this suspension was cyto-spun onto slides at 800rpm for 5 minutes. The slides were then stained with the Giemsa as described earlier.

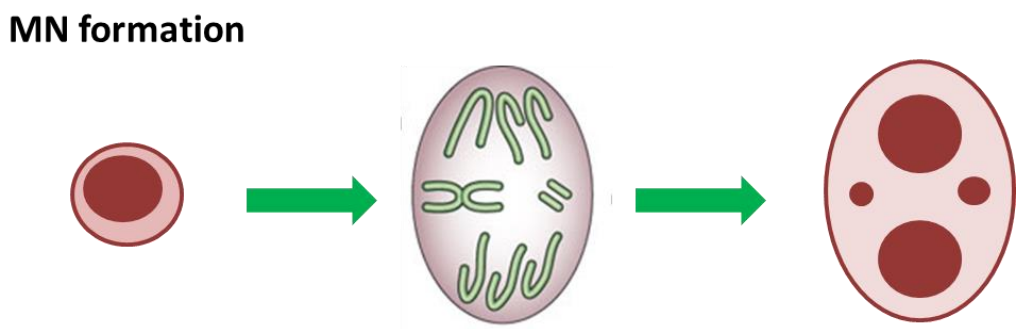

Figure 2-3. Schematic diagram showing formation of micronuclei (MN).

MN is formed when fragments of chromosome does not segregate and results in formation of mini nuclei during cellular division (Author's own representation).

2.4 Interphase Quantitative Fluorescence *in situ* Hybridization (I-QFISH)

2.4.1 Pre-hybridisation washes

The slides containing samples were washed with PBS for 5 min on the shaker. After that the samples were treated with 4% formaldehyde for 2 minutes, the next step was washing in PBS for 3x5 minutes. In order to remove unwanted proteins, 500µl of pepsin (10% pepsin; Sigma) was mixed with 50ml of acidified dH_2O of pH2 (49.5ml of deionized water added to 0.5ml HCl) and then added to 50 ml PBS and incubated at 37°C in water bath for 10 minutes. Next cells were washed 2x2 minutes with PBS on the shaker, and fixed for the second time with 4% formaldehyde for about 2 minutes. Subsequently after washing the slides 3x5 minutes with PBS, dehydrated with ethanol series (70%, 90%, 100%) and left to dry at room temperature (Figure 2.4).

2.4.2 Hybridisation

A total of 20µl of the PNA probe specific for the telomeric DNA sequence $(CCCTAA)_3$ labelled with FITC, was added to the slides. The slides were then heated on the heating block for 2 minutes at 70-75°C. Slides were left in a dark and humid chamber for 2 hours to allow for hybridisation.

2.4.3 Post-hybridisation washes

The slides were washed twice in presence of 70% formamide solution for about 15 minutes followed by washing the slides 3x with PBS for 5 minutes. After dehydrated with ethanol series (70%, 90%, 100%), a total of 15µl of Vectra-shield anti-fade (DAPI) mounting medium was added to each slides and then were sealed with a clear nail varnish.

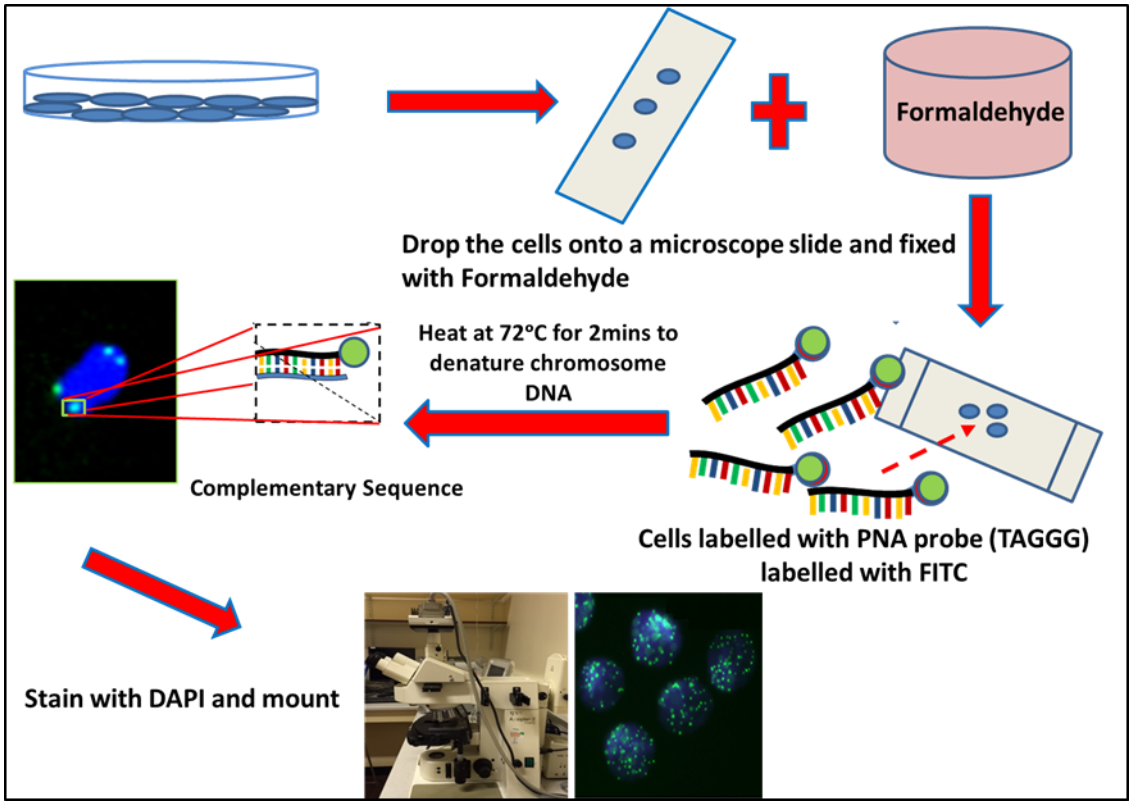

Figure 2-4. Schematic representation of the IQ-FISH workflow.

Cells are dropped and fixed onto a clean microscope slide and is hybridized with a Telomeric probe (see materials and methods for detail). The slides are then further treated and washed and images taken using a fluorescent microscope. The signal intensity from each telomeric probe is then quantified using image-processing software (Author's own representation).

2.4.4 Image capture and telomere length analysis

Images of interphase cells were acquired using the Smart Capture software (Digital Scientific, Cambridge, UK) and the analysis of telomere fluorescence using the IP lab software. The software adapted for this purpose by Digital Scientific. The software produces a combined image of the detected telomeres and the cell nucleus boundaries which are superimposed onto the telomere image. In order to maintain the accuracy of IQ-FISH methodology it was essential to have correct controls for the experiment. This is because the fluorescence microscope lamp intensity is not steady. To provide the accuracy of fluorescence intensity measurement we used to mouse cell lines, LY-R and LY-S, with long and short telomeres respectively, as calibration standards (McIlrath et al., 2001). In each experiment we captured images of LY-R and LY-S cells together with the test samples. After capturing images of interphase cells in the Smart capture 2 software, the data was sent to

the IPLab program in which telomere fluorescence intensities were measured. The procedure for IQ-FISH was described in detail in a PhD thesis by another student working in Dr. Slijepcevic's laboratory (Ojani, 2012).

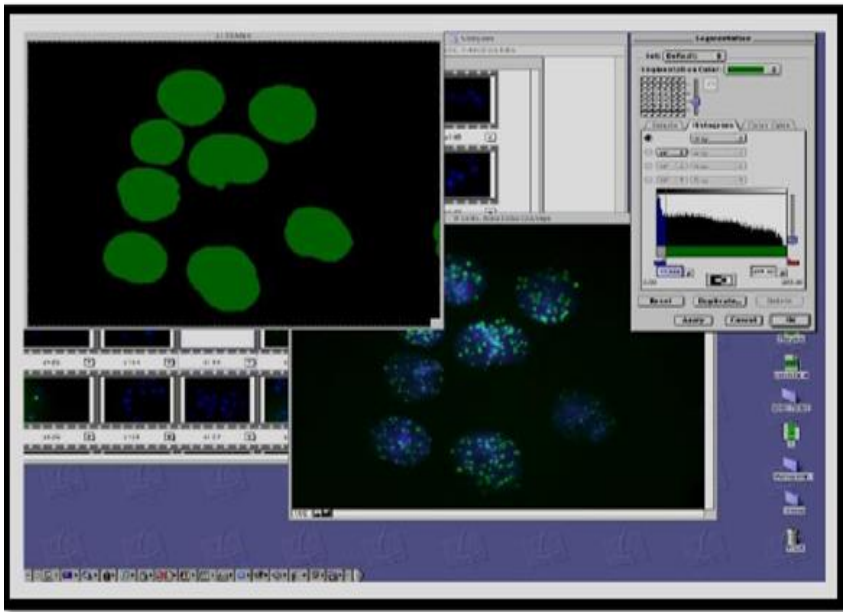

Figure 2-5- Image shows a typical segmented image with cell nuclei stained in green

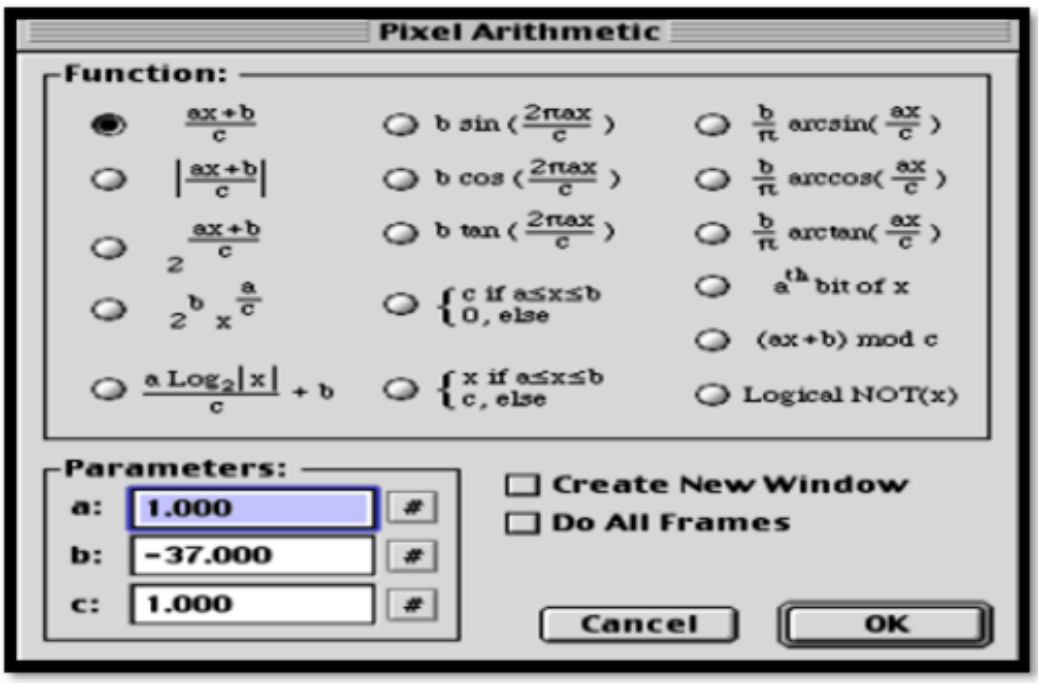

Figure 2-6- Image shows a snapshot of the mathematical manipulations behind the process of telomere fluorescence intensity measurement.

2.5 Chromosome Orientation Fluorescence *in situ* Hybridisation (CO-FISH)

CO-FISH or the technique which was originally called COD-FISH, is based on standard FISH which also has more ability to determine the absolute 5` to 3` orientation of DNA sequence relative to short arm to long arm of the chromosome. The principle of the technique is based on standard FISH, which allows hybridisation of a single standard probe to only one chromatid of a metaphase chromosome (Goodwin et al 1993). Figure 2.7 shows the main principle of this technique.

To examine the telomeric sister chromatid exchange (T-SCE), CO-FISH was used which can be seen below. The split signal shown in the image shows a T-SCE. This image was adapted and adjusted from (Bailey et al 2004).

After cell culturing the cells were placed in incubator for 20minutes and then 3µl of 5`-bromo-2-deoxyuridine (Brdu/Brdc, 3:1) at the concentration of $1x10^{-5}$ M (Sigma) was added to the cells. Following metaphase preparation slides were made and were aged overnight at 54°C to allow better preservation of chromosomes after subsequent DNA denaturing.

2.5.1 Washing, digestion, and fixation

The slides were washed with PBS for15 minutes and then stained with 2.5µl of Hoescht 33258 (0.5µl/ml), which was gently mixed with standard saline citrate (2x SSC) for 15 minutes. Slides were then exposed to 365 nm UV light for 30minutes, and a total of 100µl of Exonuclease III (Promega) (1.5µl Exonuclease III + 10µl buffer + 88.5µl H2O) was added to each slide, covered with cover slip and left at room temperature for 10 minutes. Samples were then washed with PBS for 2x5 min on the shaker. Subsequently, the slides were treated with ethanol series for about 5 minutes for dehydration (70%, 90%, and 100%), and left to air dry. Hybridisation and post-hybridisation washes are carried out as described earlier (section 2.4.2 and 2.4.3).

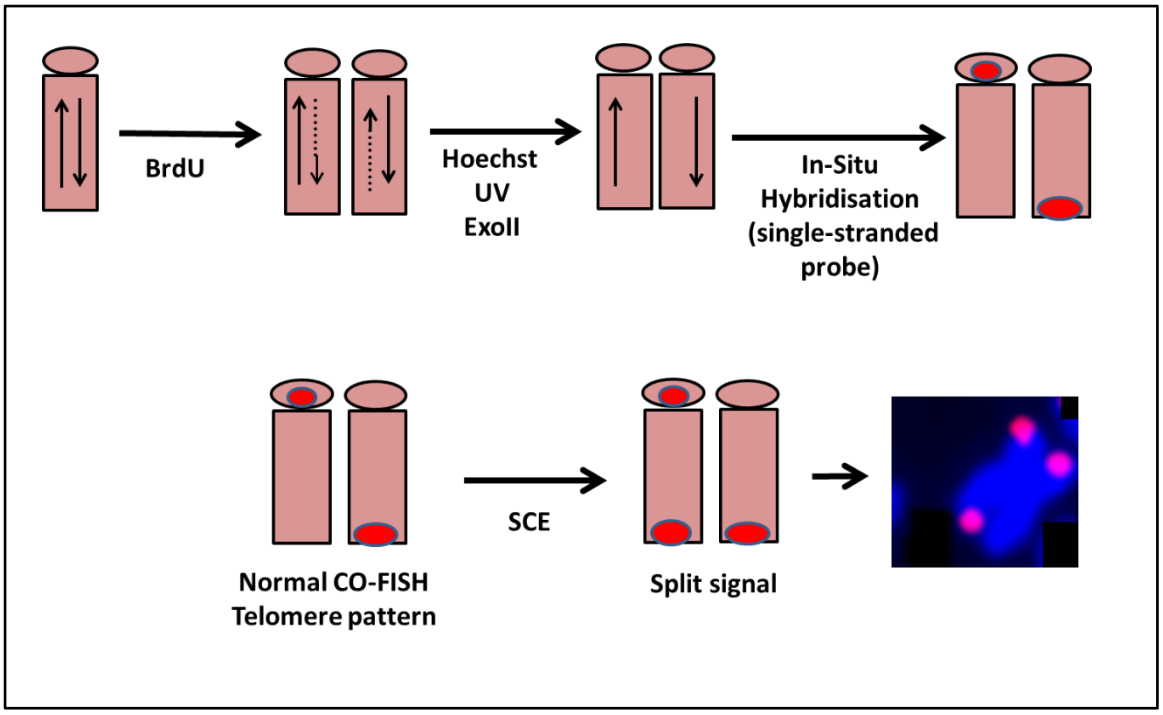

Figure 2-7. Schematic representation of CO-FISH.

Cells are left overnight in the presence of BrdU and after incooperation into the genome and metaphase preparation the slides are UV treated and digested using Exonuclease II. This causes removal of one of the strands of chromosome. The slides are then hybridized with telomeric probe and in the presence of sister chromatic exchanges three telomeric signals are observed as opposed to normal CO-FISH pattern of two telomeric signals on opposing chromatid.

2.5.2 Image Analysis

Digital images were acquired using a Zeiss fluorescence microscope equipped with a CCD camera and the ISIS captures software (*in situ* imaging system ISIS. Meta systems, Altlusshim, Germany).

2.6 Immunocytochemistry

2.6.1 Single immunofluorescence detection of γ-H2AX foci

Ionizing radiation or cytotoxic agents are mechanisms that induced double strand breaks; subsequently γ-H2AX foci quickly form and can be used as a biomarker for DNA damage. Therefore, γ-H2AX assay is one of the most popular technique for detection of DNA double strand breaks. Interphase cells were examined using a monocolonal anti-body against the γ-H2AX protein. We used a simple cytospin procedure to spreads non-adherent cells onto microscope slides using gentle fixative reagents (2% formaldehyde for 10 min). Cells were grown in T25cm^2 flasks (Nunc) and attached to poly-prep L-lysin slides (Sigma-Aldrich) by cytospin centrifuge at 1000 rpm for 5 min. after fixation with 2% paraformaldehyde for 10

min, washed with PBS for 5 min, permeabilized with 0.05% Triton X-100 solution (Sigma-Aldrich) in PBS for 10 min at 4°C. Non-specific sites on the cells were then blocked using blocking buffer (0.1 gram BSA + 10ml PBS + 10µl Tween20). A total of 100µl of blocking buffer was added to each slide and covered with parafilm for 30 minutes in dark. Cells were then incubated with mouse monoclonal anti-phospho-histon H2AX (γ-H2AX, Millipore) at 1:500 following manufacturer`s instructions in blocking buffer for 1 hour at room temperature. Cells were then washed and incubated with a species specific secondary IgG FITC conjugated antibody (FITC labelled anti-mouse, Invitrogen) at 1:1000 for 1 hour at room temperature. Cells were then washed in PBS several times and covered with vectashield mounting medium (Vector Laboratories, California, USA) containing 1.5 µg/ml DAPI.

2.6.2 Telomere dysfunction-induced foci (TIF) assay

Combined immunofluorescence (γ-H2AX) and FISH (telomeric PNA probe) to detect the DNA damage at telomeres is named TIF. First, detection of γ-H2AX foci by immunofluorescence was performed. Slides were incubated overnight in a dark container at room temperature. On the next day the FISH method, described in previous section (2.4) was applied with a Cy3-conjugated PNA probe $(C_3T_2A)_3$, followed by standard formamide and SSC washes. Cells were counterstained with DAPI in fluorescence anti-fade medium. The slides were then analysed using the computerized Axioskop 2 Zeiss fluorescence microscope equipped with a CCD camera and Metasystem software.

2.6.3 Single immunofluorescence detection of PML foci

A total of $5x10^5$ cells were grown on poly-L-lysine- coated slides (poly-Prep slides, Sigma-Aldrich) for 24 hours prior to immunofluorescence staining. The slides were fixed in 4% paraformaldehyde for 10 minutes and were washed three times in PBS. Cells were then permeabilised in 0.25% Triton-X 100 (Sigma- Aldrich) for 10 minutes at room temperature and were washed in PBS 3X5 min. Cells were blocked with 1% Bovine serum albumin (BSA) in PBS for 30 minutes and were covered with parafilm in a humid container. Promyelocytic leukemia (PML) primary antibody (Mouse monoclonal antibody against PML, MAB3738, Millipore) was added to the slides at the desired concentration (1:100), for 1 hour in humid

container covered with parafilm. Slides were washed in PBS three times for 5 minutes. The anti-mouse secondary antibody labelled with FITC (Invitrogen) was added to the slides at a dilution rate of 1:1000 and slides were incubated for 1 hour in a dark and humid container. The slides were washed in PBS 3x5min in the dark on the shaker.15µl of Vectashield with fluorescence DAPI mounting medium was then added to the slides and the slides were covered with a coverslip prior to sealing with clear nail varnish.

2.6.4 Immunofluorescence and FISH (Immuno-FISH)

After immunostaining with anti-PML antibodies, as described earlier. The FISH method was applied with a Cy3-conjugated PNA probe $(C_3TA_2)_3$ followed by standard formamide and SSC washes (section 2.4). Cells were counterstained with DAPI, and covered with a coverslip and were sealed with clear nail varnish.

2.6.5 Single immunofluorescence detection of ATRX foci

Immunofluorescent staining was performed on cells grown on poly-L-lysine-coated slides (Sigma-Aldrich), fixed for 10 min at room temperature in a 3% paraformaldehyde-buffered solution, and permeabilised 10 min on ice with cold 0.5% Triton X-100 (Sigma-Aldrich). Cells then were washed with cold PBS 4x5min and were blocked with PBG (PBS+BSA+ Gelatine Fish) for at least 30 minutes at room temperature. Alpha-thalassemia/mental retardation syndrome X-linked (ATRX) primary antibody (Rabbit polyclonal antibody against ATRX, ab97508, Abcam) was added to the slides at the relevant concentration (1:100) and incubated 1.5 hrs at 37°C. the slides were washed in PBS three times for 5 minutes. Cells then were incubated for 30 minutes at 37°C with anti-rabbit secondary antibody labelled with FITC (Cat no.: F1262, Sigma) (1:100) diluted in PBG. The slides were washed in PBS three times for 5 minutes on the shaker and mount on slides using Vectashield containing DAPI.

Immune-FISH was performed following by immunostained. The FISH method was applied with a Cy3-conjugated PNA probe $(CCCTAA)_3$. Cells were counterstained with DAPI and were sealed with clear nail varnish.

2.6.6 Single immunofluorescence detection of BRCA1 foci

Cells were grown on coverslips (Poly-L-lysine-coated slides, Sigma-Aldrich) and fixed for 10 minutes with 4% paraformaldehyde at room temperature. Cells then were washed in PBS three times for 5 minutes and were permeabilised with 0.5% Triton X-100 (Sigma-Aldrich) for 10 min on ice. The cells were then blocked with 1% BSA in PBS for 30 minutes at room temperature and were covered with parafilm in a humid container. 100µl of mouse monoclonal anti BRCA1 (Thermo scientific, 6B4) was added to the slides at the desired concentration (1:400) and the slides were incubated for 1 hour in humid container. The slides were each rinsed three times for 5 minutes. 100µl of secondary FITC-conjugated anti mouse IgG antibody (Invitrogen) was added to the slides at the desired concentration (1:500) and the slides were incubated for 1 hour in a dark and humid container covered with parafilm. The slides were each washed in TBST (Tris-Buffered Saline with 0.1% Twee20) three times for 5 minutes in the dark on the shaker. 15µl of vectashield with fluorescence DAPI mounting medium was then added to the slides and the slides were covered with coverslip prior to sealing with clear nail varnish.

2.6.7 Single immunofluorescence detection of BLM foci

Cells were grown on poly-prep slides (Sigma-Aldrich) for 24 hours before fixation in 4% formaldehyde in PBS for 10 minutes and were permeabilised with 0.5% Triton X-100 (Sigma-Aldrich) for 10 minutes at 4°C. cells were then washed with PBS 3x5 min and were incubated with blocking buffer 1% BSA in PBS for 30 minutes in humid container. 100µl of Blooms Syndrome (BLM) primary antibody (Rabbit polyclonal antibody against BLM, PA5-27384, Thermo Scientific) was added to the slides at the desired concentration (1:100) and the slides were incubated for 1 hour in a humid container covered with parafilm. The slides were washed in PBS three times for 5 minutes. Then, 100µl FITC secondary anti-rabbit were added (diluted 1:100 with 1% BSA) for one hour in dark, damp conditions and washed with PBS for five minutes, three times in a dark coupling jar and on an orbital shaker. Cells were fixed again with 4% formaldehyde for 20 minutes at room temperature and left overnight.

2.6.8 Double immunofluorescence detection of BRCA1 with BLM

Cells were spread onto poly-L-lysine-coated slides. For the simultaneous visualisation of BRCA1-BLM foci, cells were fixed as mentioned in previous section. Cells preparation were blocked for 1 h in 10% FBS/PBS, rinsed, and incubated with primary antibodies. Double staining with antibodies was performed for 1 hour at room temperature or overnight at 4°C, whereas species-specific FITC and Texas Red-conjugated secondary antibodies were applied for 1 h at room temperature followed by counterstaining for 5 min at room temperature with 0.5µg/ml DAPI. Slides were mounted in vectashield and analysed by fluorescence microscopy. All primary antibodies were used at 1: 100-400 dilutions, whereas the secondary antibodies were employed at a 1: 100 dilutions.

2.7 Western Blot

Cells were grown as described before, and after typsinaisation a total of 15 x10^5 cells centrifuged and washed with ice-cold PBS for 5 minutes at 4°C then lysed on ice for 15 min in 60µl of lysis buffer (Tris-HCl (1M,PH7.4), NaCl (5M), EDTA (0.5M,PH8.0), Triton X (100%), SDS (10% w/v), Na-deoxycholate (10% w/v), Protease Inhibitor (100x) dH_2O) (Peplab, Germany). Samples then were centrifuged at 14,000rpm for 15 min and the supernatant transfer to new Eppendorf tubes. The total protein extracts were and stored at -20°C.

For each samples approximately 30µg of protein was prepared in 2x Laemmli buffer (2-mercaptoethanol 0.1%, Bromophenol blue 0.0005%, Glycerol 10%, Sodium dodecyl sulfate (SDS) 2%, and Tris-HCl 63mM (pH6.8)) and boiled in 100°C for 10 min to denature the globular structure of the proteins and then loaded onto a 4-20% precast gradient gel (Bio-rad). The lower the molecular weight of a protein of interest, the higher the percentage of gel that is required.

2.7.1 Protein gel electrophoresis

30µg of protein were loaded carefully onto each well. The protein marker was normally loaded on the first well. The interior and exterior of the tank was filled with 1x running buffer made with 3.0g (w/v) of tris base, 14.4g (w/v) of glycine, 1g of SDS, and distilled water to 1

litter. The samples were initially run at 25mA with a constant voltage of 150V until proteins were evenly located in the gel for approximately 90 minutes. The samples were checked regularly to prevent running off of the protein samples.

2.7.2 Blotting and transfer

Once proteins were separated in the gel based on their size and mobility (heavier proteins move slower and hence were at the top of the gel, whereas smaller proteins move faster and were found near the bottom of the gel), proteins were stained with 0.1% Coomassie Brilliant Blue (Thermo Fisher Scientific) (50% methanol, 10% acetic acid and 40% H_2O) for 1hr on the shaker and then destained with destaining solution (50% methanol, 10% acetic acid and 40% H_2O) with at least two changes until all stains is removed. Coomassie blue dye is a colorimetric method that in an acidic condition the dye binds to proteins primarily through basic amino acids (arginine, lysine, and histidine) (Syrovy and Hodny 1991). Then proteins were transferred onto a blotting paper Polyvinylidine fluoride (PVDF). PVDF is a non-reactive membrane that has a non-specific affinity to amino acids. PVDF was activated by soaking in 100% methanol for 10 seconds. A sandwich of filter pad, 3mm filter paper, activated PVDF membrane, gel, 3mm filter paper, and filter pad was assembled according to the manufactures protocol (Bio-Rad). A small magnetic stirrer was placed in the tank, topped with 1x transfer buffer made with 11.25g (w/v) of glycine, 2.42g (w/v) of tris base, 200ml (v/v) of methanol and distilled water to 1 litter. The blotter was placed inside the tank and the tank was run at 100V for 90 minutes on a magnetic stirrer to create an even distribution of the electrolysis. An ice pack was also placed inside the tank to prevent overheating of the buffer solution. Next we stain the blotting membrane using 1x concentration of Ponceau S (Sigma-Aldrich) for 5 minutes on the shaker to make sure that all proteins have been transferred equally across from the gel. Ponceau S is a sodium salt of a diazo dye with a light red color that specifically stains proteins on the PVDF blotting paper.

2.7.3 Blocking and antibody incubation

Once the transfer of protein from gel onto the PVDF membrane was complete the proteins were blocked with 5% blocking reagent containing 5g (w/v) of semi-skimmed milk (Marvel) in

100ml of Tris buffer saline-Tween (TBST) made with 16g (w/v) of NaCl, 0.2g (w/v) KCl, 3g (w/v) of Tris base, 0.1% (v/v) Tween-20 added to 880ml of distilled water adjusted pH to 7.6, and distilled water added to 1 litre. The membrane was left in 30ml of blocking solution for about one hour on a shaker at room temperature. The milk mixture blocks the unspecific binding of an antibody with the membrane. the membrane was incubated with the primary antibody (1:1000 dilution) according to the manufacturer`s recommendation and was further optimized by the user. Table 2-2 below shows all antibodies used in our experiment with optimized dilution ranges. Primary antibodies were diluted in one in five dilutions in 5% blocking buffer in 1x TBST and added to the membrane overnight on a shaker set at medium pace (200rpm/minutes) at 4°C. The following day the membrane was washed four times with 0.1% PBS IGEPAL (IGEPAL CA-630, Sigma) for 10 minutes each and incubated with a secondary antibody diluted in one in five dilutions of 5% blocking buffer on a shaker at 4°C for at least one hour.

2.7.4 Protein detection with chemiluminescence

After one hour incubation with a secondary antibody the membrane was washed four times in 0.1% PBS Igpal for 10 minutes. Meanwhile ECL plus (Enhanced chemiluminescence) kit (GE Healthcare) was taken out of the fridge and left at RT to warm up. The amount of ECL required for detection was based on the size of the membrane and was recommended by the manufacturer to be of a final volume of 0.125m/cm^2 of membrane. The manufacturer`s protocol was consulted for the exact mixture of chemical A and chemical B. as a rule of thumb, 2ml of reagent A was mixed with 50µl of reagent B. that is 1 part of reagent A mixed with 40 parts of reagent B. The ECL mixture was added onto the membrane and covered with Saran wrap for 5 minutes in a dark room. The excess of the ECL was tipped off onto a paper towel, wrapped in the membrane facing down onto a piece of clean Saran wrap and placed in an X-ray cassette.

Unexposed ECL plus hyperfilm (GE healthcare) was put on top of the membrane and the cassette closed and left for exposure for 5 minutes. The X-ray films were developed using an

automatic machine (Xograph). The exposure time was assessed accordingly depending on the size of the exposed bands. If the protein bands were faint and could not be visualized then a second film was exposed for a longer period. The ECL chemiluminescence was active for at least one hour.

Table 2-2. Summary of antibodies used in this thesis.
WB: western blotting (WB); IF: immunofluorescence; M: monoclonal; P: polyclonal.

Antibody	Cat.No.	Type	Source	Application	Concentration
Anti-BRCA1	MA1-23164	M	Thermo Fisher Scientific	WB/IF	1:400 (IF) 1:1000 (WB)
Anti-BLM	PA5-27384	P	Themo Fisher Scientific	IF	1:100 (IF)
Anti-ATRX	Ab97508	P	Abcam	IF	1:100 (IF)
Anti-PML	MAB3738	M	Millipore	IF	1:100 (IF)
Anti-y-H2AX (Ser139)	05-636	M	Millipore	IF	1:500 (IF)
Anti-β-actin	A-2228	M	Sigma	WB	1:10,000 (WB)
Goat anti-rabbit IgG (H+L)	A-110088	P	Thermo Fisher Scientific	IF	1:100 (IF)
Goat anti-rabbit IgG (H+L)	T-2767	P	Thermos Fisher scientific	IF	1:100 (IF)
Rabbit anti mouse IgG	A-11054	P	Thermo Fisher scientific	IF	1:100 (IF)
Goat anti rabbit IgG	A-11054	P	Thermo Fisher scientific	IF	1:100 (IF)
Goat anti mouse IgG	A-11001	P	Thermo Fisher scientific	IF	1:100 (IF) 1:5000 (WB)

2.8 Quantitative telomere-repeat amplification (TRAP) assay

2.8.1 Protein isolation

Cell lines to be analysed were grown to 80-90% confluence on a P100 petridish. At this point cells were harvested and total cell number was determined. The cell pellet was obtained by centrifuging at 15,000*rcf* for 5 minutes. The pellet was washed once with pre-warmed PBS. Sample pellets were left on wet ice and 200µl CHAPS lysis buffer (TRAPEZE 1x CHAPS MILLIPORE Company) per 10^5-10^6 cells was used to re-suspend the pellets. All samples were retro-pipetted several times and the cell suspension was transferred to a new tube. The suspension was incubated on the ice for 30 minutes before centrifugation at 12,000 *rcf* for 20 minutes at 4°C. 150µl of the supernatant was transferred into a fresh tube and determined the protein concentration for all the samples including the one was going to be used as the standard curve. The remaining extract was aliquotted and immediately stored at -80°C until required.

2.8.2 Determination of protein concentration

The protein concentration of samples was measured using the Pierce BCA Protein Assay Kit (Thermo Scientific). Pierce BCA Protein Assay is a detergent-compatible formulation based on Bicinchoninic Acid (BCA) for the colorimetric detection and quantitation of total protein. The assay was performed according to manufacturer's guidelines. A standard calibration curve was set up using BSA diluted in CHAPS lysis buffer, ranging from concentration 0-2µg/ml (Figure 2.8, Table 2-3). All unknown sample protein concentrations were measured against the standard curve (data not shown).

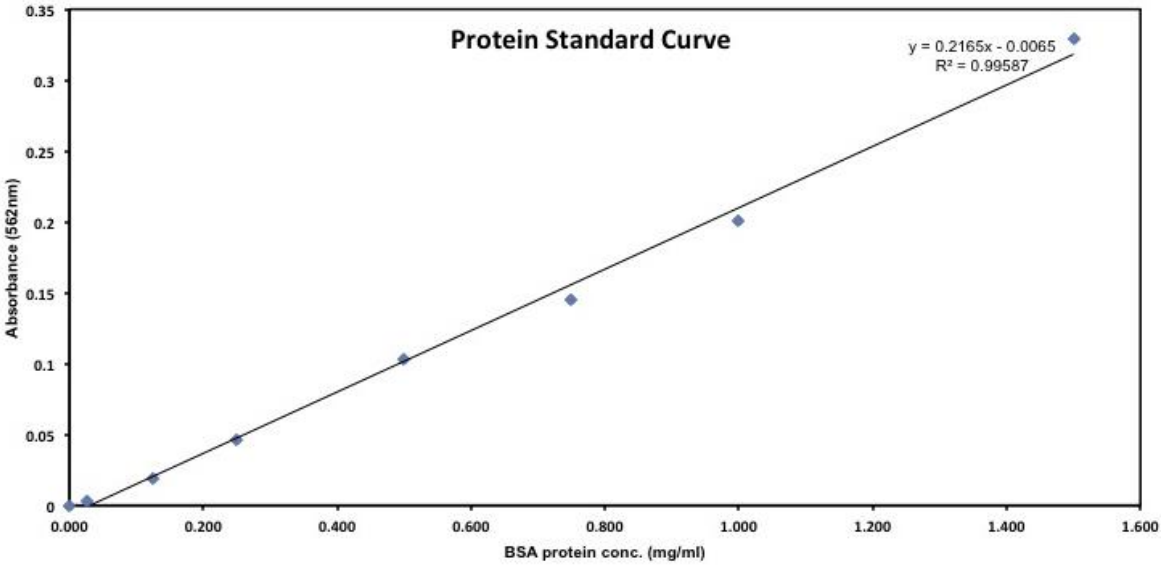

Figure 2-8. BSA standard curve for protein estimation.

Table 2-3. Preparation of diluted BSA standards for BCA analysis.

Tube	Final BSA concentration	Volume of BSA	Volume of dH2O
A	1500 µg/ml	30 µl	10 µl
B	1000 µg/ml	20 µl	20 µl
C	750 µg/ml	20 µl of A	20 µl
D	500 µg/ml	20 µl of B	20 µl
E	250 µg/ml	20 µl of C	20 µl
F	125 µg/ml	20 µl of D	20 µl
G	25 µg/ml	40 µl of E	40 µl
H	0 µg/ml	40 µl of F	40 µl

A total of 200µl of Working Reagent (BCA protein assay reagent A/B diluted 50:1) was prepared for each aliquot of protein extract and BSA protein standard concentration. To each 5µl of protein lysate, 200µl of the Working Reagent was added and the samples were vortexed thoroughly on a shaker for 30 second. The tube was incubated at 37°C for 30 minutes in the incubator and then allowed to cool at room temperature. The A562 of the standards and protein lysates was then measured using a plate reader (BP 800, BioHit). A standard curve was prepared by plotting the blank-corrected measurement for each BSA standard against its concentration. The standard curve was then used to determine the protein concentration of each study sample.

2.8.3 TRAP PCR reaction set-up

Telomerase activity was measured using a quantitative TRAP assay (Paraskeva, Atzberger et al.1998). Bench-top surfaces and pipettes were cleaned with RNAse Zap (Ambion) in preparation for the assay. Samples to be analysed were thawed on ice and diluted to a final concentration of 200ng/µl in CHAPS lysis buffer. Stock solutions were immediately quick-frozen and stored at -80°C to prevent protein degradation. Reaction mixtures for each of the samples to be analysed were made up using the following components and volumes:

Component and volume of reaction mix:
5µl 10X TRAP reaction Buffer
1µl 50X dNTP Mix
1µl telomerase primer (TS primer) (0.1µg/µl) (5`-AATCCGTCGAGAGTT-3`)
1µl telomerase primer (ACX primer mix) (0.05µg/ml)(5`-GCGCGG (CTTACC) 3CTAACC-3`)
0.4µL Taq Polymerase
39.6µl dH2O
2µl protein samples
Total volume = 50µl

Reaction mixtures were thawed on ice to prevent protein degradation, vortexed and centrifuged briefly. Samples were assayed in triplicate and each assay run included a telomerase positive, negative and non-template control. As an additional negative control, 10µl of each target sample was heat-treated to inactivate the enzyme by incubating at 85°C for 10 minutes. The microtitre plate was then placed into the thermocycler block and PCR amplification carried out with the following reaction conditions. The reaction mixture was first incubated at 25°C for 20 minutes. PCR was then started at 95°C for 10 minutes, followed by a two-step PCR amplification of 35 cycles at 95°C for 30s and 60°C for 90s.

The 10% Native (non-denaturing) PAGE gel was made using the following ingredients:

10% Native (non-denaturing) PAGE gel ingredients:
32.2ml distilled water
12.5ml 40% Acrylamide mix (19:1 acrylamide/bisacrilamide) (Protogel EC890)
5ml 10X TBE
100µl 10%ammonium persulphate (APS) freshly made
75µl TEMED

The above formula will give a 10% gel that is poured into the gel glass plate. The gel glass plate was set up following the manufacturer`s protocol. The above gel was loaded immediately onto the gel tank, and left for 30 minutes to set with a separation comb in place.

2.8.4 PAGE-gel electrophoresis and data analysis

A total of 1µl of loading dye containing bromophenol blue and xylene cyanol (0.25% each in 50% glycerol/ 50mM EDTA) was added into each reaction tube. Samples were loaded with 25µl of the telomerase PCR assay on a 10% non-denaturing PAGE (no urea) in 0.5X TBE buffer. A 25bp DNA ladder (Lifetechnologies, CA, USA) by diluting the stock concentration 1:10 in dH2O (2µl DNA ladder, 17µl dH2O, 1µl loading dye).

We used extreme care to prevent sample carry-over into adjacent wells, which may produce false-positive results. For optimal interpretation of results, we loaded heat-treated and non-heat-treated samples in alternating lanes (i.e., extract 1+heat, extract 1-heat, extract 2+heat, etc.). The TSR8 quantitation control was added on the last lanes of the gel including CHAPS-only buffer.

All samples were run at 300volts until the xylene cyanol runs 70-75% the length of the gel. This took on average between 3 to 3.5 hours. The smallest telomerase product band should be 50bp and the S-IC internal control band is 36bp. After electrophoresis, we stained the gel with SYBR Green according to the manufacturer's instructions. For SYBR Green we diluted the stock solution 1:10,000 in deionized water. The gels were stained for 30 minutes at room temperature on a shaker set at low speed to prevent breakup of the gel (Figure 2.9).

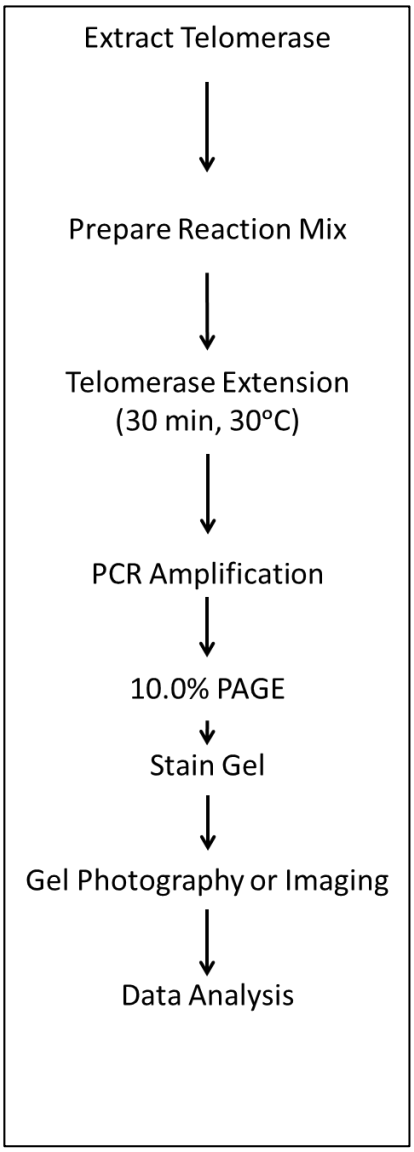

Figure 2-9. Workflow used for TRAP measurement.

2.8.5 Quantitation and data analysis using Image-Lab software

The Image-Lab software (Bio-rad) was used to quantify pixel intensities from the TRAP gels. We followed the manufacturer's guideline in estimating band intensity for this purpose. In brief, each lane was detected using the automated lane detection function and then adjusted to contain all samples in the gel. Each lane was then assessed for bands and band intensity using the automated function of the Image-Lab. Background correction was applied and the average background was subtracted from the intensity value. The intensity values for all bands were then summed up and the total sum of all bands in each lane used in the formula

to measure relative telomerase activity. The manufactures' guideline was followed in estimating the levels of telomerase activity in each sample.

$$Telomerase\ activty = \frac{(x-x_0)/c}{(r-r_0)/c_R} \times 100$$

Whereby,

x = product ladder bands from all samples including non-heat-treated

xo = heat-treated sample extracts

ro = 1X CHAPS lysis Buffer only control (primer-dimer/PCR contamination control)

r = TSR8 quantitation control (0.2 amole)

c = signal from the internal standard (S-IC) in non-heat-treated samples

cR = TSR8 quantitation control

2.9 C-Circle assay for detection of *A*lternative *L*engthening of *T*elomeres (ALT) activity

ALT^+ cancer cells have several characteristics that are unique and are not found telomerase-positive cancer or mortal cells. These unique characteristics make identification of ALT activity in cells particularly robust. They include, i) association of telomeric sequence with promyelocytic leukemia nuclear bodies (known as APBs), ii) heterogeneous telomeric lengths as a result of rolling mechanism such as rolling circle amplification (RCA), iii) recombination-dependant DNA replication, iv) low levels of ARTX protein activity, and v) circular c-rich single stranded DNA known as C-circle (CC). The levels of CC is measured through a two-step process: DNA amplification using phi29 DNA polymerase and nucleotide lacking dCTP followed by radio-labelled (P^{32}) probing and hybridization using $(CCCTAA)_3$ oligonucletoide.

2.9.1 Genomic DNA extraction

Total genomic DNA was extracted from cell pellets of various cell lines using Qiagen QIAmp DNA Mini Kit by following the manufacturer's guideline. This is a column-based technique

that does not require phenol-chloroform and DNA specifically binds to the QIAmp silica-based membrane while other contaminant from cell extract passes through. The washing steps removes all PCR contaminants such as divalent cations and proteins leaving pure gDNA. The detail step of DNA extraction is shown below:

1. Cell pellets were collected by spinning at 800g for five minutes.
2. The media is removed and cells are washed with 1ml of phosphate buffered saline (PBS) twice to remove any residual medium and proteins that could inhibit the action of DNA extraction mini kit. Cells were pelleted again at 800g for five minutes. Supernatant is removed carefully without disturbing the cell pellet.
3. Cell pellets are then suspended in 200µl of PBS. 20µl of protein K followed by 4µl of RNAse A. These ensure that RNAs and proteins are degraded in the cell pellets.
4. This is followed by the addition of 200µl of nuclear lysis solution (Buffer AL) and the samples were vortex for 15 seconds intermittently. It is important not to vortex the cells continuously as this may shear the gDNA.
5. The samples are then heated for 10 minutes at 56°C in a heating block.
6. Spin down the sample for ten second at 12000g to collect cellular debris.
7. Add 200µl of ethanol to precipitate the nucleic acid followed by a short spin for 10 seconds at 12000g.
8. The supernatant is then transferred into QIAmp column attached to a collection tube and spun down for 60 seconds at 8000g. The DNA is now attached to the silica-based membrane and the flow through is discarded.
9. The DNA is now washed with 500µl of solution AW1 and AW2 separately and spun down for 3 minutes seconds at 8000g in each wash. The flow through is discarded in each step.
10. Next new collection tube is placed and the column is spun down for additional 60 seconds at 14000g to remove any residual washing solution.

11. Finally DNA is eluted with 50µl of elution buffer (AE) that contained Tris-EDTA (10mM, pH 7.6) at room temperature for one minute. TE buffer ensures that the DNA is stable and not digested as elution in water can shear DNA for long-term storage. Then the sample is collected by centrifuging at 8000g for 1 minute in a new Eppendorf (1.5ml) tube with led.
12. Samples are frozen down at -80°C.

2.9.2 DNA quantification

The quality and quantity of extracted DNAs were measured using 1µl of total gDNA calibrated against the elution buffer using Nanodrop (lifetehcnologies). Table 2-4 below summarises the quality (A260/280) and quantity (ng/µl) of each sample.

Table 2-4. DNA concentration of all samples

Sample name	DNA concentration in (ng/µl)	DNA quality and purity (A260/280)
U2OS	147.5	1.88
HeLa	200.6	1.88
SKLU-1	182.1	1.85
G292	169.5	1.84
HCC1937	546.3	1.88
GM00893	50.4	1.86
GM13705	439.9	1.86
LY-R	464.4	1.87
LY-S	92.3	1.84
E14	146.5	1.84
408	322.4	1.86

2.9.3 C-circle amplification

The first step of the CC assay involves amplification of the C-circles utilising the RCA (Rolling Circular Amplification) of partially double-stranded C-circles by Φ29 DNA polymerase (NEB) is auto-primed by the partial G-strand ([TTAGGG]n) (from the leading strand of the DNA). DNA samples were diluted to 10ng/ul after quantification and 30ng of DNA was used in the amplification using the following reaction:

Stock concentration	Volume (µl)	Final concentration
1M DTT	0.8	4mM
10x Φ29 buffer	2.0	1x Conc
10mg/ml BSA	0.4	0.2 mg/ml
10% Tween	0.2	0.1%
1mM dATP/dTTP/dCTP/dGTP	0.8	0.1mM
Φ29 DNA polymerase (10,000 U/ml)	1.5	15 U
Nuclease-Free water	4.3	
Total volume	10ul	

10ul of the above reaction mixture is then added to 10ul volume containing 30ng of DNA. The samples were then incubated at 30°C for 8hrs followed by 65°C for 20 minutes. Samples were immediately slot-blotted or stored at -20°C.

2.9.4 Slot-blotting

Samples were slot-blotted using Amersham Biosciences Slot blot filtration manifolds. In brief, samples were diluted with 40µl of 2xSSC and mixed well. The slot-blot apparatus were assembled using 1x nitrocellulose membrane (GE Healthcare) and 1x Whatman filter paper pre-soaked in 2xSSC (see figure xx). Next, the suction unit was turned on to full and the samples were added gently on each slot. The location of each slots were recorded. Care was taken not to touch the nitrocellulose membrane. Samples were vacuumed for two minutes and laid with 100µl of 2xSSC to wash remaining sample. Following which the apparatus was dismantled and the membrane allowed to dry. The membrane was immediately cross-linked using UV cross-linker (GE Healthcare) at 1,200J twice.

2.9.5 Hybridization with P^{32}-labelled telomeric probe

2.9.5.1 Preparation of P^{32} probe

The c-rich telomere specific $(CCCTAA)_3$ (Thermo Fisher) oligonucleotide was end-labelled with ATP [γ-^{32}P] (Perking Elmer) using DNA 5' end labelling system (Promega) as follows:

Stock concentration	Volume
Oligonucleotide 100µM	5µl
T4 polynucleotide kinase buffer 10x	1µl
T4 polynucleotide kinase enzyme	1µl
ATP [γ-^{32}P] 3000Ci/mmol 10mCi/ml	3µl
Total volume	10µl

- Incubate the above mixture at 37°C for ten minutes in water bath
- Stop the reaction by adding 1µl of 0.5M EDTA
- Add 40µl of saline TE (STE) buffer to the above 10µl probe buffer

2.9.5.2 Purification of P^{32} probe

The newly prepared probe must be washed to remove any unbound nucleotide or probe using column base chromatography (Perkin Elmer). The full protocols were as follows:

- Re-suspend the resin in the column by vortexing for few seconds
- Twist off the bottom cap of the column and spun down to remove solutions from the resin at 735xg for 1 minute
- Immediately add the probe mix samples (50µl in total volume) to the resin before resin bed became dried
- The column is placed into a new clean 1.5ml Eppendorf collection tube and the column spun down for 2 minutes at 735xg
- The purified probe is then stored at -20°C

2.9.5.3 Hybridization

The nitrocellulose membrane containing slot-blotted CC assay amplified samples was placed in a glass hybridization bottle and incubated with 10ml of pre-warmed Hybridization

buffer (PerfectHyb Plus, Sigma-Aldrich) at 37°C for 15 minutes to block the membrane for unspecific binding. Finally, the freshly prepared P^{32}-labelled C-rich telomeric probe was added to the Hybridization bottle and allowed to hybridize overnight at 37°C.

The next day the membrane was washed with high stringency wash buffer containing 0.5xSSC and 0.1%SDS at 37°C with shaking for three-times. After washing the membrane was wrapped in an hybridization bag and exposed overnight onto x-ray film in dark. The exposed x-ray film was then developed using automated system (Xograph) and images were scanned for analysis.

2.9.5.4 Image analysis of CC assay (Quantification)

Each X-ray film containing developed images of the CC assay was scanned and Image J software (NIH) was used to analyse slot-blot pixel intensity (Figure 2.10).

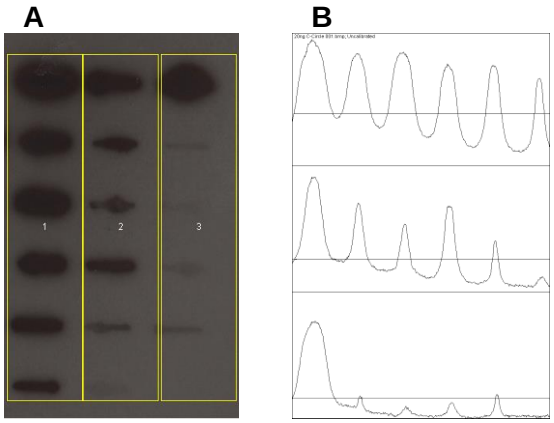

Figure 2-10. CC quantification using Image J.

A) Each X-ray film was scanned and each band were automatically recognised using the Image J software. **B)** The band intensity is then generated and the area under each peak is used to generate intensity value. This value is used and normalised to U2OS for human samples or E14 for the mouse cells.

The Microsoft Excel was used to analyse data and generate mean CC activity for each sample.

2.10 Graphical display and Statistical Analysis

Three major types of graphical representation used to display the data. These are:

- Bar charts and line graphs. In all bar charts we used either standard deviation (SD) or standard error of mean (SEM) to display variation among the data.
- Scatter plots. Used to display individual data point across samples. Average is shown using a green bar in all cases. No SD or SEM is displayed in these types of graphs since the spread of data can be visualised by the spread of the data represented by dots, but SD were used separately for t-test analysis.
- Whisker box-plot. In some cases we used the box-plot to display the spread of data as well as the mini/max. The line across the box displays the median. SD was used separately to perform t-test.

We only used the student's *t*-test to perform full statistical analysis. We used the 95% confidence interval as our cut off point with α set at 0.05 and where indicated the exact p value is displayed. In some cases the significance of each compared data is represented using * ($P < 0.05$), ** ($P < 0.001$) or *** ($P < 0.0001$). The latter means the difference between the mean is highly significant.

All statistical analysis or graphical drawing was performed on GraphPad PRISM 6 version. In some rare cases we used Microsoft Excel 2007 software.

CHAPTER 3

3 Analysis of Telomere Function in *BRCA1* Defective Human Cell Lines

3.1 Introduction

BRCA1 plays major roles in DNA damage and repair through NHEJ and HR (Moynahan et al., 1999, Davalos and Campisi, 2003, Cao et al., 2003, Ohta et al., 2011). BRCA1 is recruited to the DNA damage sites through the damage sensor, the MRN complex, and it provides a scaffold for and recruits other proteins involved in the DNA DSB repair pathway (See Chapter 1 for details). BRCA1 is also involved as a regulator of key effectors in the G2/M phases of the cell cycle by with the final result of activating the checkpoint kinase 1 (CHK1) prior to the onset of mitosis (Yarden et al., 2002). The earliest evidence linking DNA damage response and *BRCA1* was in a research pertaining to *Brca1*-defecient fibroblasts

and tumours, which revealed evidence of extensive genomic instability, such as chromosomal aberrations, centrosomal amplification and aneuploidy (Tirkkonen et al., 1997, Xu et al., 1999b, Weaver et al., 2002). The co-localisation of BRCA1 with the various DNA damage response factors, and involvement of BRCA1 in DNA DSB repair via HR and NHEJ is well documented (Powell and Kachnic, 2003). For example, BRCA1 role in NHEJ is thought to include end-resection and interaction with Ku and DNA-PKcs. These and other proteins (discussed in detail in Chapter 1) are also located at telomeres and their absence leads to telomere dysfunction as reported previously (for a review of DNA damage response proteins at telomeres see Slijepcevic, 2006). Therefore, BRCA1 is involved in the genome stability maintenance through its interaction with DNA damage response proteins. Furthermore, BRCA1 is recognised as an important tumour suppressor as BRCA1 defects are associated with familial breast and ovarian cancers (Claus et al., 1996, Ford et al., 1994, Whittemore et al., 1997, Jiang and Greenberg, 2015). Recently published work has demonstrated that a BRCA1 mutation in immortalised human primary epithelial cell creates halpoinsufficiency leading to premature senescence with increased genomic instability, as well as increased rate of telomere erosion (Sedic et al., 2015), further highlighting the role of BRCA1 in cellular senescence, genome stability and telomere maintenance. Interestingly, BRCA1 is shown to play important role in response to DNA damage induced by IR. For example, cells from *BRCA1* mutation carriers show increased sensitivity to IR, suggesting that genomic instability might occur even when a single copy of *BRCA1* is mutated (Foray et al., 1999, Trenz et al., 2002, Sedic et al., 2015). The breast cancer cell line, HCC1937, containing defects in both *BRCA1* alleles, is sensitive to IR (Abbott et al., 1999), it shows karyotypic alterations and loss of heterozygosity at many loci (Tomlinson et al., 1998).

The earliest evidence linking BRCA1 to telomere maintenance was, however, provided by McPherson et al. (2004) after examination of Brca1 and Chk2 in murine tumourigenesis models. Results showed elevated frequencies of end-to-end chromosome fusion due to Brca1 disruption - an observation pointing towards the role of BRCA1 in telomere capping

function (McPherson et al., 2004). Further evidence was provided by (Al-Wahiby and Slijepcevic, 2005) in the study of human cells lacking functional BRCA1 resulting in elevated levels of end-to-end chromosomal fusions (a phenotypic hallmark of dysfunctional telomeres due to loss of capping function). McPherson et al, provided more robust evidence for the involvement of BRCA1 in telomere maintenance using *Brca1*$^{-/-}$ murine T-cells. These cells were characterized by the presence of telomeric fusions (McPherson et al., 2006). Similarly, knockdown of BRCA1 in the breast adenocarcinoma cell line, MCF7, and the non-tumorigenic breast epithelial cell line, MCF10A, caused increased frequencies of anaphase-bridge due to telomere dysfunction (Cabuy et al., 2008). Interestingly, BRCA1 interacts with TRF1 and TRF2 at telomeres (Ballal et al., 2009). BRCA1 has been implicated in regulating telomerase (Xiong et al., 2003) most likely through acting as its negative-regulator (Ballal et al., 2009). Recent evidence indicates that BRCA1, through its interacting partner CtIP, promotes telomere fusion via A-NHEJ in an ATM-independent telomere damage-signalling manner in mouse embryonic fibroblast (MEFs) lacking functional TRF2 (Badie et al., 2015). This suggests that BRCA1 may mediate telomere repair through A-NHEJ in telomerase-positive cells through the MRN complex (Badie et al., 2015). It must be noted that uncapped telomeres are recognised by DNA damage sensing mechanism as broken ends and therefore mediate end-joining through the NHEJ mechanism; either through classical NHEJ (c-NHEJ) involving KU70/80 and LIG4 (Celli and de Lange, 2005, Celli et al., 2006) or the alternative NHEJ (A-NHEJ) involving PARP1 and LIG3 (Rai et al., 2010, Sfeir and de Lange, 2012).

The above observations strongly implicate BRCA1 in telomere maintenance through the conventional telomerase-based mechanisms. Given the role of BRCA1 in HR it is possible that it may play a role in the ALT pathway. It is known that BRCA1 interacts with APB (ALT associated PML bodies) in ALT positive cells (Wu et al., 2003) and that BRCA1 recruits recQ-like helicases WRN and BLM to facilitate intra-strand cross-link repair and DSB repair at telomeres (Cheng et al., 2006) (Gocha et al., 2014). The activities of BRCA1 and BLM at

telomeres has only been recognised recently (Acharya et al., 2014). BRCA1 is required for recombination proteins to promote strand processing and invasion, and to form recombination intermediates, and this process requires BLM during G2 phase of the cell cycle (Acharya et al., 2014). This role is different from the role played by the BRCA1-RAD50 complex found at the S-phase (Zhong et al., 1999) (Davalos and Campisi, 2003). Although, BRCA1 may have important functional role in the ALT-positive cells (which utilise HR for telomere length homeostasis) this is not well understood.

In this chapter, we set out to investigate the role of BRCA1 in HR mediated telomeric recombination through measuring levels of telomere-sister chromatid exchanges (T-SCE) in cell lines from BRCA1 mutation carriers. Moreover, we aim to characterise the consequence of BRCA1 defect on telomere length and assess the role of BRCA1 defect on telomere function through measuring frequencies of radiation-induced telomere dysfunction induced foci (TIF) as well as measuring the role of BRCA1 defect on genome instability and chromosomal aberrations following exposures to IR.

3.2 Results

3.2.1 Cell lines and rationale

We used two human lymphoblastoid *BRCA1* defective cell lines (*BRCA1+/-*), GM13705 and GM14090, obtained from *BRCA1* mutation carriers and one control cell line, GM00893 (*BRCA1* +/+). The GM13705 cell line had a four base-pair deletion at positions 3875 (3875 del 4) in exon 11 (frameshift mutation), resulting in a premature termination at codon 1252 (http://ccr.coriell.org) (Coriell 2009). The cell line, GM14090 had double base-pair deletion at position 185 (185delAG) in exon 3 (frameshift mutation), resulting in a premature termination at codon 37 (http://ccr.coriell.org) (Coriell 2009). Both cell lines have been purchased form Coriell Cell Repositories. The GM00893 cell line originated from a normal individual, and was used as BRCA1 (WT) control. Furthermore, LY-R and LY-S mouse cell lines were used as calibration standards for telomere length measurements.

3.2.2 Telomere sister chromatid exchange in *BRCA1* lymphoblastoid cell lines

One of the frequent events occurring in eukaryotic chromosomes is the exchange of genetic/chromosomal material between two sister chromatids known as the sister chromatid exchange (SCE) (Wolff, 1977). This process occurs during DNA replication (S phase of the cell cycle) and it is dependent on HR (Bailey et al., 2004b). The technique known as CO-FISH is capable of identifying SCEs occurring specifically within telomeres termed telomere SCEs (T-SCEs). It is well established that T-SCEs constitute one of the markers of the ALT pathway. This may serve as a means of recombination-based telomere length maintenance. In addition, a high level of T-SCEs has been associated with the ALT phenotype (Bailey et al., 2004b, Bechter et al., 2004b, Londono-Vallejo et al., 2004). However, high T-SCE frequencies have also been reported in some telomerase positive cells (Vera et al., 2008).

One of the aims of this chapter is to investigate whether human lymphoblastoid cell lines that have BRCA1 mutations exhibit altered recombination rates at telomeres. Consequently, the frequencies of T-SCEs in the above lymphoblastoid cell lines were assessed by CO-FISH (Figure 3.1). A total of 100 metaphase cells per cell line were analysed by CO-FISH to delineate the number of T-SCE events (Figure 3.2)**.** The experiment was performed twice to ensure reproducibility and precision of results. Statistical analysis revealed a significant increase ($P<0.001$) in T-SCE levels of the BRCA1 defective cell lines (GM13705 and GM 14090) in comparison with the control (GM 00893) (Figure 3.2)**.** Our results suggest that T-SCE occur more frequently in the *BRCA1* defective cells than the normal cells, thus implicating BRCA1 in ALT mechanism in these cells.

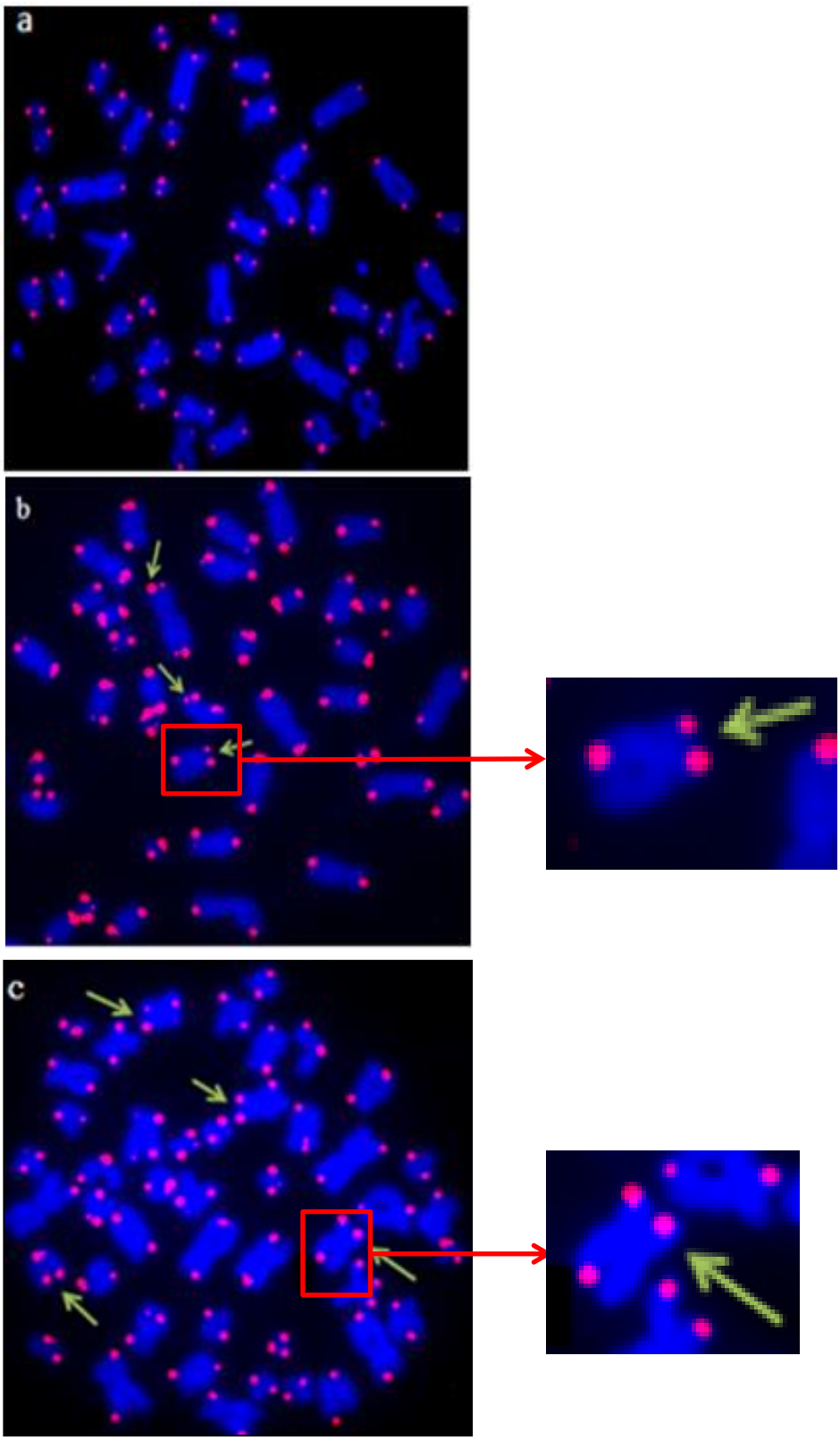

Figure 3-1. Examples of T-SCEs in lymphoblastoid cell lines after CO-FISH.

a) A metaphase spread from the GM00893 control cell line with no T-SCEs. **b)** GM 13705, and **c)** GM 14090 BRCA1 defective cell lines showed multiple T-SCE events indicated by arrows.

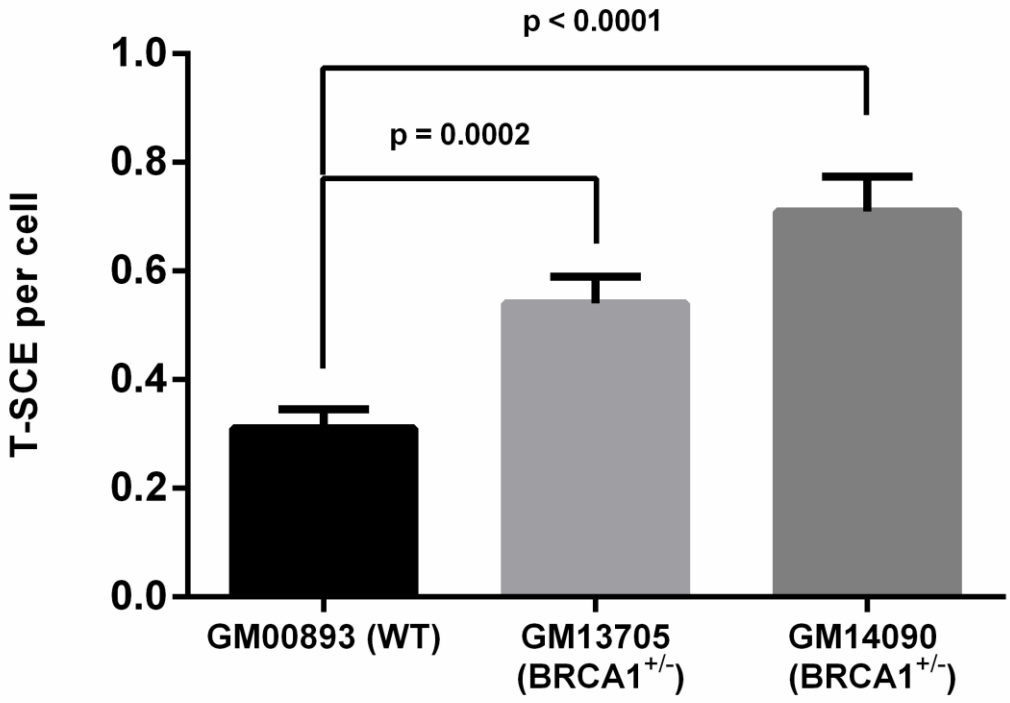

Figure 3-2. T-SCE analysis of human lymphoblastoid cells by CO-FISH.

Both BRCA1 defective cell lines showed a significant increase in T-SCE levels compared to the control cell line. Error bars indicate standard error of the mean (SEM). T-test performed for all statistical analysis.

3.2.3 Telomere length analysis in *BRCA1* lymphoblastoid cell lines

To measure the telomere length in our set of cell lines we used the IQ-FISH method which measures average telomere length in interphase cells. The method was described in a PhD thesis by another student from our laboratory (Ojani 2013). A total of 50 interphase cells per cell line were analysed and the mean telomere fluorescence intensity was determined for each cell line. Representative images of telomeres in interphase cells after this procedure are shown in Figures 3.3 and 3.4. The integral part of the method is the use of two mouse lymphoma cell lines, LY-R and LY-S, as calibration standards (Figure 3.5). These cell lines have stable telomere lengths of 49kb and 7kb, respectively (McIlrath et al., 2001) (Cabuy et al., 2004, Yasaei and Slijepcevic, 2010). Using the values of telomere fluorescence obtained for LY-R and LY-S cells (Figure 3.5 A and B) corrected calibrated fluorescence (CCFL) was calculated for the three human lymphoblastoid cell lines (Figure 3.5C) BRCA1 defective cell

lines (GM13705 and GM14090) showed significantly decreased telomeric fluorescence compared to the control GM00893 cell line (Figure 3.5).

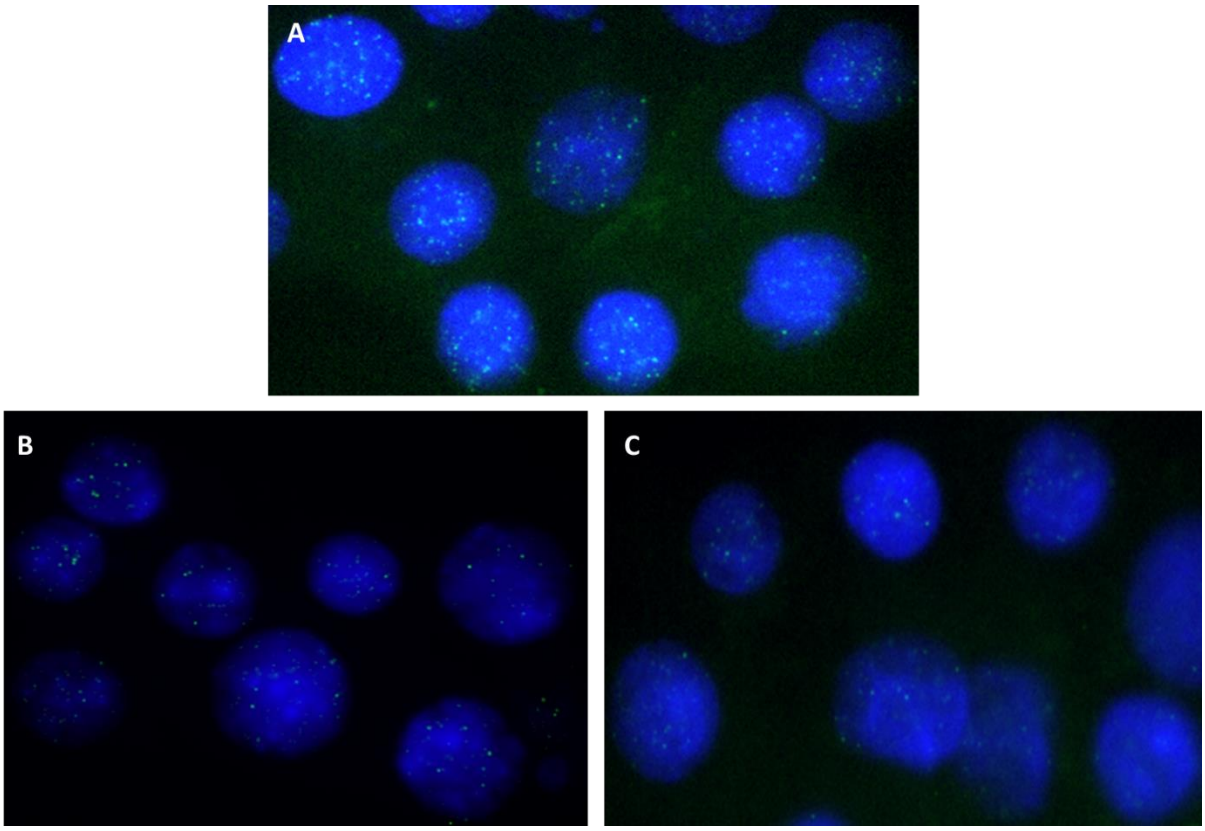

Figure 3-3. Representative examples of telomere FISH in the interphase nuclei of human lymphoblastoid cell lines.

A) GM00893 BRCA1 WT cell line (used as control). **B)** GM13705 BRCA$^{+/-}$. **C)** GM14090 BRCA1$^{+/-}$. In all cases telomere FISH probe is tagged with FITC (green) and the cell nuclei is counterstained with DAPI (blue).

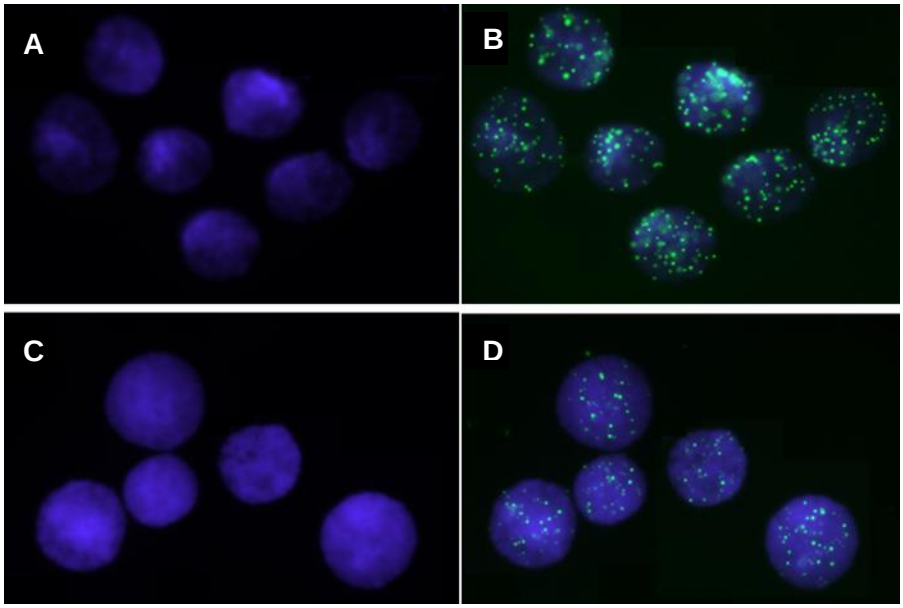

Figure 3-4. Representative examples of telomere FISH in mouse LY-R (A and B) LY-S cells (C and D). Blue: nuclei stained with DAPI (A and C). Green: telomere staining by the FITC labelled probe (B and D).

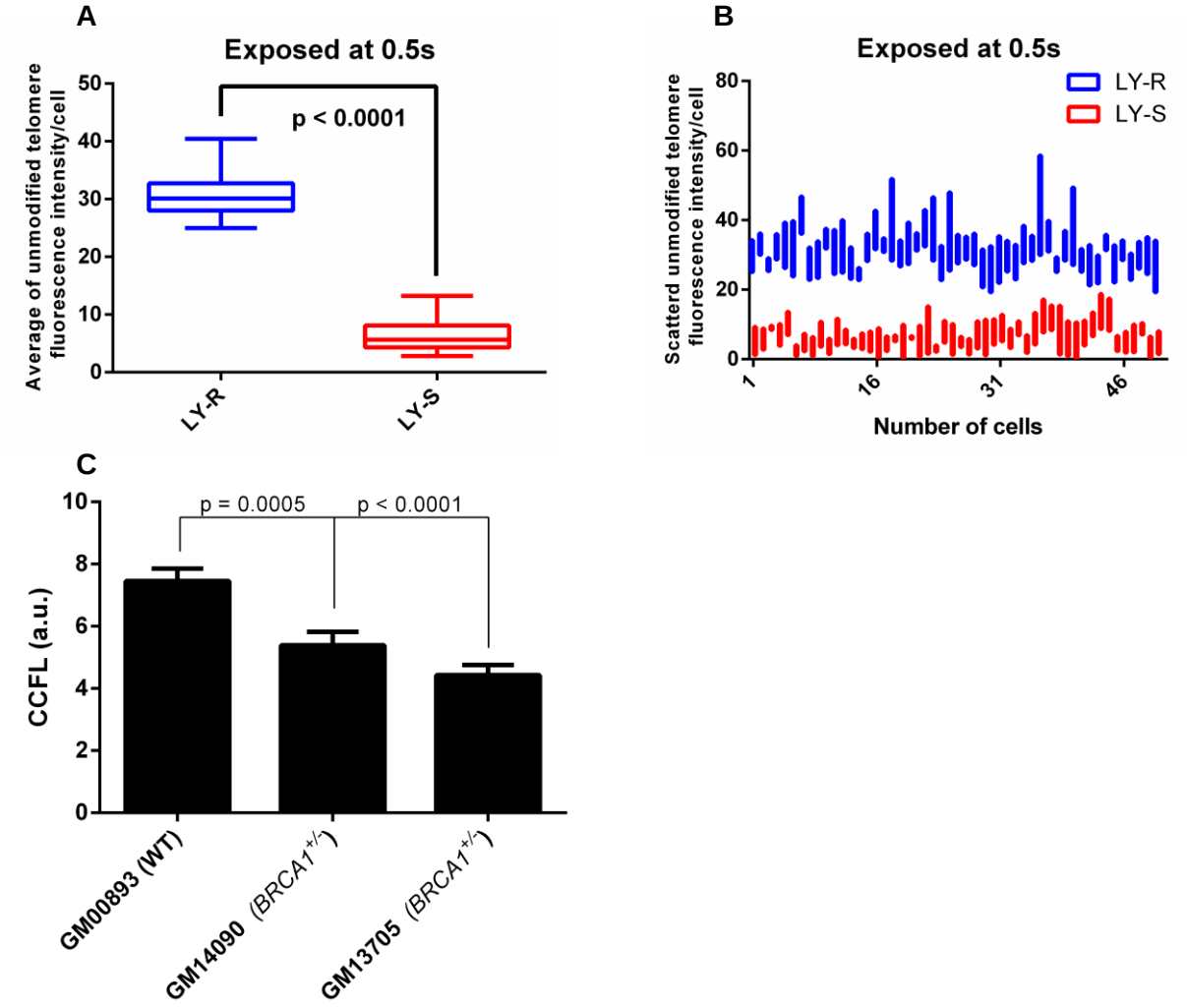

Figure 3-5. Mean values of telomere fluorescence measured using IQ-FISH.

A) Mean telomere fluorescence intensity from unmodified signals from LY-R and LY-S mouse lymphoma cell lines used here as calibration standards. **B)** A scattered plot of unmodified fluorescence intensity from 50 cells/cell line. **C)** *C*orrected *C*alibrated *FL*uorescence (CCFL) of mean telomere length from the BRCA1 WT (GM00893) and two BRCA1 mutant cell lines, GM14090 and GM 13705. Error bars represent SE. Figures A and B are based on the analysis of 50 cell nuclei/cell line performed in five independent experiments to ensure consistency. All measurements are done using the exposure of 0.5 second (s). Figure C is based on the analysis of 100 nuclei/cell line in two independent experiments. T-test used for statistical comparison.

3.2.4 Cytogenetic analysis of chromosomal aberrations in human lymphoblastoid BRCA1 defective cell lines

It is known that genes participating in genome stability maintenance could also be affecting the function of telomeres. For instance, Ku and DNA-PKcs that take part in DNA DSB repair are situated at telomeres (Riha et al., 2006, Wang et al., 2009, Ruis et al., 2008, Indiviglio and Bertuch, 2009). Some other DDR proteins, such as ATM, NBSI, PARP and FANCA are also implicated in telomere maintenance (Cabuy et al., 2004). Since genes encoding the above proteins are also involved in cellular response to IR, we refer to the family of these

genes as TERAGENE (Telomere and Radiosensitivity Gene Network) (Cabuy et al., 2004). Genes encoding RAD54, RAD51D and PARP2 are considered the most recent additions to the TERAGENE family (Jaco et al., 2003, Dantzer et al., 2004, Tarsounas et al., 2004a). Research suggests that the TERAGENE family will indeed grow further and that BRCA1 is a TERAGENE candidate (Al-Wahiby and Slijepcevic, 2005). Consistent with this notion, BRCA1 deficient cells show sensitivity to IR (Shen et al., 1998, Foray et al., 1999) (Abbott et al., 1999) (Trenz et al., 2002), while mouse cells with targeted truncation in exon 11 of *BRCA1* show dicentric chromosomes (Xu et al., 1999b, Weaver et al., 2002), which possibly result from end-to-end chromosome fusions or telomeric fusions. That, in itself, represents a signature of telomere dysfunction. Furthermore, higher levels of end-to-end chromosome fusions are observed in BRCA1$^{-/-}$ P53$^{-/-}$ mouse T-cells in comparison with cells from P53$^{-/-}$ mice (McPherson et al., 2004). Therefore, we wanted to examine response to IR in our set of cell lines and determine the involvement of telomeres in this process.

3.2.5 Chromosomal abnormalities in the BRCA1 defective human cells – the G1 assay

We started by analysing chromosomal abnormalities in G1 phase of the cell cycle after exposure to 0.5 Gy, 1.0 Gy and 2.0 Gy of gamma radiation. Representative images of radiation induced chromosomal aberrations in G1 phase (dicentric chromosomes) are shown in Figure 3.6.

A total of 100 metaphases per cell line were analysed to examine the frequencies of spontaneous and induced chromosomal abnormalities in each cell line. The results obtained showed that the spontaneous chromosomal abnormalities as well as the radiation induced levels of chromosomal abnormalities were significantly higher ($p<0.05$, $p<0.01$, and $p<0.001$) in BRCA1 deficient cell lines (GM14090 and GM13705) compared to the control cell line (GM00893) (Figure 3.7). This observation indicates that BRCA1 defective cells have a defect

in DSB as radiation induced chromosomal aberrations result from IR induced DSBs (McPherson et al., 2006, Cabuy et al., 2008).

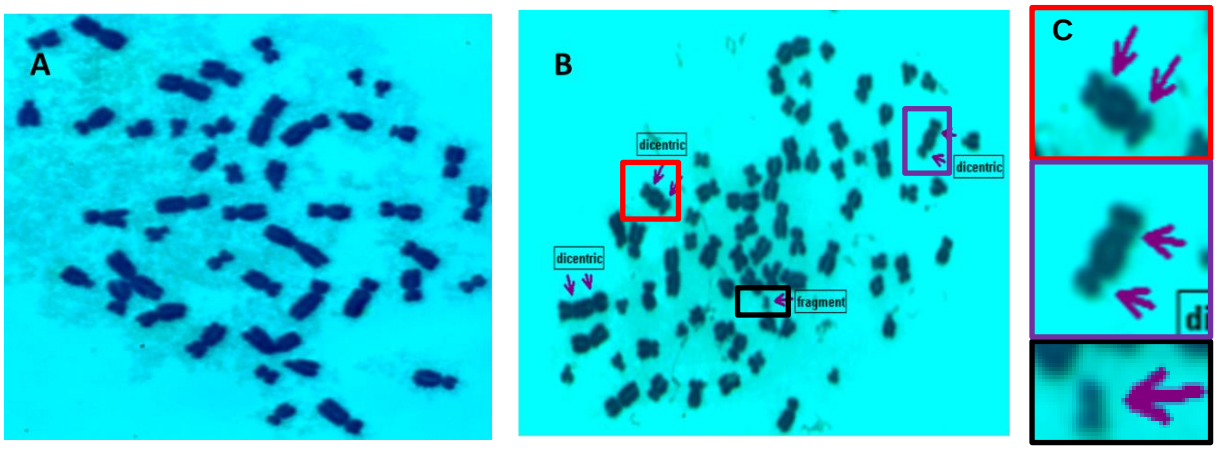

Figure 3-6. Representative example of radiation-induced CA in G1 from the BRCA1 defective human cells.

A) Un-irradiated metaphase cells of GM14090 stained with Giemsa. **B)** Examples of dicentric chromosomes (resulting from end-to-end chromosome fusions) and chromosome fragments in GM14090 shows with pink arrows, after exposure with 2.0Gy of gamma radiation, **C)** Enlarged examples of dicentric (red and purple boxes) and chromosome fragment (black box).

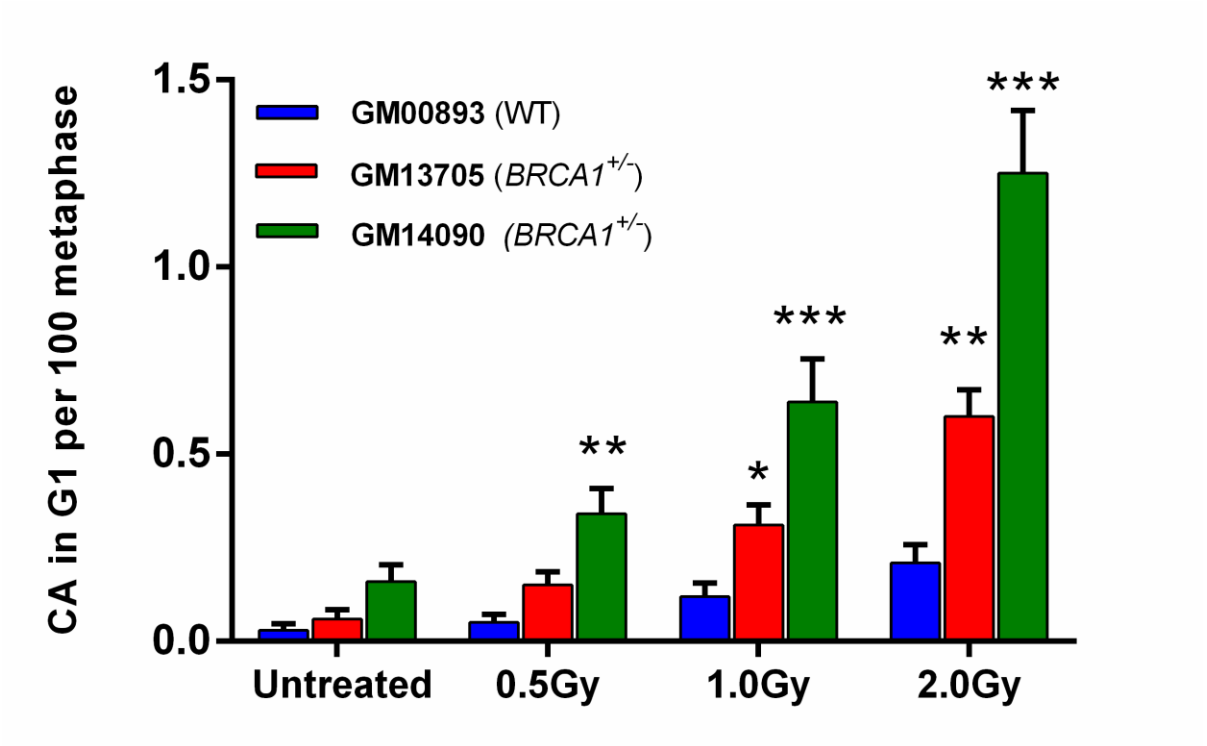

Figure 3-7. Frequencies of chromosomal abnormalities in three human cell lines after exposure to various doses of gamma radiation.

The total number of chromosomal aberrations (dicentric chromosomes, fragments and ring chromosome) are shown above from a total of 100 metaphases/cell line/dose. Each analysis is based on at least two independent experiments. Error bars represent SEM. *P<0.05, **P<0.01, and ***P<0.001.

3.2.6 Chromosomal abnormalities in the BRCA1 defective human cells – the G2 assay

In order to assess chromatid damage following exposure to IR we performed the so-called G2 assay, which captures only chromosomal damage induced in the G2 phase (Terzoudi et al., 2009, Hatzi et al., 2009).

Cells have been exposed to a single dose of 0.5 Gy and a total of 100 metaphase cells/sample were analysed 1.5 hours, 3 hours and 4 hours after exposure to gamma-rays (Figure 3.9). The average frequencies of chromatid breaks and gaps were significantly higher ($P<0.05$, $P<0.01$, and $P<0.001$) in the *BRCA1* defective cell lines (GM13705 and GM14090) than in the control cell line (GM00893) (Figure 3.8). The persistence of chromatid damage in the *BRCA1* defective cells after 0.5 Gy gamma-irradiation suggests a deficiency or imbalance in DNA repair or processing of the radiation- induced DNA DSBs. In other words, DNA damage during induced in G2 is potentially irreparable suggesting a deficiency or deficiencies in DNA repair which results in the enhanced radiosensitivity and cancer proneness characterizing *BRCA1* gene carriers. Representative examples of IR induced chromatid breaks are shown in Figure 3.9.

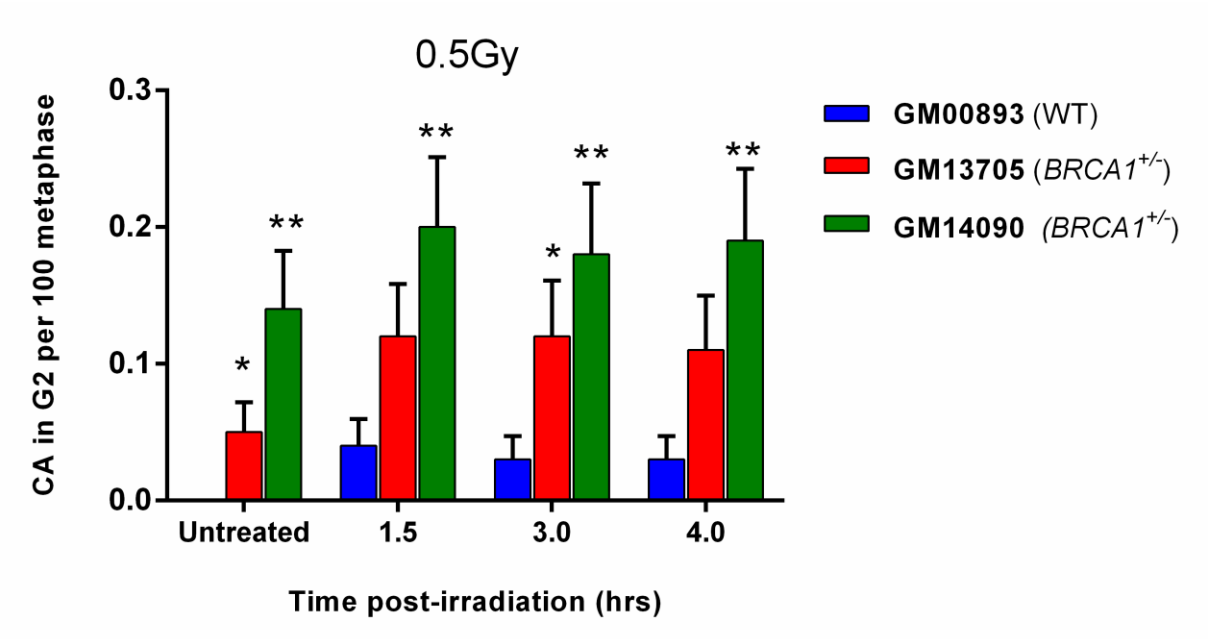

Figure 3-8. Frequencies of radiation induced chromatid breaks and gaps (G2 assay) in the BRCA1 defective cell lines (GM13705 and GM14090) and the control cell line (GM00893).

*=P<0.05, **=P<0.01, ***=P<0.001, Error bars represent SEM.

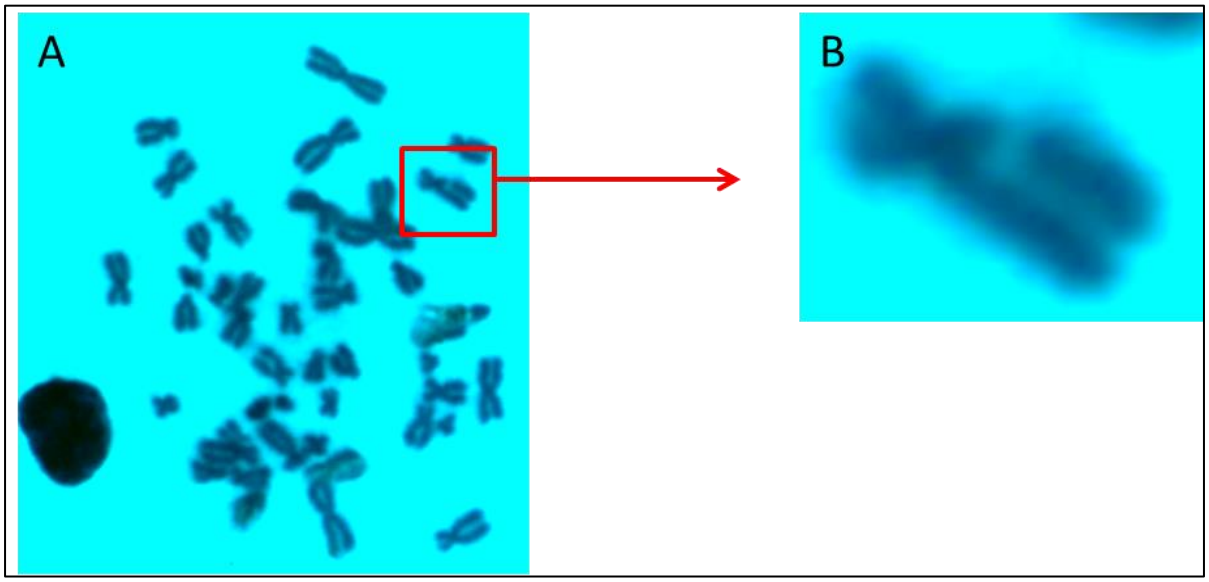

Figure 3-9. An example of chromosomal abnormalities in the G2 phase of the cell cycle in a human lymphoblastoid cell line.

A) Chromatid break in BRCA1 defective lymphoblastoid cell line GM14090, **B)** Enlarged image from A.

3.2.7 Establishment of micronucleus assay for assessing chromosome damage in BRCA1 defective cell lines

One of the most important events in carcinogenesis is chromosomal damage that occurs via DNA damage (DSBs) at the chromosome level. Therefore, investigating DNA damage at the

chromosome level is an essential part of genetic toxicology. The micronucleus assays come into view as one of the approved methods for estimating chromosome damage. This assay is important due to its ability to detect chromosome loss, chromosome breakage and chromosome rearrangement (nucleoplasmic bridges). The technique is now applied to various cell types for population monitoring of genetic damage, screening of chemicals for genotoxic potential and for specific purposes, such as the prediction of the radiosensitivity of tumours and the inter-individual variation in radiosensitivity (Fenech, 2000). Initially, several parameters were analysed to establish the optimal experimental conditions for using micronuclei tests to determine the level of chromosomal damage after exposure to gamma radiation (it is important to note that this test is not used routinely in our laboratory, hence we need to ensure that it will work in our hands consistently).

First, multiple flasks were prepared for each cell line to determine the optimal concentration of Cyt-B (3µg/ml or 6µg/ml) and optimal harvesting time (24 h or 48 h) after Cyt-B treatment. After Giemsa staining, the microscope analysis revealed that the optimal bi-nucleated cells and visible cytoplasm formed after 48hrs with the optimal concentration of Cyt-B being 6µg/ml (Figure 3.10). Since these results were consistent repeatedly we used the above concentration and timing in subsequent experiments.

A total of 500 bi-nucleated cells were scored to determine the presence or absence of MN in all cell lines after exposure to 0.5Gy, 1.0Gy, 2.0Gy and 4.0Gy of gamma rays. We observed a difference in spontaneous MN frequency between cell lines (Figure 3.11). Surprisingly, the amount of IR-induced MN was not particularly high at higher doses as reported in the literature (Slavotinek et al., 1993, Stopper and Lutz, 2002). This could be due to our inexperience with the methodology. Nevertheless, statistical analysis revealed that no significant difference in mean MN frequency was observed between untreated cells (GM00893, GM13705, and GM14090) and low dose rate (0.5Gy) (Figure 3.11 B) whereas at higher doses the difference was significant.

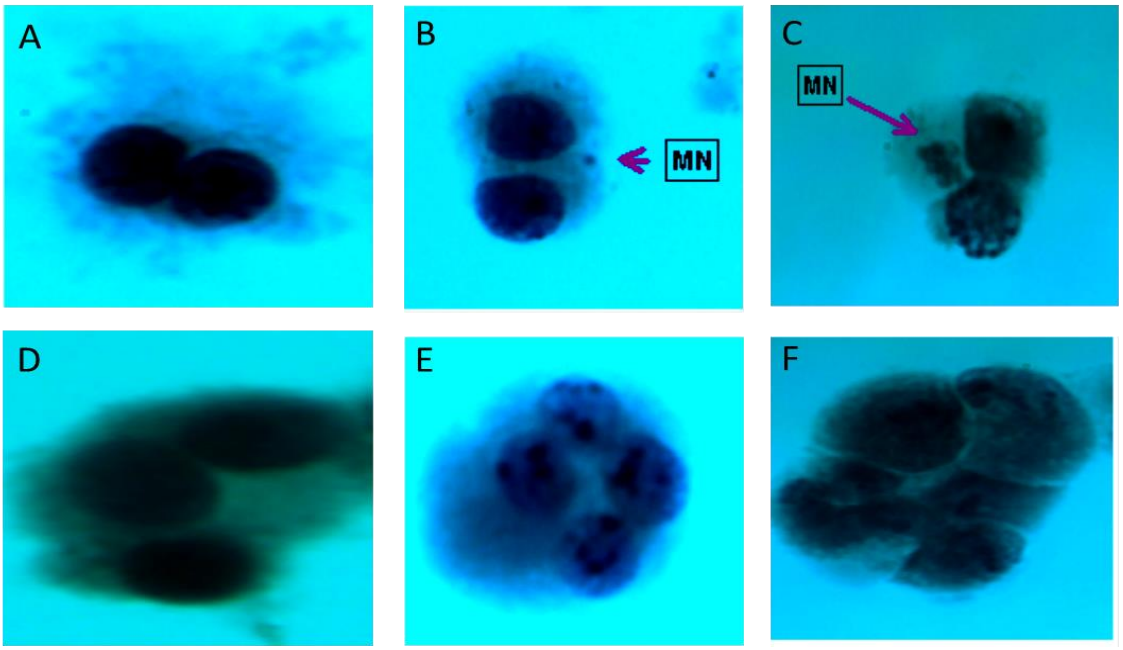

Figure 3-10. Analysis of binucleated cells in *BRCA1* human lymphoblastoid cell lines.

A) a normal binucleated cell after the cytokinesis block MN assay; **B)** bionucleated cell containing one MN; **C)** a binucleated cell with a group of MN; **D** and **E)** tri- and quadrinuclear cells; **F)** multinucleated cell.

A

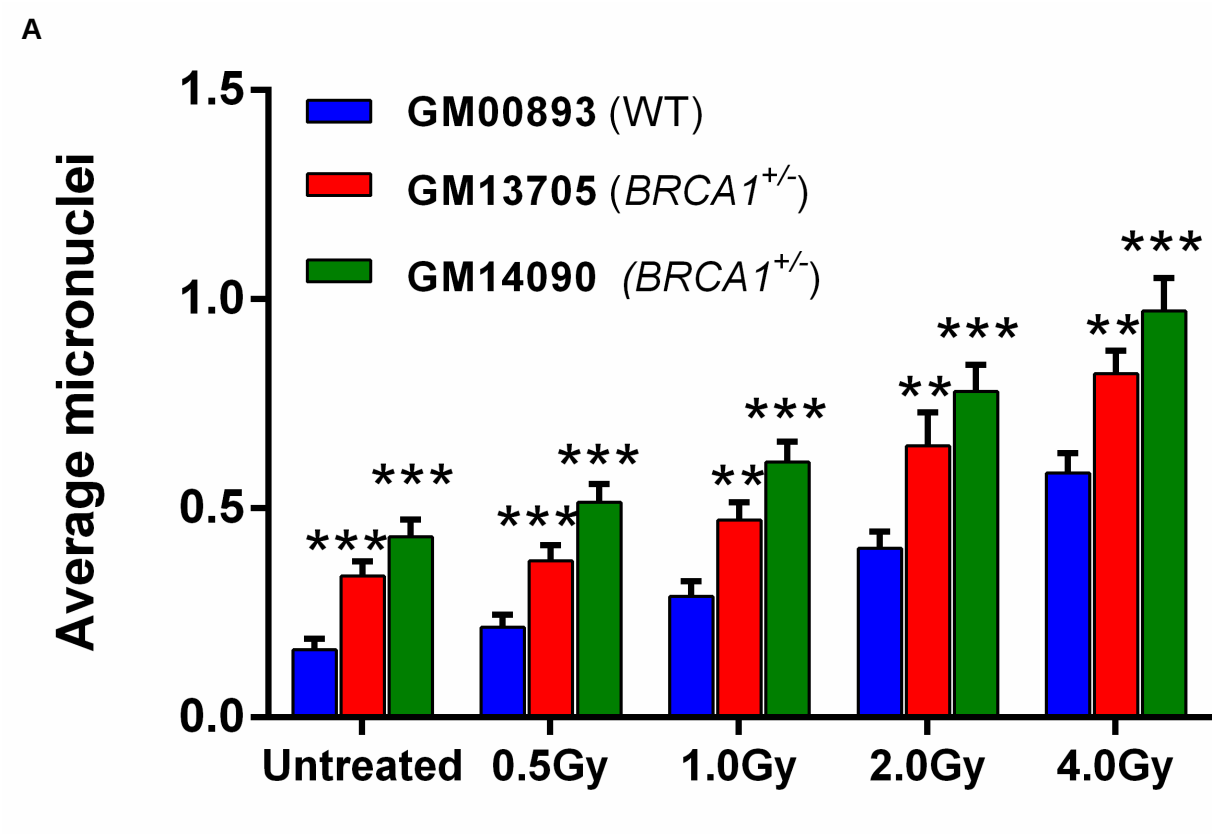

B

	0.5Gy *MN/cell*	1.0Gy *MN/cell*	2.0Gy *MN/cell*	4.0Gy *MN/cell*
GM00893 (WT)	0.216 (p=0.167)	0.290 (p=0.0038)	0.404 (p=4.85E-07)	0.584 (p=2.86E-14)
GM13705 (BRCA1$^{+/-}$)	0.374 (p=0.482)	0.472 (p=0.015)	0.65 (p=0.0003)	0.822 (p=1.96E-13)
GM14090 (BRCA1$^{+/-}$)	0.514 (p=0.173)	0.61 (p=0.0056)	0.78 (p=4.26E-06)	0.972 (1.69E-09)

Figure 3-11. Mean frequency of micronuclei in un-irradiated and irradiated cell lines.

A) Graph showing average MN per cell in untreated and irradiated cells. **B)** T-test analysis comparing the untreated with irradiated. The were no significant differences between the untreated MN frequency per cell and 0.5Gy IR in all three samples. Error bar represent SEM. **=P<0.01, ***=P<0.001. T-test used in all statistical comparison.

3.2.8 Immunofluorescence analysis of γ-H2AX in human lymphoblastoid cell lines

3.2.8.1 Analysis of γ-H2AX kinetics in human lymphoblastoid cell lines

In order to confirm cytological results at the more sophisticated level we examined IR induced DNA damage by measuring γ-H2AX levels. Frequencies of spontaneous DNA damage foci were higher in BRCA1 defective cell lines (Figure 3.12 A). All normal cell lines usually show some DNA damage foci. In our case the normal line had on average 2 foci/cell, whereas BRCA1 defective lines showed ~ 4-5 foci/cell (Figure 3.12 A). We then exposed cells to 1.0 Gy of gamma rays and quantified IR induced DNA damage foci at several time

intervals post-exposure (Figure 3.12 B). Statistical analysis shown in the Figure 3.12 C suggests persistence of IR induced DNA damage in BRCA1 defective lines relative to the control line. This observation is consistent with the notion that BRCA1 deficiency causes radiosensitivity due to ineffective repair processes.

Representative examples of IR-induced DNA damage foci are shown in Figure 3.13.

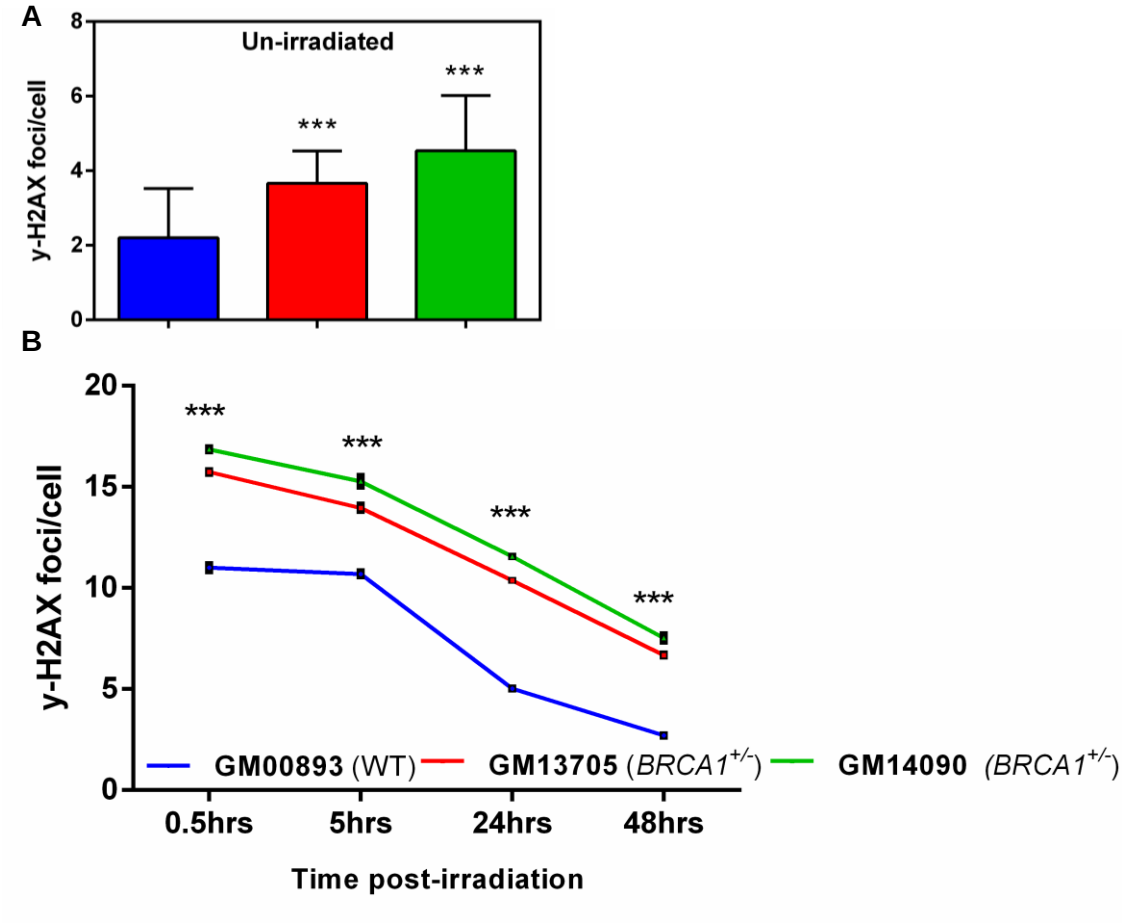

C

	0.5hrs	5.0hrs	24hrs	48hrs
	γH2AX/cell	*γH2AX/cell*	*γH2AX/cell*	*γH2AX/cell*
GM00893 (WT)	11.00 (p=6.51E-38)	10.70 (p=1.03E-42)	5.02 (p=4.58E-17)	2.70 (p=0.072)
GM13705 (BRCA1$^{+/-}$)	15.74 (p=7.78E-55)	13.96 (p=2.60E-40)	10.38 (p=5.07E-51)	6.68 (p=1.43E-18)
GM14090 (BRCA1$^{+/-}$)	16.86 (p=9.80E-59)	15.28 (p=8.37E-35)	11.56(p=4.26E-44)	7.52 (p=3.83E-11)

Figure 3-12. Frequencies of γ-H2AX foci induced with 1.0Gy of gamma-rays.

A) Average frequencies of spontaneous γ-H2AX foci. **B)** Time-course experiment from a total of 50 nuclei scored based on two independent experiments, **C)** T-test analysis comparing untreated γ-H2AX foci per cell in each sample with 1.0Gy irradiation. Asterisks indicate the level of significance (***P<0.001). Error bars represent SEM. T-test used in all statistical comparison.

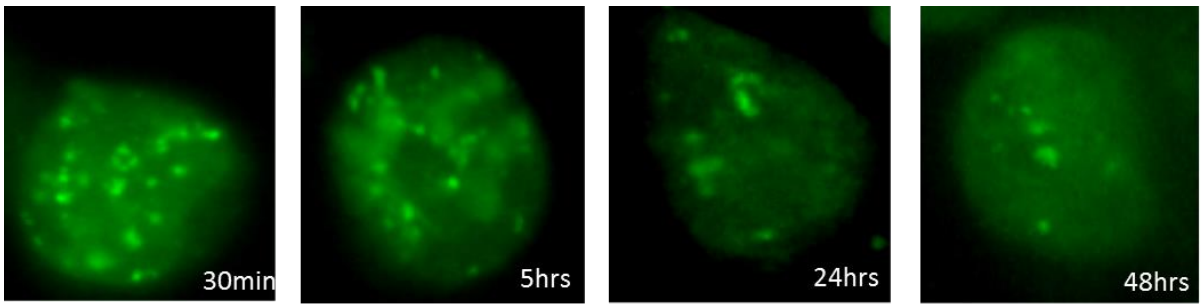

Figure 3-13. Representative example of γ-H2AX foci detected by immunofluorescence in human lymphoblastoid cell line GM14090 (BRCA1$^{+/-}$) induced with 1.0Gy gamma radiation.

3.2.8.2 Analysis of γ-H2AX after exposure to different doses of gamma rays

We also wanted to establish if radiosensitivity of BRCA1$^{+/-}$ cells detectable through defective repair kinetics (Figure 3.12) can be observed by generating dose response curves. To that end we exposed cells to 0.5 Gy, 1.0 Gy, and 2.0 Gy of gamma radiation and quantified γ-H2AX foci 30 min following exposure. Statistical analysis revealed that significant difference was observed between high dose (2.0Gy) and low doses (0.5Gy) of gamma radiation (Figure 3.14). This suggests that increasing of gamma radiation doses can cause accumulation of DDR markers in mono-allelic mutant *BRCA1* cell lines. Therefore, our results indicate that the BRCA1 defective cells accumulate higher rate of DNA damage compare to wild type when exposed to IR, pointing to the fact that BRCA1 is an important DNA DSB protein even in a heterozygous *BRCA1* situation. Figure 3.15 shows microscope analysis of γ-H2AX foci induced by IR.

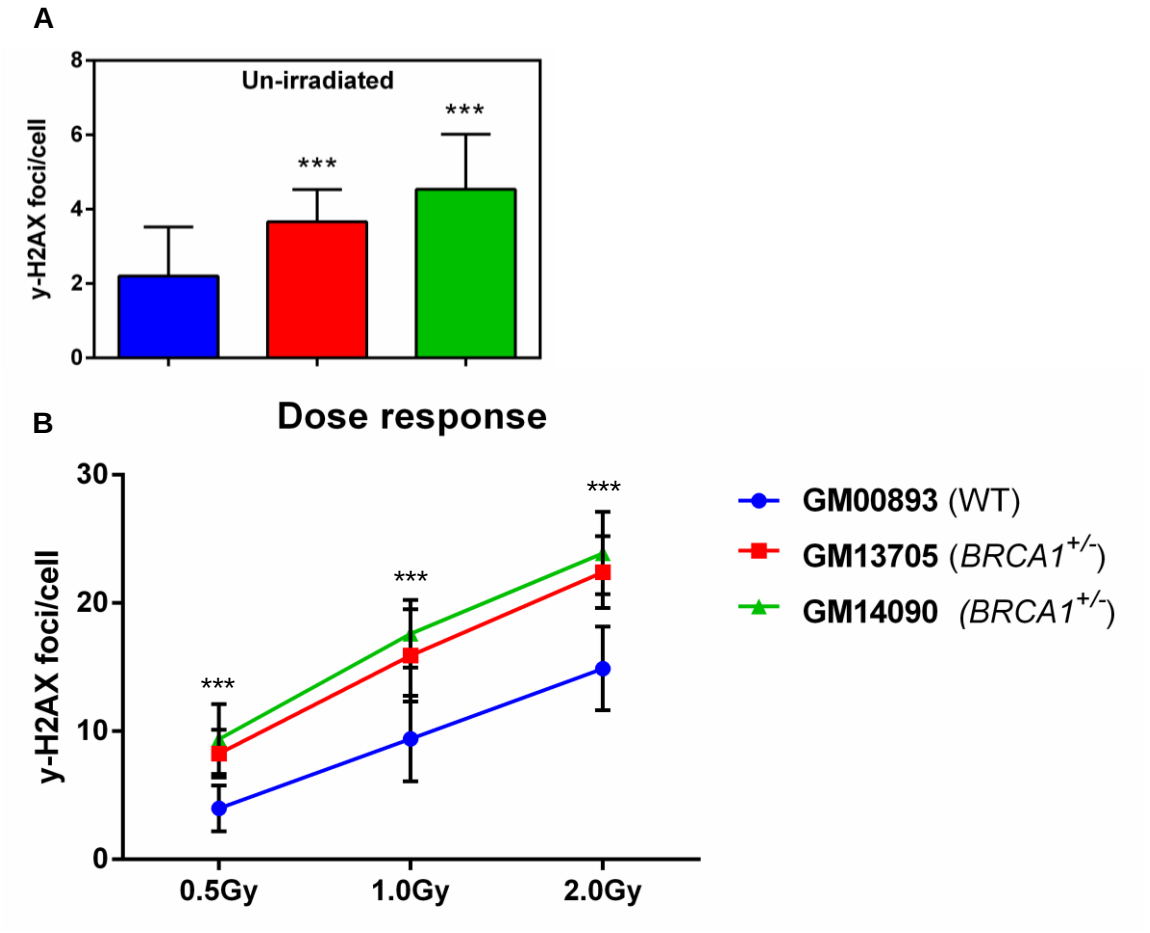

Figure 3-14. Frequencies of γ-H2AX and TIF foci after exposure to 0.5Gy, 1.0Gy, and 2.0Gy of gamma rays in BRCA1 defective cell lines (GM14090 and GM13705) and the control cell line (GM00893). A) Average frequencies of spontaneous γ-H2AX foci. **B)** The difference in the levels of γ-H2AX was significant between the two BRCA1 defective (GM14090 and GM13705) cell lines and the BRCA1 WT control (GM00893) (***P<0.001). Asterisks indicate significant differences between the BRCA1 and control cell lines (*P<0.5; **P< 0.001; ***P< 0.0001). T-test used in all statistical comparison.

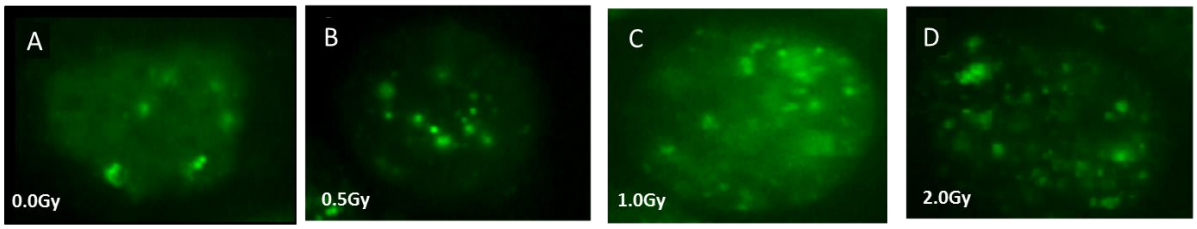

Figure 3-15. Immunofluorescence microscopy showing γ-H2AX foci formation in nuclei of human lymphoblastoid cell line GM14090.

A) γ-H2AX foci in un-irradiated cells **B)** γ-H2AX foci after irradiation with 0.5Gy, **C)** γ-H2AX foci after exposure to 1.0Gy, and **D)** The cells exposed with 2.0Gy of gamma radiation.

3.2.9 Telomere dysfunction-induced foci (TIF) analysis in human lymphoblastoid cell lines

3.2.9.1 Analysis of TIF kinetics in human lymphoblastoid cell lines

Next, in order to evaluate contribution of telomeres to the observed radiosensitivity in cell lines from BRCA1 carriers we used TIF assay as a marker for telomere dysfunction. Telomere dysfunction or loss of telomere function can be caused by telomere uncapping that occurs when either shortened telomeres or telomere-protective factors are impaired, and subsequently cell cycle arrest, senescence, apoptosis, and chromosome end fusions. TIF assay detects DNA damage exclusively at telomeres by counting dual staining: γ-H2AX (FITC) and telomere probe (Cy3) (for details see Chapter 2). Representative TIF images are shown in Figure 3.16. Our analysis revealed that slower processing of repair kinetics occurs at telomeres in cells from *BRCA1* carriers (GM13705 and GM14090) compared to the control cell line (GM00893). However, previous study revealed that the co-localisation of DDR foci with telomeric signal gradually increases because telomeres are potentially irreparable (Fumagalli et al., 2012). Our data support this finding only to a degree because we observed evidence of repair at telomeres in both normal and BRCA1$^{+/-}$ cells (Figure 3.17).

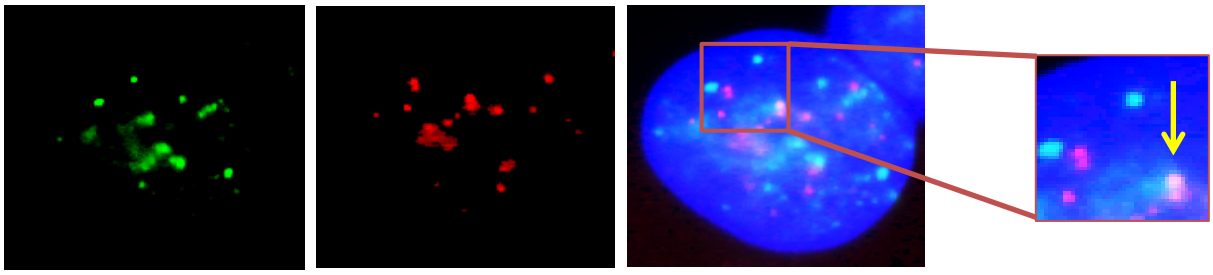

Figure 3-16. An example of TIF foci in BRCA1 carrier (GM14090).

Microscope analysis shows co-localisation of y-H2AX and telomere. Interphase cells were permeabilised and stained with anti-γH2AX (green) and telomeric Cy3-labeled PNA probes (red). Nuclei were counterstained with DAPI.

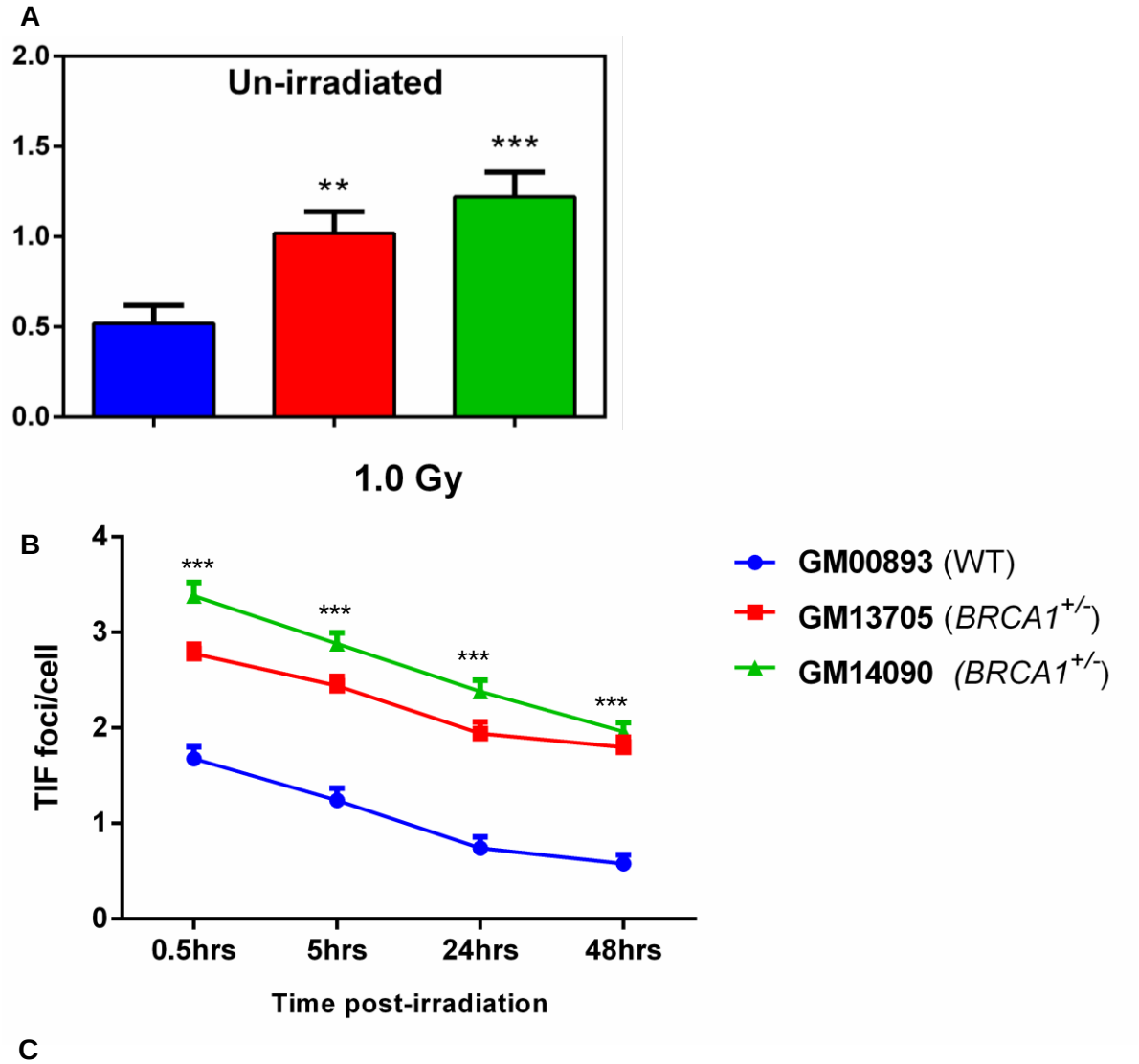

C

	0.5hrs *TIF/cell*	5.0hrs *TIF/cell*	24hrs *TIF/cell*	48hrs *TIF/cell*
GM00893 (WT)	1.68 (p=7.86E-11)	1.24 (p=2.90E-05)	0.74 (p=0.15)	0.58 (p=0.65)
GM13705 (BRCA1$^{+/-}$)	2.78 (p=1.43E-19)	2.44 (p=1.21E-14)	1.94 (p=5.21E-07)	1.80 (p=3.24E-06)
GM14090 (BRCA1$^{+/-}$)	3.38 (p=1.44E-18)	2.88 (p=8.45E-15)	2.38 (p=5.62E-09)	1.96 (p=2.78E-05)

Figure 3-17. Average frequencies of TIF foci in each cell line irradiated with 1.0Gy.

A) Levels of TIFs per cell nuclei measured in the un-irradiated lymphoblastoid lines. **B)** A total of 50 nuclei scored for each time point and cell line in two independent experiments. **C)** Repair of TIFs in the WT samples riches normal status within 24hrs after 1.0Gy of IR whereas in the BRCA1-defective cells there is a significant difference in the levels of TIFs after 48hrs when compared to the un-irradiated counterparts. Asterisks indicate significant differences between the BRCA1 defective cell lines and control cell lines at all time-points post-irradiation (**P<0.001; ***P<0.0001). Error bars represent SEM. T-test used for all statistical comparison.

3.2.9.2 Analysis of TIF response after acute dose response in human lymphoblastoid cell lines.

Detection of TIFs was carried out in *BRCA1* defective cell lines (GM14090 and GM13705) and control cell line (GM00893) following low dose (0.5 Gy) and high dose (1.0Gy and 2.0 Gy) of gamma radiation (Figure 3.18). A total of 50 nuclei were analysed to assess the mean

of TIFs foci in each cell lines. As is evidenced, the frequencies of TIF foci were significantly higher in *BRCA1* defective cells in comparison with the control (P<0.001) (Figure 3.18). To conclude, TIF results in cells with deficiency in *BRCA1* could reveal telomere dysfunction and subsequently lead to genome instability during tumourigenesis.

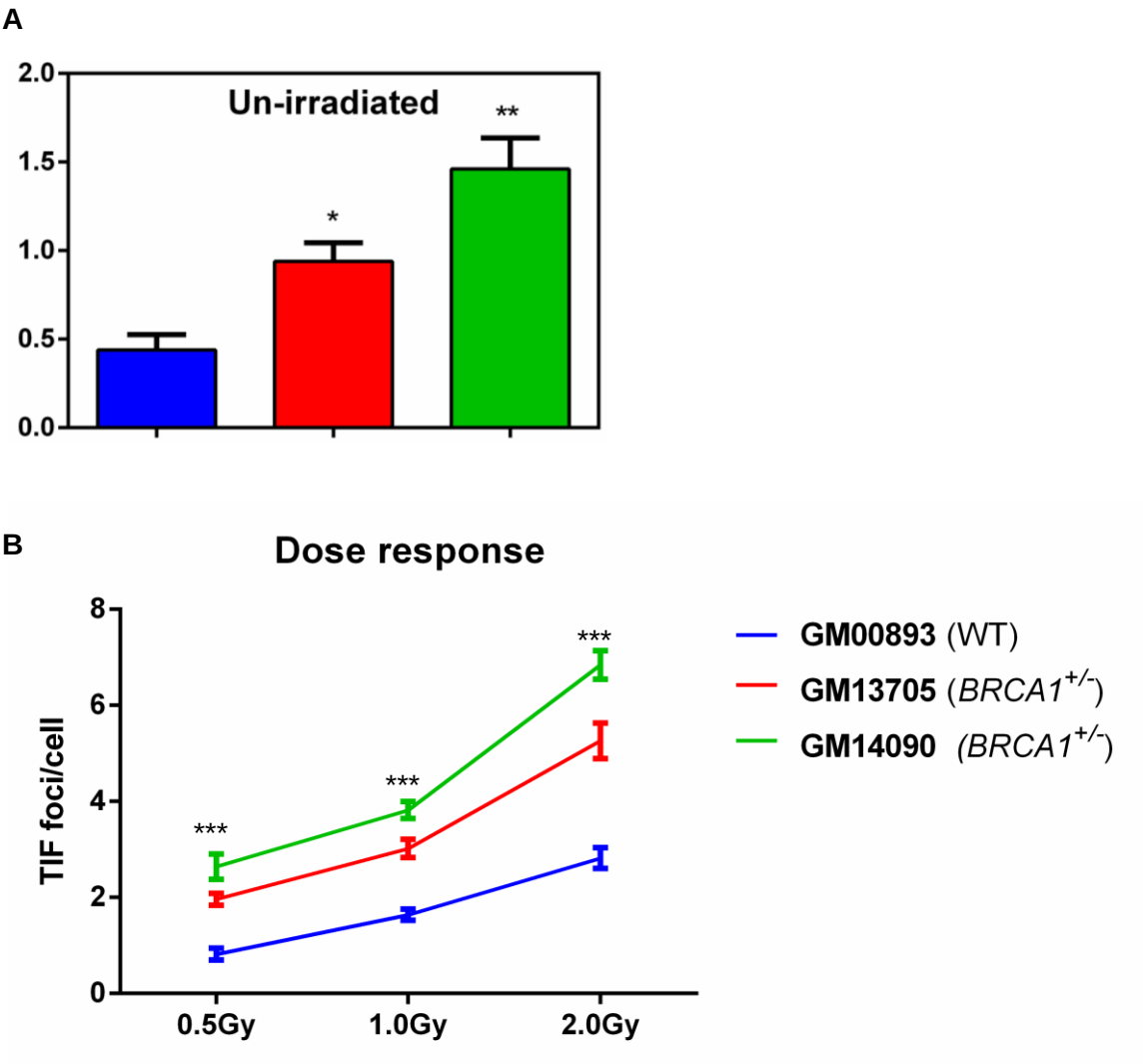

Figure 3-18 Average TIFs in BRCA1 defective cell lines (GM14090 and GM13705) and control cell lines (GM00893) exposed to various doses of IR.

A) Levels of TIFs measured per cell in the un-irradiated samples showing levels of spontaneously generated TIFs. **B)** TIFs were scored 30 minutes post-irradiation for each dose level. Asterisks indicate significant differences between the BRCA1 and control cell lines (*P<0.5; **P< 0.001; ***P< 0.0001). T-test used in all statistical comparison.

3.3 Discussion

Numerous researchers have highlighted the fact that in the mammalian cells DDR proteins also affect telomere maintenance (Verdun and Karlseder, 2007, d'Adda di Fagagna et al.,

2004). The co-operation between DNA damage response mechanisms and telomere maintenance is required to protect telomeres so that they are distinguished from DNA DSBs (Slijepcevic, 2006),(De Lange, 2005b), suggesting that DDR and telomere maintenance are functionally related.

The aim of this chapter was to evaluate the effect of BRCA1 defect on telomeres in the human lymphoblastoid cells using various telomere-specific techniques. The first results indicate elevated frequencies of T-SCEs in the two BRCA1 carrier cell lines as compared to the normal BRCA1 cell line. The dysfunctional copy of the *BRCA1* gene in two human lymphoblastoid cell line GM13705 (3875del4 in exon 11) (Castilla et al., 1994) and GM14090 (185delAG in exon 2 causing a premature termination codon at position 39) (Struewing et al., 1995) cause an elevation in the T-SCE frequencies, and an alteration in telomere length regulation which was evidenced via telomere length analysis in these cell lines (Figures 3.2 and 3.5C).

We have also shown that a lymphoblastoid cell line from a BRCA1 carrier showed elevated levels of spontaneous dicentric chromosomes resulting from end-to-end chromosome fusions (G1) and chromatid breaks (G2) (Figures 3.7 and 3.8). We have also shown that the exposure to IR causes CAs, resulting from interaction between telomeres and DSBs in the above cell lines. Our findings are in agreement with previous studies showing increased chromosomal radiation sensitivity of BRCA1 mutation carriers (Ernestos et al., 2010). The same results were observed by (Barwell et al., 2007). Another published study by (Kote-Jarai et al., 2006) and colleagues used M-FISH to show increased levels of radiation-induced chromosomal aberration in heterozygous BRCA1 mutation carriers compared with controls. They found that all chromosomes were equally involved in translocations or breaks when the data were corrected for chromosomal length. In contrast to these data, other investigators have not found an association between BRCA1 heterozygosity and radiosensitivity (Baria et al., 2001, Nieuwenhuis et al., 2002, Baeyens et al., 2004).

MN assay was another cytogenetic technique we used to assess radiosensitivity in heterozygous BRCA1 mutation carriers. Surprisingly, we observed low frequencies of MN induced by IR in BRCA1 carrier cell lines, which is not in the line with previous work that had shown high level of MN at higher doses (Slavotinek et al., 1993, Stopper and Lutz, 2002). In contrast to these data, other study (Trenz et al., 2002) have found no systematic difference in radiation sensitivity between lymphoblastoid cell lines with and without a BRCA1 mutation. Spontaneous and gamma radiation-induced MN frequencies were in same range.

Additionally, it is clear that telomere dysfunction is critically involved in the deficiency of DNA damage response in these cells. Our examination of γ-H2AX foci frequencies as a marker of DNA damage after exposure to IR in *BRCA1* carrier cell lines (GM13705 and GM14090) revealed that part of DNA damage foci placed at telomeres, is caused by dysfunctional telomeres. This assessment of DNA damage kinetics suggests that damage at telomeres, in the form of TIFs, are reparable at all-time points post-exposure in two *BRCA1* carrier cell lines (GM13705 and GM14090). On the other hand, our data are not in the line with other study (Fumagalli et al., 2012) that support telomeric DNA are irreparable and trigger persistent DDR and cellular senescence.

Previously, it has been revealed that there could be a potential mechanism for BRCA1 due to its effects on telomeres and DNA damage response (McPherson et al., 2004, Deng and Wang, 2003). It was also reported that BRCA1 regulates telomerase activity (Xiong et al., 2003); therefore, *BRCA1* deficiency can lead to an alteration of normal telomerase function, resulting in telomere shortening similar to that observed in (Figure 3.5). Additionally, it was found that BRCA1 knockdown resulted in increased telomerase activity and significant telomere lengthening in tumour cells (Ballal et al., 2009). Also, studies have suggested an interaction and co-localization of BRCA1 with shelterin proteins TRF1 and TRF2, and RAD50 (a component of the MRN complex) (Ballal et al., 2009). Furthermore, it was demonstrated that the length of the 3`G-rich overhang regulated via BRCA1, and also over-expression of BRCA1 caused lengthening, and knockdown of BRCA1 or RAD50 caused

shortening of the 3`overhang (Ballal et al., 2009). All these observations clearly suggest the role of *BRCA1* in DNA damage response and subsequently on telomeres, providing further confirmation that DNA damage response and telomere maintenance are closely associated.

In conclusion results presented in this chapter clearly indicate *BRCA1* mutation carriers show telomere dysfunction as evidenced by altered telomere length, increased TIF frequencies and elevated levels of T-SCE. Thus our results are in line with some earlier studies (Al-Wahiby and Slijepcevic, 2005, McPherson et al., 2006) (Wang et al., 2007, Ernestos et al., 2010).

An additional function of BRCA1 with regards to DSB repair may result from the up-regulation of the activity of base excision repair (BER) via a transcriptional mechanism, which in turn involves the stimulation of the expression of several key BER enzymes (OGG1, NTH1, and REF1/APE1) (Ballal et al., 2009). All in all, BRCA1 plays a vital role in the error-free repair of DSBs of DNA through HR. This role is indeed very critical for the tumour-suppressing nature of BRCA1. Nevertheless, the role of BRCA1 in non-homologous end joining remains to be settled (Rosen, 2013).

CHAPTER 4

4 DNA damage response in mouse embryonic stem cells

4.1 Introduction

The ability of mouse embryonic stem cells (mESC) to maintain pluripotency and differentiation into all somatic cell types is well documented and can be characterised by a high proliferation of activity. One of the significant factors in mouse and monkey embryonic stem cells is an unusual cell cycle; they have a very short G1 phase (~ 1.5 h) and lack a G1 checkpoint (Aladjem et al., 1998) (Malashicheva et al., 2000, Fluckiger et al., 2006). Owing to the defect of wild type p53 and low levels of CDK inhibitor p21/Waf1 expression (Aladjem et al., 1998) (Malashicheva et al., 2000) (Stead et al., 2002) (Burdon et al., 2002), ESCs do not undergo cell cycle arrest following exposure to DNA damaging agents and stress factors (Fluckiger et al., 2006) (Schratt et al., 2001), (Malashicheva et al., 2002). Therefore, this raises the question: how do mESCs maintain genome integrity when p53 is not activated? Is there any other mechanism involved in the activation of DNA damage response and

genomic integrity? There are several possibilities that have been described to provide such protection to the mouse ESCs. These include: (i) p53-independent apoptosis (Aladjem et al., 1998) (Malashicheva et al., 2000) (ii) lower mutation rates in the mouse ESCs as compared to the adult somatic cells or mouse embryonic fibroblasts (MEFs) by a factor of 100-fold, eliminating the need for constant monitoring of the genome for stability (Stambrook, 2007).

Two DNA damage responses is activated by ATM (ataxia-telangiectasia mutated) and ATR (ATM-and Rad3-related) (Bakkenist and Kastan, 2004) (Lavin and Kozlov, 2007) which subsequently activate other proteins such as: Chk1 and Chk2 kinase, p53, MDM2, H2AX, proteins of the MRE11 complex, and many others (Helt et al., 2005a), (Shiloh, 2006) (Hurley and Bunz, 2007) (Lin et al., 2005). One question that needs to be explored is whether these pathways are functional in mESC in the same was as in somatic cells. Recently, some studies have suggested that p53 can be activated by DNA damage following the suppression of Nanog promoter activities; therefore, differentiation and DDR must be coordinated (Lin et al., 2005). Moreover, the similarity of the mESC and the mouse embryonic carcinoma cell line F9 (ECC) in terms of short cell cycles, reduced duration of the G1 phase, as well as a high proliferation rate has been reported (Chuykin et al., 2008a). Ideas relating to how stem cells are over sensitive to DNA damage and easily undergo apoptosis or differentiation which eliminates impaired cells from the pluripotent pool are well documented (Van Sloun et al., 1999) (de Waard et al., 2003). It is clear enough that the loss of impaired self-renewing cells effectively maintains genetic integrity of the proliferating cell population. Consistent with this view, ESCs lack a functional G1 checkpoint, partially due to the sequestration of P53 in the cytoplasm. Therefore, an absence of the G1 checkpoint in the cells with DNA damage results in the transit from G1 into S phase and accumulation of damage (Aladjem et al., 1998, Prost et al., 1998) (Hong and Stambrook, 2004). Recently, some studies demonstrated that differentiation can be promoted by p53 translocation to the nucleus and also the transcription of p53 is inhibited through the Nanog promotor,

suggesting that the role of p53 is more important during differentiation than in responding to DNA damage in ESCs (Lin et al., 2005).

The most toxic DNA lesions are DSBs (Valerie and Povirk, 2003). ESCs show extremely high frequency of spontaneous γ-H2AX foci relative to non ESCs (Giachino et al., 2013). One of the possible reasons for this could be the replication fork collapse or reactive oxygen species (ROS) from oxidative metabolism. However, (Saretzki et al., 2004) have demonstrated that ESCs can be grown in hyperoxic conditions (40% O_2) with little effect on cell proliferation compared with cells grown under normoxic culture conditions. It, therefore, seems likely that spontaneous γ-H2AX foci observed in ESCs do not result from DNA damage but rather from the physiological interplay between different factors in these cells aimed at balancing DDR and differentiation.

Generally, two major mechanisms are associated with DNA DSB repair: HR and NHEJ. The HR pathway is active in the late S to G2 phases of the cell cycle where sister chromatids are available to serve as templates (Morrison et al., 2000) (Takata et al., 1998, Haber, 2000), whereas the NHEJ pathway requires little or no homology sequence for repair; it can also be error-free or error-prone. In contrast to HR, NHEJ takes place in the early G1 and S phases of the cell cycle (sister chromatids are not accessible during this stage).

It is noticeable that ESCs utilize HR rather than NHEJ as the principle mechanism of repair (Donoho et al., 1998) (Hasty et al., 1992) (Smih et al., 1995). This theory has been proven by gene targeting experiments. The introduction of a DSB into the targeting vector increases significantly HR activity in ESCs (Donoho et al., 1998, Hasty et al., 1992) (Smih et al., 1995). Also, prolonged S phase in ESCs might stimulate the HR pathway rather than NHEJ preferentially. Moreover, a short G1 phase can lead to the majority of ESC genomes having sister chromatids which would be more efficient for the recombination mediated repair. Clarity of research has been hampered by the fact that genetically modified mice frequently suffer from an early embryonic lethality (Friedberg and Meira, 2006). This suggests that

affected proteins may be essential for the continued proliferation of ESCs. Additionally, Rad51 plays an important role in the strand invasion process, an integral part of the HR mechanism (Baumann et al., 1996). Mice nullizygous for Rad51 die in the early stages of development. Doubly targeted ESCs lacking Rad51 cannot be obtained, and cells derived from Rad51 null blastocysts do not proliferate, suggesting that Rad51 protein plays an essential role either in cell proliferation or in the repair of DSBs generated by the endogenous processes (Tsuzuki et al., 1996, Lim and Hasty, 1996). A deletion of Rad51 on the p53 deficient backgrounds yielded similar results, although development proceeded to embryonic day 8.5 (Lim and Hasty, 1996). Consistent with the contention that HR is a major repair pathway in ESCs, Rad51 protein levels are approximately 20-fold higher in ESCs than in MEFs where NHEJ predominates.

The aim of this chapter is to investigate the effect of *Brca1* on telomeres in mESCs where both copies of *Brca1* were disrupted by gene targeting (Snouwaert et al., 1999). As explained earlier, telomere maintenance mechanisms and DDR appear to be functionally related providing us with a further possibility to examine this relationship.

We focused on investigating repair of IR induced DSBs in mESCs: 408 (*Brca1*$^{-/-}$) and E14 (*Brca1*$^{+/-}$) cell lines. Also, we performed analysis of chromosomal aberration induced in G1 and G2 phases of the cell cycle after exposure of the cells to IR. Furthermore, we have conducted experiments similar to that in the previous chapter, namely an analysis of micronuclei to identify the frequencies of chromosomal damage induced by IR.

4.2 Results

4.2.1 Establishment of an immunofluorescence assay protocol in mESCs cells

It is now well accepted that mESCs have high spontaneous levels of γ-H2AX positive foci even without exposure to genotoxic agents (Turinetto et al., 2012). Our first aim was to show that this is the case with the 408 E14 cell lines. However, the first obstacle we encountered was related to growth properties of mESCs. These cells do not grow as a monolayer but rather form multilayers of cells, thus preventing an accurate analysis of individual cells. In

order to quantify γ-H2AX positive foci in individual cells 3D multilayers of cells must be disrupted and cells separated from each other. In order to facilitate this we disrupted monolayers by trypsinization, re-suspended cells and used the Shandon Cytospin to deposit a thin layer of individually separated cells on microscope slides. However, establishing the right conditions for the cytospin protocol required time and frequent changes in the protocol. Table 4-1 shows a summary of changes in experimental conditions required to establish optimal conditions for the analysis of γ-H2AX positive in mESCs.

Table 4-1- Establishment of the H2AX assay protocol.

All experiments were performed on mESC lacking functinal *Brca1*(408) and normal *Brca1*(E14). Cells were attached to polyprep slides using a cytospin centrifudge at 800 rpm for 5min (see Chapter 2 for the methodology).

Experiment no.	Aim	Method used	Change (s) to the method	Outcome
Experiment 1	To test the Cytospin speed	Immunohistochemistry	Reduce the speed from 1200 to 800	Positive
Experiment 2	Blocking buffer	Immunohistochemistry	Incubate the cells with 1% BSA instead of Milk	Positive
Experiment 3	To test the new antibody (γ-H2AX)	Immunohistochemistry	N/A	Positive
Experiment 4	To test the new Secondary antibody	Immunohistochemistry	Reduce the dilution from 1:500 to 1:1000	Positive
Experiment 5	Complete immunohistochemistry followed by FISH	Immunohistochemistry and then hybridization with PNA	N/A	PNA and γH2AX signal weak
Experiment 6	Modified experiment 5 protocol	Immunohistochemistry and then extra fixation with 4% formaldehyde, then leave at room temperature overnight, following by hybridization with PNA	Washing with TBST instead of PBS	Positive γH2AX signal, positive telomeric PNA signal. Protocol suitable for further experiment.

After establishing the γ-H2AX assay suitable for mESCs (Table 4-1), a total of 50 nuclei were analysed twice to evaluate the frequency of spontaneous γ-H2AX foci. Results of this

analysis are shown in Figure. 4.1 A. In line with previous studies we observed dramatically higher spontaneous levels of γ-H2AX positive foci in mECS than for example in human lymphoblastoid cells lines (see previous chapter). Examples of mECS stained with the H2AX antibody without any treatment are shown in Figure 4.1 B. The average number of γ-H2AX positive foci was 31.42 cells with the 408 cell line showing significantly more foci than the E14 cell line 23.56 (Figure 4.1 A).

We then exposed both cell lines to 1.0 Gy of gamma rays and quantified γ-H2AX positive foci 30min, 5hrs, 24hrs and 48hrs post exposure (Figure 4.2). Results of this analysis are shown in Figure 4.1 C. Also, it is important to indicate that we performed a statistical analysis in two different ways. First, we compared *Brca1-/-*(408) against the control cell line E14 at each individual point (control, 0.5hrs, 5hrs, 24hrs and 48hrs); the results of this analysis are demonstrated by asterisks placed immediately above the bars in Figure 4.1 C. The results of the second analysis are presented in the table (Figure 4. 1 D). The Table contains a statistical comparison between control (spontaneous) frequencies of DNA damage foci and their counterparts at each time point post-irradiation (30min, 5hrs, 24hrs and 48hrs) for each individual cell line. The frequencies of DNA damage foci 0.5hrs and 5hrs after being exposed in *Brca1*$^{-/-}$ (408) cells were significantly higher than spontaneous frequencies, as these time intervals were insufficient for the repair processes to remove large amounts of induced DNA damage. However, a significant difference between frequencies of spontaneous DNA damage and that observed 24hrs and 48hrs post-exposure in the 408 cell line indicates the presence of unrepaired DNA damage. Therefore, this may imply a DNA damage defect in this cell line.

By contrast the control E14 cell line repaired DNA damage effectively, judging by the lack of statistical differences between DNA damage 24hrs and 48hrs after exposure relative to the spontaneous DNA damage.

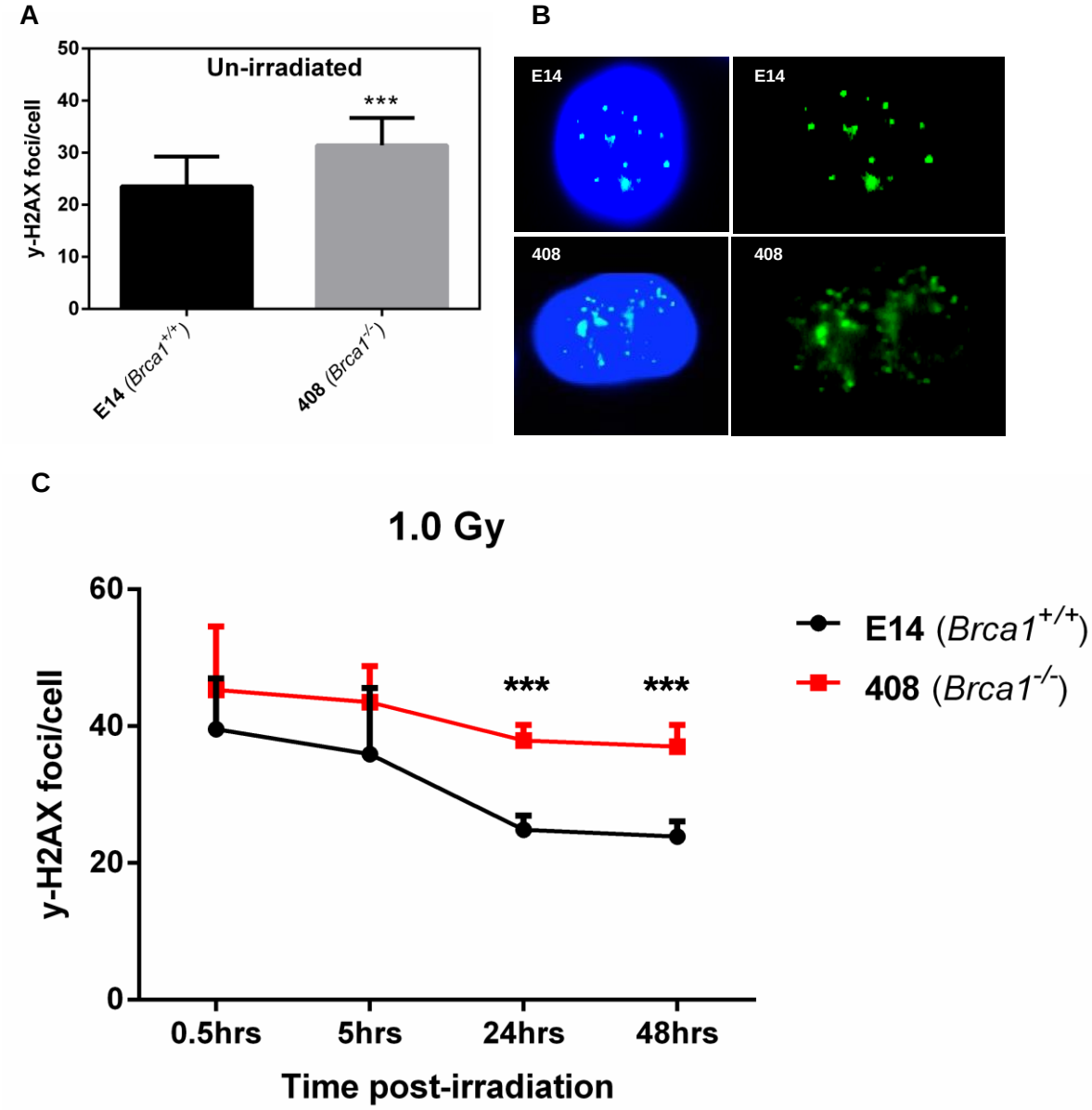

D

	0.5hrs	5.0hrs	24hrs	48hrs
	γH2AX/cell	*γH2AX/cell*	*γH2AX/cell*	*γH2AX/cell*
E14 (WT)	39.60 (p=7.13E-21)	35.94 (p=1.77E-11)	24.48 (p=0.128)	33.82 (p=0.712)
408 (BRCA1$^{-/-}$)	45.32 (p=4.17E-14)	43.54 (p=5.41E-20)	39.92 (p=2.55E-11)	37.02 (p=8.11E-09)

Figure 4-1. Analysis of γ-H2AX foci in mESCs.

A) Spontaneous levels of γH2AX foci in un-irradiated E14 and 408 cells. **B)** Examples of the γH2AX levels in E14 (top picture) and 408 cells (bottom picture). **C)** Repair kinetics in E14 and 408 cells irradiated with 1.0 Gy. T-test analysis was done to compare E14 with 408 cells (***P<0.001). (**D)** T-test analysis comparing the untreated samples with irradiated samples. There were no significant differences between the average frequency of γH2AX foci in the E14 cell line 24hrs and 48hrs post-irradiation when compared to the untreated E14 cells, whereas 408 Brca1 defective mESCs showed significantly elevated levels of γH2AX at all time points compared to the un-irradiated 408 sample. Results were obtained from two independent experiments with an average of 50 cell nuclei scored per cell line.

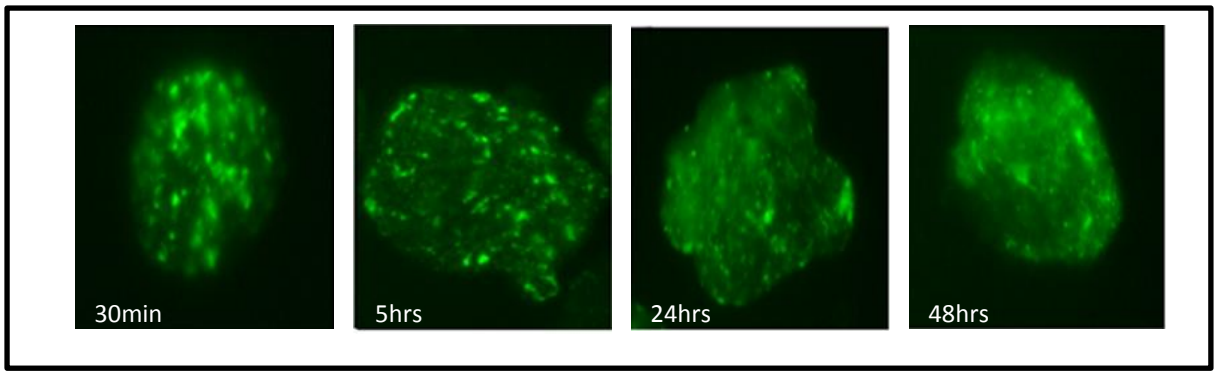

Figure 4-2. Detection of γ-H2AX by immuno-FISH in mouse embryonic stem cell line (408 Brca1$^{-/-}$) after different time post 1.0 Gy gamma irradiation.

4.2.2 Telomere dysfunction-induced foci (TIF) analysis in normal and homozygous Brca1 mESCs

We next performed the TIF assay to assess telomere function in the above cell lines. The TIF assay allows detection of γ-H2AX foci and telomeres simultaneously (Takai et al., 2003). We used a synthetic PNA (peptide nucleic acid) telomere probe to detect telomeres.

Our analysis showed that 408 cells had greater spontaneous TIF frequencies in comparison to the cell line E14 ($P<0.001$) (Figure 4.3 A). However, after treatment with IR frequencies of TIFs returend to normal levels 24hrs and 48hrs later in E14 cells (Figure 4.3 B and C). By contrast, there were significant differences between spontaneous frequencies of TIF before and those observed 24 h and 48 h after IR in the 408 cell line ($P<0.001$) (Figure 4.3 B and C). A representative image of a TIFs observed in mESCs are shown in Figure 4.4. Thus, our results suggests that 408 cells show telomere dysfunction relative to control E14 cells.

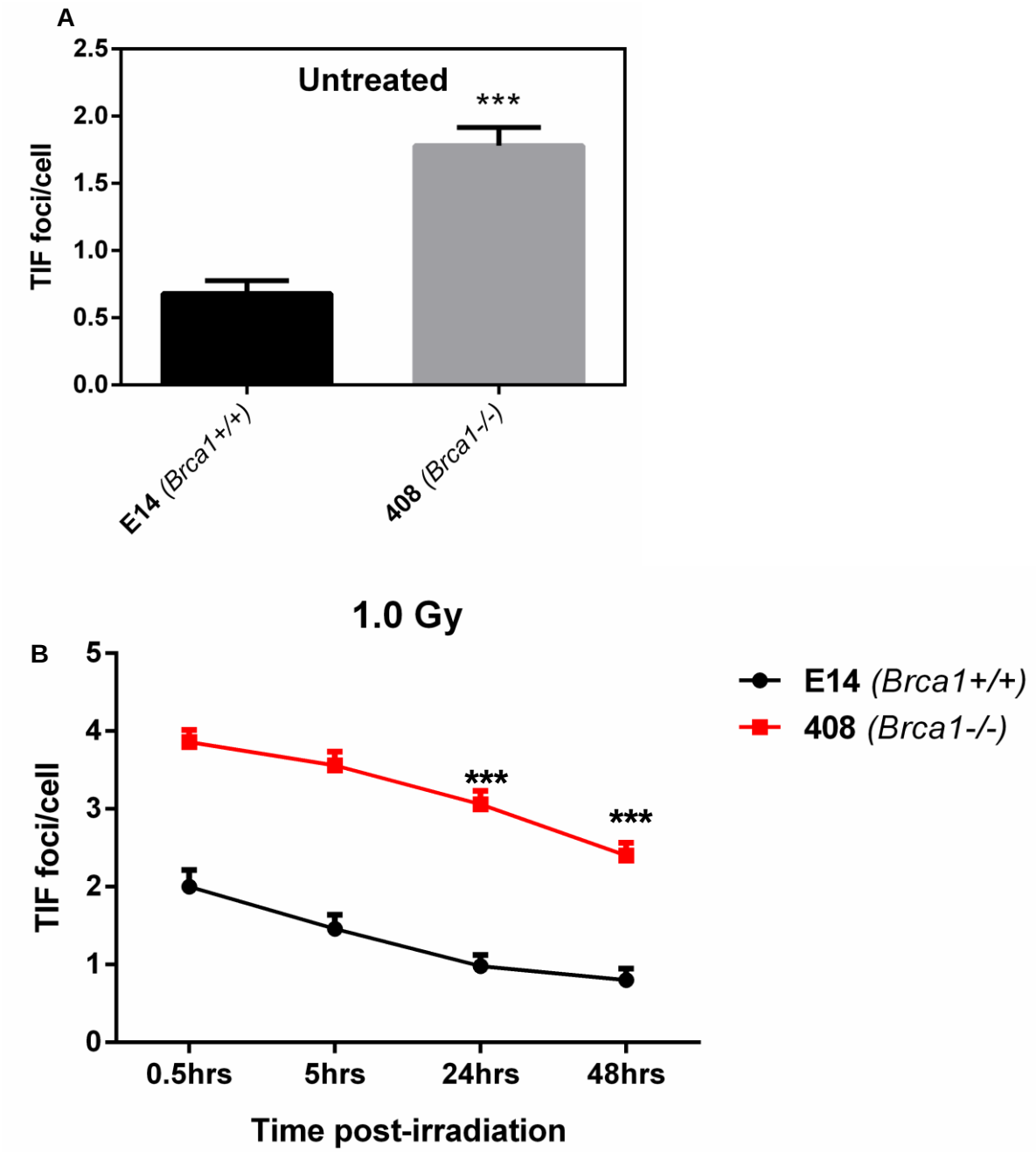

C

	0.5hrs *TIF/cell*	5.0hrs *TIF/cell*	24hrs *TIF/cell*	48hrs *TIF/cell*
E14 (WT)	2 (p=4.46E-07)	1.46 (p=0.0002)	0.96 (p=0.088)	0.8 (p=0.500)
408 (BRCA1$^{-/-}$)	3.86 (p=6.36E-17)	3.56 (p=2.42E-12)	3.06 (p=7.43E08)	2.4 (p=0.0044)

Figure 4-3. Average frequencies of TIF foci in each cell line after 0.5hrs, 5hrs, 24hrs and 48hrs post-irradiation. A) levels of TIFs per cell nuclei measured in the un-irradiated E14 and 408 cell lines. **B)** a total of 50nuclei scored for each time point and cell line (E14 and 408) in two independent experiments. **C)** T-test analysis comparing the untreated samples with irradiated samples. There were no significant differences between the average frequency of TIF foci in the E14 cell line 24hrs and 48hrs post-irradiation when compared to the untreated E14 cells, whereas 408 Brca1 defective mESC showed significantly elevated levels of TIF at all time points compared to the un-irradiated 408 sample but to a lesser extent at 48hrs. Error bars indicate SEM and asterisks indicate significant differences between the 408 and the control cell line (E14) (***P<0.001).

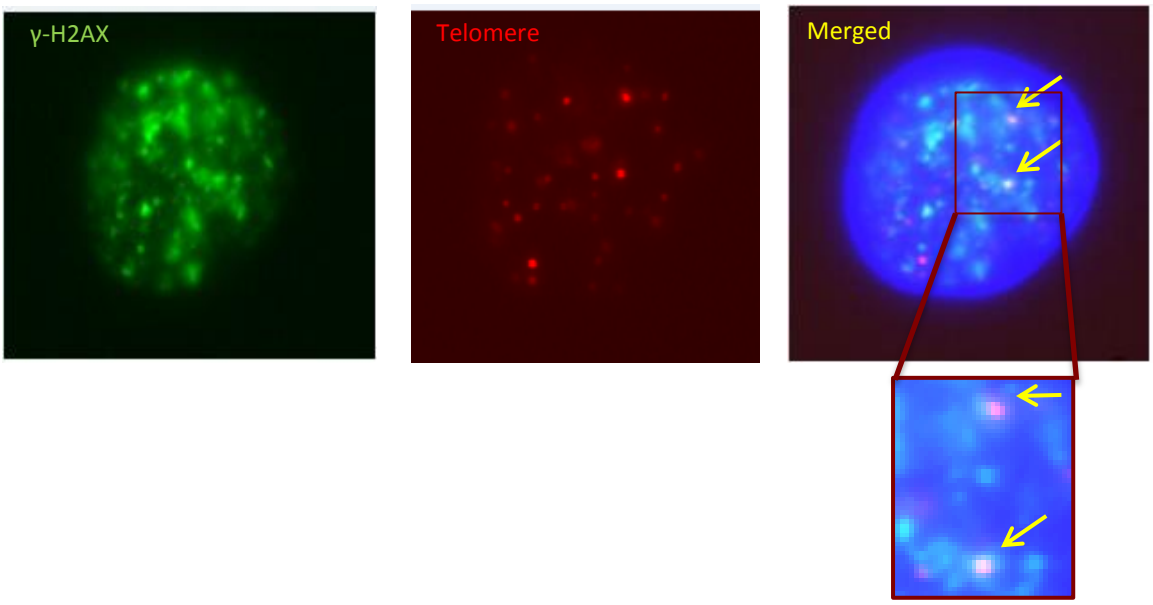

Figure 4-4. **Detection of TIF in mESC*: Brca1+/+* and *Brca1-/-* (E14 and 408 respectively).** Interphase cells were permeabilised and stained with antiphospho-histon γ- H2AX (green) and telomeric Cy3-labeled PNA probes (red). Nuclei were counterstained with DAPI.

4.2.3 Radiation induced chromosomal abnormalities in Brca1 mutant mouse embryonic stem cells

To investigate whether *Brca1* defecincy results in IR sensitivity, the G1and G2 assay was performed in the E14 (*Brca1*$^{+/+}$) and 408 (*Brca1*$^{-/-}$) cell lines after exposure to increasing doses of IR. IR induces DSBs effectively and these may convert in cytologically visible chromosoml damage. Some studies have reported that *BRCA1* mutant HCC193 carcinoma cell line is hypersensitive to IR, and that this sensitivity is partlly relieved by the expression of wild-type *BRCA1*. Morover, *Brca1* mutant mESC, 236.44, is also sensitive to IR (Moynahan et al., 2001). Also, mouse cells with targeted deletion in exon 11 of *Brca1* show severe genomic instability including the presence of multiple chromosomal aberrations (CAs) in individual cells (Xu et al., 1999b, Weaver et al., 2002). Mouse embryos carrying a *Brca1* null mutation and mouse thymocytes lacking functional *Brca1* are hypersensitive to IR (Shen et al., 1998, Mak et al., 2000). This idea suggests that *Brca1* deficiency results in chromosome instability in mESCs, however, this is different to the dramatic instability detected in MEFs.

4.2.4 Analysis of CAs induced by IR in mESCs

Cell lines were subjected to 0.5 Gy, 1.0 Gy, 2.0 Gy and 4.0 Gy of gamma rays for the G1 assay, while cells were exposed to 0.5 Gy for the G2 assay. The protocols for G1 and G2

assay are used routinely in our laboratory and are based on the following references (Al-Wahiby and Slijepcevic, 2005). We used the clasical Giemsa staining method to identify CAs, such as dicentric chromosomes, chromosome fragments (Figure 4.5). As expected, the statistical analysis of the mouse embryonic *Brca1*$^{-/-}$ stem cell line (408) showed significantly higher frequencies of CAs, relative to the control cell line *Brca1*$^{+/+}$ (E14) in the G1 assay ($P<0.05$, $P<0.01$, and $P<0.001$) (Figure 4.6).

Similarly, the G2 assay showed same results. A statistical analysis after 1.5hrs post-radiation of both cell lines (E14 and 408) showed a significantly higher level of chromosome breaks relative to the untreated cell lines ($P<0.05$) (Figure 4.7). A similar situation was also observed after 3hrs and 4hrs of post-radiation which is also statistically significant ($P<0.05$, $P<0.01$). Our results clearly demonstrate that the 408 cell line is IR sensitive relative to the E14 cell line pointing further in the direction of a defective DNA damage response.

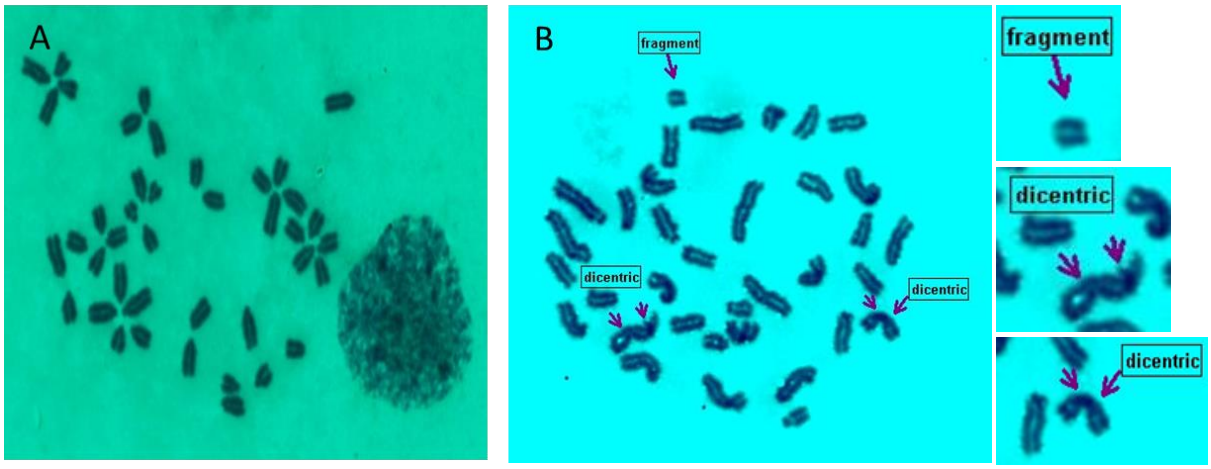

Figure 4-5. Examples of chromosomal abnormalities in mouse embryonic stem cells. A) Untreated cells, with classical Giemsa staining method, **B)** chromosomal abnormalities in 408 cell line (dicentric and fragment) after exposure with IR.

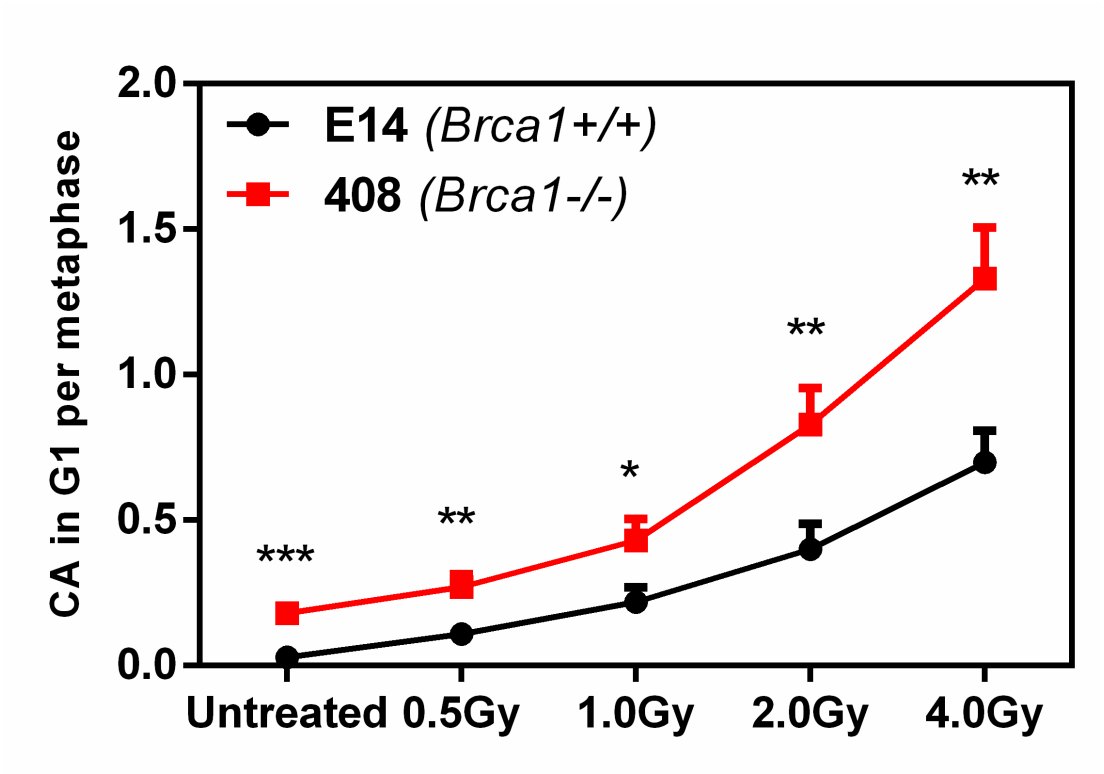

Figure 4-6. Frequency of chromosomal abnormalities in mouse embryonic stem cell lines: E14 (*Brca1+/+)* and 408 (*Brca1-/-)* induced by IR in the G1 phase. *=P<0.05, **=P<0.01, ***=P<0.001. The error bars represent SEM.

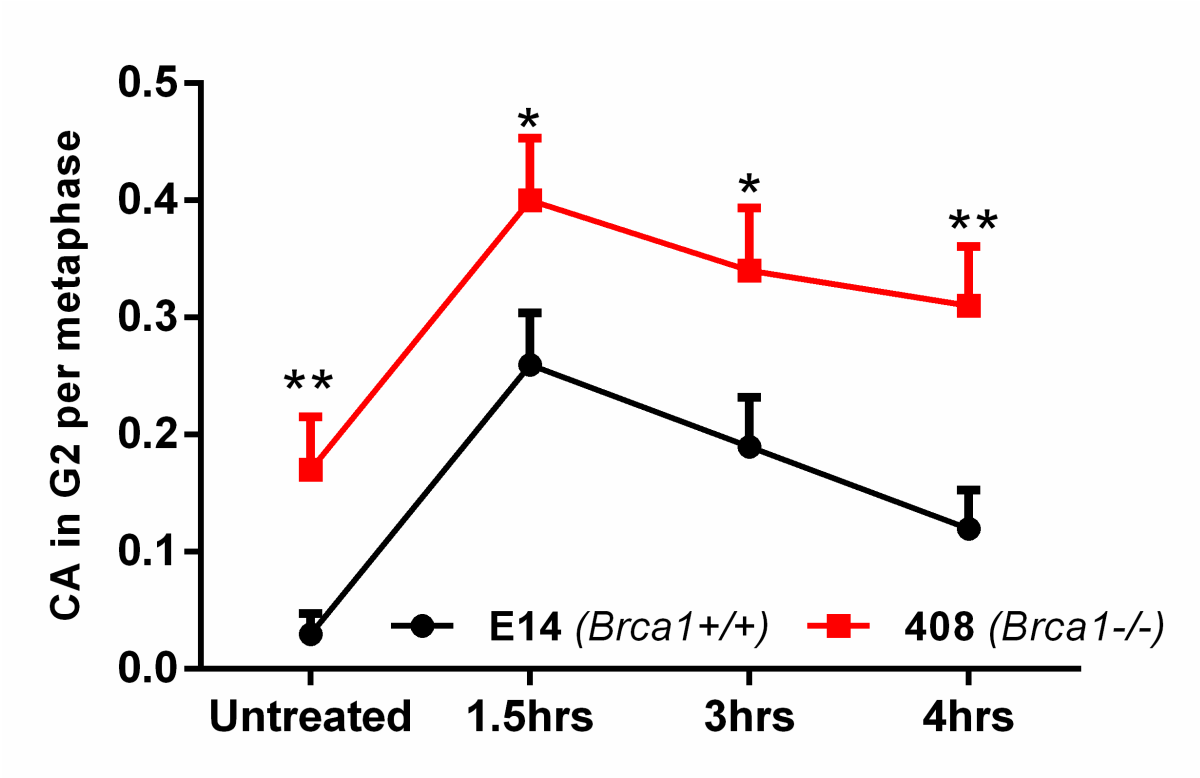

Figure 4-7. **Relative frequencies of chromatid breaks in mouse embryonic stem cell lines (E14 and 408):** all cells collected at 1.5hrs, 3hrs and 4hrs after exposuere to 0.5Gy IR. The error bars represent SEM.

4.2.4.1 Setting up a modified micronuclei assay protocol for assessing chromosome damage in mouse BRCA1 homozygous embryonic stem cells

In the previous chapter, we attempted to optimise the MN assay in *BRCA1* carrier lymphoblastoid cell lines. Here, we also attempted to investigate DNA damage at the chromosome level in mESCs using the MN assay. Therefore, we carried out a series of experiments (Table 4-2) to optimize the MN assay in mESCs. Figures 4.8 and 4.10 illustrate differences between initial results (Figure 4.8) which indicated poorly stained cells, lack of differentiation between nuclei and cytoplasm, lack of accuracy in detecting MN and results after the protocol optimization (Figure 4.10) showing clear distinction between nuclei and cytoplasm, clarity of identifying MN and clarity of identifying binucleate cells. The final results (Table 4-2) revealed that the optimal binucleated cells and clear cytoplasm formed 48hrs after treating cells with 6µg/ml of Cyt-B.

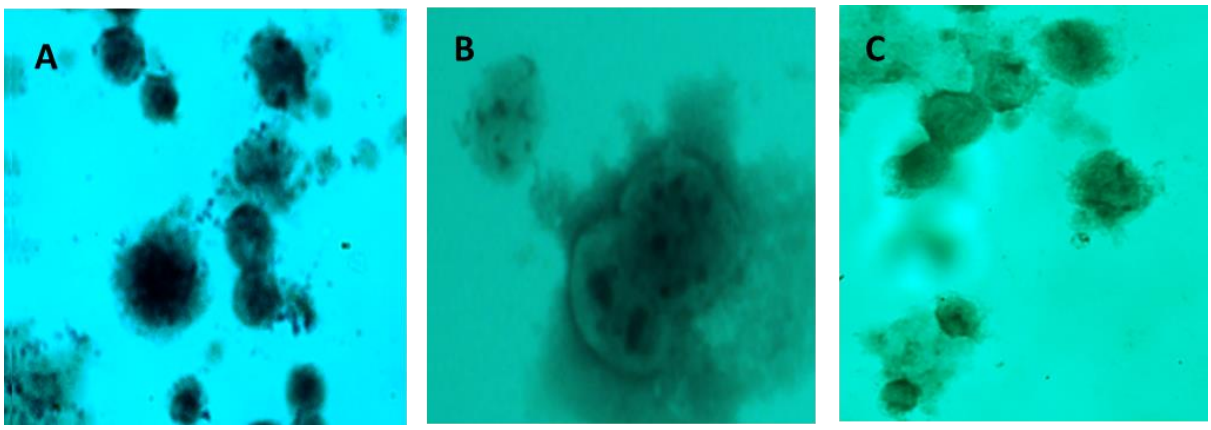

Figure 4-8. Examples of initial images generated by the MN assay in mESCs A) after 24hrs with 3µg/ml of Cyt-B, **B)** after 24hrs with 6µg/ml Cyt-B, **C)** after 48hrs with 3µg/ml of Cyt-B.

Table 4.2- Establishment of a micronucleus assay.
All experiments were performed on normal (E14) and mutant mouse embryonic stem cells (408).

Experiment no.	Aim	Method used	Outcome
Experiment 1	To test the dose of Cyt-B (3 or 6 µg/ml)	Both doses of Cyt-B were added	Visible and clear MN of 6 µg/ml dose
Experiment 2	To test the optimum time for radiation-induced MN	MN was found between 24 hrs and 48 hrs post-radiation	Increase the level of MN 48 hrs post-radiation
Experiment 3	Modified Experiment 2 protocol as the optimum experimental conditions	Micronuclei assay and then Giemsa staining	Positive MN measurement at 48 hrs in the presence of 6 µg/ml Cyt-B

It is now established that micronuclei are derived from acentric chromatid fragments, acentric chromosome fragments or whole chromosomes that fail to segregate properly in anaphase (Fenech, 2010).

Our analysis revealed a clear distinction regarding the spontaneous level of MN frequencies between E14 and 408 cell lines as shown in Figure 4.9. The level of MN formed following IR was higher in the 408 cell line compared to the normal E14 cell line. The highest level of MN was observed after exposure to 2.0 Gy and 4.0 Gy in 408 cells. The statistical analysis revealed frequencies of MN are higher in the 408 cell line ($P<0.05$) than in the normal E14 cell line after 2 Gy and 4 Gy (Figure 4.6). Taken together these results show greater sensitivity to IR in 408 cells relative to E14 cells, suggesting a DDR defect.

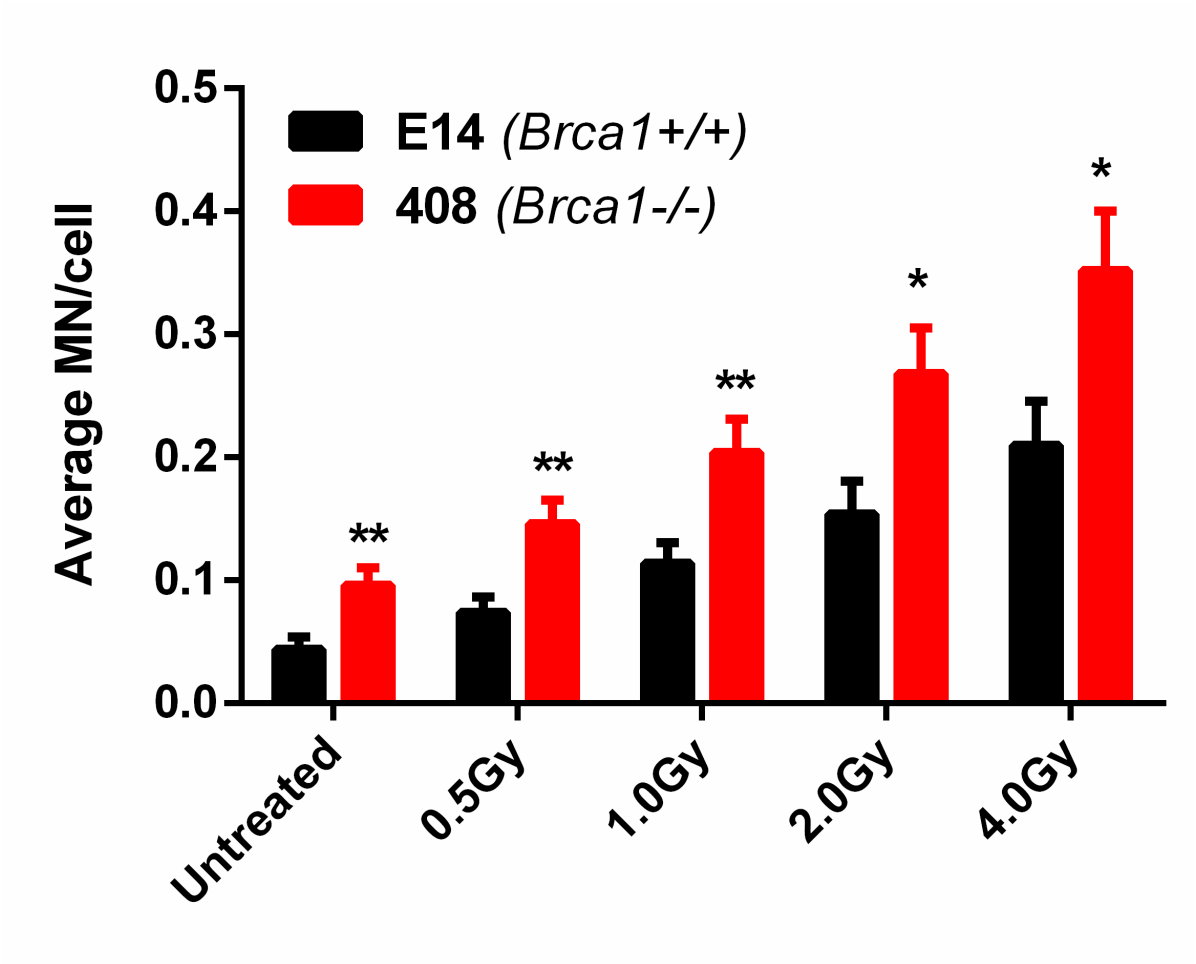

Figure 4-9. Mean MN after irradiation in mouse embryonic stem cell lines: E14 (Brca1+/+) and 408 (Brca1-/-). The basal levels of MN induced by IR 48hrs after exposure to different Gy in cultures of normal *Brca1* cell line (E14) and *Brca1* homozygous cell line (408) treated with cytochalasin B. Mean ± SEM from 500 scored binucleated cells. T-test used for statistical analysis. * (P<0.05); ** (P<0.001).

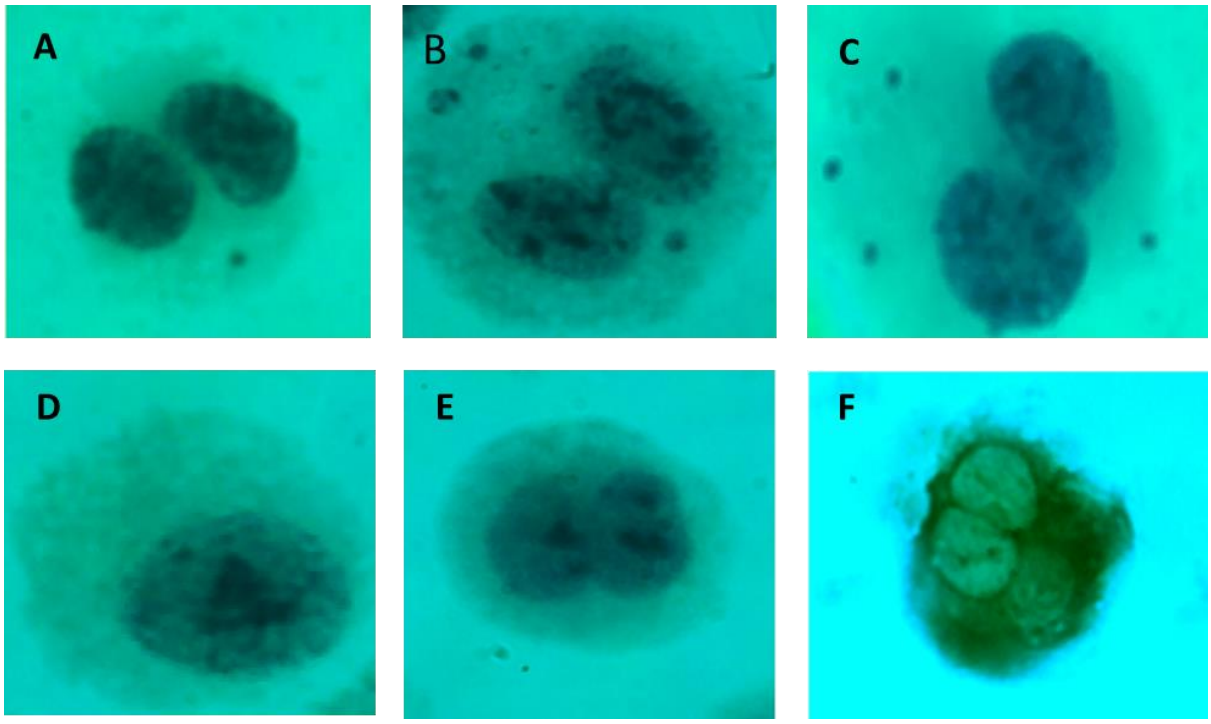

Figure 4-10. **Scoring binucleated cells in mESC. A)** an examlpe of a MN; **B and C)** binucleated cells with three MN; **D, E and F)** viable mono, di and quadrinuclear cells.

4.3 Discussion

Previous investigations showed that telomere dysfunction induces a DNA damage response in mammalian cells (Takai et al., 2003). Also γ-H2AX, 53BP1, RAD17, RAD51D, and ATM as DNA damage response factors, were discovered to become associated with dysfunctional, uncapped telomeres (Takai et al., 2003) (d'Adda di Fagagna et al., 2003, Herbig et al., 2004), (Tarsounas et al., 2004b). Moreover, it has been reported that embryonic tissue with BRCA1 deficiency revealed IR hypersensitivity, consistent with a defect in DSB repair (Sharan et al., 1997) (Deng and Brodie, 2000).

The first aim of this chapter was to evaluate the influence of BRCA1 defect on DDR mechanisem in mESCs (E14 and 408). It was shown previously that mESCs show very high basal levels of γH2AX without exposure to any genotoxic agents (Turinetto et al., 2012, Fernandez-Capetillo et al., 2002, Banath et al., 2009) argued that this could be due to chromatin decondensation rather than pre-existing DNA damage which potentially explains a

new role for γ-H2AX in mECCs. We have also observed the high level of γ-H2AX foci in both un-treated mouse ESCs (E14 and 408) which are consistent with their results.

Additionally, it is well documented that γ-H2AX is essential for the recruitment of BRCA1 and other DNA repair and damage-response factors like 53BP1, MDC1, and the MRN complex to the site of DNA damage (Fernandez-Capetillo et al., 2002, Stewart et al., 2003). Similar to the previous study by (Shen et al., 1998), we also know that murine BRCA1 is responsible for genomic integrity and murine embryos carrying a *Brca1* null mutation exhibited hypersensitivity to γ-irradiation and chromosomal abnormalities, suggesting an involvement of BRCA1 in DDR. The DNA damage kinetics analysis in mESCs after exposure to IR shows full repair in the control cell line (E14) 24hrs post-radiation, whereas, the *Brca1*$^{-/-}$ cell line (408) shows a defect in DNA repair kinetics as exemplifed by the presence of residual damage 48 hrs after (Stewart et al., 2003) exposure to IR (Figure 4.1). Analysis of DNA damage at telomeres also suggests lack of repair in the 408 cell line but not its full absences(Figure 4.3). The normal cell line, E14, was able to repair TIFs effectively (Figure 4.3). Thus our evaluation of DNA damage kinetics suggests that damage at telomeres (TIFs) is not irreparable in the case of the normal cell line. Our results contrast recent published resulsts suggesting that DNA damage at telomeres is irreparable irrespective of the genetic status of the cells (Fumagalli et al., 2012).

A high level of γH2AX has also been associated with the single-strand breaks occuring in the S phase of the ESC population, as rapidly dividing cells have increased proportion of cells in S phase, compared to many somatic cells (Chuykin et al., 2008b). Many studies have reported on the differences in sensitivity to DNA damaging agents between telomeric sequences and the rest of the genome. Furthermore, a number of studies have also demonstrated that the absence of a G1 checkpoint leads to cell death in S phase; it is also well documented that HR is the predominant DSB repair pathway in mESCs but when ESC cells start to differentiate, the HR levels are reduced whereas the NHEJ levels are increased (Tichy and Stambrook, 2008).

The second aim of this chapter was to determine whether the *Brca1* defect in mESCs leads to IR sensitivity. Our results clearly show that this is the case as shown by elevated frequencies of CAs in both G1 and G2 phases of the cell cycle (Figures 4.6, 4.7). The first evidence of elevated CAs in the 408 cell lines as a result of telomere dysfunction was presented by Al-Wahiby and Slijepcevic (2005). Their analysis revealed significantly higher levels of CAs after being exposed to bleomycin in 408 cells relative to E14 cells. It is clear that both cell lines showed CAs involving telomere-DSB interaction after treatment with blemycin, however, the percentage of CAs due to dysfunctional telomeres in the wild type ES cell line can be explained by the fact that this cell line, also named E14TG2a, is not completely normal; i.e., it lacks the 5` portion of the *Hprt*gene and may have some other abnormalities (Snouwaert et al., 1999).

A study has examined the DSB repair at the molecular level in the *Brca1-/-* 236.44 mESC line to determine the nature of the repair defect. It is worth mentioning that this cell line was designed by several rounds of gene targeting, such that both *Brca1* allels are mutated by deletion of the 5` end of exon 11 (Gowen et al., 1996). Their results demonstrated that the 236.44 cell line has defective HR which induced chromosome breaks and reduced gene targeting; the results also support the notion that wild type *Brca1* enables functional HR. In addition, Moynahan et al. (2001) established that the *Brca1*$^{-/-}$ genetic status results in chromosome instability in mESCs, while no dramatic instability can be detected in MEFs (mouse embryonic fibroblasts). Notably, *Brca1* deficient cells show sensitivity to mitomycin-C which is more profound than the previously published IR and cisplatin sensitivities (Gowen et al., 1998, Bhattacharyya et al., 2000).

In conclusion, results in this chapter indicate that when both copies of *Brca1* are dysfunctional, as in the case of the 408 cell line, this leads to dysfunctional DNA damage response and subsequently dysfunctional telomere maintenance.

CHAPTER 5

5 Analysis of ALT markers in mESCs

5.1 Introduction

It has been documented the nuclear protein, BRCA1, is classified as a tumour suppressor based on the fact that deficiency of *BRCA1* gene can cause about 80-90% risk for breast or ovarian cancer (Ford et al., 1994, Miki et al., 1994). However, the BRCA1 protein has been shown to interact with other proteins; it can also play a supporting role in several cellular processes, such as transcription (Chapman and Verma, 1996, Monteiro et al., 1996), cell cycle transition (Xu et al., 1999a, Larson et al., 1997) and DNA repair (Scully et al., 1997, Gowen et al., 1998, Shen et al., 1998, Zhong et al., 1999). It is interesting that telomere maintenance mechanisms also act as a tumour suppression mechanism (Cesare and Reddel, 2008). Therefore, analysis of telomere maintenance in cells with null BRCA1 could potentially shed light on how this protein exerts its tumour suppression properties. Also, it has been demonstrated that *BRCA1* is expressed in only a subset of tissues (Miki et al., 1994); however, some studies that used the murine homologue Brca1 (Bennett et al., 1995, Sharan et al., 1995) have demonstrated that the expression can be detected early in the development of the embryo and continues to be expressed in a large spectrum of tissues throughout the development and into adulthood (Marquis et al., 1995, Lane et al., 1995). Other studies have also revealed that BRCA1 can be expressed in all dividing cells

throughout the cell cycle in a specific manner; the maximal expression has been shown to occur in the S phase (Chen et al., 1996, Ruffner and Verma, 1997). Functionally, BRCA1 has been examined using a number of mouse lines with disruption of *Brca1* gene-by-gene targeting (Gowen et al., 1996, Hakem et al., 1996, Liu et al., 1996, Ludwig et al., 1997, Shen et al., 1998). Unlike humans, mice with null *Brca1* do not show an increased risk of tumour formation (Cressman et al., 1999). However, mice heterozygous mutants for both *Brca1* and *P53* have been shown to develop tumours after exposure to IR (Cressman et al., 1999). Using mice with deficiency of *Brca1* as a source of primary cell lines has been restrictive because these animals die in early embryogenesis. Therefore, the mECS cell line homozygous for a mutant *Brca1* allele has been generated by two rounds of gene targeting (Snouwaert et al., 1999).

Also, two additional studies confirmed that *BRCA1* plays a role in telomere maintenance. French et al. (2006) revealed that the expression of a dominant negative *BRCA1* mutation in breast epithelial cells leads to changes in telomere length (elongation) and an increase of anaphase bridges. Moreover, previous studies using mouse *Brca1-/-* cells (McPherson et al., 2006) showed the level of telomeric fusion increases relative to control cells. On the other hand, study of the effect of telomere shortening on chromosome stability, and analysis of telomere length in two individual chromosomes (2 and 11) derived from mice lacking the telomerase RNA (mTR) gene by using quantitative fluorescence in situ hybridization, indicate that telomere length at both chromosomes decreased with increasing generations of $mTR^{-/-}$ mice.

Promyelocytic leukemia (PML) nuclear bodies regulate cellular processes, such as DNA replication, tumour suppression, gene transcription and DNA repair (Pearson et al., 2000, Salomoni and Pandolfi, 2002, Bernardi and Pandolfi, 2007). Consistent with the multi–functional role in cells, PML bodies contain a variety of regulatory proteins including PML, SP100, p53, pRb, HP-1, ATRX, DAXX and SUMO-1. Generally, in human ALT cancer cell lines PML bodies known as the ALT-associated PML bodies (APBs) are readily identifiable.

It is well documented that telomeric DNA, telomere binding proteins (TRF1, TRF2) and DNA repair protein (NBSI, Mre11, RAD50) co-localize with the APBs (Cesare and Reddel, 2010, Wu et al., 2003). Although it is still unclear whether APBs directly drive ALT activity, there is evidence that they promote ALT activity. The disassembly of APBs as a result of RNAi-mediated knockdown of either PML or Mre11/RAD50/Nbs1 (MRN) proteins leads to inhibition of telomere elongation in ALT cells (Jiang et al., 2005, Jiang et al., 2007, Wu et al., 2000). Furthermore, it has been demonstrated that NBS1 plays a key role in the recruitment of Rad50, Mre11 and BRCA1 (the latter through the binding of NH2-domain of NSB1 with the COOH-terminal domain) to the APBs (Wu et al., 2003). Thus, the study suggests the direct association of BRCA1 with APBs.

It is now well documented that mutations in the *ATRX* gene correlate with the ALT activity making this gene one of the best ALT markers (Lovejoy et al., 2012). The activation of the ALT pathway occurs in pancreatic neuroendocrine cancers, pediatric glioblastomas, and other tumours of the central nervous system when ATRX is mutated (Lovejoy et al., 2012). The molecular bases for ALT activation in human cancer cells are not yet fully known. The ALT activation occurs relatively infrequently *in vitro* during conversion of virally-transformed (p53/Rb deficient) human cells and may take months following a telomere mediated crisis (Yeager et al., 1999, Lovejoy et al., 2012). The low frequency of ALT activation in mammalian cells is thought to be due to a mechanism that requires mutation and/or epigenetic modification of the genome to unleash the ALT pathway (Lovejoy et al., 2012). The ALT pathway is suppressed in telomerase-positive mammalian cells due to the component of shelterins, such as TRF2, Rap1 and POT1 as well as KU70/80 heterodimers (Lovejoy et al., 2012, Celli et al., 2006) (Sfeir et al., 2010). ATRX and DAXX participate in chromatin remodelling at telomeres within histone H3.3; recently it has been shown that inactivating mutations in ATRX or DAXX are a common phenotype of human pancreatic neuroendocrine tumors (Heaphy et al., 2011) and cause telomere dysfunction phenotype resembling that of ALT activation in 61% of the tumours (Heaphy et al., 2011). These ALT-

associated phenotypes include increasing TTAGGG repeat containing telomeric transcripts (known as TERRA), reducing telomeric loading of HP1α and elevated DDR (Osterwald et al., 2015). Although the exact mechanism of ATRX or DAXX mutation in ALT activation is not yet known, ATRX or DAXX mutation is thought to serve as a good marker of ALT activity in vitro, as a recent study has shown that 90% of ALT-positive immortalised lines are ATRX deficient (Lovejoy et al., 2012).

In this chapter, we examined telomere maintenance in the same set of mECSs as in the previous chapter (E14, 408) in order to assess contribution of BRCA1 deficiency to this process. We analysed T-SCEs by CO-FISH, telomere length by IQ-FISH and the frequency of end-to-end chromosome fusions by conventional cytological methods. We also probed telomere association with APBs and ATRX in order to assess contribution of ALT to telomere maintenance in the BRCA1 negative environment.

5.2 Results

5.2.1 CO-FISH analysis of BRCA1-defective mouse embryonic stem cells

We started by analysing frequencies of T-SCEs. A total of 100 metaphases per cell line were analysed. Our results indicate a significant increase ($P<0.001$) in T-SCE levels in the 408 cell line relative to the E14 cell line (Figure 5.1). These results suggest that the *BRCA1* defect affects recombination rates at telomeres, and subsequently could be a contributory factor to the defective DNA damage response observed in these cells. Additionally, the results further confirm the existence of the ALT pathway in mouse *Brca1*$^{-/-}$ ESCs as T-SCEs represent one of the ALT markers (Chapter 6). Figure 5.2 shows microscopy examples of T-SCEs observed in mESCs.

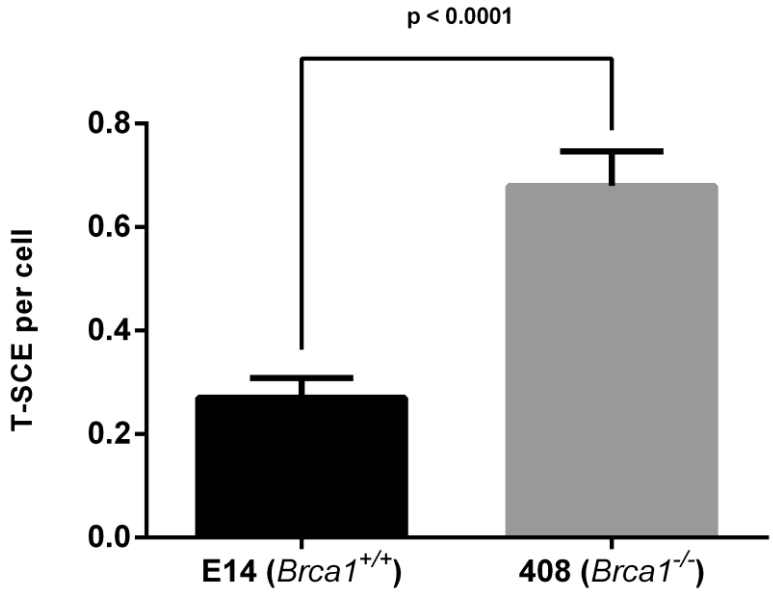

Figure 5-1. Mean value of T-SCEs in mESCs. Error bars indicate SEM. A total of 100 metaphases were scored for the presence of T-SCE in two independent experiments.

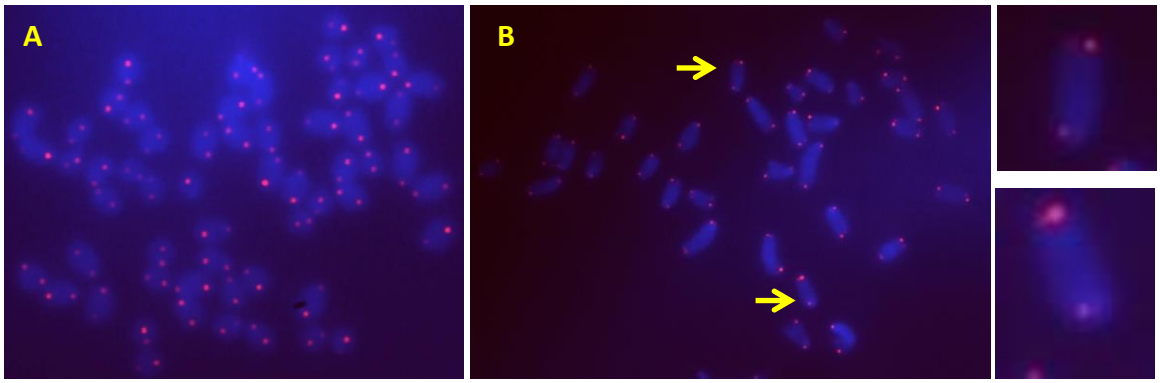

Figure 5-2. Examples of T-SCEs in the mESCs. A) A metaphase spread from the E14 cell line. **B)** A metaphase spread from the 408 cell line. The yellow arrows indicate examples of T-SCEs and enlarged on the right.

5.2.2 Analysis of end-to-end telomeric fusion in mouse embryonic stem cells

Chromosomal instability has been characterised as a one the major classes of genetic instability, which occurs at a very early stage of tumorigenesis (Shih et al., 2001). Some studies have revealed that disorder of telomere maintenance is related with end-to-end chromosome fusion in many organisms. For instance, in the fission yeast *S. pombe,* deletion of ATM homologous (*tel1*$^{+}$ and *rad3*$^{+}$*)* or telomerase reverse transcriptase gene (*trt*$^{+}$) affects

telomere shortening and leads to eventual loss of growth. To directly determine whether telomere dysfunction can induce genetic instability, we measured end-to-end chromosome fusions in E14 and 408 cell lines. We measured frequencies of end chromosome fusions (ECFs) in metaphase cells. For this purpose, we scored 100 metaphase cells by using the telomeric PNA probe. The results indicated a significant increase ($P<0.05$) in frequencies of telomeric fusion in 408 cells compared to the control E14 cell line (Figure 5.3). Our results support the idea that functional telomeres are required to maintain chromosome stability and prevent chromosome fusions. Figure 5.4 shows examples of ECFs observed.

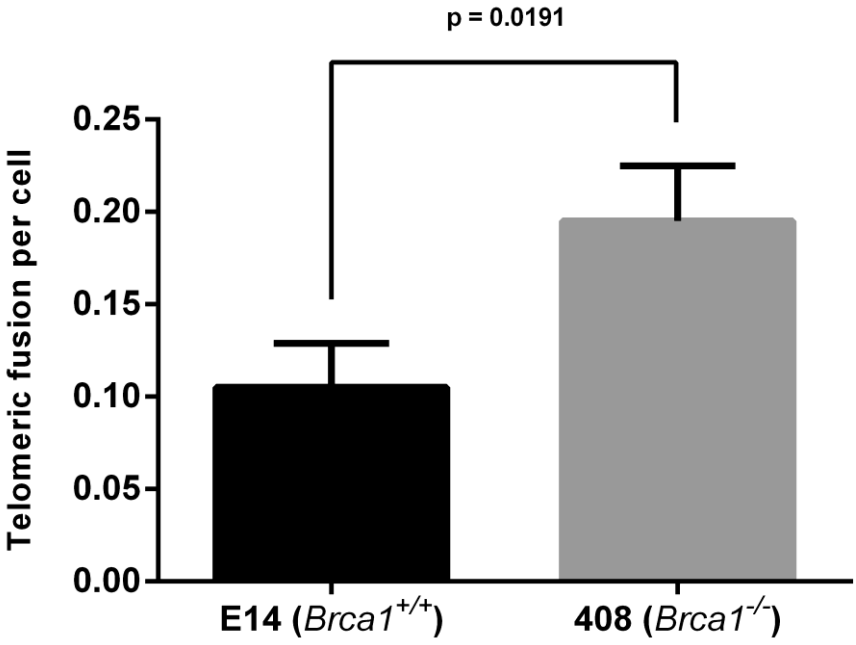

Figure 5-3. Frequencies of telomeric end-to-end fusions in E14 and 408 cell lines. The error bar indicates SEM. A total of 100 metaphases were scored for the presence of ECFs in two independent experiments.

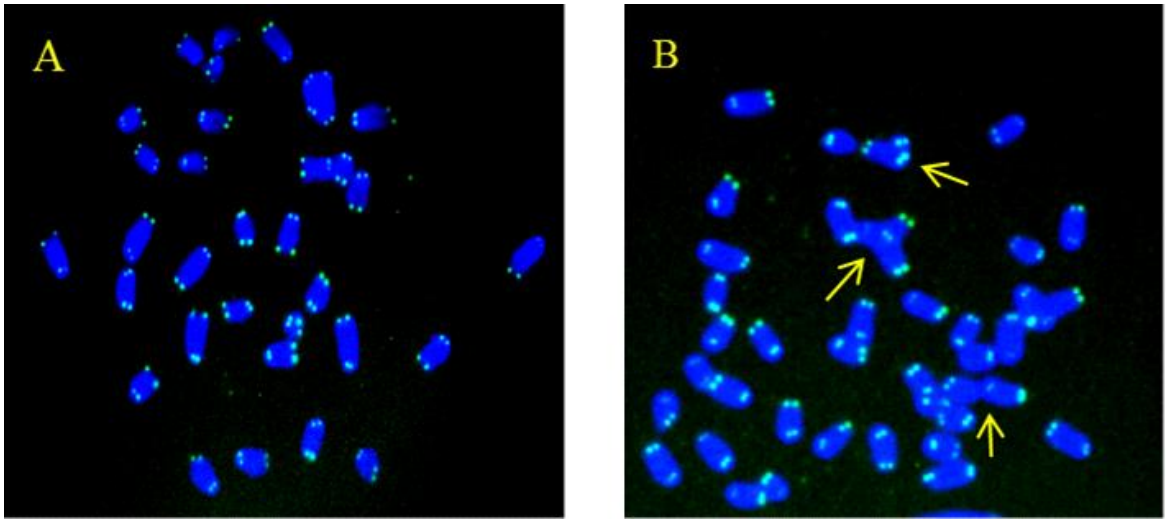

Figure 5-4. **Detection of telomeric fusion in mouse embryonic stem cells: A)** control cell line (E14), and **B)** Brca1$^{-/-}$ (408).

5.2.3 Telomere length analysis using IQ-FISH in mouse embryonic stem cells

Next, we analysed telomere fluorescence intensity in 408 and E14 cell lines using the IQ-FISH technique (see the Chapter 2). A total of 100 interphase cells per cell line were captured, and the mean telomere fluorescence intensity per cell was used to determine potential differences between cell lines. In order to ensure reproducibility of results, telomere lengths were measured in two mouse lymphoblastoid cell lines: the parental radio-resistant L5178Y-R cell line (known as LY-R) and its subtype, the radiosensitive L5178-S cell line (LY-S) (see Chapter 3; Figure 3.5 A and 3.5 B). Statistical analysis of our results revealed that the mouse *Brca1*$^{-/-}$ cell line (408) had significantly decreased telomeric DNA sequences ($P < 0.001$) compared to the control *Brca1*$^{+/+}$ cell line (E14) (Figure 5.5). Therefore, these results are similar to those observed in cell lines from *BRCA1* carriers (Chapter 3).

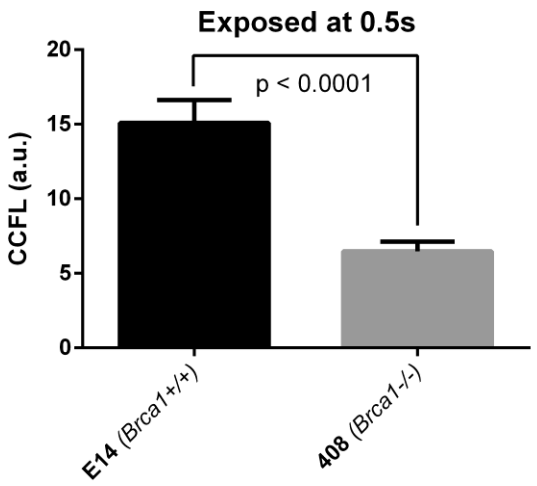

Figure 5-5. Telomere fluorescence analysis by IQ-FISH. CCFL. corrected calibrated fluorescence after calibration using LY-R and LY-S cells. Error bars indicate SEM.

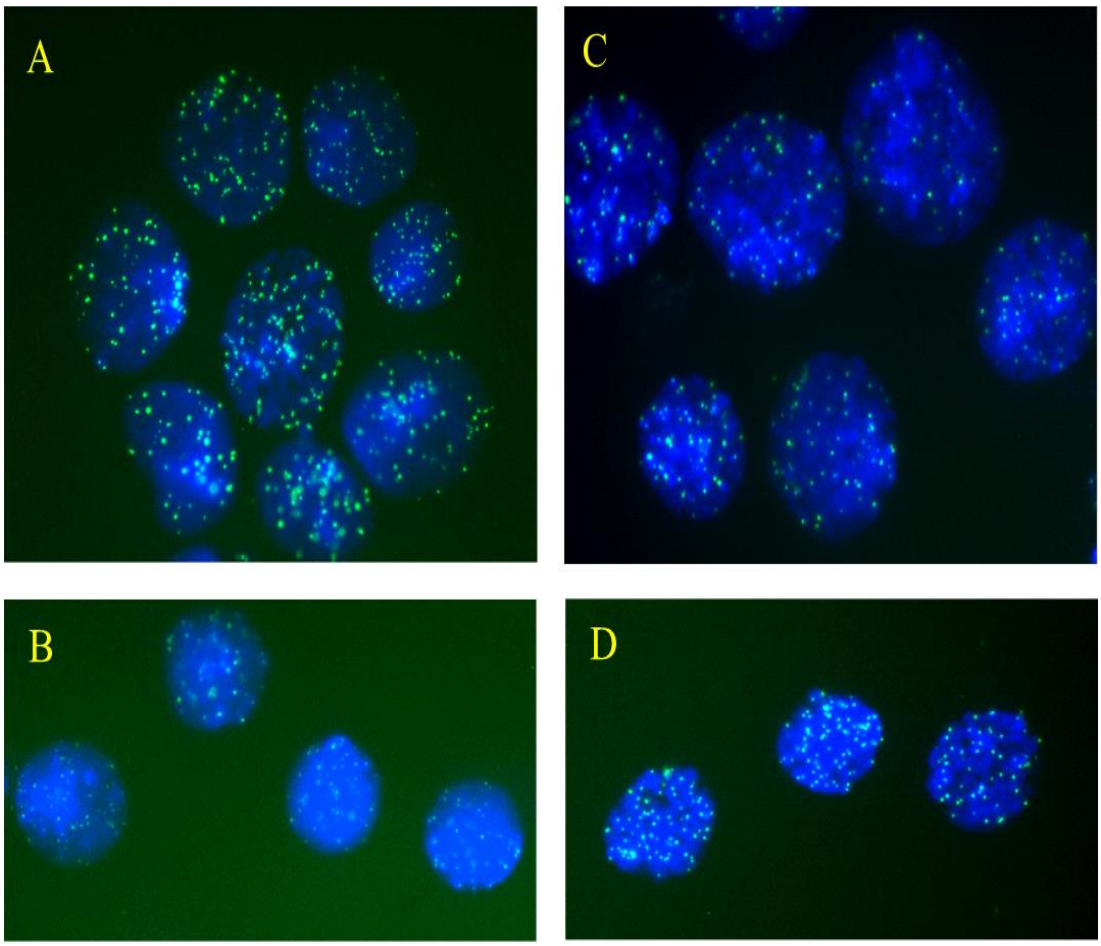

Figure 5-6. Telomere fluorescence analysis using IQ-FISH. A and **B)** Radioresistance LY-R and Radiosensitive LY-S in interphase; **C** and **D)** show mESCs: 408 and E14, respectively.

5.2.4 Co-localization of PML bodies and telomeres in mouse embryonic stem cells

Elevated frequencies of T-SCEs in 408 cells suggest on the presence of the active ALT pathway (Figure 5.1). To investigate whether these cells show further evidence of the active ALT pathway we assessed another ALT marker, APBs, in each cell line. For this purpose we used well-established positive controls: human ALT $^{+}$ and ALT $^{-}$ cell lines (U2OS as ALT positive and HeLa as ALT negative) (Figure 5.7). In addition, we included the human BRCA1 defective HCC1937 cell line and two mouse lymphoma cell lines, LY-R and LY-S (Figure 5.7). The difference in the average numbers of APBs/nuclei, were statistically significant between U2OS cells on one side and HeLa and HCC1937 on the other side (Figure 5.7). This suggests that BRCA1 deficiency present in the HCC1937 cell line does not lead to the ALT activation. However, the difference between HeLa and HCC1937 cells is significant (Figure 5.7) adding some uncertainty to our results. We have also observed statistically significant differences between 408 cells on one side and all other mouse cell lines on the other side (Figure 5.7) suggesting that the BRCA1 defect may have some effect on APBs as the ALT marker.

The analysis of co-localisation of the telomeres and APBs is shown in Figure 5.8. This analysis excludes the BRCA1 deficiency as a potential activator of ALT in human cells as the HCC1937 cell line did not show co-localisation between APBs and telomeres (Figure 5.8). Similarly, there was no difference between 408 and E14 cells in terms of co-localisation (Figure 5.8) further supporting the lack of correlation between the ALT activation and a BRCA1 defect. Interestingly, mouse lymphoma cells showed some differences relative to 408/E14 cells (Figure 5.8).

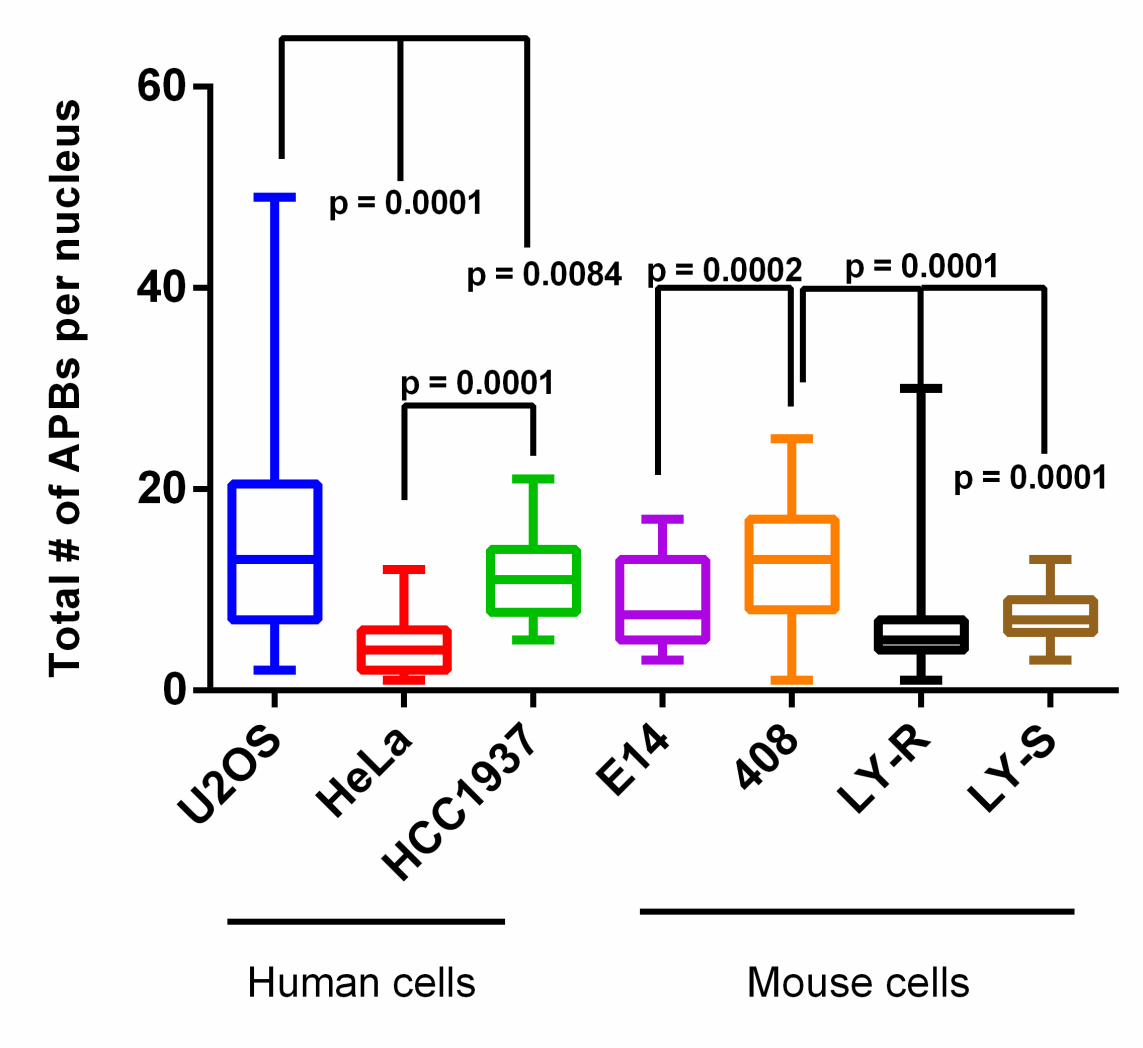

Figure 5-7. Total number of APBs in human and mouse cells. Frequency of APBs counted in: BRCA1-positive human cells (U2OS and HeLa) and BRCA1-defective human cells (HCC1937); and mouse Brca1-positive ESC (E14) and Brca1-defective ESC (408) cells; mouse Brca1-positive lymphoblastoid (LY-R and LY-S) cells. Data from 50 nuclei counted in two independent experiments. T-test used for statistical analysis.

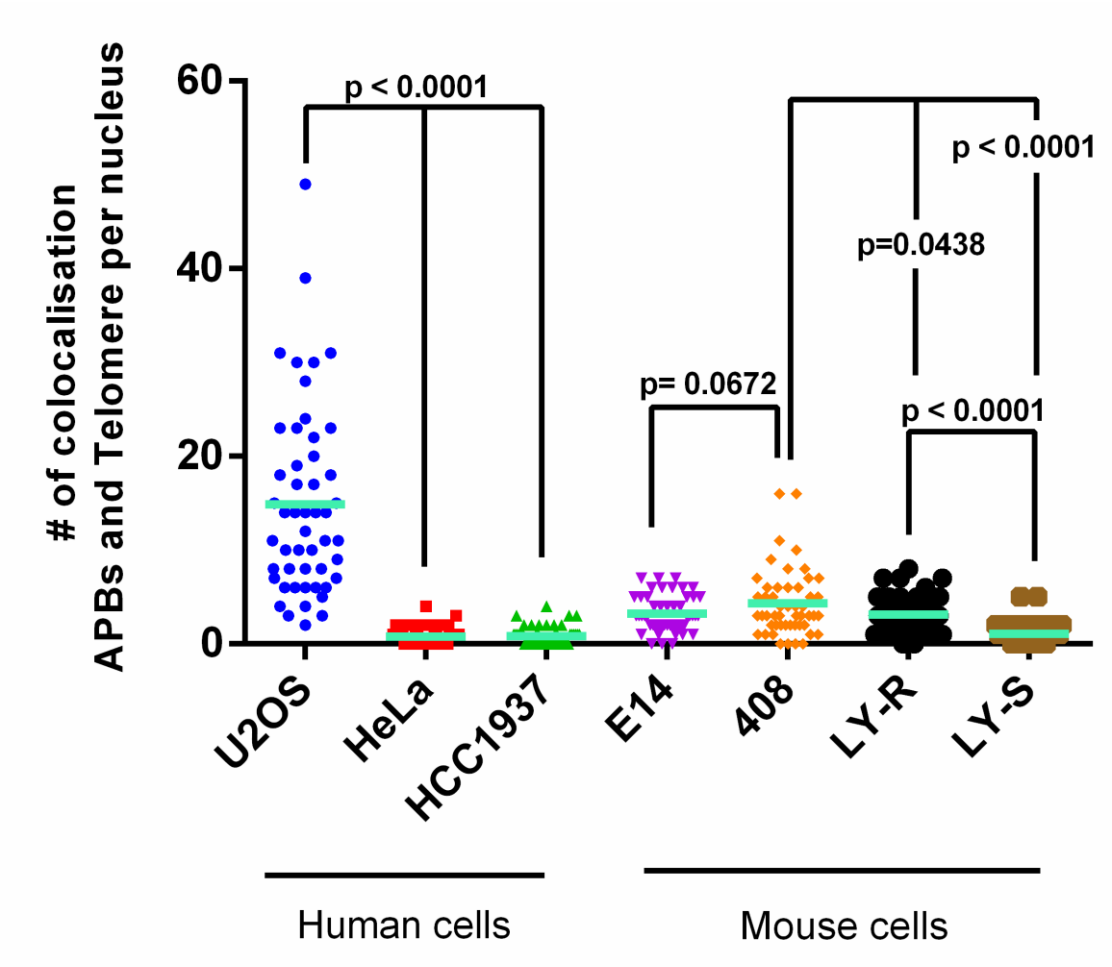

Figure 5-8. Co-localisation of APBs with telomeres in human and mouse cell lines. Green lines indicate the means. T-tests were used for statistical analysis.

Examples of images obtained after the immunofluorescence analysis with PML antibodies and telomeric probe are shown in Figures 5.9 and 5.10.

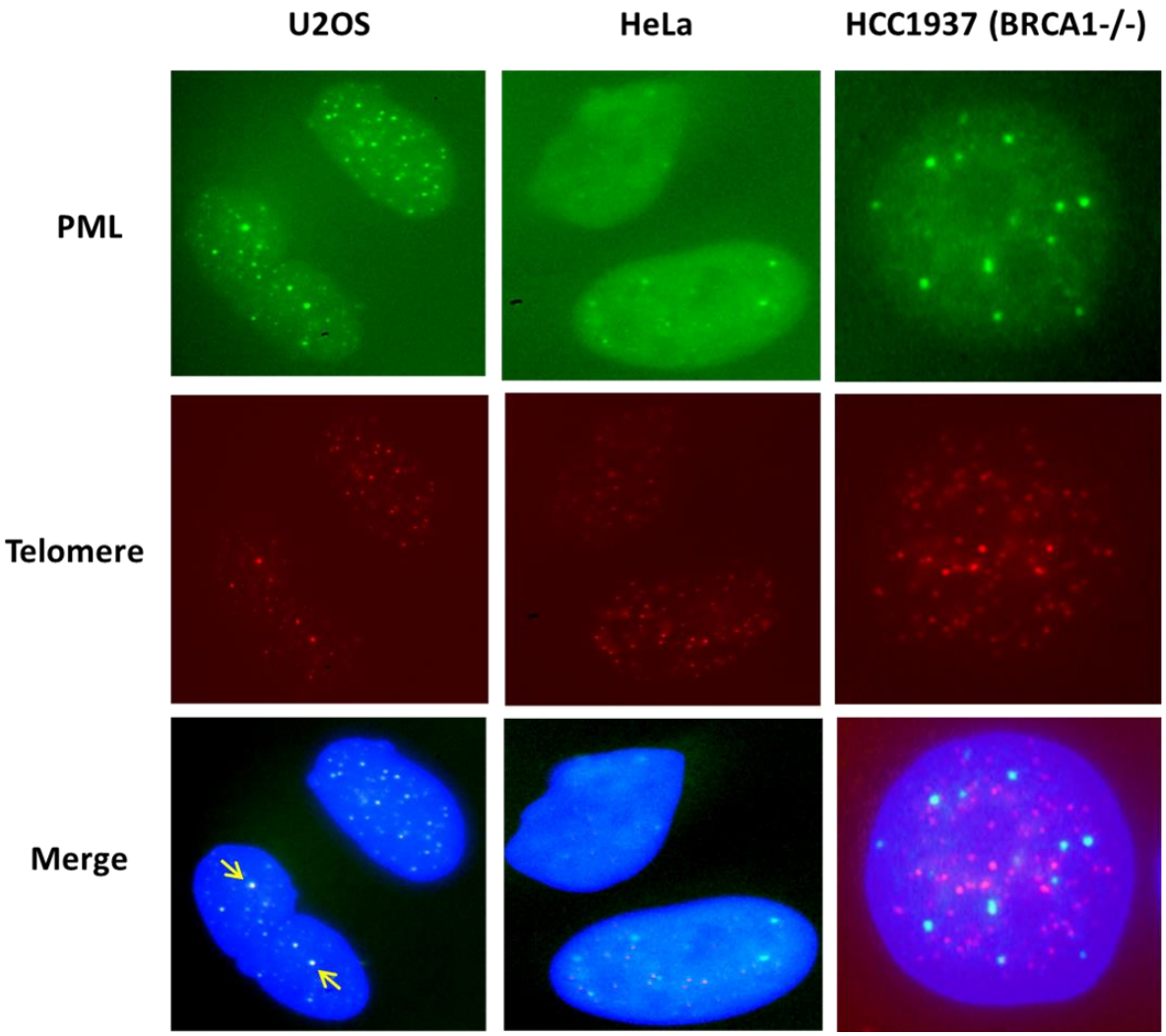

Figure 5-9. Immuno-FISH analysis in ALT$^+$ (U2OS) and ALT$^-$ (HeLa and HCC1937). U2OS was used as the positive control while HeLa served as the negative control. Interphase cells were permeabilised and stained with anti-PML (green) and telomeric Cy3-labeled PNA probes (red). Nuclei were counterstained with DAPI.

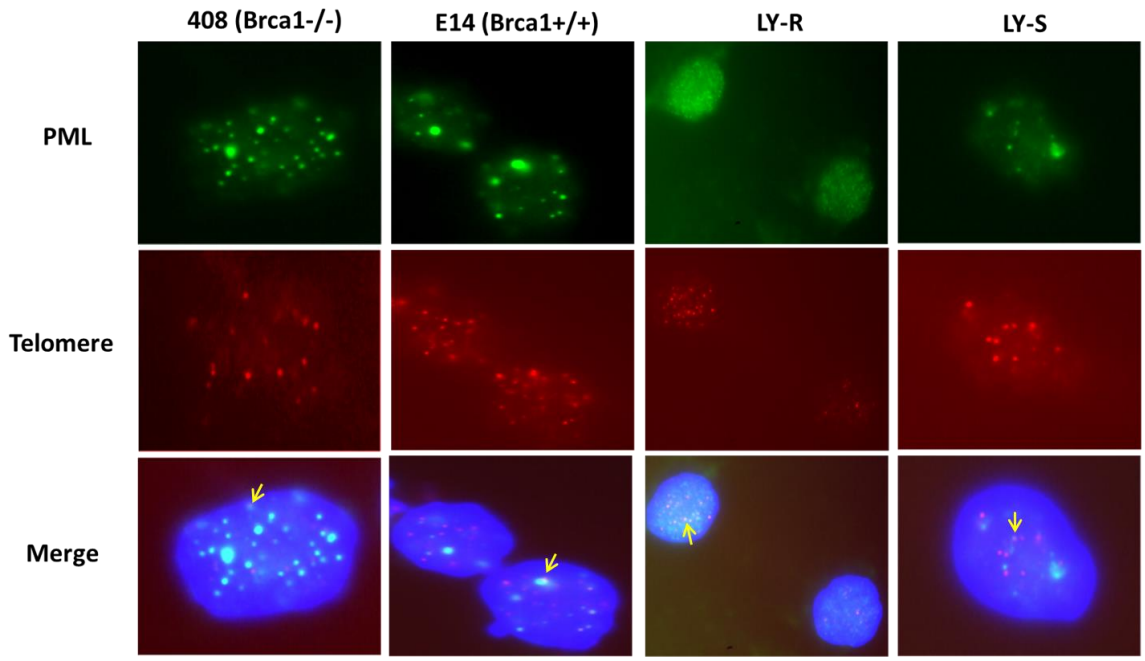

Figure 5-10. Detection of APBs by immuno-FISH in mESCs, LY-R and LY-S cells. Interphase cells were permeabilised and stained with anti-PML (green) and telomeric Cy3-labeled PNA probes (red). Nuclei were counterstained with DAPI.

5.2.5 ATRX as a marker of ALT activity

Next, we used another ALT marker, the antibody against ATRX, to check if there is a link between the ALT activation and BRCA1 defect. We looked for the presence of ATRX using immunofluorescence in the two mESC lines, as well as in human ALT^{+} U2OS (BRCA1$^{+/+}$), ALT^{-} HeLa (BRCA1$^{+/+}$) HCC1937 (BRCA1$^{-/-}$), mouse LY-R and LY-S cells. We measured the total number of ATRX foci per cell in two independent experiments in all samples (Figure 5.11). As expected, the human U-2OS ALT^{+} cell line had no ATRX foci as reported previously (Lovejoy et al., 2012), whereas there were on average between 10-11 ATRX foci per cell in both HeLa and the HCC1937 human breast cancer cell line (Figure 5.11). Also there were on average 7 ATRX foci in the two mESC lines (Figure 5.11). Therefore, judging by the presence of ATRX signals in all cell lines except the ALT positive cell line, U2OS, we have to conclude that the BRCA1 defect *per se* is not linked to the ALT activation.

Next, we analysed co-localisation of ATRX with telomeres, if any, in all cell lines (Figure 5.12). A total of 50 cell nuclei were randomly analysed in each cell line in two independent

experiments. In general, the level of co-localisation was low (Figure 5.12) and interestingly, there was a statistical difference between 408 cells and LY-R cells (p<0.0001) (Figure 5.12).

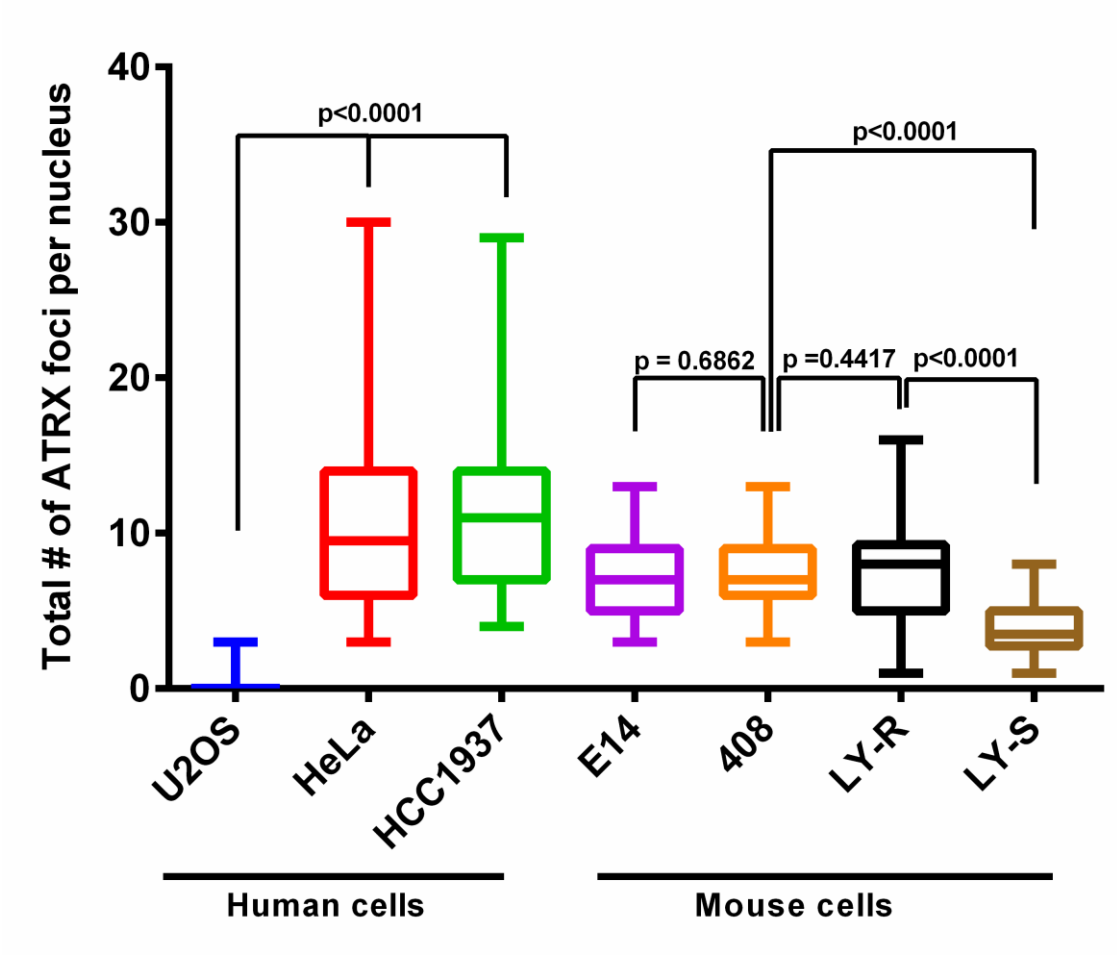

Figure 5-11. Total number of ATRX signals in human and mouse cells. Data is from 50 nuclei from two independent experiments. T-test is used for statistical comparison.

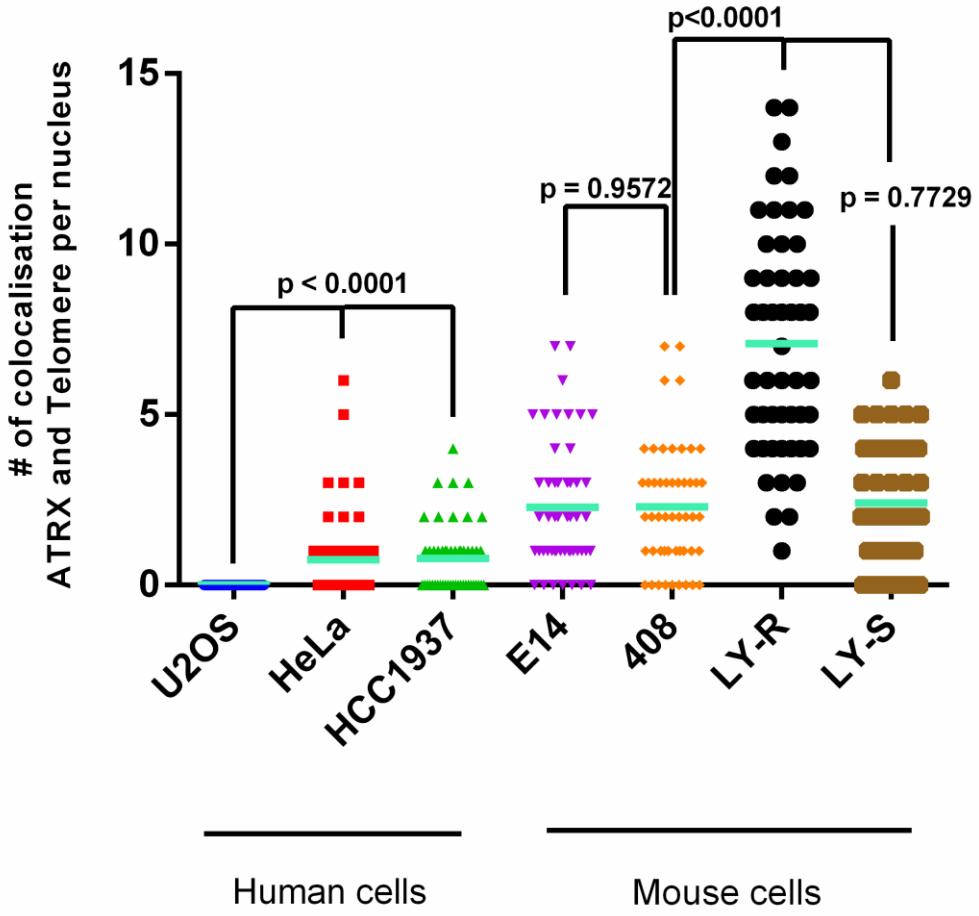

Figure 5-12. Co-localisation of ATRX with telomeres. The green bar indicates mean. T-test is used for statistical analysis.

Examples of images of cells stained with ATRX antibodies and telomeric probe are shown in Figures 5.13 and 5.14.

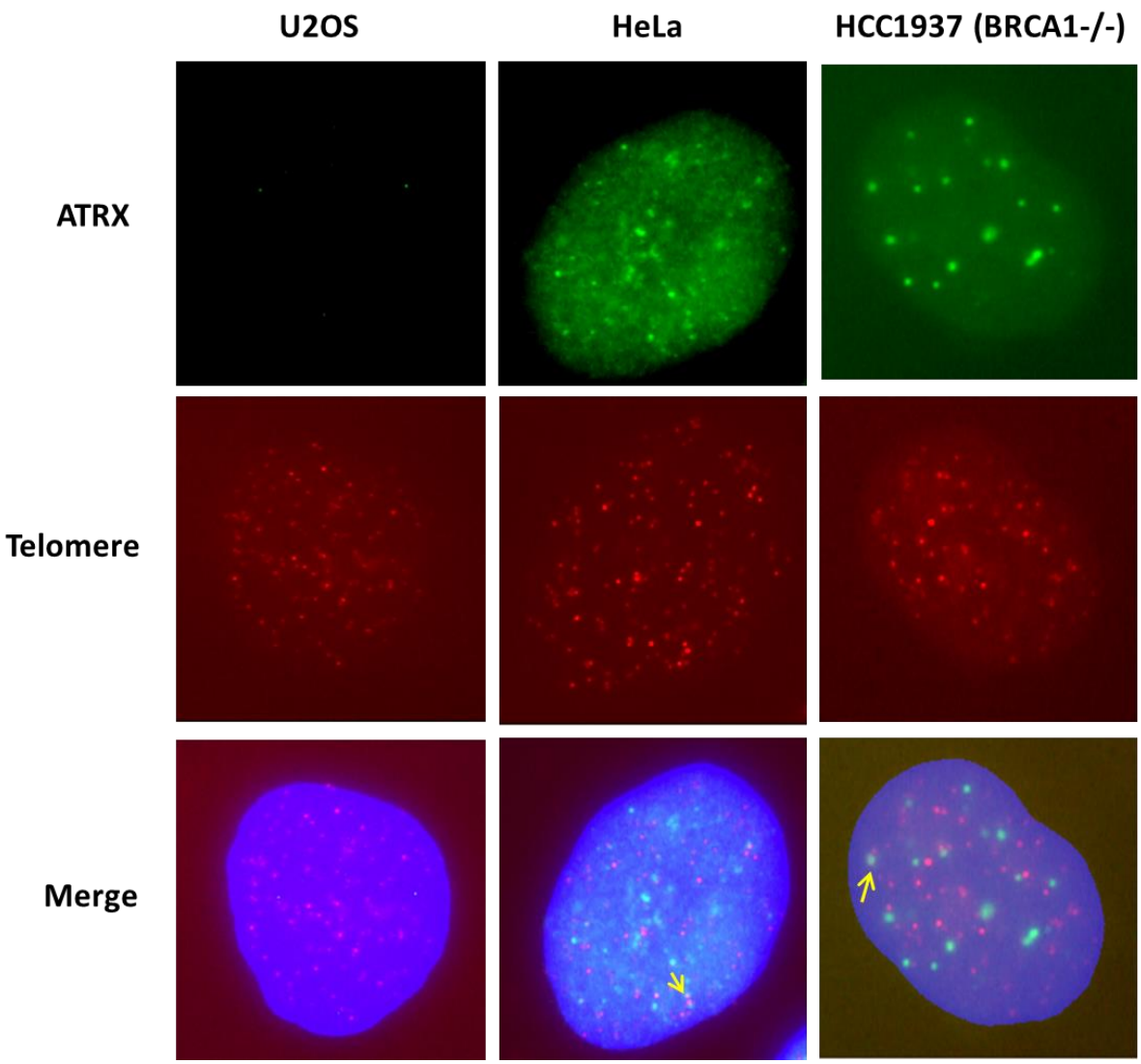

Figure 5-13. ATRX (green) is absent in U2OS cells and present in HeLa and HC1937 cells. Telomeres shown in red.

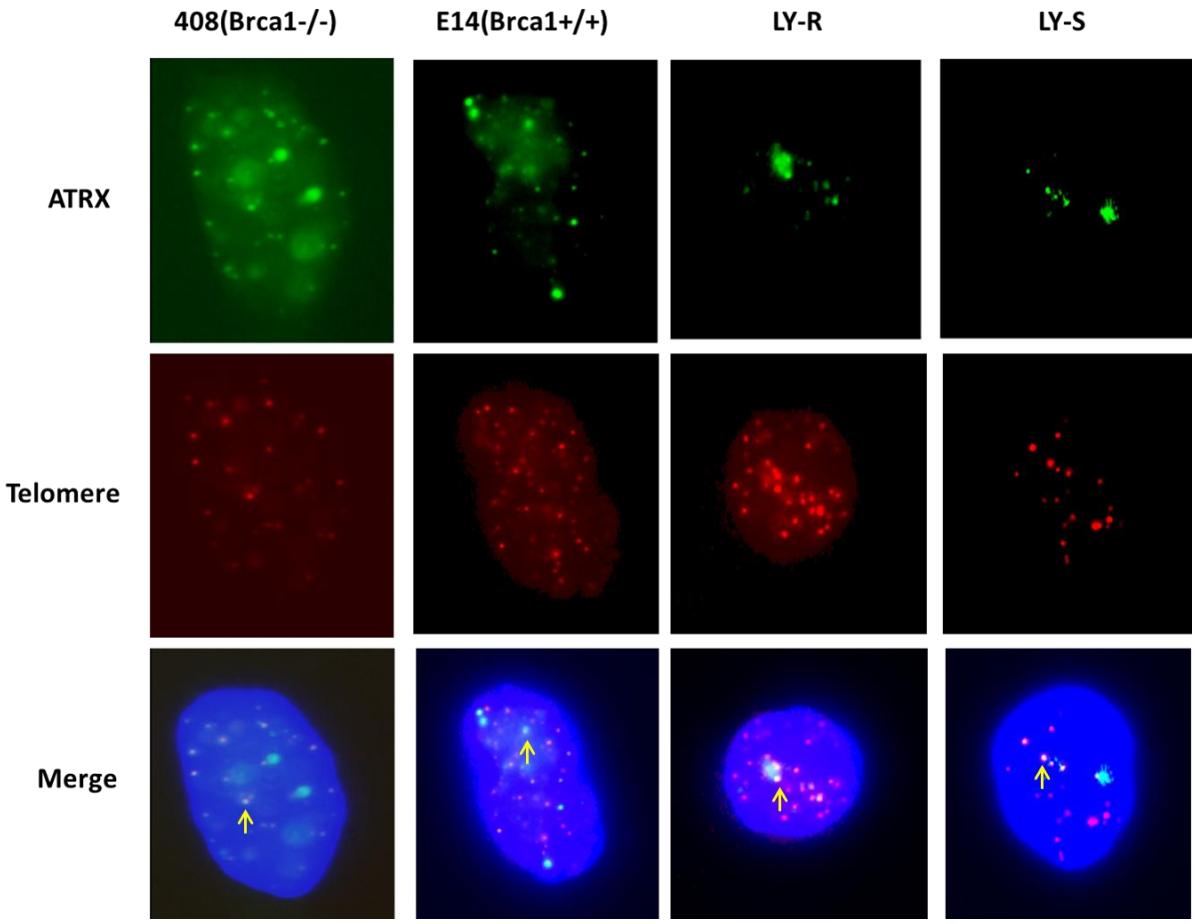

Figure 5-14. ATRX signals (green) present in all mouse cells. Telomeres shown in red.

5.3 Discussion

Mutations in breast and ovarian cancer susceptibility gene 1 (*BRCA1*) can cause about 40-45% of hereditary breast cancer cases. BRCA1 is a multi-functional protein, which is not fully understood, however, research has shown BRCA1 functions in DDR, HR, NHEJ and regulation of telomere length (Tirkkonen et al., 1997, Xu et al., 1999b, Weaver et al., 2002, Baldeyron et al., 2002, Zhong et al., 2002b, Bau et al., 2004, Moynahan et al., 1999, Moynahan et al., 2001, Merel et al., 2002, Acharya et al., 2014) (Wang et al., 2001). In mammalian cells, telomere dysfunction induces DDR. For example, a study has shown that the TRF2 deletion leads to uncapped telomeres and an association with DDR factors including 53BP1, γ-H2AX, Rad17, ATM and Mre11, and subsequent telomere dysfunction (Takai et al., 2003). The co-localisation of BRCA1 with MRN complex following DNA damage

was also reported (Zhong et al., 1999, Wang et al., 2000, Wu et al., 2003) proposing that BRCA1 plays a role in telomeres. Moreover, the results of an initial study on cultured embryonic stem cells revealed that Brca1-deficient cells in addition to hypersensitivity to γ-irradiation also showed numerical and structural chromosomal aberrations which may be a direct consequence of unrepaired DNA damage (Deng and Scott, 2000). Therefore, deficiency in BRCA1 gene affects many cellular pathways.

Results presented in this chapter indicate that the *Brca1* defect in mESC line, 408, caused elevated T-SCE frequencies (Figure 5.1) as revealed by the CO-FISH assay (Bailey et al., 2004a)Baily and Eberle 2001). This finding is in the line with a previous study (Al-Wahiby and Slijepcevic, 2005) which revealed that after treatment with bleomycin the *Brca1* deficient cell line (408) shows a higher level of T-SCEs than the parental wild type ES cell line (E14). Furthermore, we observed increased end-to-end chromosome fusion and significant telomere shortening relative to the control cell line (E14) (Figures 5.2 and 5.3).

Elevated T-SCE frequencies (Figure 5.1) may represent the sign of ALT activation. However, no clear difference was detected in the number of APB or ATRX signals in the set of several relevant cell lines (Figures 5.8 and 5.12) suggesting the lack of association between the ALT activation and BRCA1 defect. The observed elevated T-SCE frequencies in 408 cells probably reflect the HR deficiency as a result of BRCA1 absence rather than the ability of BRCA1 to affect HR at telomeres.

We also measured telomere length by IQ-FISH techniques (see Chapter 2). We found a significant difference between Brca1$^{-/-}$ (408) and the matching control cell (E14) (Figure 5.5). This result suggests that telomeres in mouse Brca1$^{-/-}$ degraded more rapidly than telomeres in Brca1$^{+/+}$ (E14) due to telomere dysfunction. Our measurements are in agreement with previously published studies, which analysed telomere maintenance in mESCs deficient in *Brca1*, which revealed accelerated telomere shortening and mild telomere dysfunction in comparison to control cells (Cabuy et al., 2005). Furthermore, their results revealed

accelerated telomere shortening in cells defective in ligase I, ligase IV, Artemis, AT, NBS, FA, patient with a defect in DNA DSB repair and patient diagnosed with Xeroderma Pigmentosum (Cabuy et al., 2005). However this accelerated telomere shortening was accompanied by signs of telomere dysfunction including anaphase bridges (formation of bridge during anaphase separation of chromosomes), end-to-end chromosome fusions and early loss of telomere capping function (Cabuy et al., 2005).

In conclusion, results presented in this chapter indicate (i) elevated T-SCE frequencies and some other signs of telomere dysfunction in the mouse *Brca1* deficient cell line (408) and (ii) lack of correlation between the ALT and the BRCA1 defect.

CHAPTER 6

6 Assessment of additional ALT markers in mouse and human cells

6.1 Introduction

In the previous chapter we used markers of ALT (T-SCE, APBs, and ATRX) in human cells and mESCs to detect correlation between BRCA1 deficiency and ALT activity. However, none of the ALT markers we used gave us enough confidence to think that Brca1 is actively involved in the ALT pathway. For example, even though frequencies of T-SCEs were elevated in Brca1 defective mECSs (Figure 5.1) other ALT markers (APBs and ATRX) could not be correlated with the Brca1 mediated defect (Figures 5.8-5.12). Therefore, we set out to use a more robust marker of ALT activity to clarify this uncertainty. At present the most reliable indicator of ALT activity is the C-Circle (CC) assay (Henson et al., 2009). The CC assay provides a rapid and sensitive measure of the ALT activity (Henson and Reddel, 2010).

Human and rodent cells maintain their telomere length through the use of telomerase enzyme (Greider and Blackburn, 1985). However the fundamental difference between the two types of cells is that most human somatic cells have a repressed telomerase activity - apart from mitotically active cells such as skin, hair follicle cells, lymphocytes and endometrial cells that shows low levels of telomerase (Hiyama et al., 1995, Härle-Bachor and Boukamp, 1996, Yasumoto et al., 1996). Nevertheless, telomerase enzyme is found active in human germ cells (Hahn et al., 1999) and 85% of human tumour cell lines (Kim et al., 1994). Interestingly, recent evidence has suggested that ALT may indeed be active in mouse somatic cells *in vivo*, but the level of the activity is insufficient to maintain or elongate telomere lengths and that during *in vitro* immortalisation or in cancers this level is increased (Neumann et al., 2013). So far, there is no evidence that ALT activity is present in normal human somatic cells. ALT is specific to some forms of tumors such as osteosarcomas (Cesare and Reddel, 2010).

Rodent cells including mouse do not shut down telomerase activity in transition from stem to differentiated cells and therefore possess longer telomeres (20kb) compared to the human cells (9-12kb) (Hemann and Greider, 2000, Newbold, 2002, Rangarajan and Weinberg, 2003, Calado and Dumitriu, 2013). Mouse cells have longer telomeres and inhibition of telomerase enzyme in these cells, like the $mTR^{-/-}$ mouse embryo fibroblast (MEFs), stop cell division only after 10-15 population doublings long before appreciable telomere shortening occurs (Blasco et al., 1997), indicating that mouse cells do not use telomere lengths as a mechanism to limit cell division and therefore, other events may exist (Wright and Shay, 2000). Could the other factor be the co-existence between the telomerase and ALT in maintaining telomere lengths dynamics in mouse cells? Indeed, in experiments whereby telomerase was exogenously activated through the *hTERT* transfection in ALT positive GM847 human cells, data showed that telomerase did not abolish ALT activity and only when the GM847 telomerase+/ALT+ cells were fused with telomerase-positive tumour cell lines this caused inhibition of ALT activity (Perrem et al., 2001), suggesting that other factors

could be responsible for inhibition of the ALT pathway (Perrem et al., 2001). These intriguing observations show that both telomerase and ALT can co-exist in the same cell and their activities depend on unknown factors. However, it is not clear whether there could exist human tumour cells with both ALT and telomerase activity, suggesting that one mechanism is sufficient to combat the process of telomere erosion in cancer cells.

However, the co-existence between telomerase and ALT activity in the mouse cells have been reported recently (Neumann et al., 2013). Therefore, the aim of this chapter is to probe for the activity of ALT in the same set of cell lines as in Chapter 5 (extended by two more ALT+ human cell lines) using the CC assay. Other aims include (i) measuring telomerase activity and (ii) analysis of colocalisation of BRCA1 and BLM with telomeres as a recent study has suggested that BRCA1 and BLM co-localise with RAD50 in ALT positive human cells (Acharya et al., 2014).

6.2 Results

6.2.1 Cell lines

A total of eleven cell lines were analysed in this chapter including: U2OS, HeLa, G292, SKLU-1, HCC1937, mESCs E14 and 408, human lymphoblastoid cells lines GM00893 and GM13705 (*BRCA1*$^{+/-}$) and mouse lymphoma cell lines LY-R and LY-S. All cell lines were analysed using (i) the CC assay (ii) the telomerase activity TRAP assay and (iii) immunofluorescence with the BLM antibody combined with other relevant antibodies or telomeric PNA probes.

6.2.2 Detection of ALT activity by C-circles assay

Results presented in Chapter 5 were inconclusive regarding the link between BRCA1 and ALT activity. For example, although we observed significant differences in the number of APBs between the 408 and E14 cell lines (Figure 5.7) there was no difference between the cell lines in terms of co-localisation of APBs and telomeres (Figure 5.8). Similarly, we observed identical situation with human HCC1937 (Figures 5.7 and 5.8) known to be defective in BRCA1.

However, to assess the presence of ALT in the most accurate way we measured ALT activity using a sensitive CC assay. This assay measures levels of self-priming circular telomeric C-strand templates for rolling circle amplification (RCA) (Henson et al., 2009, Henson and Reddel, 2010) that is shown to be 1000-fold overexpressed in ALT+ cells relative to ALT- cells and therefore provides the most accurate measure of ALT activity available at present. However, it must be pointed out that it is not yet clear whether CC's are integral part of the ALT pathway and therefore the data must be interpreted with caution (Henson and Reddel, 2010). Furthermore, it must be noted that the CCs are different to the t-circles found in ALT+ cells that contain nicks and gaps in both strands and therefore unable to sustain RCA. The CC assay protocol is described in detail in Chapter 2 (Materials and Methods).

The CC assay was carried out using 30ng of gDNA from the ALT$^+$ human cell lines (U2OS, G292 and SKLU-1), ALT$^-$ cell lines (HeLa and HCC1937) and human lymphoblastoid lines (GM00893 and GM13705) as well as mESCs (E14 and 408) and mouse lymphoblastoid cell lines, LY-R and LY-S (Figure 6.1A).

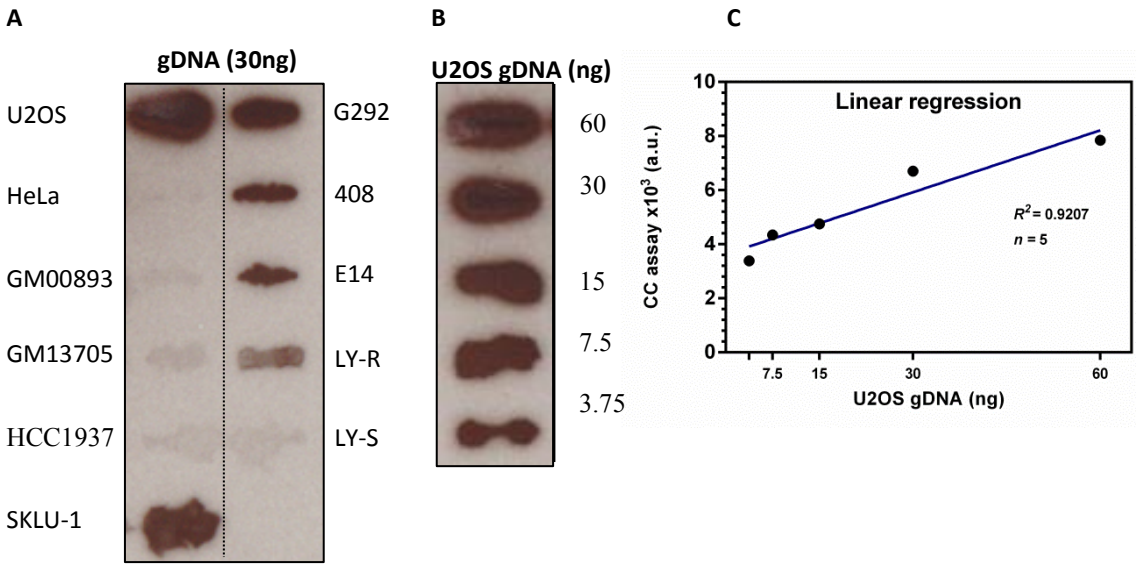

Figure 6-1. The CC assay in human and mouse cells. A) Slot-blot examples of the CC assay using 30ng of gDNA. **B)** The human ALT-positive U2OS cells used to create a standard curve with concentrations of DNA ranging from 3.75ng-60ng. **C)** Standard curve of the CC assay of the ALT-positive U2OS. The R^2 was equal to 0.9207. The CC assay unit is calculated based on arbitrary unit (a.u.).

The gDNA from all samples were slot blotted onto a nitrocellulose membrane and probed with P^{32}-labelled C-rich telomeric oligonucleotide $(CCCTAA)_3$ (Figure 6.1). To establish that the increases in the ALT activity measured through CC assay are dependent on the gDNA concentration we performed a serial dilution experiment using various concentrations of the ALT+ U2OS (Figure 6.1B). Regression analysis showed a linear correlation (R^2=0.9207) between concentrations of gDNA of U2OS and CC activity (Figure 6.1C) suggesting that the activity of CC assay is dependent on the input gDNA and consistent with the published data (Henson and Reddel, 2010).

Data from the CC assay showed ALT activity in both mESCs in the range similar for the human ALT+ cell lines with the exception of (i) the 408 cell line which had the highest ALT activity and (ii) the LY-S cell line which lacked ALT activity completely (Figure 6.2). To confirm this observation further and to assess the differences is not due to the input gDNA, we repeated the CC assay using 20ng of freshly extracted gDNA from the mouse ES cells and the LY-R and LY-S on two independent experiments and measured the average ALT activity by quantifying the blot images as before. Data showed similar results in that the mouse ES 408 had higher activity on average 1.5 fold more CC activity than the isogenic E14 (not shown). This confirms that the Brca1 defective mESC line, 408, has the highest level of ALT activity in our set of mouse cell lines (Figure 6.2) (p= 0.0341).

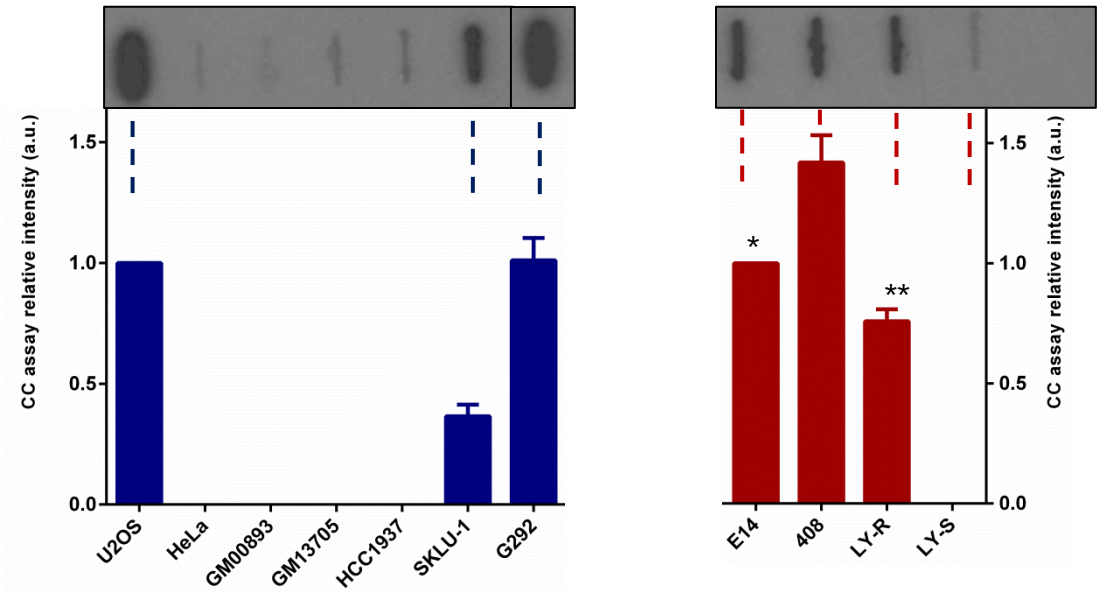

Figure 6-2 CC assay on 30ng genomic DNA. A) from U2OS (ALT^{+}), HeLa, GM00893, GM13705 (BRCA1$^{+/-}$), HCC1937 (BRCA1$^{-/-}$), SKLU-1, G292. **B)** E14 (Brca1$^{+/+}$), 408 (Brca1$^{-/-}$), LY-R, and LY-S. The quantitation was done using the Image J software. Error bars indicates SD. T-test used for statistical analysis. *P= 0.0341, **P=0.0169.

The complete lack of ALT in LY-S cells is surprising, as normal mouse somatic cells have readily detectable ALT activity (Neumann et al., 2013). Interestingly, the levels of ATRX in the LY-S cell line was significantly lower than in the LY-R line (Figure 5.11). This reduction of ATRX in the LY-S cell line apparently does not affect ALT which is contrary to results of (Clynes et al., 2014) showing that the complete absence of ATRX activates ALT. Therefore, ablation of ATRX alone is not sufficient to trigger ALT in mouse cells possibly suggesting the involvement of other factors in ALT activation. It has been reported that mouse cells with reduced ATRX activity show DNA damage at telomeres and higher levels of γH2AX (Clynes et al., 2014, Lovejoy et al., 2012). This is true in respect to the radio-sensitive LY-S cells and could suggest an important role of ATRX in the DNA damage response.

6.2.3 Detection of Telomerase activity in mESCs

As discussed previously, mammalian cells maintain their telomere length through two major known pathways: telomerase or ALT (Cerone et al., 2001, Bednarek et al., 1995, Chadeneau et al., 1995, Blasco et al., 1996, Broccoli et al., 1996). To assess whether the ALT activity observed mESCs (Figures 6.1 and 6.2) has an effect on the telomerase levels

we measure telomerase activity using the gold standard PCR-based *T*elomerase *R*epeat *A*mplification *P*rotocol (TRAP) assay (Kim et al., 1994, Harley et al., 1994, Kim and Wu, 1997). Using this assay we measured telomerase activity in all mouse cell lines (E14, 408, LY-R and LY-S) with two different concentrations of protein (200ng and, 400ng data doesn't shown) (Figure 6.3). Two human cell lines, HeLa (telomerase positive) and U2OS (ALT+; telomerase negative) served as controls (Figure 6.3). Since the TRAP assay is enzyme based we heat-treated each sample to inactivate the telomerase enzyme and to identify false positive reactions. The data revealed high telomerase activity in the HeLa cells as expected and consistent with previously published observations (Shay et al., 2001, Ivankovic et al., 2007) and low telomerase activity in U2OS cell line as expected (Bryan et al., 1997b, Vonderheide et al., 1999, Tilman et al., 2009, Lovejoy et al., 2012) (Figures 6.3 and 6.4). Interestingly, the two mESC lines showed ~5 fold and ~3 fold less telomerase activity relative to HeLa cells respectively (Figure 6.4), when quantified using Image J. Although the 408 cells had slightly higher levels of telomerase activity compared to E14 cells the difference was not significant ($p=0.149$), whereas, we observed significant difference ($p=0.0026$) in telomerase activity between LY-S and LY-R cells (Figures 6.3 and 6.4). To confirm these observations we repeated the TRAP assay using 400ng of total Chaps-lysed protein and quantified the telomerase levels (data doesn't show). The levels of telomerase activity in the U2OS, E14, 408 and LY-R were largely consistent with the previous TRAP assay in terms of levels of telomerase activity (200ng in Figure 6.3). However, the levels of telomerase activity in the HeLa and LY-S cells increased significantly when the concentrations of the telomerase were doubled (data doesn't show) possibly suggesting the importance of the activity of telomerase in the maintenance of telomeres in these two cell lines.

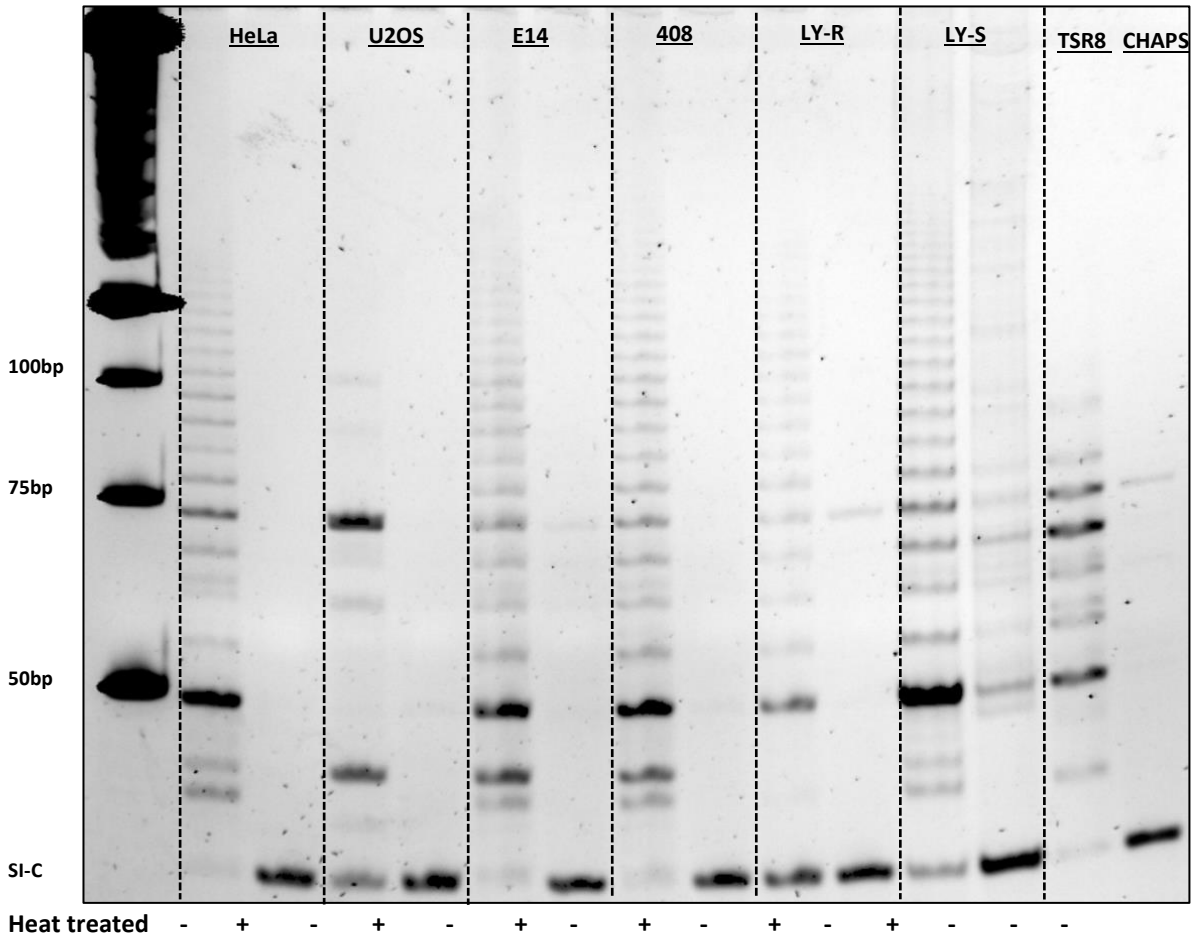

Figure 6-3. Telomere Repeat Amplification Protocol (TRAP). 200ng of CHAPS lysed proteins used in all samples. The heat-treated samples were heated at 85°C for 10 minutes to inactivate the telomerase enzyme. The Standanrd Internal Control (SI-C) at 36bp is indicative of complete PCR amplification. In high telomerase samples the SI-C is weaker than in low telomerase samples since the SI-C competes proportionaly with the telomerase enzyme. The 25bp DNA ladder is shown in the first lane. The last lanes are TSR8 (2 units of telomerase quantitation positive control. TSR8 is an oligonucleotide with a sequence identical to the TS primer extended with 8 telomeric repeats AG(GGTTAG)$_7$. This control serves as a standard for estimating the amount of TS primers with telomeric repeats extended by telomerase in a given extract provided by the kit manufacturer) and CHAPS buffer used as internal positive and negative controls respectively.

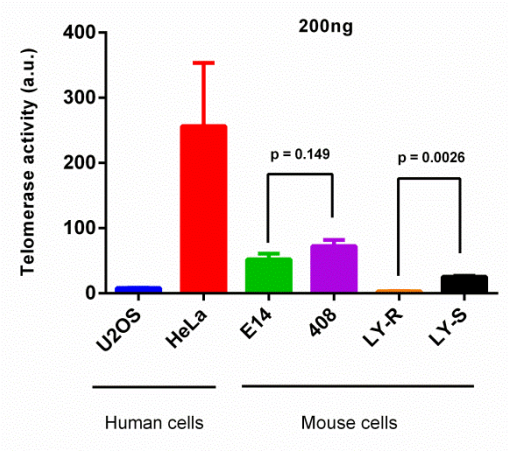

Figure 6-4 Telomerase activity in the human and mouse cell lines. U2OS (ALT^+), HeLa (ALT^-), LY-R, LY-S, E14 ($Brca1^{+/+}$), and 408 ($Brca1^{-/-}$) calculated using the TRAP gels from the 200ng protein . The artibtary unit of telomerase units calcualted using the formula described in chapter 2. T-test is used for statistical analysis. The 200ng data is based on three independent experiments from two independent CHAPS lysed proteins.

6.2.4 Investigation of BRCA1 protein in ALT and non ALT cell lines

Given the differences observed in terms of ALT activity between mESCs and mouse lymphoma cell lines we thought that it is important to verify presence/absence of BRCA1 in all cell lines before moving further. First, we performed immunoblot analysis to measure levels of Brca1 in the mouse and human cells (Figure 6.5). Protein lysates were extracted from $1.6x10^6$ cells from each cell line and total protein lysate (60µl from human cells and 30µl from mouse cells) were separated on a 4-20% a gradient gel (See Chapter 2 for detail). The Brca1 immunoblot confirmed the lack of Brca1 activity in the mouse ES cell 408 compared to the E14 (Brca1 WT) and slightly lower Brca1 activity in the LY-S cells compared to the LY-R (45% and 75% respectively) (Figure 6.5A-C). The immunoblot revealed some BRCA1 activity (7%) in human BRCA1 defective breast cancer line HCC1937 compared with the BRCA1 WT HeLa and U2OS lines (Figure 6.5B).

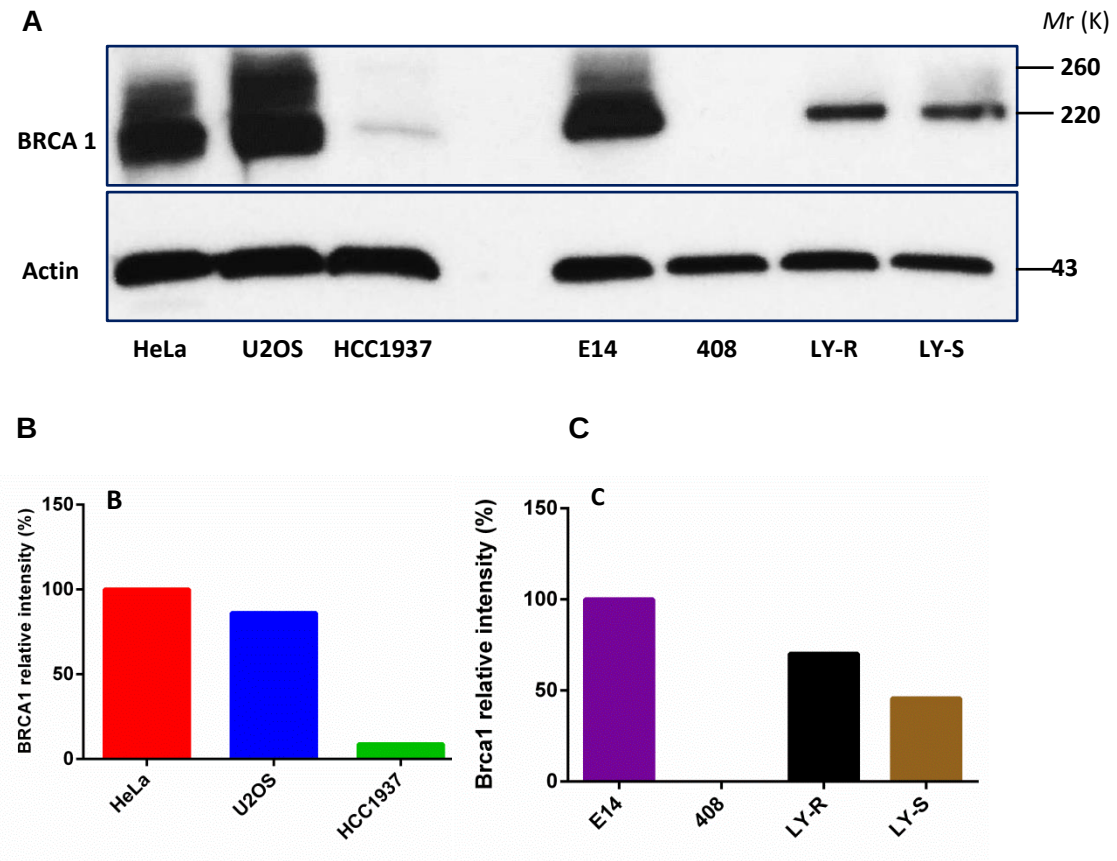

Figure 6-5 Immunoblotting of BRCA1 in the human and mouse cell lines. A) Western blot showing the BRCA1 expression. **B)** Protein bands were quantified by densitometry, expressed relative to actin, and normalized to the control (HeLa). **C)** Protein bands were quantified by densitometry, expressed relative to actin, and normalized to the control (E14).

6.2.5 Immunofluorescence analysis of BRCA1, BLM and ATRX

A recent study shows that BRCA1 interacts with the BLM helicase exclusively in ALT+ cells (Acharya et al., 2014). Although the exact mechanism of ALT activation in human tumor lines are not yet clear, it is suggested to involve several proteins central to the HR pathway including BRCA1 and BLM helicase (Acharya et al., 2014). This is interesting in the present context as we have shown that the ALT activity is extremely high in mouse Brca1 defective 408 cells (Figure 6.1 and 6.2). To study the possible role of BLM interactions with BRCA1 in the ALT pathway we set out to use immunofluorescence experiments to assess co-localisation between BLM, BRCA1, ATRX and telomeres in our set of cell lines. Thus, this section is divided into 4 parts examining interactions between:

- BRCA1 and telomeres

- BLM and telomeres
- BRCA1 and BLM
- BRCA1 and ATRX.

BRCA1 and telomeres

First, all cell lines were examined for the presence of BRCA1 foci using immunofluorescence (Figure 6.6). As expected significant differences were observed in the number and distribution of BRCA1 foci in human ALT^+ (U2OS) and human ALT^- (HeLa and HCC1937) (Figure 6.7 and 6.8) ($p<0.0001$). For example, U2OS cells showed on average 18.14 foci per cell compared to HeLa (13.38 foci per cell) and HCC1937 (4.14 foci per cell) (Figure 6.7). Similarly, we observed significant difference between the Brca1 foci in the E14 and 408 ($p<0.0001$) (Figure 6.8) with E14 showing on average 11.78 foci per cell and 408 showing 1.56 foci per cell of Brca1. These data are in agreement with the immunoblot shown in the previous section (Figure 6.5). However, we did notice a small number of Brca1 foci in the $Brca1^{-/-}$ mouse ES 408 cells (1.56 foci per cell) and we believe this could be due to the unspecific binding of Brca1 antibody to other transcript variants of the *Brca1* gene (in human cells these are reported to be 5 BRCA1 gene isoforms with molecular weight range of 70-220 kDa) (Monteiro et al., 1996, Bork et al., 1997). This unspecific binding of the Brca1 antibody was also observed in the immunoblot image at ~ molecular weight of 120 kDa (data not shown). Due to the extremely low occurrence of these unspecific Brca1 foci in mouse ES 408 cells we decided to continue with analysing for the colocalisation of the Brca1 with telomeres.

Next we probed the BRCA1 immunostained slides with telomeric PNA FISH probes to scan for colocalisation between BRCA1 and telomeres (Figure 6.6 and 6.7). The results of our analysis are shown in Figures 6.8 and 6.9. The low levels of BRCA1 staining in HCC1937 and 408 cells are most likely due to non-specific staining.

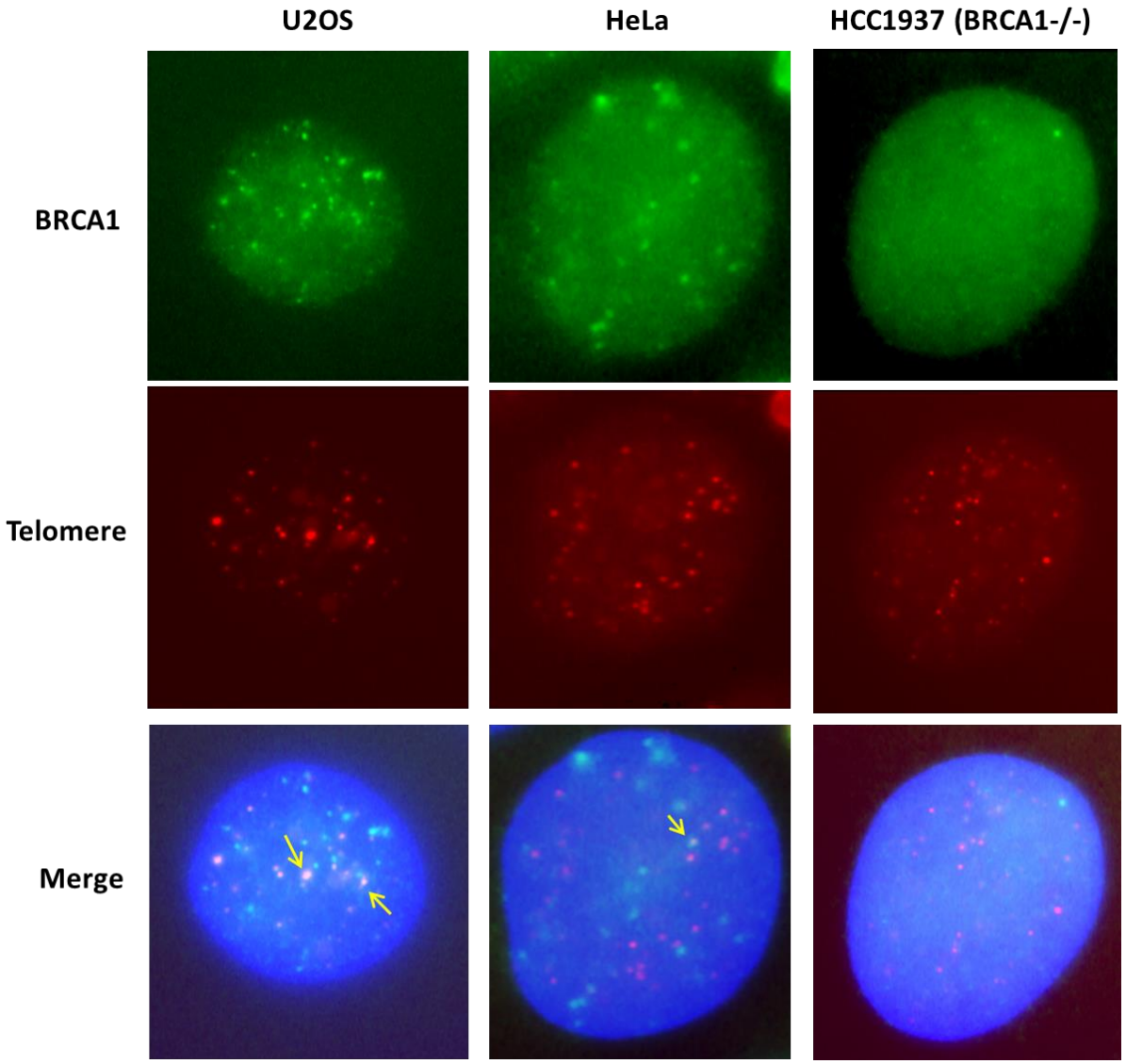

Figure 6-6- BRCA1 co-localise at telomere in human cell lines. Examples of immunofluorescence colocalisation of BRCA1 with telomeres in the human HCC1937 BRCA defective and HeLa and U2OS BRCA1 positive cells. . Interphase cells were permeabilised and stained with anti-BRCA1 (green) and telomeric Cy3-labeled PNA probes (red). Nuclei were counterstained with DAPI.

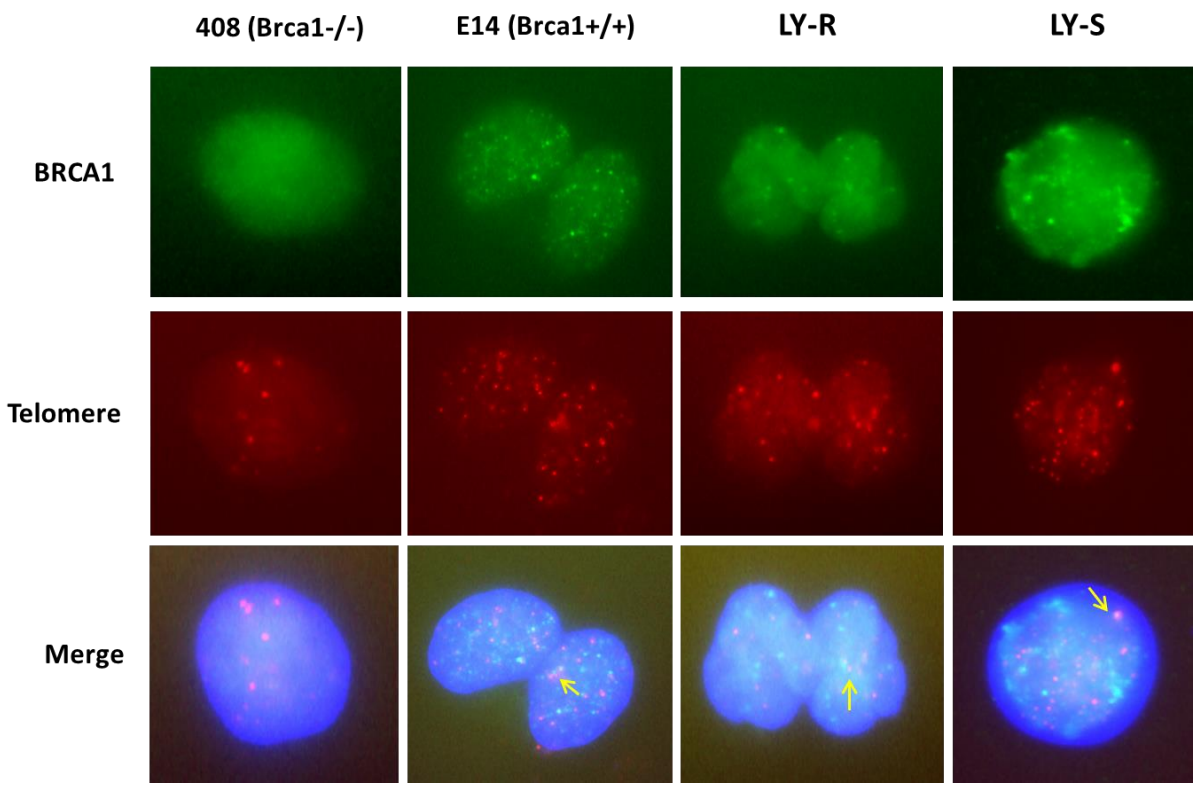

Figure 6-7- BRCA1 co-localise at telomere in mouse cell lines. Examples of BRCA1 colocalisation with telomeres. 408 cell line served as the negative controls, and E14 was used as the positive control. Interphase cells were permeabilised and stained with anti-BRCA1 (green) and telomeric Cy3-labeled PNA probes (red). Nuclei were counterstained with DAPI.

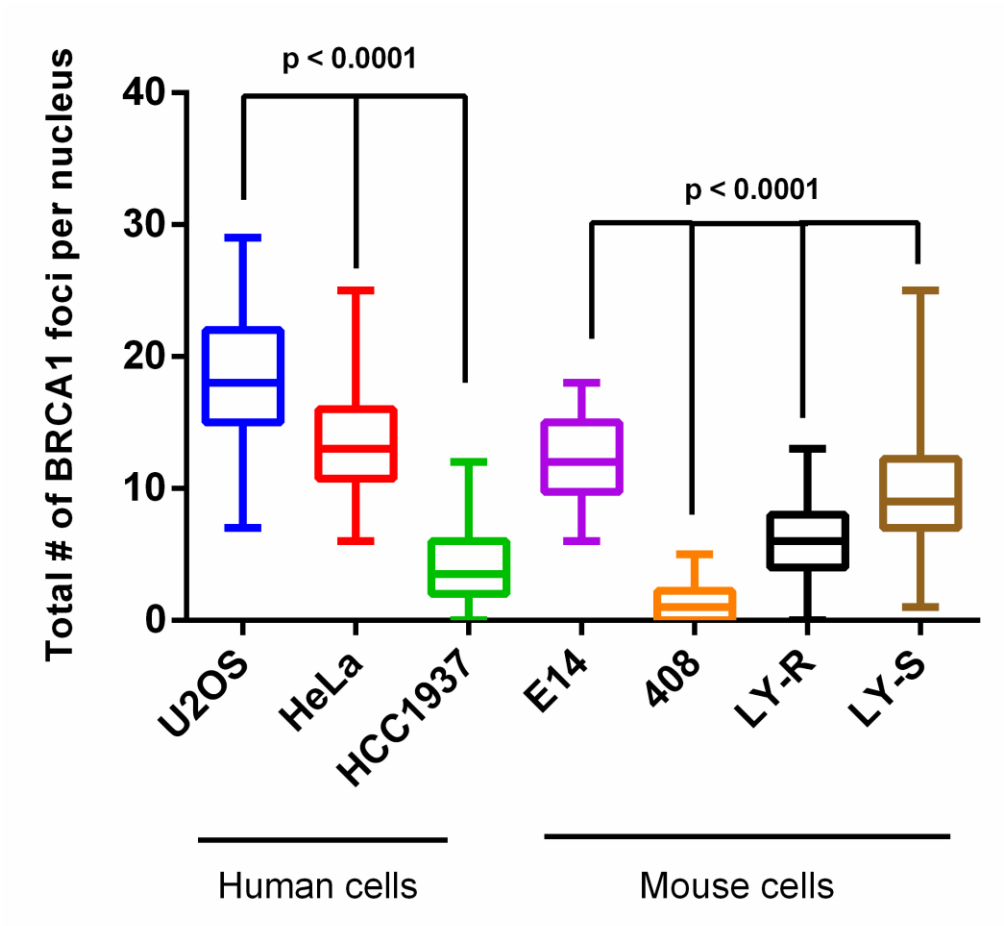

Figure 6-8- Total number of BRCA1 foci per cell in the human and mouse cells. Immunofluoresence of the total number of BRCA1 foci in the human ALT-positive (U2OS) and ALT-negative (HeLa and HCC1937) cells and the mouse ES cells (E14 and 408) and lymphoblastoid (LY-R and LY-S) counted in 50 cell nuclei in two independent experiments. T-test is used for statistical analysis.

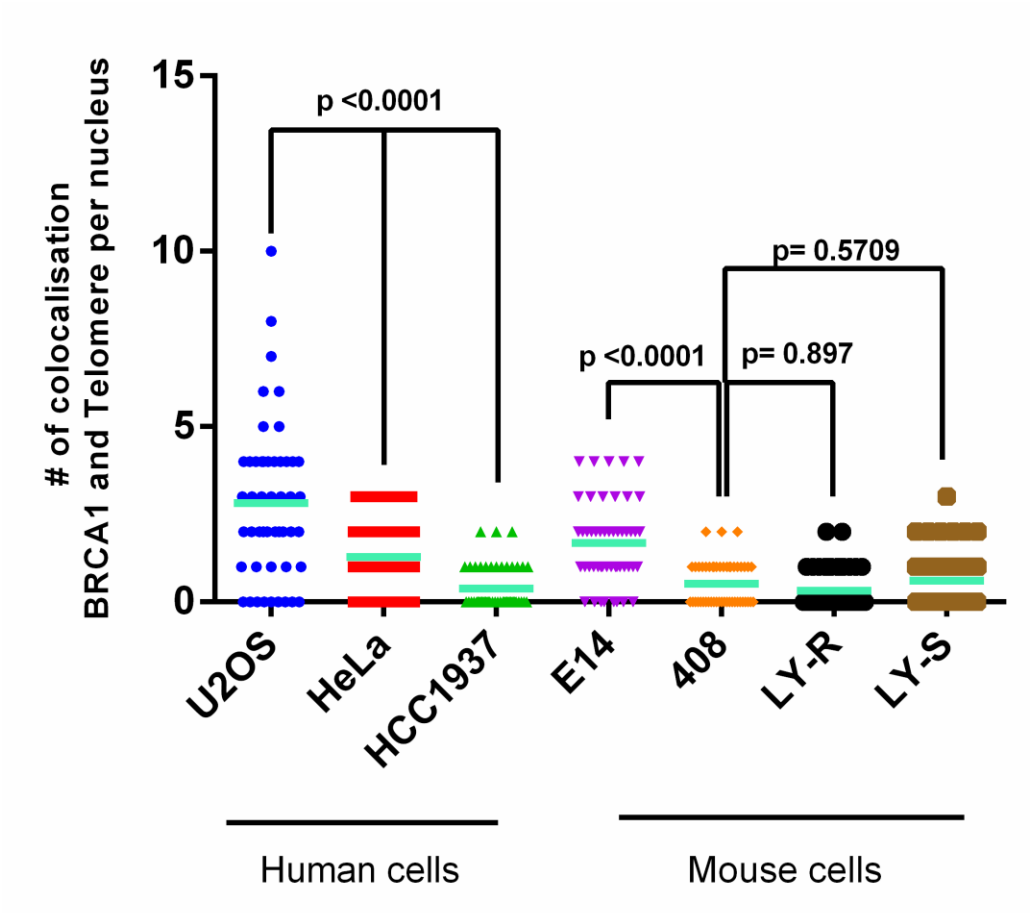

Figure 6-9- Co-localisation of BRCA1 with telomeres in the human and mouse cells and human cell lines. Number of BRCA1 foci colocalised with telomeres in the human ALT-positive (U2OS) and ALT-negative (HeLa and HCC1937) cells and the mouse ES cells (E14 and 408) and lymphoblastoid (LY-R and LY-S) cells. In total 50 cell nuclei counted in two independent experiments. The green bar indicates mean. T-test is used for statistical analysis.

BLM and telomeres

Images of BLM staining in different cell lines are shown in Figures 6.10 and 6.11. The ALT$^+$ U2OS cells had on average 6.5 BLM foci per cell whereas the ALT$^-$/telomerase$^+$ HeLa and HCC1937 had on average 8.24 and 9.8 foci per cell respectively (Figure 6.12 and 6.13). U2OS had significantly lower levels of BLM foci per cell when compared to both HeLa ($p=0.0024$) and HCC1937 ($p<0.0001$). However, when levels of BLM associated with telomeres were analysed in the human cells, the U2OS ALT$^+$ cells showed higher levels of colocalisation (3.06 foci per cell) as compared to the ALT- HeLa (0.62) and HCC1937 (0.62) further indicating the involvement of BLM in the ALT activity (Figure 6.12 and 6.13). This difference was highly significant ($p<0.0001$). In the mESCs, level of average BLM foci per cell was slightly higher in the E14 cells (7.32) compared to 408 (6.68 foci per cell) but not significant ($p=0.2287$) (Figure 6.12). Interestingly, when BLM colocalisation with telomere was assessed in the two mESCs, E14 cells had much higher levels of BLM-telomere colocalisation (2.32 foci per cell) than 408 cells (0.44 foci per cell) (Figure 6.13). This significant difference ($p<0.0001$) backs up similar observation seen in the human ALT$^+$ cells where BRCA1 was crucial in maintaining BLM association with telomeres further suggesting and important role of BLM, BRCA1 and ALT activity and in line with the recently published data (Acharya et al., 2014). Furthermore, LY-R and LY-S cells had the highest levels of average BLM foci per cells 10.44 and 11.72 respectively (Figure 6.12), but showed similar levels of BLM-telomere colocalisation (1.70 foci per cell in LY-R and 1.78 foci per cell in LY-S) (Figure 6.13).

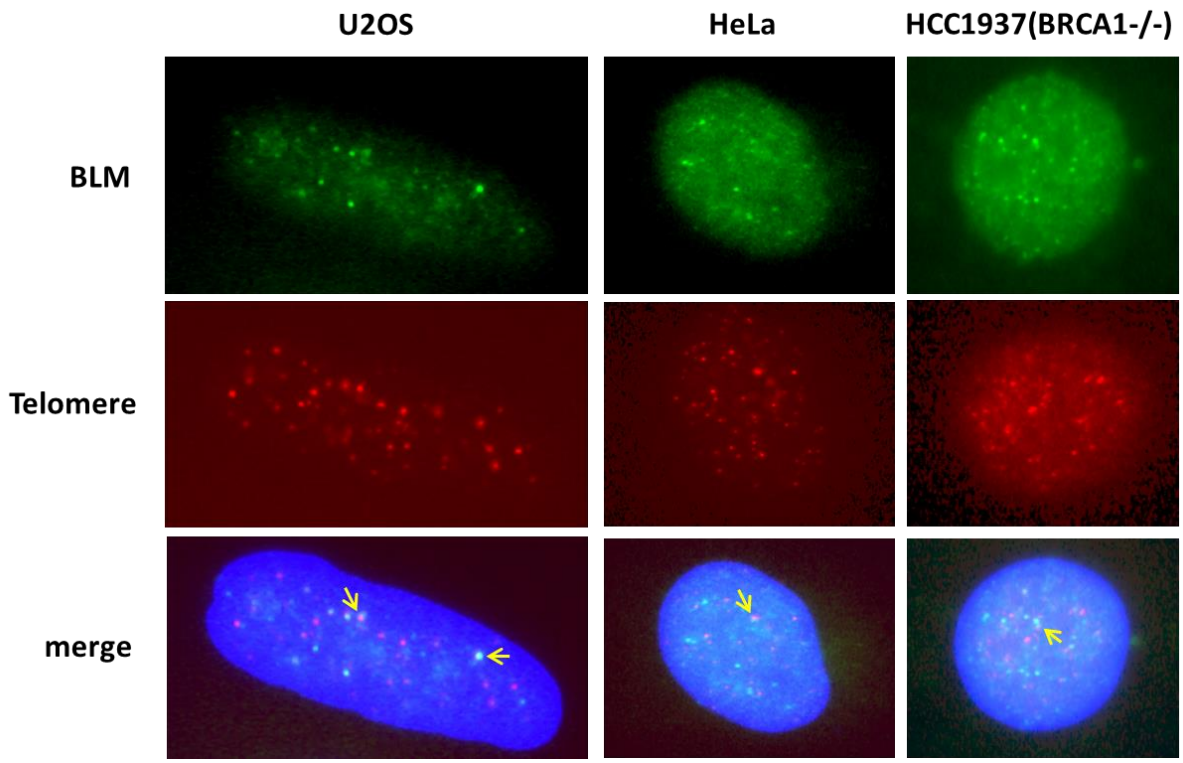

Figure 6-10- BLM (green) co-localisation with telomeres (red) in the human cell lines. . Interphase cells were permeabilised and stained with anti-BLM (green) and telomeric Cy3-labeled PNA probes (red). Nuclei were counterstained with DAPI.

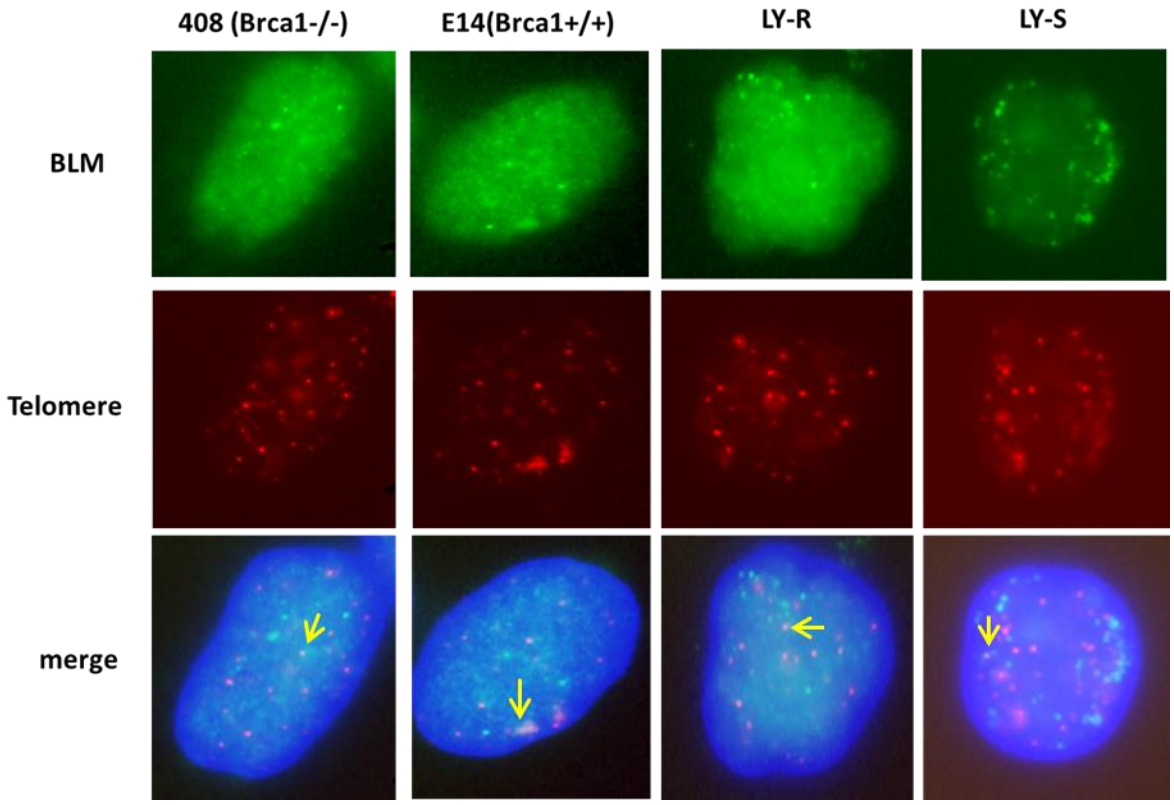

Figure 6-11- BLM (green) co-localisation with telomeres (red) in the mouse cell lines.

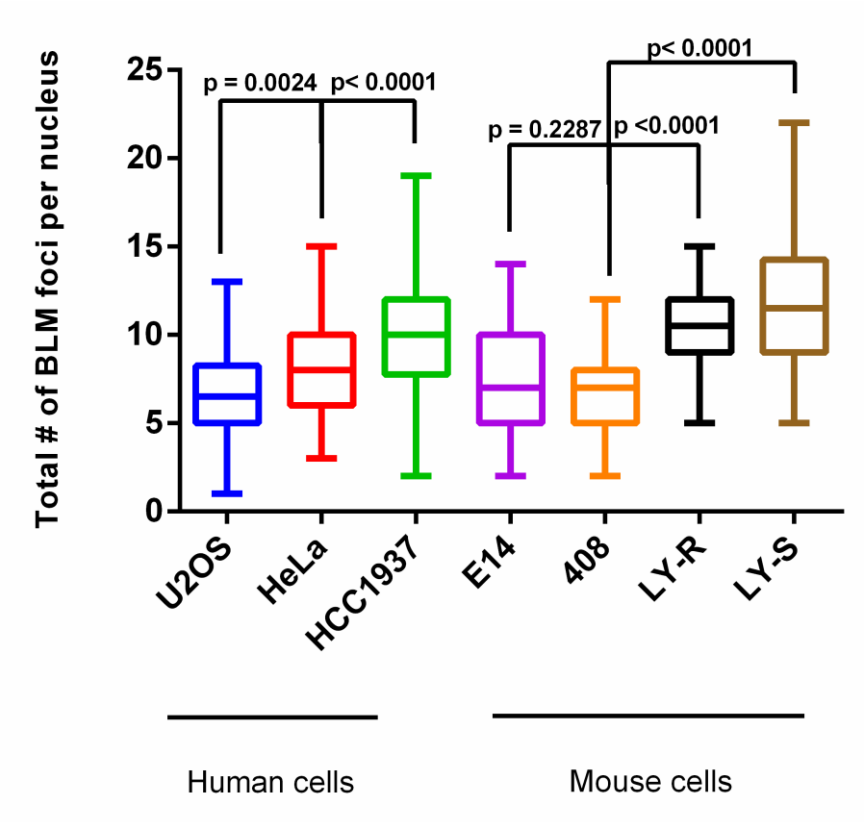

Figure 6-12- Number of BLM foci per cell in the human and mouse cells. A total of 50 cell nuclei in two independent experiments were analysed. Statistical analysis carried out by T-test.

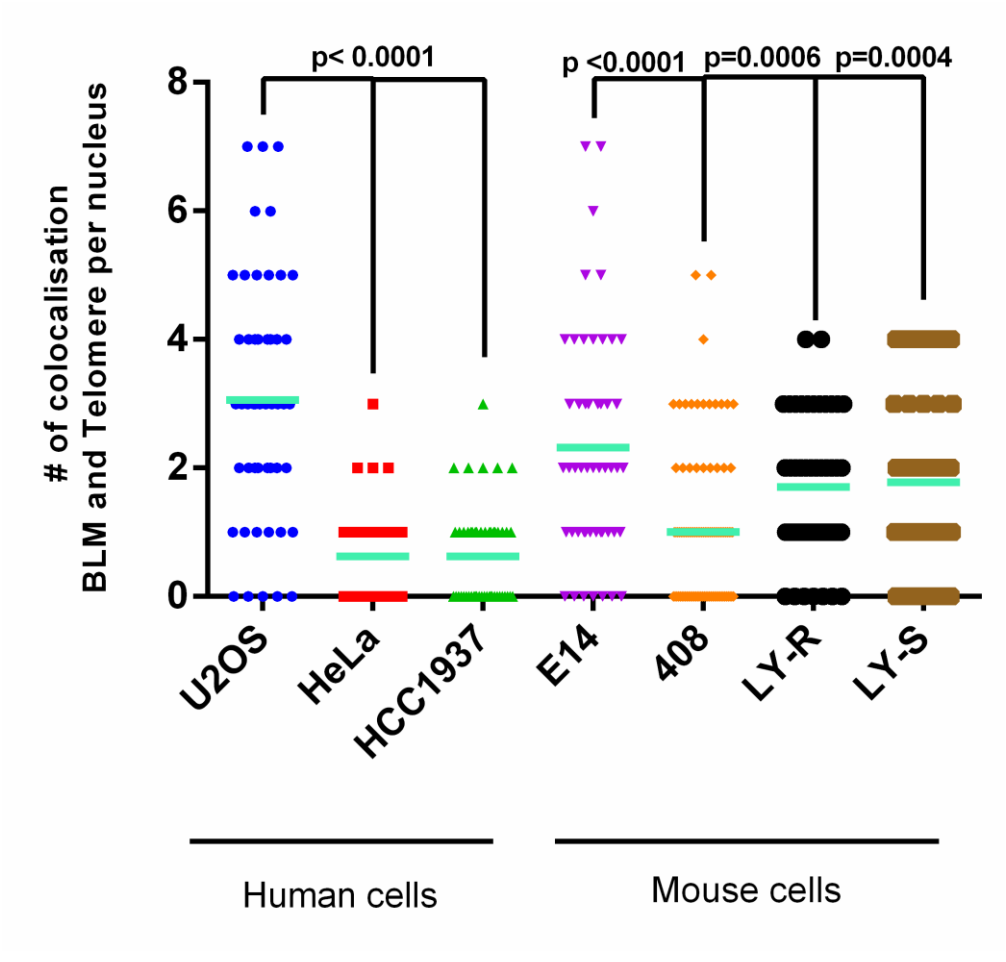

Figure 6-13- Co-localisation of BLM with telomeres in the human and mouse cells. A total 50 cell nuclei/sample counted in two independent experiments. The green bars indicate the means. T-test is used for statistical analysis.

BRCA1 and BLM

Bloom syndrome (BS) is an uncommon cancer-predisposing autosomal recessive disorder characterized by genomic instability, immunodeficiency, infertility, and small stature (German, 1993, Ellis and German, 1996). *BLM*, the gene mutated in Bloom syndrome encodes a DNA helicase of the RecQ family (Ellis et al., 1995). Moreover, BLM associates with numerous proteins involved in DNA repair including BRCA1, DNA mismatch repair proteins, DNA topoisomerases, and Fanconi anemia proteins. BLM is a component of the BRCA1-associated genome surveillance complex (BASC) (Wang et al., 2000, Chaudhury et al., 2013, Wu et al., 2001). Interestingly BLM also associated with several telomere-specific proteins, such as POT1, TRF1 and TRF2 (Stavropoulos et al., 2002, Sun et al., 1998), (Temime-Smaali et al., 2008, Bhattacharyya et al., 2010).

Next, we carried out immunofluorescence analysis using combination of BLM and BRCA1 antibodies (Figures 6.14 and 6.15). Number of foci per cells and mean number of co-localisation are shown in Figures 6.16. Our results indicate that HeLa as telomerase-positive cells contained a high frequency of BLM-BRCA1 co-localised foci (Figure 6.16A), but none are found at telomeres. Whereas only in ALT cells BLM and BRCA1 co-localise at telomeres. Interestingly all mouse cell lines (E14, LY-R, and LY-S) show less than 10% of co-localisation of BLM with BRCA1 (Figure 6.16B). Also data shows that BLM and BRCA1 physically interact.

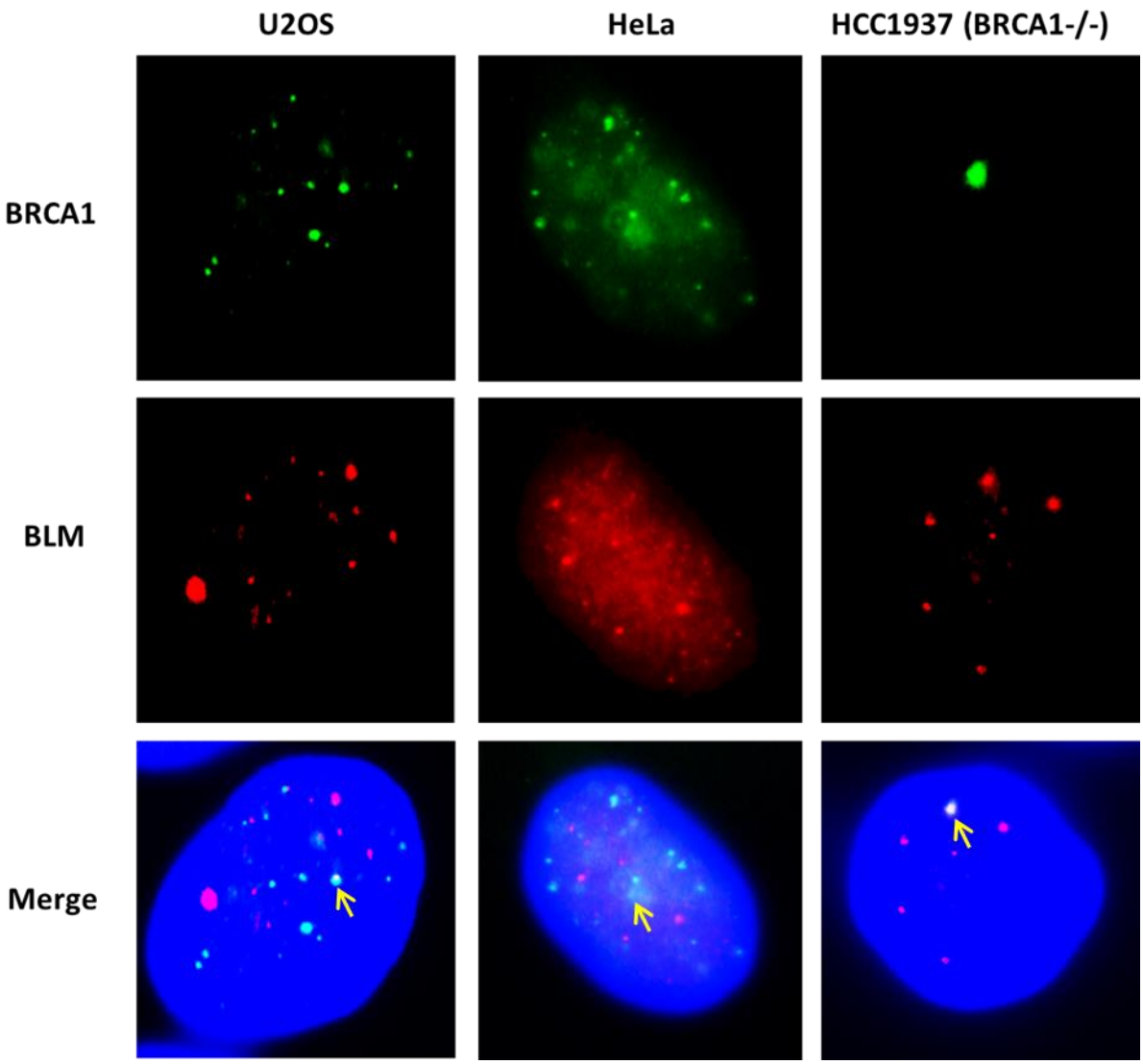

Figure 6-14- Examples of immunofluorescence showing co-localisation of BRCA1 with BLM in human cell lines. Interphase cells were permeabilised and stained with anti-BRCA1 (green) and anti-BLM (red) antibodies. Nuclei were counterstained with DAPI.

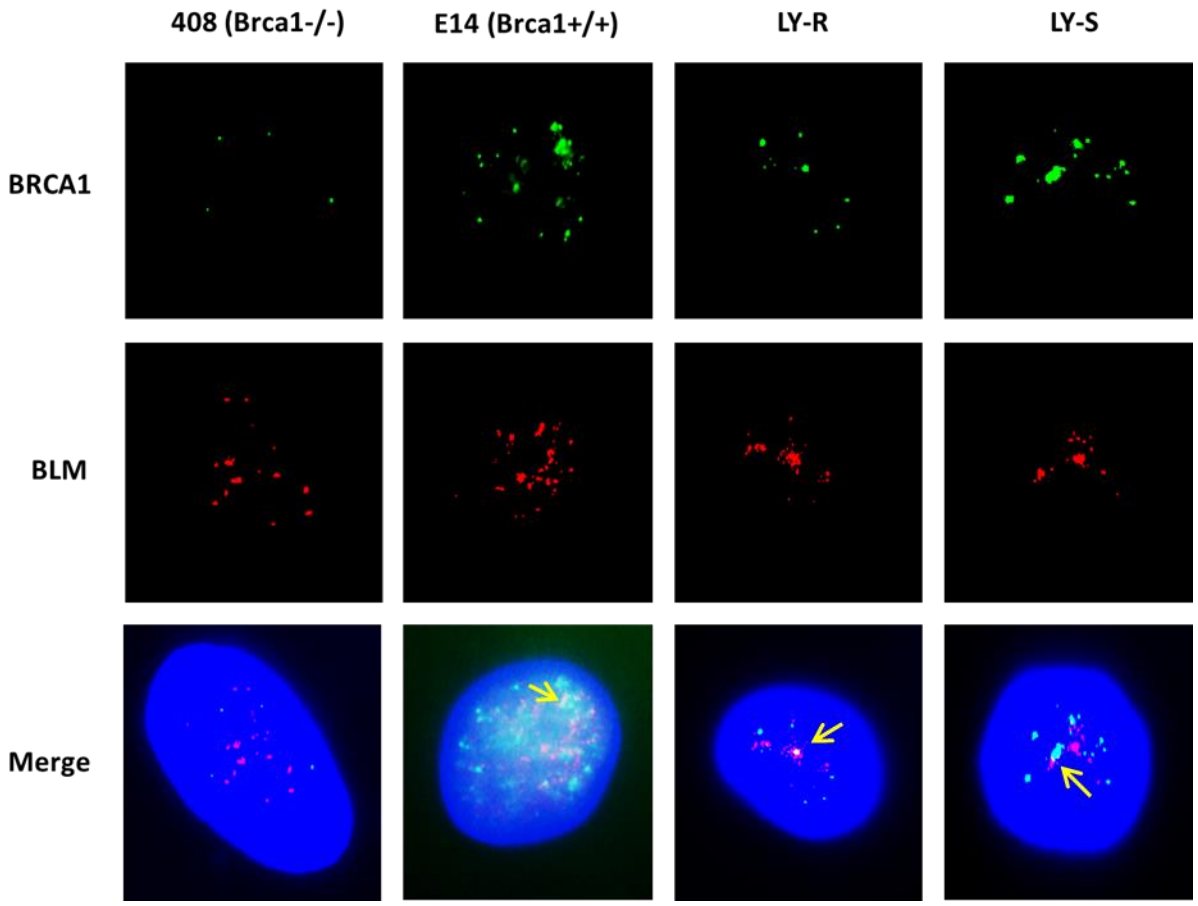

Figure 6-15- Examples of immunofluorescence showing co-localisation of BRCA1 with BLM in mouse cell lines. Interphase cells were permeabilised and stained with anti-BRCA1 (green) and anti-BLM (red) antibodies. Nuclei were counterstained with DAPI.

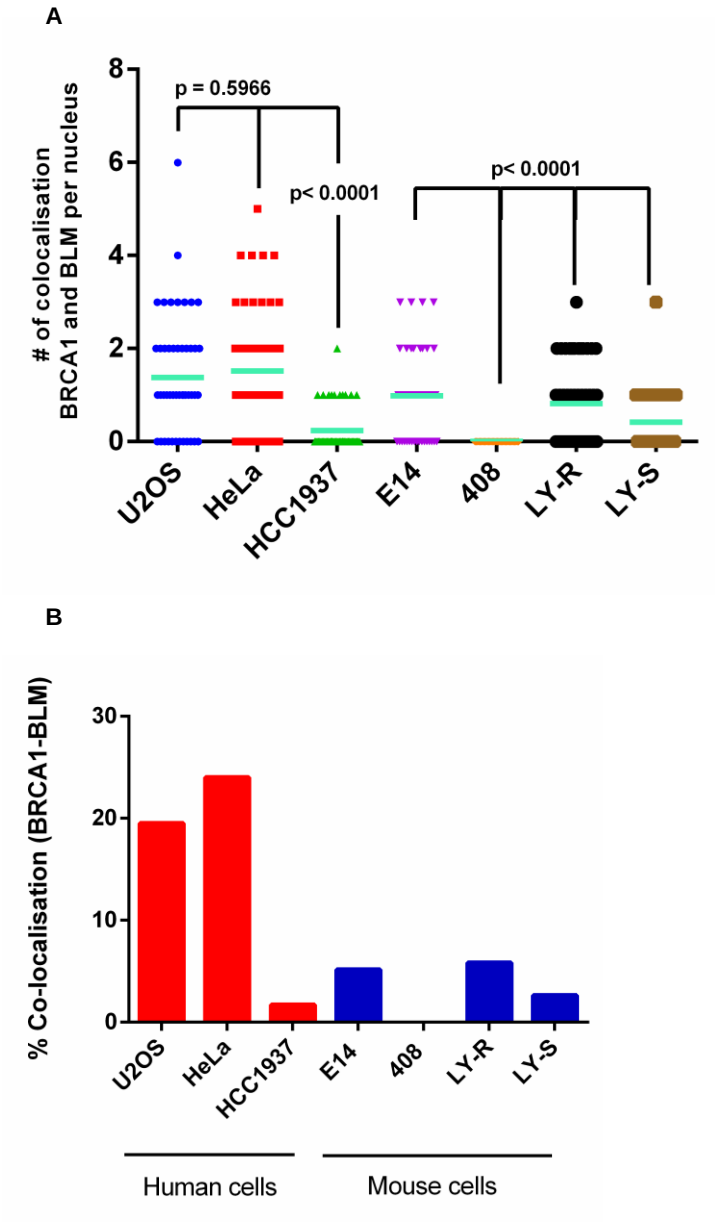

Figure 6-16- A) Co-localisation of BRCA1 with BLM in the human and mouse cells. **B)** Quantitation of percentage of cells with BRCA1-BLM co-localisation. A total 50 cell nuclei/sample counted in two independent experiments. The green bar indicate the means. T-test is used for statistical analysis.

BRCA1 and ATRX

To investigate whether ATRX co-localises with BRCA1 in our set of cell lines the Abcam antibody against ATRX was used in co-localisation experiments (Figures 6.17 and 6.18). The results of our analysis are presented in Figure 6.19. It is likely that the BRCA1 positive signals observed in HCC1937 (Figure 6.19) are the result of non-specific staining. The rest

of results are in line with expectation. In particular, we would like to highlight LY-S cells which showed the lowest level of co-localisation between BRCA1 and ATRX (Figure 6.19).

At the end of this analysis it is important to provide some kind of summary which is presented in Figure 6.20. This Figure combines the result of APB analysis (Figure 5.8), ATRX analysis (Figure 5.12) with all Figures presented in this Chapter (Figures 6.9 and 6.13).

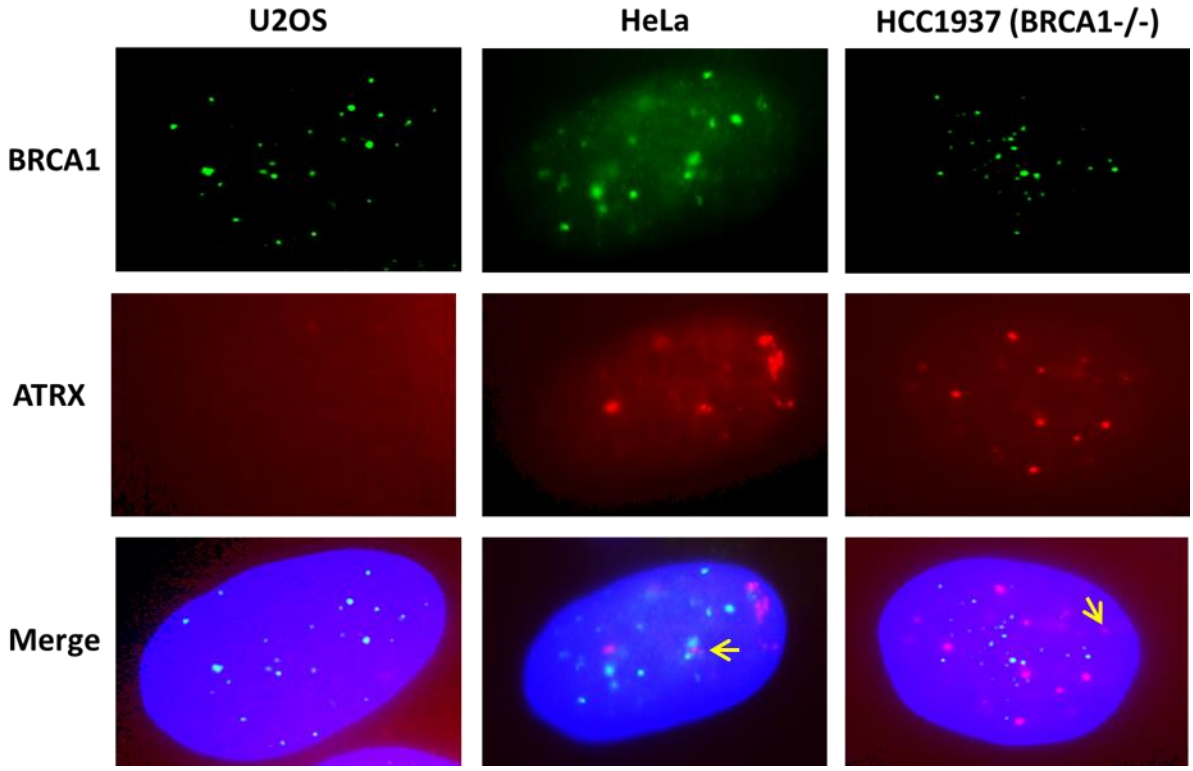

Figure 6-17- Examples of immunofluorescence showing co-localisation of BRCA1 with ATRX in the human cell lines. Interphase cells were permeabilised and stained with anti-BRCA1 (green) and anti-ATRX (red) antibodies. Nuclei were counterstained with DAPI.

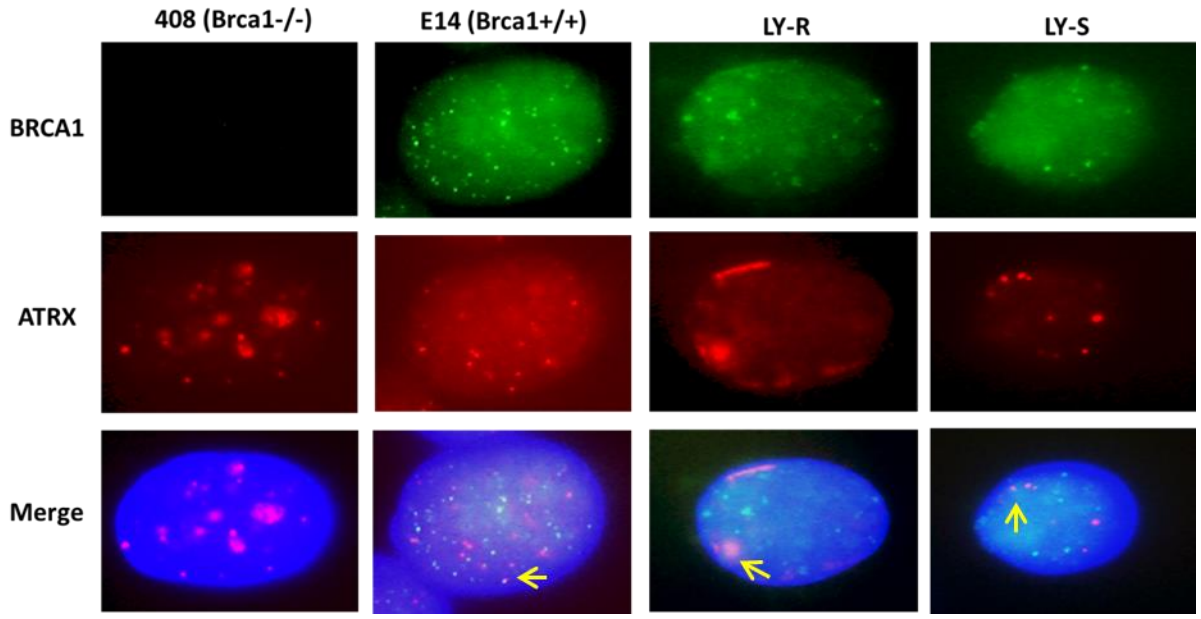

Figure 6-18- Examples of immunofluorescence showing co-localisation of BRCA1 with ATRX in the mouse cell lines. Interphase cells were permeabilised and stained with anti-BRCA1 (green) and anti-ATRX (red) antibodies. Nuclei were counterstained with DAPI.

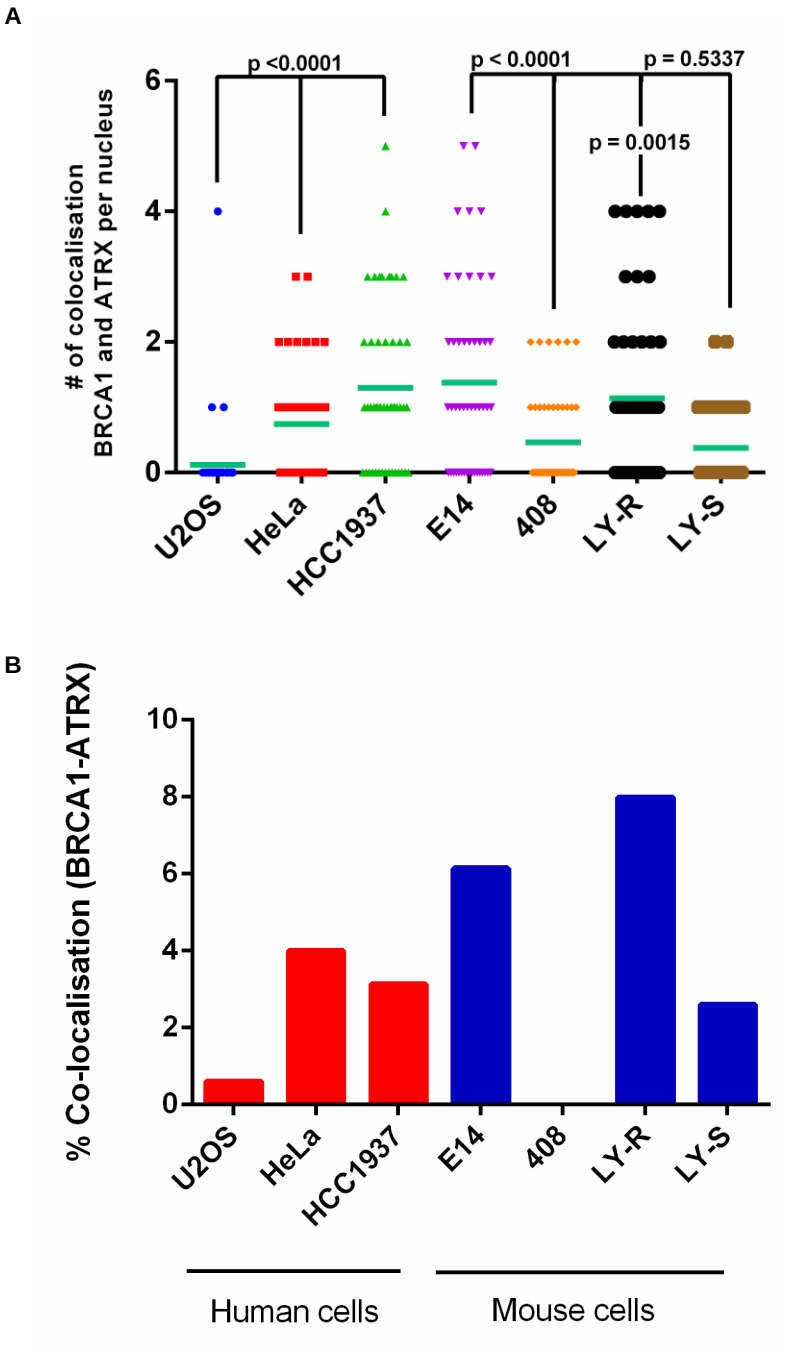

Figure 6-19- Co-localisation of BRCA1 with ATRX in the human and mouse cells. A) Number of BRCA1 and ATRX colocalisation in the human ALT-positive (U2OS) and ALT-negative (HeLa and HCC1937) cells and the mouse ES cells (E14 and 408) and lymphoblastoid (LY-R and LY-S) cells. **B)** Quantitation of percent of cells with ATRX-BRCA1 colocalisations in the human and mouse cells. In total 50 cell nuclei counted in two independent experiments. The green bar indicates mean. T-test is used for statistical analysis.

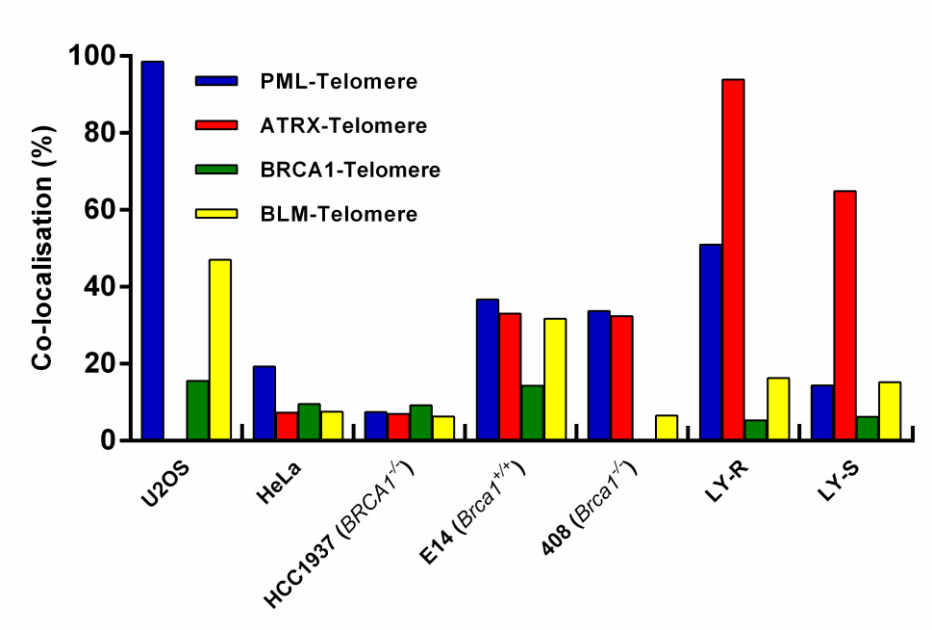

Figure 6-20- Co-localised foci of APBs, ATRX, BRCA1 and BLM with telomeres in human and mouse cells.

6.3 Discussion

In previous chapters (4 and 5) we provided some evidence for the presence of ALT-like activity associated with the Brca1 defect but this was not conclusive. For example, we have shown elevated frequencies of T-SCEs in 408 cells relative to control cells (Figure 5.1) and increased numbers of APBs (Figure 5.7). However, the rest of ALT markers used indicated lack of differences between 408 and E14 cells (Figures 5.8, 5.12).

The aim of this chapter was to use a more sensitive ALT marker known as the CC assay to assess the presence of ALT activity in the mESCs and other cell lines more accurately. The most accurate method for assessing the ALT activity at present is the CC assay that quantifies the levels of rolling circles generated as a result of recombination at telomeres (Henson et al., 2009, Henson and Reddel, 2010). Using this method we identified elevated levels of CC activity in the mouse ES cells E14, 408 and the lymphoblastoid LY-R cells (Figure 6.2). Further examination and quantification of the CC activity revealed that the Brca1 defective 408 cells had 50% more CC activity than the isogenic control counterpart E14 (Figure 6.2). We have also identified CC activity in the LY-R cells but no such activity

was observed in the LY-S cells (Figure 6.2). To our knowledge this is the first reported evidence of CC activity in the pair of mouse LY cells and ESCs, E14 and 408.

It must be mentioned that the ALT activity in the mouse tissues has been reported previously (Neumann et al., 2013) suggesting that normal mouse somatic cells use the ALT pathway. However, it is not clear whether ALT activity in the mouse tissues have any telomere lengthening function. For example, it has also been demonstrated quite clearly that in some strains of laboratory mice telomere lengths are much longer (30-150kb) as compared to the wild-derived mouse strains with shorter telomere lengths of about 10-25kb (Hemann and Greider, 2000). Whether, the differences in the mouse telomeres are due to ALT activities is not known at present. The low activity of ALT was suggested to inhibit the elongation of telomeres by telomerase by trimming the long telomeres through recombination and production of t-circles (Neumann et al., 2013). To identify whether the high levels of CC activity in the mouse cells and subsequently ALT-type activity has replaced telomerase, we measured the levels of telomerase enzyme activity using the TRAP assay. Quantifying the TRAP data revealed some interesting points: (i) that levels of telomerase enzyme in E14 and 408 were similar and (ii) levels of telomerase were significantly higher in LY-S cells than in the LY-R cells (Figure 6.4; $p=0.0026$). Interestingly, we observed differences in the level of enzyme activity between 200ng and 400ng protein extract concentrations between LY-R and LY-S cells (Figure 6.4). However, this was replicated in the case of the telomerase positive HeLa cell line (Figure 6.4) possibly suggesting that the importance of the activity of telomerase in the maintenance of telomeres in this two cell lines.

This suggested that the co-existence of ALT and telomerase in the mouse cells might serve different functions depending on the type of cells. For instance, the elevated levels of telomerase in the LY-S cells may serve to maintain the shorter telomere lengths of the LY-S whereas in the LY-R the low levels of telomerase may have canonical function other than telomere length elongation and maintenance since ALT in the LY-R cells, may be the prominent mechanism of telomere length maintenance. Alternatively, functional activity of

ALT and telomerase in the mESCs, regardless of the levels of Brca1 activity, might serve independent roles. It would be of interest to study the telomere length role of telomerase and ALT in mESCs by inhibiting telomerase enzyme using specific telomerase inhibitor such as Imetelstat (GRN163L; Geron) and subsequently measuring telomere length. However, due to lack of time this hypothesis was not followed.

We also measured levels of Brca1 protein using western blotting to check whether Brca1 was fully expressed in all cell lines and to define the levels of Brca1 activity in the mutant lines, especially in the mutant human BRCA1-defective cell line (HCC1937) and the mouse ES cell line 408. The results further confirmed the published observation that there is a leaky expression of BRCA1 protein in the human HCC1937 extracts as previously described (Figure 6.5) (Tulchin et al., 2013). The 408 cell line did not have any detectable levels of Brca1 expression. Once we were confident of the levels of Brca1 activity, we set out, in a series of single and double immunofluorescence experiments, to measure the co-localisation of Brca1 with telomeres, BLM, and ATRX in all seven human and mouse cell lines (Figures 6.15-6.20).

When assessing the co-localisation of BRCA1 with ATRX and we found that two mouse cell lines, E14 and LY-R (both ALT-positive) showed significantly higher level of co-localisation in comparison with 408 (ALT-positive) and the LY-S (ALT-negative) respectively (Figure 6.18; $p<0.0001$ and $p=0.0002$). These are the first ever-reported data, to our knowledge, of colocalisation amongst Brca1 and ATRX in the mouse cells and our data clearly suggest that the ATRX and Brca1 co-localises at higher levels in the ALT-positive cells. However, these data are in contradiction to the functional role of ATRX in the human cells. It has been shown that the level of ATRX is diminished in 90% of human ALT-positive cells and that ATRX can be a marker of ALT activity in the human cells (Lovejoy et al., 2012). In the mouse cells we have found that ATRX is much lower in the LY-S cells and this low levels of ATRX does not correlate to the ALT activity whereas the LY-R and E14 have elevated levels of ATRX as well as ATRX co-localisation with Brca1. Why the ATRX levels are lower in the LY-S cells

and not in the 408 cells are puzzling. However, in ALT-negative human cell lines; HeLa and HCC1937 (BRCA1-/-); the high frequencies of co-localisation were observed.

It is now clear that only in ALT cells, BRCA1 and BLM co-localise with RAD50 (Acharya et al., 2014). We presented evidence that in mESCs, LY-R and LY-S cells only a fraction of BRCA1 co-localises with BLM at telomeres (10% percentage) (Figure 6.16B). Our data from the human cells HeLa and U2OS are in agreement with the results obtained by Acharya et al. (2014), which shows HeLa cells have higher frequency of co-localisation than the U2OS cells.

Perhaps, the most interesting observation in this Chapter was the highest level of ALT activity in 408 cells (Figure 6.2). This finding suggests that, at least in the context of mouse cells, defective Brca1 may contribute to increase in the ALT pathway. In the human BRCA1 negative cells, HCC1937, the ALT activity was absent (Figure 6.2). Further investigation is required to expand upon these initial findings and assess their relevance. In the same context, it is important to highlight the situation with the pair of well characterized mouse lymphoma cell lines, LY-R and LY-S cells (Figure 6.2). Surprisingly, the only mouse cell line with no evidence of ALT was the LY-S cell line (Figure 6.2) thus contradicting observations by Neumann et al. (2013) that mouse somatic cells use ALT regularly as a method for telomere maintenance. It will be of importance to understand the nature of this observation in the context of LY-S cells radiosensitivity. All known components of DSB repair, that mediate radiosensitivity, are normal in LY-S cells (McIlrath et al., 2001). Given that telomere maintenance and DDR mechanisms are functionally linked (d'Adda di Fagagna et al., 2003) it would be of interest to assess to which extent potentially defective telomere maintenance in LY-S cells contributes to radiosensitivity. By the same token, our results argue that defective BRCA1 alters telomere homeostasis in favour of ALT perhaps acting as its de-repressor. This finding may have implications for cancer therapy based on targeting telomere maintenance.

CHAPTER 7

7 General Discussion and Future Research Direction

7.1 Introduction

BRCA1 is an important tumour suppressor protein that plays a key role in the DDR and DNA repair (Roy et al., 2011, Jiang and Greenberg, 2015). Germline mutations in *BRCA1* increase the life-time risk of developing breast (40-80%) and ovarian cancer (11%-50%) (Roy et al., 2011, Petrucelli et al., 2013). The main role of BRCA1 in DNA repair is fulfilled via the HR mechanism, an important DNA repair pathway that uses the undamaged sister chromatid to carry out high-fidelity repair of predominantly replication-associated DSB (Roy et al., 2013). BRCA1 also has a critical role in sensing DNA damage and therefore it is vital to the DDR and cell cycle checkpoint activation (Roy et al., 2013), making the role of BRCA1 in the genome integrity indispensible in the mammalian cell. More recently, it has been suggested that BRCA1 plays an active role in ALT-positive cancer cells but not telomerase-

positive cancer cells with the help of BLM and RAD50 (Acharya et al., 2014). However, the exact role of BRCA1 in telomere maintenance in ALT-positive cells is still unclear.

In this thesis we explored the role of BRCA1 from a telomere biology point of view by assessing markers of telomere dysfunction and ALT activity in the human and mouse cells. Our data revealed additional evidence for the role of BRCA1 in telomere dysfunction in the mammalian cells (Chapter 3; 4). Furthermore our data provided a new line of evidence for the relationship between BRCA1 and ALT activity in the mouse cells (Chapter 5; 6). These results are briefly summarized below.

7.2 Telomere dysfunction in *BRCA1* mutation carriers

Telomere dysfunction can lead to premature senescence (de Lange, 2006) and cancer (Blackburn et al., 2006, Donate and Blasco, 2011) if left unrepaired. The current known mechanisms behind telomere dysfunction are (a) disrupted shelterin proteins leading to unprotected telomeric ends (de Lange, 2006), (b) telomere length shortening and loss of the t-loops (Blackburn et al., 2006), (c) defective DNA damage repair and sensing proteins (d'Adda di Fagagna et al., 2004). To assess the role of BRCA1 in telomere dysfunction in the human cells, we used two markers of telomere dysfunction i.e. T-SCE and telomere length using human cell lines from BRCA1 carriers. Our findings specific to cells from BRCA1 carriers, described in detail in Chapter 3, indicate (i) higher frequencies of T-SCE, (ii) significantly shorter telomeres and (iii) defective DDR that also affects telomeres. Previous studies have shown that BRCA1 deficiency leads to telomere dysfunction, as evidenced by elevated chromosome fusions and translocations involving telomeres and telomere shortening (Cabuy et al., 2008, McPherson et al., 2006). To our knowledge in this thesis we reported first evidence of elevated T-SCEs in the two BRCA1 mutation carrier human cell lines and our observation of telomere shortening is consistent with the function of BRCA1 on telomeres that has been previously demonstrated (McPherson et al., 2006). However, the exact role of BRCA1 in telomere length homeostasis is conflicting. For example, Ballal et al. (2009) has shown that knock-down of BRCA1 protein using siRNA in two breast cancer cell

lines (MCF7 and T47D) led to increases in telomere length by an average of 3.45kb with 45% increase in the activity of the telomerase enzyme. The same study also showed that co-knock-down of the hTERT (the catalytic subunit of the telomerase enzyme) and BRCA1 did not result in telomere shortening suggesting that the mechanism of telomere lengthening by BRCA1 may be independent of the telomerase enzyme. In contrast, in another study, Cabuy et al., (2008) did not find changes in telomere length or the telomerase enzyme activity when BRCA1 was knocked down in the mammary epithelial cells, although the frequencies of anaphase-bridges (normally is indicative of dysfunctional telomeres) was elevated in those cells. The authors, therefore, suggested that the role of BRCA1 on telomeres might have a protective function rather than affect telomere length maintenance. Moreover, increased frequency of TIFs observed in cells from BRCA1 carriers shown in Chapter 3, further highlights the role of BRCA1 in telomere integrity maintenance. Taken together, our data presented in Chapter 3 seems to be in agreement with the published data (Cabuy et al., 2008, Ballal et al., 2009, Al-Wahiby and Slijepcevic, 2005, McPherson et al., 2006) pointing towards the active role of BRCA1 in telomere maintenance and length stability. However, the exact mechanism behind BRCA1 function in telomere length maintenance remains unclear.

7.3 Evidence for ALT activity in BRCA1 defective mESCs

ALT is another mechanism used in mammalian cells to maintain or increase telomere lengths. Roughly 15% of human cancers use ALT as the preferred mechanism of telomere length maintenance (Bryan et al., 1995, Bryan et al., 1997b, Bryan and Reddel, 1997, Hande et al., 1999). The currently accepted explanation for telomere elongation in the ALT positive cells is through the HR mechanism (Dunham et al., 2000). Interestingly, it has been proposed that recombination-mediated telomere synthesis was the archetypal telomere lengthening mechanism when eukaryotes first evolved linear chromosomes and that this was permanently repressed when it was superseded by telomerase in later eukaryotes (de Lange, 2004). It has recently been shown that the ALT activity is present in normal mouse tissues but this activity may be repressed in the mouse germline cells (Neumann et al., 2013). The exact molecular mechanism behind ALT repression or derepression in the

mammalian cells is not fully understood. A recent study have suggested that BRCA1, through its interaction with BLM and RAD50, accumulates and co-localises at telomeres in the ALT+ human cells but not in telomerase+ cells (Acharya et al., 2014). Our results presented in Chapters 4, 5 and 6 of this thesis, provided novel insights into the mechanism of ALT in mammalian cells. We demonstrated that levels of T-SCE (one of the markers of ALT activity) were significantly higher in the mESC line, 408 (Brca1$^{-/-}$) and lymphoblastoid cells from BRCA1 carriers. These initial observations suggested that at least one recognized ALT marker (T-SCEs) was positive. However, when we looked at other markers, such as ATRX and APBs we did not find significant differences between Brca1 defective cells and the control cells suggesting lack of association between Brca1 and ALT in these cells.

Nevertheless, when we assayed for the occurrence of ALT using a more sensitive assay (the CC assay) we found ALT activity in both mESCs and mouse lymphoblastoid LY-R cells. The ALT activities in these cells were accompanied with telomerase and this data confirm the previous finding that ALT may be expressed at low levels in all mouse somatic tissues (Neumann et al., 2013). However, to our surprise, the 408 cells had 1.5 fold higher activity than the isogenic normal counterpart. This clearly provided additional evidence for the involvement of Brca1 in ALT derepression mechanism in the mouse cells. However, we believe factors might be at play in addition to Brca1. Our results indicate the non-canonical role of ALT in the mouse cells. For example, higher activity of ALT in the 408 cells may serve a different function possibly more related to the DNA repair and the HR than telomere length synthesis whereas, the activity of ALT in the LY-R cells may serve as telomere length maintenance. Our results strongly suggest that the ALT activity is suppressed in the LY-S cells. This finding is of great interest for future research. We therefore, provided first strong evidence of higher ALT activity in the Brca1 defective mESCs on the absence of ALT in LY-S cells. But it must be pointed out that, that we do not have direct evidence for some of the hypotheses we postulated above, namely the different functional role of ALT. We believe these can be the basis for further investigation.

7.4 Future Research Direction

As mentioned above the novel findings of this thesis are:

- Identification of elevated levels of T-SCE in the human BRCA1 defective cells;
- Telomere dysfunction phenotype in the human and mouse Brca1 defective cells;
- Elevated ALT activity in the mouse Brca1 defective cells;
- Absence of ALT activity in the LY-S mouse lymphoma cells.

As a result of the above findings several line of new research could be pursued. Firstly, it would be of interest to further investigate, at molecular level, the mechanism behind BRCA1 and ALT derepression in the mammalian cells to identify whether BRCA1 cooperates with other factors such as BRCA2, BLM, WRN, Rad50 etc in providing ALT repression and if so to what extent. These can be performed using shRNA library screening or with the help of genome editing using CRISPR/Cas9. For example, conditional *in vitro* knock-out of BRCA1 and BRCA2 in normal human and mouse cells may provide further insight into the biochemical and functional activities of BRCA1/BRCA2 from telomere maintenance perspective. These cells can be subjected to detailed cytogenetic analysis using double colour CO-FISH to measure the levels of chromatid exchanges and imbalances or telomere probe STORM imaging to quantify levels of t-loop formation.

Secondly, the alternative functions of the ALT in mouse cells could be further investigated. For example, the co-existence of telomerase and ALT in the mouse cells provides a nice model to study telomere length synthesis role of ALT in the mouse 408 and LY-R/LY-S cells by inhibiting the telomerase activity either through inhibitor of the telomerase enzyme or knock-down of the mouse *Tert* gene. This will enable identification of the role of ALT on telomere length maintenance. Telomere length measurement could quickly be performed using qPCR or IQ-FISH methods.

Of particular importance would be examination of the nature or radiosensitivity in LY-S cells in light of ALT absence. A strong body of data indicate functional link between DDR and telomere maintenance (d'Adda di Fagagna et al., 2004).

Finally, it would be of interest to identify genes that may play important roles in ALT derepression by performing large-scale RNAi screening coupled with transcriptomics (RNAseq) to identify genes that may activate ALT phenotype in normal human cells. Data generated here will enable identification of functional role of set of gene(s) that can further be investigated through single-gene knock-outs experiment. Finding out the exact mechanism of ALT derepression and activity in maintaining the telomere length will have

important clinical uses. For example, it can be used to design novel anti-ALT inhibitors as an anti-tumour drugs.

8 References

ABBOTT, D. W., THOMPSON, M. E., ROBINSON-BENION, C., TOMLINSON, G., JENSEN, R. A. & HOLT, J. T. 1999. BRCA1 expression restores radiation resistance in BRCA1-defective cancer cells through enhancement of transcription-coupled DNA repair. *J Biol Chem,* 274**,** 18808-12.

ABREU, E., ARITONOVSKA, E., REICHENBACH, P., CRISTOFARI, G., CULP, B., TERNS, R. M., LINGNER, J. & TERNS, M. P. 2010. TIN2-tethered TPP1 recruits human telomerase to telomeres in vivo. *Mol Cell Biol,* 30**,** 2971-82.

ACHARYA, S., KAUL, Z., GOCHA, A. S., MARTINEZ, A. R., HARRIS, J., PARVIN, J. D. & GRODEN, J. 2014. Association of BLM and BRCA1 during Telomere Maintenance in ALT Cells. *PLoS One,* 9**,** e103819.

AL-WAHIBY, S. & SLIJEPCEVIC, P. 2005. Chromosomal aberrations involving telomeres in BRCA1 deficient human and mouse cell lines. *Cytogenet Genome Res,* 109**,** 491-6.

ALADJEM, M. I., SPIKE, B. T., RODEWALD, L. W., HOPE, T. J., KLEMM, M., JAENISCH, R. & WAHL, G. M. 1998. ES cells do not activate p53-dependent stress responses and undergo p53-independent apoptosis in response to DNA damage. *Curr Biol,* 8**,** 145-55.

ANTONIOU, A. C., FOULKES, W. D. & TISCHKOWITZ, M. 2014. Breast-cancer risk in families with mutations in PALB2. *N Engl J Med,* 371**,** 1651-2.

ARAT, N. O. & GRIFFITH, J. D. 2012. Human Rap1 interacts directly with telomeric DNA and regulates TRF2 localization at the telomere. *J Biol Chem,* 287**,** 41583-94.

BADIE, S., CARLOS, A. R., FOLIO, C., OKAMOTO, K., BOUWMAN, P., JONKERS, J. & TARSOUNAS, M. 2015. BRCA1 and CtIP promote alternative non-homologous end-joining at uncapped telomeres. *Embo j.* England.

BAEYENS, A., THIERENS, H., CLAES, K., POPPE, B., DE RIDDER, L. & VRAL, A. 2004. Chromosomal radiosensitivity in BRCA1 and BRCA2 mutation carriers. *Int J Radiat Biol,* 80**,** 745-56.

BAILEY, S. M., BRENNEMAN, M. A. & GOODWIN, E. H. 2004a. Frequent recombination in telomeric DNA may extend the proliferative life of telomerase-negative cells. *Nucleic Acids Res,* 32**,** 3743-51.

BAILEY, S. M., CORNFORTH, M. N., KURIMASA, A., CHEN, D. J. & GOODWIN, E. H. 2001. Strand-specific postreplicative processing of mammalian telomeres. *Science,* 293**,** 2462-5.

BAILEY, S. M., GOODWIN, E. H. & CORNFORTH, M. N. 2004b. Strand-specific fluorescence in situ hybridization: the CO-FISH family. *Cytogenet Genome Res,* 107**,** 14-7.

BAKKENIST, C. J. & KASTAN, M. B. 2004. Phosphatases join kinases in DNA-damage response pathways. *Trends Cell Biol,* 14**,** 339-41.

BALDEYRON, C., JACQUEMIN, E., SMITH, J., JACQUEMONT, C., DE OLIVEIRA, I., GAD, S., FEUNTEUN, J., STOPPA-LYONNET, D. & PAPADOPOULO, D. 2002. A single mutated BRCA1 allele leads to impaired fidelity of double strand break end-joining. *Oncogene,* 21**,** 1401-10.

BALLAL, R. D., SAHA, T., FAN, S., HADDAD, B. R. & ROSEN, E. M. 2009. BRCA1 localization to the telomere and its loss from the telomere in response to DNA damage. *J Biol Chem,* 284**,** 36083-98.

BANATH, J. P., BANUELOS, C. A., KLOKOV, D., MACPHAIL, S. M., LANSDORP, P. M. & OLIVE, P. L. 2009. Explanation for excessive DNA single-strand breaks and endogenous repair foci in pluripotent mouse embryonic stem cells. *Exp Cell Res,* 315**,** 1505-20.

BARIA, K., WARREN, C., ROBERTS, S. A., WEST, C. M. & SCOTT, D. 2001. Chromosomal radiosensitivity as a marker of predisposition to common cancers? *Br J Cancer,* 84**,** 892-6.

BARWELL, J., PANGON, L., GEORGIOU, A., KESTERTON, I., LANGMAN, C., ARDEN-JONES, A., BANCROFT, E., SALMON, A., LOCKE, I., KOTE-JARAI, Z., MORRIS, J. R., SOLOMON, E., BERG, J., DOCHERTY, Z., CAMPLEJOHN, R., EELES, R. & HODGSON, S. V. 2007. Lymphocyte radiosensitivity in BRCA1 and BRCA2 mutation carriers and implications for breast cancer susceptibility. *Int J Cancer,* 121**,** 1631-6.

BAU, D. T., FU, Y. P., CHEN, S. T., CHENG, T. C., YU, J. C., WU, P. E. & SHEN, C. Y. 2004. Breast cancer risk and the DNA double-strand break end-joining capacity of nonhomologous end-joining genes are affected by BRCA1. *Cancer Res,* 64**,** 5013-9.

BAUMANN, P., BENSON, F. E. & WEST, S. C. 1996. Human Rad51 protein promotes ATP-dependent homologous pairing and strand transfer reactions in vitro. *Cell,* 87**,** 757-66.

BAUMANN, P. & PRICE, C. 2010. Pot1 and telomere maintenance. *FEBS Lett,* 584**,** 3779-84.

BECHTER, O. E., SHAY, J. W. & WRIGHT, W. E. 2004a. The frequency of homologous recombination in human ALT cells. *Cell Cycle,* 3**,** 547-9.

BECHTER, O. E., ZOU, Y., WALKER, W., WRIGHT, W. E. & SHAY, J. W. 2004b. Telomeric recombination in mismatch repair deficient human colon cancer cells after telomerase inhibition. *Cancer Res,* 64**,** 3444-51.

BEDNAREK, A., BUDUNOVA, I., SLAGA, T. J. & ALDAZ, C. M. 1995. Increased telomerase activity in mouse skin premalignant progression. *Cancer Res,* 55**,** 4566-9.

BENNETT, L. M., HAUGEN-STRANO, A., COCHRAN, C., BROWNLEE, H. A., FIEDOREK, F. T., JR. & WISEMAN, R. W. 1995. Isolation of the mouse homologue of BRCA1 and genetic mapping to mouse chromosome 11. *Genomics,* 29**,** 576-81.

BERNARDI, R. & PANDOLFI, P. P. 2007. Structure, dynamics and functions of promyelocytic leukaemia nuclear bodies. *Nat Rev Mol Cell Biol,* 8**,** 1006-16.

BHATTACHARYYA, A., EAR, U. S., KOLLER, B. H., WEICHSELBAUM, R. R. & BISHOP, D. K. 2000. The breast cancer susceptibility gene BRCA1 is required for subnuclear assembly of Rad51 and survival following treatment with the DNA cross-linking agent cisplatin. *J Biol Chem,* 275**,** 23899-903.

BHATTACHARYYA, S., SANDY, A. & GRODEN, J. 2010. Unwinding Protein Complexes in ALTernative Telomere Maintenance. *J Cell Biochem,* 109**,** 7-15.

BILAUD, T., BRUN, C., ANCELIN, K., KOERING, C. E., LAROCHE, T. & GILSON, E. 1997. Telomeric localization of TRF2, a novel human telobox protein. *Nat Genet,* 17**,** 236-9.

BLACKBURN, E. H. & GALL, J. G. 1978. A tandemly repeated sequence at the termini of the extrachromosomal ribosomal RNA genes in Tetrahymena. *J Mol Biol,* 120**,** 33-53.

BLACKBURN, E. H., GREIDER, C. W. & SZOSTAK, J. W. 2006. Telomeres and telomerase: the path from maize, Tetrahymena and yeast to human cancer and aging. *Nat Med,* 12**,** 1133-8.

BLASCO, M. A. 2007. Telomere length, stem cells and aging. *Nat Chem Biol,* 3**,** 640-9.

BLASCO, M. A., LEE, H. W., HANDE, M. P., SAMPER, E., LANSDORP, P. M., DEPINHO, R. A. & GREIDER, C. W. 1997. Telomere shortening and tumor formation by mouse cells lacking telomerase RNA. *Cell,* 91**,** 25-34.

BLASCO, M. A., RIZEN, M., GREIDER, C. W. & HANAHAN, D. 1996. Differential regulation of telomerase activity and telomerase RNA during multi-stage tumorigenesis. *Nat Genet,* 12**,** 200-4.

BORK, P., HOFMANN, K., BUCHER, P., NEUWALD, A. F., ALTSCHUL, S. F. & KOONIN, E. V. 1997. A superfamily of conserved domains in DNA damage-responsive cell cycle checkpoint proteins. *Faseb j,* 11**,** 68-76.

BROCCOLI, D., GODLEY, L. A., DONEHOWER, L. A., VARMUS, H. E. & DE LANGE, T. 1996. Telomerase activation in mouse mammary tumors: lack of detectable telomere shortening and evidence for regulation of telomerase RNA with cell proliferation. *Mol Cell Biol,* 16**,** 3765-72.

BRYAN, T. M., ENGLEZOU, A., DALLA-POZZA, L., DUNHAM, M. A. & REDDEL, R. R. 1997a. Evidence for an alternative mechanism for maintaining telomere length in human tumors and tumor-derived cell lines. *Nature Medicine,* 3**,** 1271-1274.

BRYAN, T. M., ENGLEZOU, A., DALLA-POZZA, L., DUNHAM, M. A. & REDDEL, R. R. 1997b. Evidence for an alternative mechanism for maintaining telomere length in human tumors and tumor-derived cell lines. *Nat Med,* 3**,** 1271-4.

BRYAN, T. M., ENGLEZOU, A., GUPTA, J., BACCHETTI, S. & REDDEL, R. R. 1995. Telomere elongation in immortal human cells without detectable telomerase activity. *Embo j,* 14**,** 4240-8.

BRYAN, T. M. & REDDEL, R. R. 1997. Telomere dynamics and telomerase activity in in vitro immortalised human cells. *Eur J Cancer,* 33**,** 767-73.

BUGREEV, D. V., ROSSI, M. J. & MAZIN, A. V. 2011. Cooperation of RAD51 and RAD54 in regression of a model replication fork. *Nucleic Acids Res,* 39**,** 2153-64.

BUIS, J., STONEHAM, T., SPEHALSKI, E. & FERGUSON, D. O. 2012. Mre11 regulates CtIP-dependent double-strand break repair by interaction with CDK2. *Nat Struct Mol Biol,* 19**,** 246-52.

BURDON, T., SMITH, A. & SAVATIER, P. 2002. Signalling, cell cycle and pluripotency in embryonic stem cells. *Trends Cell Biol,* 12**,** 432-8.

BURMA, S., CHEN, B. P., MURPHY, M., KURIMASA, A. & CHEN, D. J. 2001. ATM phosphorylates histone H2AX in response to DNA double-strand breaks. *J Biol Chem,* 276**,** 42462-7.

CABUY, E., NEWTON, C., JOKSIC, G., WOODBINE, L., KOLLER, B., JEGGO, P. A. & SLIJEPCEVIC, P. 2005. Accelerated telomere shortening and telomere abnormalities in radiosensitive cell lines. *Radiat Res,* 164**,** 53-62.

CABUY, E., NEWTON, C., ROBERTS, T., NEWBOLD, R. & SLIJEPCEVIC, P. 2004. Identification of subpopulations of cells with differing telomere lengths in mouse and human cell lines by flow FISH. *Cytometry A,* 62**,** 150-61.

CABUY, E., NEWTON, C. & SLIJEPCEVIC, P. 2008. BRCA1 knock-down causes telomere dysfunction in mammary epithelial cells. *Cytogenet Genome Res,* 122**,** 336-42.

CALADO, R. T. & DUMITRIU, B. 2013. Telomere dynamics in mice and humans. *Semin Hematol,* 50**,** 165-74.

CAMPISI, J., KIM, S. H., LIM, C. S. & RUBIO, M. 2001. Cellular senescence, cancer and aging: the telomere connection. *Exp Gerontol,* 36**,** 1619-37.

CAO, L., LI, W., KIM, S., BRODIE, S. G. & DENG, C. X. 2003. Senescence, aging, and malignant transformation mediated by p53 in mice lacking the Brca1 full-length isoform. *Genes Dev,* 17**,** 201-13.

CASTILLA, L. H., COUCH, F. J., ERDOS, M. R., HOSKINS, K. F., CALZONE, K., GARBER, J. E., BOYD, J., LUBIN, M. B., DESHANO, M. L., BRODY, L. C. & ET AL. 1994. Mutations in the BRCA1 gene in families with early-onset breast and ovarian cancer. *Nat Genet,* 8**,** 387-91.

CELLI, G. B. & DE LANGE, T. 2005. DNA processing is not required for ATM-mediated telomere damage response after TRF2 deletion. *Nat Cell Biol,* 7**,** 712-8.

CELLI, G. B., DENCHI, E. L. & DE LANGE, T. 2006. Ku70 stimulates fusion of dysfunctional telomeres yet protects chromosome ends from homologous recombination. *Nat Cell Biol,* 8**,** 885-90.

CERONE, M. A., AUTEXIER, C., LONDONO-VALLEJO, J. A. & BACCHETTI, S. 2005. A human cell line that maintains telomeres in the absence of telomerase and of key markers of ALT. *Oncogene,* 24**,** 7893-901.

CERONE, M. A., LONDONO-VALLEJO, J. A. & BACCHETTI, S. 2001. Telomere maintenance by telomerase and by recombination can coexist in human cells. *Hum Mol Genet,* 10**,** 1945-52.

CESARE, A. J. & GRIFFITH, J. D. 2004. Telomeric DNA in ALT cells is characterized by free telomeric circles and heterogeneous t-loops. *Mol Cell Biol,* 24**,** 9948-57.

CESARE, A. J. & REDDEL, R. R. 2008. Telomere uncapping and alternative lengthening of telomeres. *Mech Ageing Dev,* 129**,** 99-108.

CESARE, A. J. & REDDEL, R. R. 2010. Alternative lengthening of telomeres: models, mechanisms and implications. *Nat Rev Genet,* 11**,** 319-30.

CHADENEAU, C., SIEGEL, P., HARLEY, C. B., MULLER, W. J. & BACCHETTI, S. 1995. Telomerase activity in normal and malignant murine tissues. *Oncogene,* 11**,** 893-8.

CHAPMAN, M. S. & VERMA, I. M. 1996. Transcriptional activation by BRCA1. *Nature,* 382**,** 678-9.

CHAUDHURY, I., SAREEN, A., RAGHUNANDAN, M. & SOBECK, A. 2013. FANCD2 regulates BLM complex functions independently of FANCI to promote replication fork recovery. *Nucleic Acids Res,* 41**,** 6444-59.

CHEN, T., STEPHENS, P. A., MIDDLETON, F. K. & CURTIN, N. J. 2012. Targeting the S and G2 checkpoint to treat cancer. *Drug Discov Today,* 17**,** 194-202.

CHEN, Y., FARMER, A. A., CHEN, C. F., JONES, D. C., CHEN, P. L. & LEE, W. H. 1996. BRCA1 is a 220-kDa nuclear phosphoprotein that is expressed and phosphorylated in a cell cycle-dependent manner. *Cancer Res,* 56**,** 3168-72.

CHENG, W. H., KUSUMOTO, R., OPRESKO, P. L., SUI, X., HUANG, S., NICOLETTE, M. L., PAULL, T. T., CAMPISI, J., SEIDMAN, M. & BOHR, V. A. 2006. Collaboration of Werner syndrome protein and BRCA1 in cellular responses to DNA interstrand cross-links. *Nucleic Acids Res,* 34**,** 2751-60.

CHUYKIN, I. A., LIANGUZOVA, M. S., POSPELOVA, T. V. & POSPELOV, V. A. 2008a. Activation of DNA damage response signaling in mouse embryonic stem cells. *http://dx.doi.org/10.4161/cc.7.18.6699*.

CHUYKIN, I. A., LIANGUZOVA, M. S., POSPELOVA, T. V. & POSPELOV, V. A. 2008b. Activation of DNA damage response signaling in mouse embryonic stem cells. *Cell Cycle,* 7**,** 2922-8.

CLARK, S. L., RODRIGUEZ, A. M., SNYDER, R. R., HANKINS, G. D. & BOEHNING, D. 2012. Structure-Function Of The Tumor Suppressor BRCA1. *Comput Struct Biotechnol J,* 1.

CLARKE, P. R. & SANDERSON, H. S. 2006. A mitotic role for BRCA1/BARD1 in tumor suppression? *Cell,* 127**,** 453-5.

CLAUS, E. B., SCHILDKRAUT, J. M., THOMPSON, W. D. & RISCH, N. J. 1996. The genetic attributable risk of breast and ovarian cancer. *Cancer,* 77**,** 2318-24.

CLYNES, D., JELINSKA, C., XELLA, B., AYYUB, H., TAYLOR, S., MITSON, M., BACHRATI, C. Z., HIGGS, D. R. & GIBBONS, R. J. 2014. ATRX dysfunction induces replication defects in primary mouse cells. *PLoS One,* 9**,** e92915.

COLGIN, L. M., BARAN, K., BAUMANN, P., CECH, T. R. & REDDEL, R. R. 2003. Human POT1 facilitates telomere elongation by telomerase. *Curr Biol,* 13**,** 942-6.

CRABBE, L., VERDUN, R. E., HAGGBLOM, C. I. & KARLSEDER, J. 2004. Defective telomere lagging strand synthesis in cells lacking WRN helicase activity. *Science,* 306**,** 1951-3.

CRESSMAN, V. L., BACKLUND, D. C., AVRUTSKAYA, A. V., LEADON, S. A., GODFREY, V. & KOLLER, B. H. 1999. Growth retardation, DNA repair defects, and lack of spermatogenesis in BRCA1-deficient mice. *Mol Cell Biol,* 19**,** 7061-75.

CRISTOFARI, G. & LINGNER, J. 2006. Telomere length homeostasis requires that telomerase levels are limiting. *Embo j,* 25**,** 565-74.

D'ADDA DI FAGAGNA, F., REAPER, P. M., CLAY-FARRACE, L., FIEGLER, H., CARR, P., VON ZGLINICKI, T., SARETZKI, G., CARTER, N. P. & JACKSON, S. P. 2003. A DNA damage checkpoint response in telomere-initiated senescence. *Nature,* 426**,** 194-8.

D'ADDA DI FAGAGNA, F., TEO, S. H. & JACKSON, S. P. 2004. Functional links between telomeres and proteins of the DNA-damage response. *Genes Dev,* 18**,** 1781-99.

DANTZER, F., GIRAUD-PANIS, M. J., JACO, I., AME, J. C., SCHULTZ, I., BLASCO, M., KOERING, C. E., GILSON, E., MENISSIER-DE MURCIA, J., DE MURCIA, G. & SCHREIBER, V. 2004. Functional interaction between poly(ADP-Ribose) polymerase 2 (PARP-2) and TRF2: PARP activity negatively regulates TRF2. *Mol Cell Biol,* 24**,** 1595-607.

DAVALOS, A. R. & CAMPISI, J. 2003. Bloom syndrome cells undergo p53-dependent apoptosis and delayed assembly of BRCA1 and NBS1 repair complexes at stalled replication forks. *J Cell Biol,* 162**,** 1197-209.

DAVIS, A. J. & CHEN, D. J. 2013. DNA double strand break repair via non-homologous end-joining. *Transl Cancer Res,* 2**,** 130-143.

DE LANGE, T. 2004. T-loops and the origin of telomeres. *Nat Rev Mol Cell Biol,* 5**,** 323-9.

DE LANGE, T. 2005a. Shelterin: the protein complex that shapes and safeguards human telomeres. *Genes Dev,* 19**,** 2100-10.

DE LANGE, T. 2005b. Telomere-related genome instability in cancer. *Cold Spring Harb Symp Quant Biol,* 70**,** 197-204.

DE LANGE, T., SHIUE, L., MYERS, R. M., COX, D. R., NAYLOR, S. L., KILLERY, A. M. & VARMUS, H. E. 1990. Structure and variability of human chromosome ends. *Mol Cell Biol,* 10**,** 518-27.

DE WAARD, H., DE WIT, J., GORGELS, T. G., VAN DEN AARDWEG, G., ANDRESSOO, J. O., VERMEIJ, M., VAN STEEG, H., HOEIJMAKERS, J. H. & VAN DER HORST, G. T. 2003. Cell type-specific hypersensitivity to oxidative damage in CSB and XPA mice. *DNA Repair (Amst),* 2**,** 13-25.

DENCHI, E. L. & DE LANGE, T. 2007. Protection of telomeres through independent control of ATM and ATR by TRF2 and POT1. *Nature,* 448**,** 1068-71.

DENG, C. X. & BRODIE, S. G. 2000. Roles of BRCA1 and its interacting proteins. *Bioessays,* 22**,** 728-37.

DENG, C. X. & SCOTT, F. 2000. Role of the tumor suppressor gene Brca1 in genetic stability and mammary gland tumor formation. *Oncogene,* 19**,** 1059-64.

DENG, C. X. & WANG, R. H. 2003. Roles of BRCA1 in DNA damage repair: a link between development and cancer. *Hum Mol Genet,* 12 Spec No 1**,** R113-23.

DOKSANI, Y., WU, J. Y., DE LANGE, T. & ZHUANG, X. 2013. Super-resolution fluorescence imaging of telomeres reveals TRF2-dependent T-loop formation. *Cell,* 155**,** 345-56.

DONATE, L. E. & BLASCO, M. A. 2011. Telomeres in cancer and ageing. *Philos Trans R Soc Lond B Biol Sci,* 366**,** 76-84.

DONOHO, G., JASIN, M. & BERG, P. 1998. Analysis of gene targeting and intrachromosomal homologous recombination stimulated by genomic double-strand breaks in mouse embryonic stem cells. *Mol Cell Biol,* 18**,** 4070-8.

DOWNS, J. A. & JACKSON, S. P. 2004. A means to a DNA end: the many roles of Ku. *Nat Rev Mol Cell Biol,* 5**,** 367-78.

DUCREST, A. L., SZUTORISZ, H., LINGNER, J. & NABHOLZ, M. 2002. Regulation of the human telomerase reverse transcriptase gene. *Oncogene,* 21**,** 541-52.

DUNHAM, M. A., NEUMANN, A. A., FASCHING, C. L. & REDDEL, R. R. 2000. Telomere maintenance by recombination in human cells. *Nat Genet,* 26**,** 447-50.

DURANT, S. T. & NICKOLOFF, J. A. 2005. Good timing in the cell cycle for precise DNA repair by BRCA1. *Cell Cycle,* 4**,** 1216-22.

EICKBUSH, T. H. 1997. Telomerase and retrotransposons: which came first? *Science,* 277**,** 911-2.

ELLIS, N. A. & GERMAN, J. 1996. Molecular genetics of Bloom's syndrome. *Hum Mol Genet,* 5 Spec No**,** 1457-63.

ELLIS, N. A., LENNON, D. J., PROYTCHEVA, M., ALHADEFF, B., HENDERSON, E. E. & GERMAN, J. 1995. Somatic intragenic recombination within the mutated locus BLM can correct the high sister-chromatid exchange phenotype of Bloom syndrome cells. *Am J Hum Genet,* 57**,** 1019-27.

ERNESTOS, B., NIKOLAOS, P., KOULIS, G., ELENI, R., KONSTANTINOS, B., ALEXANDRA, G. & MICHAEL, K. 2010. Increased chromosomal radiosensitivity in women carrying BRCA1/BRCA2 mutations assessed with the G2 assay. *Int J Radiat Oncol Biol Phys,* 76**,** 1199-205.

ESCRIBANO-DIAZ, C., ORTHWEIN, A., FRADET-TURCOTTE, A., XING, M., YOUNG, J. T., TKAC, J., COOK, M. A., ROSEBROCK, A. P., MUNRO, M., CANNY, M. D., XU,

D. & DUROCHER, D. 2013. A cell cycle-dependent regulatory circuit composed of 53BP1-RIF1 and BRCA1-CtIP controls DNA repair pathway choice. *Mol Cell,* 49**,** 872-83.

FENECH, M. 2000. The in vitro micronucleus technique. *Mutat Res,* 455**,** 81-95.

FENECH, M. 2010. The lymphocyte cytokinesis-block micronucleus cytome assay and its application in radiation biodosimetry. *Health Phys,* 98**,** 234-43.

FENG, J., FUNK, W. D., WANG, S. S., WEINRICH, S. L., AVILION, A. A., CHIU, C. P., ADAMS, R. R., CHANG, E., ALLSOPP, R. C., YU, J. & ET AL. 1995. The RNA component of human telomerase. *Science,* 269**,** 1236-41.

FENG, L., FONG, K. W., WANG, J., WANG, W. & CHEN, J. 2013. RIF1 counteracts BRCA1-mediated end resection during DNA repair. *J Biol Chem,* 288**,** 11135-43.

FERNANDEZ-CAPETILLO, O., CHEN, H.-T., CELESTE, A., WARD, I., ROMANIENKO, P. J., MORALES, J. C., NAKA, K., XIA, Z., CAMERINI-OTERO, R. D., MOTOYAMA, N., CARPENTER, P. B., BONNER, W. M., CHEN, J. & NUSSENZWEIG, A. 2002. DNA damage-induced G2|[ndash]|M checkpoint activation by histone H2AX and 53BP1. *Nature Cell Biology,* 4**,** 993-997.

FLUCKIGER, A. C., MARCY, G., MARCHAND, M., NEGRE, D., COSSET, F. L., MITALIPOV, S., WOLF, D., SAVATIER, P. & DEHAY, C. 2006. Cell cycle features of primate embryonic stem cells. *Stem Cells,* 24**,** 547-56.

FORAY, N., RANDRIANARISON, V., MAROT, D., PERRICAUDET, M., LENOIR, G. & FEUNTEUN, J. 1999. Gamma-rays-induced death of human cells carrying mutations of BRCA1 or BRCA2. *Oncogene,* 18**,** 7334-42.

FORD, D., EASTON, D. F., BISHOP, D. T., NAROD, S. A. & GOLDGAR, D. E. 1994. Risks of cancer in BRCA1-mutation carriers. Breast Cancer Linkage Consortium. *Lancet,* 343**,** 692-5.

FRIEDBERG, E. C. & MEIRA, L. B. 2006. Database of mouse strains carrying targeted mutations in genes affecting biological responses to DNA damage Version 7. *DNA Repair (Amst),* 5**,** 189-209.

FUMAGALLI, M., ROSSIELLO, F., CLERICI, M., BAROZZI, S., CITTARO, D., KAPLUNOV, J. M., BUCCI, G., DOBREVA, M., MATTI, V., BEAUSEJOUR, C. M., HERBIG, U., LONGHESE, M. P. & D'ADDA DI FAGAGNA, F. 2012. Telomeric DNA damage is irreparable and causes persistent DNA-damage-response activation. *Nat Cell Biol,* 14**,** 355-65.

GELL, D. & JACKSON, S. P. 1999. Mapping of protein-protein interactions within the DNA-dependent protein kinase complex. *Nucleic Acids Res,* 27**,** 3494-502.

GERMAN, J. 1993. Bloom syndrome: a mendelian prototype of somatic mutational disease. *Medicine (Baltimore),* 72**,** 393-406.

GIACHINO, C., ORLANDO, L. & TURINETTO, V. 2013. Maintenance of Genomic Stability in Mouse Embryonic Stem Cells: Relevance in Aging and Disease. *Int J Mol Sci.*

GILLEY, D., LEE, M. S. & BLACKBURN, E. H. 1995. Altering specific telomerase RNA template residues affects active site function. *Genes Dev,* 9**,** 2214-26.

GOCHA, A. R., ACHARYA, S. & GRODEN, J. 2014. WRN loss induces switching of telomerase-independent mechanisms of telomere elongation. *PLoS One,* 9**,** e93991.

GOWEN, L. C., AVRUTSKAYA, A. V., LATOUR, A. M., KOLLER, B. H. & LEADON, S. A. 1998. BRCA1 required for transcription-coupled repair of oxidative DNA damage. *Science,* 281**,** 1009-12.

GOWEN, L. C., JOHNSON, B. L., LATOUR, A. M., SULIK, K. K. & KOLLER, B. H. 1996. Brca1 deficiency results in early embryonic lethality characterized by neuroepithelial abnormalities. *Nat Genet,* 12**,** 191-4.

GREIDER, C. W. & BLACKBURN, E. H. 1985. Identification of a specific telomere terminal transferase activity in Tetrahymena extracts. *Cell,* 43**,** 405-13.

GREIDER, C. W. & BLACKBURN, E. H. 1989. A telomeric sequence in the RNA of Tetrahymena telomerase required for telomere repeat synthesis. *Nature,* 337**,** 331-7.

GRIFFITH, J. D., COMEAU, L., ROSENFIELD, S., STANSEL, R. M., BIANCHI, A., MOSS, H. & DE LANGE, T. 1999. Mammalian telomeres end in a large duplex loop. *Cell,* 97**,** 503-14.

GROBELNY, J. V., GODWIN, A. K. & BROCCOLI, D. 2000. ALT-associated PML bodies are present in viable cells and are enriched in cells in the G(2)/M phase of the cell cycle. *J Cell Sci,* 113 Pt 24**,** 4577-85.

GUDMUNDSDOTTIR, K. & ASHWORTH, A. 2006. The roles of BRCA1 and BRCA2 and associated proteins in the maintenance of genomic stability. *Oncogene,* 25**,** 5864-74.

HABER, J. E. 2000. Partners and pathwaysrepairing a double-strand break. *Trends Genet,* 16**,** 259-64.

HACKETT, J. A. & GREIDER, C. W. 2003. End resection initiates genomic instability in the absence of telomerase. *Mol Cell Biol,* 23**,** 8450-61.

HAHN, W. C., STEWART, S. A., BROOKS, M. W., YORK, S. G., EATON, E., KURACHI, A., BEIJERSBERGEN, R. L., KNOLL, J. H., MEYERSON, M. & WEINBERG, R. A. 1999. Inhibition of telomerase limits the growth of human cancer cells. *Nat Med,* 5**,** 1164-70.

HAKEM, R., DE LA POMPA, J. L., SIRARD, C., MO, R., WOO, M., HAKEM, A., WAKEHAM, A., POTTER, J., REITMAIR, A., BILLIA, F., FIRPO, E., HUI, C. C., ROBERTS, J., ROSSANT, J. & MAK, T. W. 1996. The tumor suppressor gene Brca1 is required for embryonic cellular proliferation in the mouse. *Cell,* 85**,** 1009-23.

HALL, J. M., LEE, M. K., NEWMAN, B., MORROW, J. E., ANDERSON, L. A., HUEY, B. & KING, M. C. 1990. Linkage of early-onset familial breast cancer to chromosome 17q21. *Science,* 250**,** 1684-9.

HANAOKA, S., NAGADOI, A. & NISHIMURA, Y. 2005. Comparison between TRF2 and TRF1 of their telomeric DNA-bound structures and DNA-binding activities. *Protein Sci,* 14**,** 119-30.

HANDE, M. P., SAMPER, E., LANSDORP, P. & BLASCO, M. A. 1999. Telomere length dynamics and chromosomal instability in cells derived from telomerase null mice. *J Cell Biol,* 144**,** 589-601.

HÄRLE-BACHOR, C. & BOUKAMP, P. 1996. Telomerase activity in the regenerative basal layer of the epidermis inhuman skin and in immortal and carcinoma-derived skin keratinocytes. *Proc Natl Acad Sci U S A,* 93**,** 6476-81.

HARLEY, C. B. 2002. Telomerase is not an oncogene. *Oncogene,* 21**,** 494-502.

HARLEY, C. B., FUTCHER, A. B. & GREIDER, C. W. 1990. Telomeres shorten during ageing of human fibroblasts. *Nature,* 345**,** 458-60.

HARLEY, C. B., KIM, N. W., PROWSE, K. R., WEINRICH, S. L., HIRSCH, K. S., WEST, M. D., BACCHETTI, S., HIRTE, H. W., COUNTER, C. M., GREIDER, C. W. & ET AL. 1994. Telomerase, cell immortality, and cancer. *Cold Spring Harb Symp Quant Biol,* 59**,** 307-15.

HARLEY, C. B. & VILLEPONTEAU, B. 1995. Telomeres and telomerase in aging and cancer. *Curr Opin Genet Dev,* 5**,** 249-55.

HARRINGTON, L., ZHOU, W., MCPHAIL, T., OULTON, R., YEUNG, D. S., MAR, V., BASS, M. B. & ROBINSON, M. O. 1997. Human telomerase contains evolutionarily conserved catalytic and structural subunits. *Genes Dev,* 11**,** 3109-15.

HASTY, P., RIVERA-PEREZ, J. & BRADLEY, A. 1992. The role and fate of DNA ends for homologous recombination in embryonic stem cells. *Mol Cell Biol,* 12**,** 2464-74.

HATZI, V. I., TERZOUDI, G. I., MAKROPOULOS, V. & PANTELIAS, G. E. 2009. A cytogenetic methodology to evaluate in vitro the G2-chromosomal radiosensitization induced by chemicals at non-clastogenic doses. *J Genet,* 88**,** 349-51.

HAYFLICK, L. 1965. Mycoplasmas and human leukemia. *Wistar Inst Symp Monogr,* 4**,** 157-65.

HAYFLICK, L. & MOORHEAD, P. S. 1961. The serial cultivation of human diploid cell strains. *Exp Cell Res,* 25**,** 585-621.

HEAPHY, C. M., DE WILDE, R. F., JIAO, Y., KLEIN, A. P., EDIL, B. H., SHI, C., BETTEGOWDA, C., RODRIGUEZ, F. J., EBERHART, C. G., HEBBAR, S.,

OFFERHAUS, G. J., MCLENDON, R., RASHEED, B. A., HE, Y., YAN, H., BIGNER, D. D., OBA-SHINJO, S. M., MARIE, S. K., RIGGINS, G. J., KINZLER, K. W., VOGELSTEIN, B., HRUBAN, R. H., MAITRA, A., PAPADOPOULOS, N. & MEEKER, A. K. 2011. Altered telomeres in tumors with ATRX and DAXX mutations. *Science,* 333**,** 425.

HEIN, A. L., OUELLETTE, M. M. & YAN, Y. 2014. Radiation-induced signaling pathways that promote cancer cell survival (Review). *International Journal of Oncology,* 45**,** 1813-1819.

HEINE, B., HUMMEL, M., DEMEL, G. & STEIN, H. 1998. Demonstration of constant upregulation of the telomerase RNA component in human gastric carcinomas using in situ hybridization. *J Pathol,* 185**,** 139-44.

HELT, C. E., CLIBY, W. A., KENG, P. C., BAMBARA, R. A. & O'REILLY, M. A. 2005a. Ataxia telangiectasia mutated (ATM) and ATM and Rad3-related protein exhibit selective target specificities in response to different forms of DNA damage. *J Biol Chem,* 280**,** 1186-92.

HELT, C. E., WANG, W., KENG, P. C. & BAMBARA, R. A. 2005b. Evidence that DNA damage detection machinery participates in DNA repair. *Cell Cycle,* 4**,** 529-32.

HEMANN, M. T. & GREIDER, C. W. 2000. Wild-derived inbred mouse strains have short telomeres. *Nucleic Acids Res.*

HEMANN, M. T., STRONG, M. A., HAO, L. Y. & GREIDER, C. W. 2001. The shortest telomere, not average telomere length, is critical for cell viability and chromosome stability. *Cell,* 107**,** 67-77.

HENSON, J. D., CAO, Y., HUSCHTSCHA, L. I., CHANG, A. C., AU, A. Y., PICKETT, H. A. & REDDEL, R. R. 2009. DNA C-circles are specific and quantifiable markers of alternative-lengthening-of-telomeres activity. *Nat Biotechnol,* 27**,** 1181-5.

HENSON, J. D., NEUMANN, A. A., YEAGER, T. R. & REDDEL, R. R. 2002. Alternative lengthening of telomeres in mammalian cells. *Oncogene,* 21**,** 598-610.

HENSON, J. D. & REDDEL, R. R. 2010. Assaying and investigating Alternative Lengthening of Telomeres activity in human cells and cancers. *FEBS Lett,* 584**,** 3800-11.

HERBIG, U., JOBLING, W. A., CHEN, B. P., CHEN, D. J. & SEDIVY, J. M. 2004. Telomere shortening triggers senescence of human cells through a pathway involving ATM, p53, and p21(CIP1), but not p16(INK4a). *Mol Cell,* 14**,** 501-13.

HERRERA, E., SAMPER, E., MARTIN-CABALLERO, J., FLORES, J. M., LEE, H. W. & BLASCO, M. A. 1999. Disease states associated with telomerase deficiency appear earlier in mice with short telomeres. *Embo j,* 18**,** 2950-60.

HIYAMA, K., HIRAI, Y., KYOIZUMI, S., AKIYAMA, M., HIYAMA, E., PIATYSZEK, M. A., SHAY, J. W., ISHIOKA, S. & YAMAKIDO, M. 1995. Activation of telomerase in human lymphocytes and hematopoietic progenitor cells. *J Immunol,* 155**,** 3711-5.

HOCKEMEYER, D., DANIELS, J. P., TAKAI, H. & DE LANGE, T. 2006. Recent expansion of the telomeric complex in rodents: Two distinct POT1 proteins protect mouse telomeres. *Cell,* 126**,** 63-77.

HOCKEMEYER, D., SFEIR, A. J., SHAY, J. W., WRIGHT, W. E. & DE LANGE, T. 2005. POT1 protects telomeres from a transient DNA damage response and determines how human chromosomes end. *Embo j,* 24**,** 2667-78.

HOLT, S. E., AISNER, D. L., BAUR, J., TESMER, V. M., DY, M., OUELLETTE, M., TRAGER, J. B., MORIN, G. B., TOFT, D. O., SHAY, J. W., WRIGHT, W. E. & WHITE, M. A. 1999. Functional requirement of p23 and Hsp90 in telomerase complexes. *Genes Dev,* 13**,** 817-26.

HONG, Y. & STAMBROOK, P. J. 2004. Restoration of an absent G1 arrest and protection from apoptosis in embryonic stem cells after ionizing radiation. *Proc Natl Acad Sci U S A,* 101**,** 14443-8.

HURLEY, P. J. & BUNZ, F. 2007. ATM and ATR: components of an integrated circuit. *Cell Cycle,* 6**,** 414-7.

HUYEN, Y., ZGHEIB, O., DITULLIO, R. A., JR., GORGOULIS, V. G., ZACHARATOS, P., PETTY, T. J., SHESTON, E. A., MELLERT, H. S., STAVRIDI, E. S. &

HALAZONETIS, T. D. 2004. Methylated lysine 79 of histone H3 targets 53BP1 to DNA double-strand breaks. *Nature,* 432**,** 406-11.

INDIVIGLIO, S. M. & BERTUCH, A. A. 2009. Ku's essential role in keeping telomeres intact. *Proc Natl Acad Sci U S A,* 106**,** 12217-8.

IVANKOVIC, M., CUKUSIC, A., GOTIC, I., SKROBOT, N., MATIJASIC, M., POLANCEC, D. & RUBELJ, I. 2007. Telomerase activity in HeLa cervical carcinoma cell line proliferation. *Biogerontology,* 8**,** 163-72.

IWANO, T., TACHIBANA, M., RETH, M. & SHINKAI, Y. 2004. Importance of TRF1 for functional telomere structure. *J Biol Chem,* 279**,** 1442-8.

JACO, I., MUNOZ, P., GOYTISOLO, F., WESOLY, J., BAILEY, S., TACCIOLI, G. & BLASCO, M. A. 2003. Role of mammalian Rad54 in telomere length maintenance. *Mol Cell Biol,* 23**,** 5572-80.

JIANG, Q. & GREENBERG, R. A. 2015. Deciphering the BRCA1 Tumor Suppressor Network. *J Biol Chem,* 290**,** 17724-32.

JIANG, W. Q., ZHONG, Z. H., HENSON, J. D., NEUMANN, A. A., CHANG, A. C. & REDDEL, R. R. 2005. Suppression of alternative lengthening of telomeres by Sp100-mediated sequestration of the MRE11/RAD50/NBS1 complex. *Mol Cell Biol,* 25**,** 2708-21.

JIANG, W. Q., ZHONG, Z. H., HENSON, J. D. & REDDEL, R. R. 2007. Identification of candidate alternative lengthening of telomeres genes by methionine restriction and RNA interference. *Oncogene,* 26**,** 4635-47.

JOHNSON, F. B., MARCINIAK, R. A., MCVEY, M., STEWART, S. A., HAHN, W. C. & GUARENTE, L. 2001. The Saccharomyces cerevisiae WRN homolog Sgs1p participates in telomere maintenance in cells lacking telomerase. *Embo j,* 20**,** 905-13.

KARLSEDER, J., HOKE, K., MIRZOEVA, O. K., BAKKENIST, C., KASTAN, M. B., PETRINI, J. H. & DE LANGE, T. 2004. The telomeric protein TRF2 binds the ATM kinase and can inhibit the ATM-dependent DNA damage response. *PLoS Biol,* 2**,** E240.

KARLSEDER, J., KACHATRIAN, L., TAKAI, H., MERCER, K., HINGORANI, S., JACKS, T. & DE LANGE, T. 2003. Targeted deletion reveals an essential function for the telomere length regulator Trf1. *Mol Cell Biol,* 23**,** 6533-41.

KASTAN, M. B., ONYEKWERE, O., SIDRANSKY, D., VOGELSTEIN, B. & CRAIG, R. W. 1991. Participation of p53 protein in the cellular response to DNA damage. *Cancer Res,* 51**,** 6304-11.

KIM, N. W., PIATYSZEK, M. A., PROWSE, K. R., HARLEY, C. B., WEST, M. D., HO, P. L., COVIELLO, G. M., WRIGHT, W. E., WEINRICH, S. L. & SHAY, J. W. 1994. Specific association of human telomerase activity with immortal cells and cancer. *Science,* 266**,** 2011-5.

KIM, N. W. & WU, F. 1997. Advances in quantification and characterization of telomerase activity by the telomeric repeat amplification protocol (TRAP). *Nucleic Acids Res,* 25**,** 2595-7.

KIM, S. H., BEAUSEJOUR, C., DAVALOS, A. R., KAMINKER, P., HEO, S. J. & CAMPISI, J. 2004. TIN2 mediates functions of TRF2 at human telomeres. *J Biol Chem,* 279**,** 43799-804.

KIM, S. H., KAMINKER, P. & CAMPISI, J. 1999. TIN2, a new regulator of telomere length in human cells. *Nat Genet,* 23**,** 405-12.

KING, M. C., MARKS, J. H. & MANDELL, J. B. 2003. Breast and ovarian cancer risks due to inherited mutations in BRCA1 and BRCA2. *Science,* 302**,** 643-6.

KLOBUTCHER, L. A., SWANTON, M. T., DONINI, P. & PRESCOTT, D. M. 1981. All gene-sized DNA molecules in four species of hypotrichs have the same terminal sequence and an unusual 3' terminus. *Proc Natl Acad Sci U S A,* 78**,** 3015-9.

KOMENAKA, I. K., DITKOFF, B. A., JOSEPH, K. A., RUSSO, D., GORROOCHURN, P., WARD, M., HOROWITZ, E., EL-TAMER, M. B. & SCHNABEL, F. R. 2004. The development of interval breast malignancies in patients with BRCA mutations. *Cancer,* 100**,** 2079-83.

KOTE-JARAI, Z., SALMON, A., MENGITSU, T., COPELAND, M., ARDERN-JONES, A., LOCKE, I., SHANLEY, S., SUMMERSGILL, B., LU, Y. J., SHIPLEY, J. & EELES, R. 2006. Increased level of chromosomal damage after irradiation of lymphocytes from BRCA1 mutation carriers. *Br J Cancer,* 94**,** 308-10.

LAFFERTY-WHYTE, K., CAIRNEY, C. J., WILL, M. B., SERAKINCI, N., DAIDONE, M. G., ZAFFARONI, N., BILSLAND, A. & KEITH, W. N. 2009. A gene expression signature classifying telomerase and ALT immortalization reveals an hTERT regulatory network and suggests a mesenchymal stem cell origin for ALT. *Oncogene,* 28**,** 3765-74.

LALLEMAND-BREITENBACH, V. & DE THE, H. 2010. PML nuclear bodies. *Cold Spring Harb Perspect Biol,* 2**,** a000661.

LANE, T. F., DENG, C., ELSON, A., LYU, M. S., KOZAK, C. A. & LEDER, P. 1995. Expression of Brca1 is associated with terminal differentiation of ectodermally and mesodermally derived tissues in mice. *Genes Dev,* 9**,** 2712-22.

LANS, H., MARTEIJN, J. A. & VERMEULEN, W. 2012. ATP-dependent chromatin remodeling in the DNA-damage response. *Epigenetics Chromatin,* 5**,** 4.

LARSON, J. S., TONKINSON, J. L. & LAI, M. T. 1997. A BRCA1 mutant alters G2-M cell cycle control in human mammary epithelial cells. *Cancer Res,* 57**,** 3351-5.

LAVIN, M. F. & KOZLOV, S. 2007. DNA damage-induced signalling in ataxia-telangiectasia and related syndromes. *Radiother Oncol,* 83**,** 231-7.

LEE, A. C., FERNANDEZ-CAPETILLO, O., PISUPATI, V., JACKSON, S. P. & NUSSENZWEIG, A. 2005. Specific association of mouse MDC1/NFBD1 with NBS1 at sites of DNA-damage. *Cell Cycle,* 4**,** 177-82.

LEE, J. H. & PAULL, T. T. 2007. Activation and regulation of ATM kinase activity in response to DNA double-strand breaks. *Oncogene,* 26**,** 7741-8.

LEI, M., PODELL, E. R. & CECH, T. R. 2004. Structure of human POT1 bound to telomeric single-stranded DNA provides a model for chromosome end-protection. *Nat Struct Mol Biol,* 11**,** 1223-9.

LENDVAY, T. S., MORRIS, D. K., SAH, J., BALASUBRAMANIAN, B. & LUNDBLAD, V. 1996. Senescence mutants of Saccharomyces cerevisiae with a defect in telomere replication identify three additional EST genes. *Genetics,* 144**,** 1399-412.

LI, B. & DE LANGE, T. 2003. Rap1 affects the length and heterogeneity of human telomeres. *Mol Biol Cell,* 14**,** 5060-8.

LI, B., OESTREICH, S. & DE LANGE, T. 2000. Identification of human Rap1: implications for telomere evolution. *Cell,* 101**,** 471-83.

LI, H., LEE, T. H. & AVRAHAM, H. 2002. A novel tricomplex of BRCA1, Nmi, and c-Myc inhibits c-Myc-induced human telomerase reverse transcriptase gene (hTERT) promoter activity in breast cancer. *J Biol Chem,* 277**,** 20965-73.

LI, M. & YU, X. 2013. Function of BRCA1 in the DNA damage response is mediated by ADP-ribosylation. *Cancer Cell,* 23**,** 693-704.

LI, X. & HEYER, W. D. 2008. Homologous recombination in DNA repair and DNA damage tolerance. *Cell Res,* 18**,** 99-113.

LI, Y. & TERGAONKAR, V. 2014. Noncanonical functions of telomerase: implications in telomerase-targeted cancer therapies. *Cancer Res,* 74**,** 1639-44.

LIM, D. S. & HASTY, P. 1996. A mutation in mouse rad51 results in an early embryonic lethal that is suppressed by a mutation in p53. *Mol Cell Biol,* 16**,** 7133-43.

LIN, T., CHAO, C., SAITO, S., MAZUR, S. J., MURPHY, M. E., APPELLA, E. & XU, Y. 2005. p53 induces differentiation of mouse embryonic stem cells by suppressing Nanog expression. *Nat Cell Biol,* 7**,** 165-71.

LINGNER, J. & CECH, T. R. 1996. Purification of telomerase from Euplotes aediculatus: requirement of a primer 3' overhang. *Proc Natl Acad Sci U S A,* 93**,** 10712-7.

LINGNER, J., HENDRICK, L. L. & CECH, T. R. 1994. Telomerase RNAs of different ciliates have a common secondary structure and a permuted template. *Genes Dev,* 8**,** 1984-98.

LINGNER, J., HUGHES, T. R., SHEVCHENKO, A., MANN, M., LUNDBLAD, V. & CECH, T. R. 1997. Reverse transcriptase motifs in the catalytic subunit of telomerase. *Science,* 276**,** 561-7.

LIU, C. Y., FLESKEN-NIKITIN, A., LI, S., ZENG, Y. & LEE, W. H. 1996. Inactivation of the mouse Brca1 gene leads to failure in the morphogenesis of the egg cylinder in early postimplantation development. *Genes Dev,* 10**,** 1835-43.

LOAYZA, D. & DE LANGE, T. 2003. POT1 as a terminal transducer of TRF1 telomere length control. *Nature,* 423**,** 1013-8.

LONDONO-VALLEJO, J. A., DER-SARKISSIAN, H., CAZES, L., BACCHETTI, S. & REDDEL, R. R. 2004. Alternative lengthening of telomeres is characterized by high rates of telomeric exchange. *Cancer Res,* 64**,** 2324-7.

LOU, Z., MINTER-DYKHOUSE, K., FRANCO, S., GOSTISSA, M., RIVERA, M. A., CELESTE, A., MANIS, J. P., VAN DEURSEN, J., NUSSENZWEIG, A., PAULL, T. T., ALT, F. W. & CHEN, J. 2006. MDC1 maintains genomic stability by participating in the amplification of ATM-dependent DNA damage signals. *Mol Cell,* 21**,** 187-200.

LOVEJOY, C. A., LI, W., REISENWEBER, S., THONGTHIP, S., BRUNO, J., DE LANGE, T., DE, S., PETRINI, J. H., SUNG, P. A., JASIN, M., ROSENBLUH, J., ZWANG, Y., WEIR, B. A., HATTON, C., IVANOVA, E., MACCONAILL, L., HANNA, M., HAHN, W. C., LUE, N. F., REDDEL, R. R., JIAO, Y., KINZLER, K., VOGELSTEIN, B., PAPADOPOULOS, N. & MEEKER, A. K. 2012. Loss of ATRX, genome instability, and an altered DNA damage response are hallmarks of the alternative lengthening of telomeres pathway. *PLoS Genet,* 8**,** e1002772.

LUDWIG, T., CHAPMAN, D. L., PAPAIOANNOU, V. E. & EFSTRATIADIS, A. 1997. Targeted mutations of breast cancer susceptibility gene homologs in mice: lethal phenotypes of Brca1, Brca2, Brca1/Brca2, Brca1/p53, and Brca2/p53 nullizygous embryos. *Genes Dev,* 11**,** 1226-41.

LY, H., XU, L., RIVERA, M. A., PARSLOW, T. G. & BLACKBURN, E. H. 2003. A role for a novel 'trans-pseudoknot' RNA-RNA interaction in the functional dimerization of human telomerase. *Genes Dev,* 17**,** 1078-83.

MAK, T. W., HAKEM, A., MCPHERSON, J. P., SHEHABELDIN, A., ZABLOCKI, E., MIGON, E., DUNCAN, G. S., BOUCHARD, D., WAKEHAM, A., CHEUNG, A., KARASKOVA, J., SAROSI, I., SQUIRE, J., MARTH, J. & HAKEM, R. 2000. Brca1 required for T cell lineage development but not TCR loci rearrangement. *Nat Immunol,* 1**,** 77-82.

MAKAROV, V. L., HIROSE, Y. & LANGMORE, J. P. 1997. Long G tails at both ends of human chromosomes suggest a C strand degradation mechanism for telomere shortening. *Cell,* 88**,** 657-66.

MAKAROV, V. L., LEJNINE, S., BEDOYAN, J. & LANGMORE, J. P. 1993. Nucleosomal organization of telomere-specific chromatin in rat. *Cell,* 73**,** 775-87.

MALASHICHEVA, A. B., KISLIAKOVA, T. V., SAVATIER, P. & POSPELOV, V. A. 2002. [Embryonal stem cells do not undergo cell cycle arrest upon exposure to damaging factors]. *Tsitologiia,* 44**,** 643-8.

MALASHICHEVA, A. B., KISLYAKOVA, T. V., AKSENOV, N. D., OSIPOV, K. A. & POSPELOV, V. A. 2000. F9 embryonal carcinoma cells fail to stop at G1/S boundary of the cell cycle after gamma-irradiation due to p21WAF1/CIP1 degradation. *Oncogene,* 19**,** 3858-65.

MAO, Z., BOZZELLA, M., SELUANOV, A. & GORBUNOVA, V. 2008. DNA repair by nonhomologous end joining and homologous recombination during cell cycle in human cells. *Cell Cycle,* 7**,** 2902-6.

MARI, P. O., FLOREA, B. I., PERSENGIEV, S. P., VERKAIK, N. S., BRUGGENWIRTH, H. T., MODESTI, M., GIGLIA-MARI, G., BEZSTAROSTI, K., DEMMERS, J. A., LUIDER, T. M., HOUTSMULLER, A. B. & VAN GENT, D. C. 2006. Dynamic assembly of end-joining complexes requires interaction between Ku70/80 and XRCC4. *Proc Natl Acad Sci U S A,* 103**,** 18597-602.

MARQUIS, S. T., RAJAN, J. V., WYNSHAW-BORIS, A., XU, J., YIN, G. Y., ABEL, K. J., WEBER, B. L. & CHODOSH, L. A. 1995. The developmental pattern of Brca1

expression implies a role in differentiation of the breast and other tissues. *Nat Genet,* 11**,** 17-26.

MARTINS, F. C., DE, S., ALMENDRO, V., GONEN, M., PARK, S. Y., BLUM, J. L., HERLIHY, W., ETHINGTON, G., SCHNITT, S. J., TUNG, N., GARBER, J. E., FETTEN, K., MICHOR, F. & POLYAK, K. 2012. Evolutionary pathways in BRCA1-associated breast tumors. *Cancer Discov,* 2**,** 503-11.

MASER, R. S. & DEPINHO, R. A. 2002. Keeping telomerase in its place. *Nat Med.* United States.

MCGINTY, R. K., HENRICI, R. C. & TAN, S. 2014. Crystal structure of the PRC1 ubiquitylation module bound to the nucleosome. *Nature,* 514**,** 591-6.

MCILRATH, J., BOUFFLER, S. D., SAMPER, E., CUTHBERT, A., WOJCIK, A., SZUMIEL, I., BRYANT, P. E., RICHES, A. C., THOMPSON, A., BLASCO, M. A., NEWBOLD, R. F. & SLIJEPCEVIC, P. 2001. Telomere length abnormalities in mammalian radiosensitive cells. *Cancer Res,* 61**,** 912-5.

MCPHERSON, J. P., HANDE, M. P., POONEPALLI, A., LEMMERS, B., ZABLOCKI, E., MIGON, E., SHEHABELDIN, A., PORRAS, A., KARASKOVA, J., VUKOVIC, B., SQUIRE, J. & HAKEM, R. 2006. A role for Brca1 in chromosome end maintenance. *Hum Mol Genet,* 15**,** 831-8.

MCPHERSON, J. P., LEMMERS, B., HIRAO, A., HAKEM, A., ABRAHAM, J., MIGON, E., MATYSIAK-ZABLOCKI, E., TAMBLYN, L., SANCHEZ-SWEATMAN, O., KHOKHA, R., SQUIRE, J., HANDE, M. P., MAK, T. W. & HAKEM, R. 2004. Collaboration of Brca1 and Chk2 in tumorigenesis. *Genes Dev,* 18**,** 1144-53.

MEEKER, A. K. & DE MARZO, A. M. 2004. Recent advances in telomere biology: implications for human cancer. *Curr Opin Oncol,* 16**,** 32-8.

MEREL, P., PRIEUR, A., PFEIFFER, P. & DELATTRE, O. 2002. Absence of major defects in non-homologous DNA end joining in human breast cancer cell lines. *Oncogene,* 21**,** 5654-9.

MEYERSON, M., COUNTER, C. M., EATON, E. N., ELLISEN, L. W., STEINER, P., CADDLE, S. D., ZIAUGRA, L., BEIJERSBERGEN, R. L., DAVIDOFF, M. J., LIU, Q., BACCHETTI, S., HABER, D. A. & WEINBERG, R. A. 1997. hEST2, the putative human telomerase catalytic subunit gene, is up-regulated in tumor cells and during immortalization. *Cell,* 90**,** 785-95.

MEYNE, J., RATLIFF, R. L. & MOYZIS, R. K. 1989. Conservation of the human telomere sequence (TTAGGG)n among vertebrates. *Proc Natl Acad Sci U S A,* 86**,** 7049-53.

MIKI, Y., SWENSEN, J., SHATTUCK-EIDENS, D., FUTREAL, P. A., HARSHMAN, K., TAVTIGIAN, S., LIU, Q., COCHRAN, C., BENNETT, L. M., DING, W. & ET AL. 1994. A strong candidate for the breast and ovarian cancer susceptibility gene BRCA1. *Science,* 266**,** 66-71.

MONTEIRO, A. N., AUGUST, A. & HANAFUSA, H. 1996. Evidence for a transcriptional activation function of BRCA1 C-terminal region. *Proc Natl Acad Sci U S A,* 93**,** 13595-9.

MORRISON, C., SONODA, E., TAKAO, N., SHINOHARA, A., YAMAMOTO, K. & TAKEDA, S. 2000. The controlling role of ATM in homologous recombinational repair of DNA damage. *Embo j,* 19**,** 463-71.

MOTEVALLI, A., YASAEI, H., VIRMOUNI, S. A., SLIJEPCEVIC, P. & ROBERTS, T. 2014. The effect of chemotherapeutic agents on telomere length maintenance in breast cancer cell lines. *Breast Cancer Res Treat.*

MOYNAHAN, M. E., CHIU, J. W., KOLLER, B. H. & JASIN, M. 1999. Brca1 controls homology-directed DNA repair. *Mol Cell,* 4**,** 511-8.

MOYNAHAN, M. E., CUI, T. Y. & JASIN, M. 2001. Homology-directed dna repair, mitomycin-c resistance, and chromosome stability is restored with correction of a Brca1 mutation. *Cancer Res,* 61**,** 4842-50.

MOYZIS, R. K., BUCKINGHAM, J. M., CRAM, L. S., DANI, M., DEAVEN, L. L., JONES, M. D., MEYNE, J., RATLIFF, R. L. & WU, J. R. 1988. A highly conserved repetitive DNA

sequence, (TTAGGG)n, present at the telomeres of human chromosomes. *Proc Natl Acad Sci U S A,* 85**,** 6622-6.

MUNTONI, A., NEUMANN, A. A., HILLS, M. & REDDEL, R. R. 2009. Telomere elongation involves intra-molecular DNA replication in cells utilizing alternative lengthening of telomeres. *Hum Mol Genet,* 18**,** 1017-27.

MURNANE, J. P., SABATIER, L., MARDER, B. A. & MORGAN, W. F. 1994. Telomere dynamics in an immortal human cell line. *Embo j,* 13**,** 4953-62.

MUSOLINO, A., BELLA, M. A., BORTESI, B., MICHIARA, M., NALDI, N., ZANELLI, P., CAPELLETTI, M., PEZZUOLO, D., CAMISA, R., SAVI, M., NERI, T. M. & ARDIZZONI, A. 2007. BRCA mutations, molecular markers, and clinical variables in early-onset breast cancer: a population-based study. *Breast,* 16**,** 280-92.

NABETANI, A. & ISHIKAWA, F. 2009. Unusual telomeric DNAs in human telomerase-negative immortalized cells. *Mol Cell Biol,* 29**,** 703-13.

NAKA, K., IKEDA, K. & MOTOYAMA, N. 2002. Recruitment of NBS1 into PML oncogenic domains via interaction with SP100 protein. *Biochem Biophys Res Commun,* 299**,** 863-71.

NAKAMURA, T. M. & CECH, T. R. 1998. Reversing time: origin of telomerase. *Cell,* 92**,** 587-90.

NAKAYAMA, J., TAHARA, H., TAHARA, E., SAITO, M., ITO, K., NAKAMURA, H., NAKANISHI, T., IDE, T. & ISHIKAWA, F. 1998. Telomerase activation by hTRT in human normal fibroblasts and hepatocellular carcinomas. *Nat Genet,* 18**,** 65-8.

NAROD, S. A. & FOULKES, W. D. 2004. BRCA1 and BRCA2: 1994 and beyond. *Nat Rev Cancer,* 4**,** 665-76.

NASIR, L., DEVLIN, P., MCKEVITT, T., RUTTEMAN, G. & ARGYLE, D. J. 2001. Telomere lengths and telomerase activity in dog tissues: a potential model system to study human telomere and telomerase biology. *Neoplasia,* 3**,** 351-9.

NEUMANN, A. A. & REDDEL, R. R. 2002. Telomere maintenance and cancer -- look, no telomerase. *Nat Rev Cancer,* 2**,** 879-84.

NEUMANN, A. A., WATSON, C. M., NOBLE, J. R., PICKETT, H. A., TAM, P. P. & REDDEL, R. R. 2013. Alternative lengthening of telomeres in normal mammalian somatic cells. *Genes Dev,* 27**,** 18-23.

NEWBOLD, R. F. 2002. The significance of telomerase activation and cellular immortalization in human cancer. *Mutagenesis,* 17**,** 539-50.

NIEUWENHUIS, B., VAN ASSEN-BOLT, A. J., VAN WAARDE-VERHAGEN, M. A., SIJMONS, R. H., VAN DER HOUT, A. H., BAUCH, T., STREFFER, C. & KAMPINGA, H. H. 2002. BRCA1 and BRCA2 heterozygosity and repair of X-ray-induced DNA damage. *Int J Radiat Biol,* 78**,** 285-95.

O'CONNELL, M. J. & CIMPRICH, K. A. 2005. G2 damage checkpoints: what is the turn-on? *J Cell Sci,* 118**,** 1-6.

O'CONNOR, M. S., SAFARI, A., XIN, H., LIU, D. & SONGYANG, Z. 2006. A critical role for TPP1 and TIN2 interaction in high-order telomeric complex assembly. *Proc Natl Acad Sci U S A,* 103**,** 11874-9.

O'DRISCOLL, M. & JEGGO, P. A. 2006. The role of double-strand break repair - insights from human genetics. *Nat Rev Genet,* 7**,** 45-54.

OGINO, H., NAKABAYASHI, K., SUZUKI, M., TAKAHASHI, E., FUJII, M., SUZUKI, T. & AYUSAWA, D. 1998. Release of telomeric DNA from chromosomes in immortal human cells lacking telomerase activity. *Biochem Biophys Res Commun,* 248**,** 223-7.

OHTA, T., SATO, K. & WU, W. 2011. The BRCA1 ubiquitin ligase and homologous recombination repair. *FEBS Lett,* 585**,** 2836-44.

OKA, Y., SHIOTA, S., NAKAI, S., NISHIDA, Y. & OKUBO, S. 1980. Inverted terminal repeat sequence in the macronuclear DNA of Stylonychia pustulata. *Gene,* 10**,** 301-6.

OKAZAKI, R., OKAZAKI, T., SAKABE, K. & SUGIMOTO, K. 1967. Mechanism of DNA replication possible discontinuity of DNA chain growth. *Jpn J Med Sci Biol,* 20**,** 255-60.

OLOVNIKOV, A. M. 1971. Principle of marginotomy in template synthesis of polynucleotides. *Dokl Akad Nauk SSSR,* 201**,** 1496-9.

OLOVNIKOV, A. M. 1973. A theory of marginotomy. The incomplete copying of template margin in enzymic synthesis of polynucleotides and biological significance of the phenomenon. *J Theor Biol,* 41**,** 181-90.

OPITZ, O. G., SULIMAN, Y., HAHN, W. C., HARADA, H., BLUM, H. E. & RUSTGI, A. K. 2001. Cyclin D1 overexpression and p53 inactivation immortalize primary oral keratinocytes by a telomerase-independent mechanism. *J Clin Invest,* 108**,** 725-32.

OPRESKO, P. L., OTTERLEI, M., GRAAKJAER, J., BRUHEIM, P., DAWUT, L., KOLVRAA, S., MAY, A., SEIDMAN, M. M. & BOHR, V. A. 2004. The Werner syndrome helicase and exonuclease cooperate to resolve telomeric D loops in a manner regulated by TRF1 and TRF2. *Mol Cell,* 14**,** 763-74.

OPRESKO, P. L., VON KOBBE, C., LAINE, J. P., HARRIGAN, J., HICKSON, I. D. & BOHR, V. A. 2002. Telomere-binding protein TRF2 binds to and stimulates the Werner and Bloom syndrome helicases. *J Biol Chem,* 277**,** 41110-9.

OSTERWALD, S., DEEG, K. I., CHUNG, I., PARISOTTO, D., WORZ, S., ROHR, K., ERFLE, H. & RIPPE, K. 2015. PML induces compaction, TRF2 depletion and DNA damage signaling at telomeres and promotes their alternative lengthening. *J Cell Sci,* 128**,** 1887-900.

PALM, W. & DE LANGE, T. 2008. How shelterin protects mammalian telomeres. *Annu Rev Genet,* 42**,** 301-34.

PEARSON, M., CARBONE, R., SEBASTIANI, C., CIOCE, M., FAGIOLI, M., SAITO, S., HIGASHIMOTO, Y., APPELLA, E., MINUCCI, S., PANDOLFI, P. P. & PELICCI, P. G. 2000. PML regulates p53 acetylation and premature senescence induced by oncogenic Ras. *Nature,* 406**,** 207-10.

PELLEGRINI, L., YU, D. S., LO, T., ANAND, S., LEE, M., BLUNDELL, T. L. & VENKITARAMAN, A. R. 2002. Insights into DNA recombination from the structure of a RAD51-BRCA2 complex. *Nature,* 420**,** 287-93.

PENDINO, F., TARKANYI, I., DUDOGNON, C., HILLION, J., LANOTTE, M., ARADI, J. & SEGAL-BENDIRDJIAN, E. 2006. Telomeres and telomerase: Pharmacological targets for new anticancer strategies? *Curr Cancer Drug Targets,* 6**,** 147-80.

PERREM, K., COLGIN, L. M., NEUMANN, A. A., YEAGER, T. R. & REDDEL, R. R. 2001. Coexistence of alternative lengthening of telomeres and telomerase in hTERT-transfected GM847 cells. *Mol Cell Biol,* 21**,** 3862-75.

PETRUCELLI, N., DALY, M. B. & FELDMAN, G. L. 2013. BRCA1 and BRCA2 Hereditary Breast and Ovarian Cancer.

PHAN, A. T., KURYAVYI, V., LUU, K. N. & PATEL, D. J. 2007. Structure of two intramolecular G-quadruplexes formed by natural human telomere sequences in K+ solution. *Nucleic Acids Res,* 35**,** 6517-25.

POWELL, S. N. & KACHNIC, L. A. 2003. Roles of BRCA1 and BRCA2 in homologous recombination, DNA replication fidelity and the cellular response to ionizing radiation. *Oncogene,* 22**,** 5784-91.

PROST, S., BELLAMY, C. O., CLARKE, A. R., WYLLIE, A. H. & HARRISON, D. J. 1998. p53-independent DNA repair and cell cycle arrest in embryonic stem cells. *FEBS Lett,* 425**,** 499-504.

RAI, R., ZHENG, H., HE, H., LUO, Y., MULTANI, A., CARPENTER, P. B. & CHANG, S. 2010. The function of classical and alternative non-homologous end-joining pathways in the fusion of dysfunctional telomeres. *Embo j,* 29**,** 2598-610.

RANGARAJAN, A. & WEINBERG, R. A. 2003. Comparative biology of mouse versus human cells: modelling human cancer in mice. *Nature Reviews Cancer,* 3**,** 952-959.

REDDEL, R. R., BRYAN, T. M. & MURNANE, J. P. 1997. Immortalized cells with no detectable telomerase activity. A review. *Biochemistry (Mosc),* 62**,** 1254-62.

RIHA, K., HEACOCK, M. L. & SHIPPEN, D. E. 2006. The role of the nonhomologous end-joining DNA double-strand break repair pathway in telomere biology. *Annu Rev Genet,* 40**,** 237-77.

RIOU, J. F., GUITTAT, L., MAILLIET, P., LAOUI, A., RENOU, E., PETITGENET, O., MEGNIN-CHANET, F., HELENE, C. & MERGNY, J. L. 2002. Cell senescence and telomere shortening induced by a new series of specific G-quadruplex DNA ligands. *Proc Natl Acad Sci U S A,* 99**,** 2672-7.

ROMERO, D. P. & BLACKBURN, E. H. 1991. A conserved secondary structure for telomerase RNA. *Cell,* 67**,** 343-53.

ROSEN, E. M. 2013. BRCA1 in the DNA damage response and at telomeres. *Front Genet,* 4**,** 85.

ROSEN, E. M., FAN, S. & MA, Y. 2006. BRCA1 regulation of transcription. *Cancer Lett,* 236**,** 175-85.

ROY, R., CHUN, J. & POWELL, S. N. 2011. BRCA1 and BRCA2: different roles in a common pathway of genome protection. *Nature Reviews Cancer,* 12**,** 68-78.

ROY, S., CHOUDHURY, S. R., SENGUPTA, D. N. & DAS, K. P. 2013. Involvement of AtPollambda in the repair of high salt- and DNA cross-linking agent-induced double strand breaks in Arabidopsis. *Plant Physiol,* 162**,** 1195-210.

RUFFNER, H., JOAZEIRO, C. A., HEMMATI, D., HUNTER, T. & VERMA, I. M. 2001. Cancer-predisposing mutations within the RING domain of BRCA1: loss of ubiquitin protein ligase activity and protection from radiation hypersensitivity. *Proc Natl Acad Sci U S A,* 98**,** 5134-9.

RUFFNER, H. & VERMA, I. M. 1997. BRCA1 is a cell cycle-regulated nuclear phosphoprotein. *Proc Natl Acad Sci U S A,* 94**,** 7138-43.

RUIS, B. L., FATTAH, K. R. & HENDRICKSON, E. A. 2008. The catalytic subunit of DNA-dependent protein kinase regulates proliferation, telomere length, and genomic stability in human somatic cells. *Mol Cell Biol,* 28**,** 6182-95.

SALOMONI, P. & PANDOLFI, P. P. 2002. The role of PML in tumor suppression. *Cell,* 108**,** 165-70.

SANCAR, A., LINDSEY-BOLTZ, L. A., UNSAL-KACMAZ, K. & LINN, S. 2004. Molecular mechanisms of mammalian DNA repair and the DNA damage checkpoints. *Annu Rev Biochem,* 73**,** 39-85.

SARETZKI, G., ARMSTRONG, L., LEAKE, A., LAKO, M. & VON ZGLINICKI, T. 2004. Stress defense in murine embryonic stem cells is superior to that of various differentiated murine cells. *Stem Cells,* 22**,** 962-71.

SARTORI, A. A., LUKAS, C., COATES, J., MISTRIK, M., FU, S., BARTEK, J., BAER, R., LUKAS, J. & JACKSON, S. P. 2007. Human CtIP promotes DNA end resection. *Nature,* 450**,** 509-14.

SCHRATT, G., WEINHOLD, B., LUNDBERG, A. S., SCHUCK, S., BERGER, J., SCHWARZ, H., WEINBERG, R. A., RUTHER, U. & NORDHEIM, A. 2001. Serum response factor is required for immediate-early gene activation yet is dispensable for proliferation of embryonic stem cells. *Mol Cell Biol,* 21**,** 2933-43.

SCULLY, R., CHEN, J., OCHS, R. L., KEEGAN, K., HOEKSTRA, M., FEUNTEUN, J. & LIVINGSTON, D. M. 1997. Dynamic changes of BRCA1 subnuclear location and phosphorylation state are initiated by DNA damage. *Cell,* 90**,** 425-35.

SCULLY, R., GANESAN, S., VLASAKOVA, K., CHEN, J., SOCOLOVSKY, M. & LIVINGSTON, D. M. 1999. Genetic analysis of BRCA1 function in a defined tumor cell line. *Mol Cell,* 4**,** 1093-9.

SEDIC, M., SKIBINSKI, A., BROWN, N., GALLARDO, M., MULLIGAN, P., MARTINEZ, P., KELLER, P. J., GLOVER, E., RICHARDSON, A. L., COWAN, J., TOLAND, A. E., RAVICHANDRAN, K., RIETHMAN, H., NABER, S. P., NAAR, A. M., BLASCO, M. A., HINDS, P. W. & KUPERWASSER, C. 2015. Haploinsufficiency for BRCA1 leads to cell-type-specific genomic instability and premature senescence. *Nat Commun,* 6**,** 7505.

SFEIR, A. & DE LANGE, T. 2012. Removal of shelterin reveals the telomere end-protection problem. *Science,* 336**,** 593-7.

SFEIR, A., KABIR, S., VAN OVERBEEK, M., CELLI, G. B. & DE LANGE, T. 2010. Loss of Rap1 induces telomere recombination in absence of NHEJ or a DNA damage signal. *Science,* 327**,** 1657-61.

SHARAN, S. K., MORIMATSU, M., ALBRECHT, U., LIM, D. S., REGEL, E., DINH, C., SANDS, A., EICHELE, G., HASTY, P. & BRADLEY, A. 1997. Embryonic lethality and radiation hypersensitivity mediated by Rad51 in mice lacking Brca2.

SHARAN, S. K., WIMS, M. & BRADLEY, A. 1995. Murine Brca1: sequence and significance for human missense mutations. *Hum Mol Genet,* 4**,** 2275-8.

SHAY, J. W. & WRIGHT, W. E. 2005. Senescence and immortalization: role of telomeres and telomerase. *Carcinogenesis,* 26**,** 867-74.

SHAY, J. W., ZOU, Y., HIYAMA, E. & WRIGHT, W. E. 2001. Telomerase and cancer. *Hum Mol Genet,* 10**,** 677-85.

SHEN, S. X., WEAVER, Z., XU, X., LI, C., WEINSTEIN, M., CHEN, L., GUAN, X. Y., RIED, T. & DENG, C. X. 1998. A targeted disruption of the murine Brca1 gene causes gamma-irradiation hypersensitivity and genetic instability. *Oncogene,* 17**,** 3115-24.

SHIH, I. M., ZHOU, W., GOODMAN, S. N., LENGAUER, C., KINZLER, K. W. & VOGELSTEIN, B. 2001. Evidence that genetic instability occurs at an early stage of colorectal tumorigenesis. *Cancer Res,* 61**,** 818-22.

SHILOH, Y. 2003. ATM and related protein kinases: safeguarding genome integrity. *Nat Rev Cancer,* 3**,** 155-68.

SHILOH, Y. 2006. The ATM-mediated DNA-damage response: taking shape. *Trends Biochem Sci,* 31**,** 402-10.

SLAVOTINEK, A., MCMILLAN, T. J. & STEEL, C. M. 1993. A comparison of micronucleus frequency and radiation survival in lymphoblastoid cell lines. *Mutagenesis,* 8**,** 569-75.

SLIJEPCEVIC, P. 2006. The role of DNA damage response proteins at telomeres--an "integrative" model. *DNA Repair (Amst),* 5**,** 1299-306.

SMIH, F., ROUET, P., ROMANIENKO, P. J. & JASIN, M. 1995. Double-strand breaks at the target locus stimulate gene targeting in embryonic stem cells. *Nucleic Acids Res,* 23**,** 5012-9.

SMOGORZEWSKA, A., KARLSEDER, J., HOLTGREVE-GREZ, H., JAUCH, A. & DE LANGE, T. 2002. DNA ligase IV-dependent NHEJ of deprotected mammalian telomeres in G1 and G2. *Curr Biol,* 12**,** 1635-44.

SMOGORZEWSKA, A., VAN STEENSEL, B., BIANCHI, A., OELMANN, S., SCHAEFER, M. R., SCHNAPP, G. & DE LANGE, T. 2000. Control of human telomere length by TRF1 and TRF2. *Mol Cell Biol,* 20**,** 1659-68.

SNOUWAERT, J. N., GOWEN, L. C., LATOUR, A. M., MOHN, A. R., XIAO, A., DIBIASE, L. & KOLLER, B. H. 1999. BRCA1 deficient embryonic stem cells display a decreased homologous recombination frequency and an increased frequency of non-homologous recombination that is corrected by expression of a brca1 transgene. *Oncogene,* 18**,** 7900-7.

SPYCHER, C., MILLER, E. S., TOWNSEND, K., PAVIC, L., MORRICE, N. A., JANSCAK, P., STEWART, G. S. & STUCKI, M. 2008. Constitutive phosphorylation of MDC1 physically links the MRE11-RAD50-NBS1 complex to damaged chromatin. *J Cell Biol,* 181**,** 227-40.

STAMBROOK, P. J. 2007. An ageing question: do embryonic stem cells protect their genomes? *Mech Ageing Dev,* 128**,** 31-5.

STAVROPOULOS, D. J., BRADSHAW, P. S., LI, X., PASIC, I., TRUONG, K., IKURA, M., UNGRIN, M. & MEYN, M. S. 2002. The Bloom syndrome helicase BLM interacts with TRF2 in ALT cells and promotes telomeric DNA synthesis. *Hum Mol Genet,* 11**,** 3135-44.

STEAD, E., WHITE, J., FAAST, R., CONN, S., GOLDSTONE, S., RATHJEN, J., DHINGRA, U., RATHJEN, P., WALKER, D. & DALTON, S. 2002. Pluripotent cell division cycles are driven by ectopic Cdk2, cyclin A/E and E2F activities. *Oncogene,* 21**,** 8320-33.

STEWART, G. S., WANG, B., BIGNELL, C. R., TAYLOR, A. M. & ELLEDGE, S. J. 2003. MDC1 is a mediator of the mammalian DNA damage checkpoint. *Nature,* 421**,** 961-6.

STOPPER, H. & LUTZ, W. K. 2002. Induction of micronuclei in human cell lines and primary cells by combination treatment with gamma-radiation and ethyl methanesulfonate. *Mutagenesis,* 17**,** 177-81.

STRUEWING, J. P., BRODY, L. C., ERDOS, M. R., KASE, R. G., GIAMBARRESI, T. R., SMITH, S. A., COLLINS, F. S. & TUCKER, M. A. 1995. Detection of eight BRCA1 mutations in 10 breast/ovarian cancer families, including 1 family with male breast cancer. *Am J Hum Genet,* 57**,** 1-7.

SUN, H., KAROW, J. K., HICKSON, I. D. & MAIZELS, N. 1998. The Bloom's syndrome helicase unwinds G4 DNA. *J Biol Chem,* 273**,** 27587-92.

TAKAI, H., SMOGORZEWSKA, A. & DE LANGE, T. 2003. DNA damage foci at dysfunctional telomeres. *Curr Biol,* 13**,** 1549-56.

TAKATA, M., SASAKI, M. S., SONODA, E., MORRISON, C., HASHIMOTO, M., UTSUMI, H., YAMAGUCHI‐IWAI, Y., SHINOHARA, A. & TAKEDA, S. 1998. Homologous recombination and non‐homologous end‐joining pathways of DNA double‐strand break repair have overlapping roles in the maintenance of chromosomal integrity in vertebrate cells.

TARSOUNAS, M., DAVIES, A. A. & WEST, S. C. 2004a. RAD51 localization and activation following DNA damage. *Philos Trans R Soc Lond B Biol Sci,* 359**,** 87-93.

TARSOUNAS, M., MUNOZ, P., CLAAS, A., SMIRALDO, P. G., PITTMAN, D. L., BLASCO, M. A. & WEST, S. C. 2004b. Telomere maintenance requires the RAD51D recombination/repair protein. *Cell,* 117**,** 337-47.

TEMIME-SMAALI, N., GUITTAT, L., WENNER, T., BAYART, E., DOUARRE, C., GOMEZ, D., GIRAUD-PANIS, M. J., LONDONO-VALLEJO, A., GILSON, E., AMOR-GUERET, M. & RIOU, J. F. 2008. Topoisomerase IIIalpha is required for normal proliferation and telomere stability in alternative lengthening of telomeres. *Embo j,* 27**,** 1513-24.

TERZOUDI, G. I., HATZI, V. I., BARSZCZEWSKA, K., MANOLA, K. N., STAVROPOULOU, C., ANGELAKIS, P. & PANTELIAS, G. E. 2009. G2-checkpoint abrogation in irradiated lymphocytes: A new cytogenetic approach to assess individual radiosensitivity and predisposition to cancer. *Int J Oncol,* 35**,** 1223-30.

TICHY, E. D. & STAMBROOK, P. J. 2008. DNA repair in murine embryonic stem cells and differentiated cells. *Exp Cell Res,* 314**,** 1929-36.

TILMAN, G., LORIOT, A., BENEDEN, A. V., ARNOULT, N., LONDOÑO-VALLEJO, J. A., SMET, C. D. & DECOTTIGNIES, A. 2009. Subtelomeric DNA hypomethylation is not required for telomeric sister chromatid exchanges in ALT cells. *Oncogene,* 28**,** 1682-1693.

TIRKKONEN, M., JOHANNSSON, O., AGNARSSON, B. A., OLSSON, H., INGVARSSON, S., KARHU, R., TANNER, M., ISOLA, J., BARKARDOTTIR, R. B., BORG, A. & KALLIONIEMI, O. P. 1997. Distinct somatic genetic changes associated with tumor progression in carriers of BRCA1 and BRCA2 germ-line mutations. *Cancer Res,* 57**,** 1222-7.

TLSTY, T. D. 2011. A twist of cell fate. *Cell Stem Cell,* 8**,** 126-7.

TOKUTAKE, Y., MATSUMOTO, T., WATANABE, T., MAEDA, S., TAHARA, H., SAKAMOTO, S., NIIDA, H., SUGIMOTO, M., IDE, T. & FURUICHI, Y. 1998. Extra-chromosomal telomere repeat DNA in telomerase-negative immortalized cell lines. *Biochem Biophys Res Commun,* 247**,** 765-72.

TOMLINSON, G. E., CHEN, T. T., STASTNY, V. A., VIRMANI, A. K., SPILLMAN, M. A., TONK, V., BLUM, J. L., SCHNEIDER, N. R., WISTUBA, II, SHAY, J. W., MINNA, J. D. & GAZDAR, A. F. 1998. Characterization of a breast cancer cell line derived from a germ-line BRCA1 mutation carrier. *Cancer Res,* 58**,** 3237-42.

TRENZ, K., ROTHFUSS, A., SCHUTZ, P. & SPEIT, G. 2002. Mutagen sensitivity of peripheral blood from women carrying a BRCA1 or BRCA2 mutation. *Mutat Res,* 500**,** 89-96.

TSUZUKI, T., FUJII, Y., SAKUMI, K., TOMINAGA, Y., NAKAO, K., SEKIGUCHI, M., MATSUSHIRO, A., YOSHIMURA, Y. & MORITAT 1996. Targeted disruption of the Rad51 gene leads to lethality in embryonic mice.

TULCHIN, N., ORNSTEIN, L., DIKMAN, S., STRAUCHEN, J., JAFFER, S., NAGI, C., BLEIWEISS, I., KORNREICH, R., EDELMANN, L., BROWN, K., BODIAN, C., NAIR, V. D., CHAMBON, M., WOODS, N. T. & MONTEIRO, A. N. 2013. Localization of BRCA1 protein in breast cancer tissue and cell lines with mutations. *Cancer Cell Int,* 13**,** 70.

TURINETTO, V., ORLANDO, L., SANCHEZ-RIPOLL, Y., KUMPFMUELLER, B., STORM, M. P., PORCEDDA, P., MINIERI, V., SAVIOZZI, S., ACCOMASSO, L., CIBRARIO ROCCHIETTI, E., MOORWOOD, K., CIRCOSTA, P., CIGNETTI, A., WELHAM, M. J. & GIACHINO, C. 2012. High basal gammaH2AX levels sustain self-renewal of mouse embryonic and induced pluripotent stem cells. *Stem Cells,* 30**,** 1414-23.

VALERIE, K. & POVIRK, L. F. 2003. Regulation and mechanisms of mammalian double-strand break repair. *Oncogene,* 22**,** 5792-5812.

VAN SLOUN, P. P., JANSEN, J. G., WEEDA, G., MULLENDERS, L. H., VAN ZEELAND, A. A., LOHMAN, P. H. & VRIELING, H. 1999. The role of nucleotide excision repair in protecting embryonic stem cells from genotoxic effects of UV-induced DNA damage. *Nucleic Acids Res,* 27**,** 3276-82.

VAN STEENSEL, B., SMOGORZEWSKA, A. & DE LANGE, T. 1998. TRF2 protects human telomeres from end-to-end fusions. *Cell,* 92**,** 401-13.

VERA, E., CANELA, A., FRAGA, M. F., ESTELLER, M. & BLASCO, M. A. 2008. Epigenetic regulation of telomeres in human cancer. *Oncogene,* 27**,** 6817-33.

VERDUN, R. E. & KARLSEDER, J. 2007. Replication and protection of telomeres. *Nature,* 447**,** 924-31.

VOGELSTEIN, B., LANE, D. & LEVINE, A. J. 2000. Surfing the p53 network. *Nature,* 408**,** 307-10.

VONDERHEIDE, R. H., HAHN, W. C., SCHULTZE, J. L. & NADLER, L. M. 1999. The Telomerase Catalytic Subunit Is a Widely Expressed Tumor-Associated Antigen Recognized by Cytotoxic T Lymphocytes. *Immunity,* 10**,** 673-679.

WALKER, J. R., CORPINA, R. A. & GOLDBERG, J. 2001. Structure of the Ku heterodimer bound to DNA and its implications for double-strand break repair. *Nature,* 412**,** 607-14.

WANG, C., JURK, D., MADDICK, M., NELSON, G., MARTIN-RUIZ, C. & VON ZGLINICKI, T. 2009. DNA damage response and cellular senescence in tissues of aging mice. *Aging Cell,* 8**,** 311-23.

WANG, H., WANG, M., BOCKER, W. & ILIAKIS, G. 2005. Complex H2AX phosphorylation patterns by multiple kinases including ATM and DNA-PK in human cells exposed to ionizing radiation and treated with kinase inhibitors. *J Cell Physiol,* 202**,** 492-502.

WANG, H., ZENG, Z. C., BUI, T. A., DIBIASE, S. J., QIN, W., XIA, F., POWELL, S. N. & ILIAKIS, G. 2001. Nonhomologous end-joining of ionizing radiation-induced DNA double-stranded breaks in human tumor cells deficient in BRCA1 or BRCA2. *Cancer Res,* 61**,** 270-7.

WANG, Q., ZHANG, H., KAJINO, K. & GREENE, M. I. 1998. BRCA1 binds c-Myc and inhibits its transcriptional and transforming activity in cells. *Oncogene,* 17**,** 1939-48.

WANG, R. C., SMOGORZEWSKA, A. & DE LANGE, T. 2004. Homologous recombination generates T-loop-sized deletions at human telomeres. *Cell,* 119**,** 355-68.

WANG, X., LIU, L., MONTAGNA, C., RIED, T. & DENG, C. X. 2007. Haploinsufficiency of Parp1 accelerates Brca1-associated centrosome amplification, telomere shortening, genetic instability, apoptosis, and embryonic lethality. *Cell Death Differ,* 14**,** 924-31.

WANG, Y., CORTEZ, D., YAZDI, P., NEFF, N., ELLEDGE, S. J. & QIN, J. 2000. BASC, a super complex of BRCA1-associated proteins involved in the recognition and repair of aberrant DNA structures. *Genes Dev,* 14**,** 927-39.

WEAVER, Z., MONTAGNA, C., XU, X., HOWARD, T., GADINA, M., BRODIE, S. G., DENG, C. X. & RIED, T. 2002. Mammary tumors in mice conditionally mutant for Brca1

exhibit gross genomic instability and centrosome amplification yet display a recurring distribution of genomic imbalances that is similar to human breast cancer. *Oncogene,* 21**,** 5097-107.

WEINRICH, S. L., PRUZAN, R., MA, L., OUELLETTE, M., TESMER, V. M., HOLT, S. E., BODNAR, A. G., LICHTSTEINER, S., KIM, N. W., TRAGER, J. B., TAYLOR, R. D., CARLOS, R., ANDREWS, W. H., WRIGHT, W. E., SHAY, J. W., HARLEY, C. B. & MORIN, G. B. 1997. Reconstitution of human telomerase with the template RNA component hTR and the catalytic protein subunit hTRT. *Nat Genet,* 17**,** 498-502.

WEST, S. C. 2003. Molecular views of recombination proteins and their control. *Nat Rev Mol Cell Biol,* 4**,** 435-45.

WHITTEMORE, A. S., GONG, G. & ITNYRE, J. 1997. Prevalence and contribution of BRCA1 mutations in breast cancer and ovarian cancer: results from three U.S. population-based case-control studies of ovarian cancer. *Am J Hum Genet,* 60**,** 496-504.

WILSON, D. M., 3RD & THOMPSON, L. H. 2007. Molecular mechanisms of sister-chromatid exchange. *Mutat Res,* 616**,** 11-23.

WOLFF, S. 1977. Sister chromatid exchange. *Annu Rev Genet,* 11**,** 183-201.

WOOSTER, R., BIGNELL, G., LANCASTER, J., SWIFT, S., SEAL, S., MANGION, J., COLLINS, N., GREGORY, S., GUMBS, C. & MICKLEM, G. 1995. Identification of the breast cancer susceptibility gene BRCA2. *Nature,* 378**,** 789-92.

WRIGHT, W. E. & SHAY, J. W. 1992. The two-stage mechanism controlling cellular senescence and immortalization. *Exp Gerontol,* 27**,** 383-9.

WRIGHT, W. E. & SHAY, J. W. 2000. Telomere dynamics in cancer progression and prevention: fundamental differences in human and mouse telomere biology. *Nat Med,* 6**,** 849-51.

WRIGHT, W. E., TESMER, V. M., HUFFMAN, K. E., LEVENE, S. D. & SHAY, J. W. 1997. Normal human chromosomes have long G-rich telomeric overhangs at one end. *Genes Dev,* 11**,** 2801-9.

WU, G., JIANG, X., LEE, W. H. & CHEN, P. L. 2003. Assembly of functional ALT-associated promyelocytic leukemia bodies requires Nijmegen Breakage Syndrome 1. *Cancer Res,* 63**,** 2589-95.

WU, G., LEE, W. H. & CHEN, P. L. 2000. NBS1 and TRF1 colocalize at promyelocytic leukemia bodies during late S/G2 phases in immortalized telomerase-negative cells. Implication of NBS1 in alternative lengthening of telomeres. *J Biol Chem,* 275**,** 30618-22.

WU, L., DAVIES, S. L., LEVITT, N. C. & HICKSON, I. D. 2001. Potential role for the BLM helicase in recombinational repair via a conserved interaction with RAD51. *J Biol Chem,* 276**,** 19375-81.

WU, W., NISHIKAWA, H., FUKUDA, T., VITTAL, V., ASANO, M., MIYOSHI, Y., KLEVIT, R. E. & OHTA, T. 2015. Interaction of BARD1 and HP1 Is Required for BRCA1 Retention at Sites of DNA Damage. *Cancer Res,* 75**,** 1311-21.

WYMAN, C. & KANAAR, R. 2006. DNA double-strand break repair: all's well that ends well. *Annu Rev Genet,* 40**,** 363-83.

XIN, H., LIU, D. & SONGYANG, Z. 2008. The telosome/shelterin complex and its functions. *Genome Biol.*

XIONG, J., FAN, S., MENG, Q., SCHRAMM, L., WANG, C., BOUZAHZA, B., ZHOU, J., ZAFONTE, B., GOLDBERG, I. D., HADDAD, B. R., PESTELL, R. G. & ROSEN, E. M. 2003. BRCA1 inhibition of telomerase activity in cultured cells. *Mol Cell Biol,* 23**,** 8668-90.

XU, X., WAGNER, K. U., LARSON, D., WEAVER, Z., LI, C., RIED, T., HENNIGHAUSEN, L., WYNSHAW-BORIS, A. & DENG, C. X. 1999a. Conditional mutation of Brca1 in mammary epithelial cells results in blunted ductal morphogenesis and tumour formation. *Nat Genet,* 22**,** 37-43.

XU, X., WEAVER, Z., LINKE, S. P., LI, C., GOTAY, J., WANG, X. W., HARRIS, C. C., RIED, T. & DENG, C. X. 1999b. Centrosome amplification and a defective G2-M cell cycle

checkpoint induce genetic instability in BRCA1 exon 11 isoform-deficient cells. *Mol Cell,* 3**,** 389-95.

YANKIWSKI, V., MARCINIAK, R. A., GUARENTE, L. & NEFF, N. F. 2000. Nuclear structure in normal and Bloom syndrome cells. *Proc Natl Acad Sci U S A,* 97**,** 5214-9.

YARDEN, R. I., PARDO-REOYO, S., SGAGIAS, M., COWAN, K. H. & BRODY, L. C. 2002. BRCA1 regulates the G2/M checkpoint by activating Chk1 kinase upon DNA damage. *Nat Genet,* 30**,** 285-9.

YASAEI, H. & SLIJEPCEVIC, P. 2010. Defective Artemis causes mild telomere dysfunction. *Genome Integr,* 1**,** 3.

YASUMOTO, S., KUNIMURA, C., KIKUCHI, K., TAHARA, H., OHJI, H., YAMAMOTO, H., IDE, T. & UTAKOJI, T. 1996. Telomerase activity in normal human epithelial cells. *Oncogene,* 13**,** 433-9.

YE, J. Z., HOCKEMEYER, D., KRUTCHINSKY, A. N., LOAYZA, D., HOOPER, S. M., CHAIT, B. T. & DE LANGE, T. 2004. POT1-interacting protein PIP1: a telomere length regulator that recruits POT1 to the TIN2/TRF1 complex. *Genes Dev,* 18**,** 1649-54.

YEAGER, T. R., NEUMANN, A. A., ENGLEZOU, A., HUSCHTSCHA, L. I., NOBLE, J. R. & REDDEL, R. R. 1999. Telomerase-negative immortalized human cells contain a novel type of promyelocytic leukemia (PML) body. *Cancer Res,* 59**,** 4175-9.

ZHANG, J. 2013. The role of BRCA1 in homologous recombination repair in response to replication stress: significance in tumorigenesis and cancer therapy. *Cell Biosci,* 3**,** 11.

ZHANG, J. & POWELL, S. N. 2005. The role of the BRCA1 tumor suppressor in DNA double-strand break repair. *Mol Cancer Res,* 3**,** 531-9.

ZHONG, Q., BOYER, T. G., CHEN, P. L. & LEE, W. H. 2002a. Deficient nonhomologous end-joining activity in cell-free extracts from Brca1-null fibroblasts. *Cancer Res,* 62**,** 3966-70.

ZHONG, Q., CHEN, C. F., CHEN, P. L. & LEE, W. H. 2002b. BRCA1 facilitates microhomology-mediated end joining of DNA double strand breaks. *J Biol Chem,* 277**,** 28641-7.

ZHONG, Q., CHEN, C. F., LI, S., CHEN, Y., WANG, C. C., XIAO, J., CHEN, P. L., SHARP, Z. D. & LEE, W. H. 1999. Association of BRCA1 with the hRad50-hMre11-p95 complex and the DNA damage response. *Science,* 285**,** 747-50.

ZHONG, Z., SHIUE, L., KAPLAN, S. & DE LANGE, T. 1992. A mammalian factor that binds telomeric TTAGGG repeats in vitro. *Mol Cell Biol,* 12**,** 4834-43.

ZHONG, Z. H., JIANG, W. Q., CESARE, A. J., NEUMANN, A. A., WADHWA, R. & REDDEL, R. R. 2007. Disruption of telomere maintenance by depletion of the MRE11/RAD50/NBS1 complex in cells that use alternative lengthening of telomeres. *J Biol Chem,* 282**,** 29314-22.

ZHU, X. D., KUSTER, B., MANN, M., PETRINI, J. H. & DE LANGE, T. 2000. Cell-cycle-regulated association of RAD50/MRE11/NBS1 with TRF2 and human telomeres. *Nat Genet,* 25**,** 347-52.